OAK RIDGE NATIONAL LABORATORY LIBRARIES
3 4456 0550291 6

CENTRAL RESEARCH LIBRARY

ORNL-TM-4356

cy. 80

HIGH-TEMPERATURE STRUCTURAL DESIGN METHODS FOR LMFBR COMPONENTS QUARTERLY PROGRESS REPORT FOR PERIOD ENDING JUNE 30, 1973

W. L. Greenstreet
J. M. Corum
C. E. Pugh

[redacted]

OAK RIDGE NATIONAL LABORATORY
CENTRAL RESEARCH LIBRARY
DOCUMENT COLLECTION
LIBRARY LOAN COPY
DO NOT TRANSFER TO ANOTHER PERSON
If you wish someone else to see this document, send in name with document and the library will arrange a loan.
UCN-7969

OAK RIDGE NATIONAL LABORATORY
OPERATED BY UNION CARBIDE CORPORATION • FOR THE U.S. ATOMIC ENERGY COMMISSION

Printed in the United States of America. Available from
the U.S. Atomic Energy Commission, Technical Information Center
P.O. Box 62, Oak Ridge, Tennessee 37830
Price: Printed Copy $7.60 ; Microfiche $1.45

This report was prepared as an account of work sponsored by the United States Government. Neither the United States nor the United States Atomic Energy Commission, nor any of their employees, nor any of their contractors, subcontractors, or their employees, makes any warranty, express or implied, or assumes any legal liability or responsibility for the accuracy, completeness or usefulness of any information, apparatus, product or process disclosed, or represents that its use would not infringe privately owned rights.

ORNL-TM-4356
UC-79e, UC-79h,
UC-79k

Contract No. W-7405-eng-26

HIGH-TEMPERATURE STRUCTURAL DESIGN METHODS FOR LMFBR COMPONENTS

QUARTERLY PROGRESS REPORT
FOR PERIOD ENDING JUNE 30, 1973

W. L. Greenstreet
J. M. Corum
C. E. Pugh

DECEMBER 1973

[redacted]

OAK RIDGE NATIONAL LABORATORY
Oak Ridge, Tennessee 37830
operated by
UNION CARBIDE CORPORATION
for the
U.S. ATOMIC ENERGY COMMISSION

OAK RIDGE NATIONAL LABORATORY LIBRARIES
3 4456 0550291 6

Previous Reports in this Series

ORNL-CF-70-6-14	March — May 1970
ORNL-CF-70-6-48	June 1970
ORNL-CF-70-8-30	July 1970
ORNL-CF-70-9-46	August 1970
ORNL-CF-70-10-56	September 1970
ORNL-CF-70-12-46	October — November 1970
ORNL-CF-71-2-48	December 1970 — January 1971
ORNL-CF-71-4-58	February — March 1971
ORNL-CF-71-6-57	April — May 1971
ORNL-CF-71-8-54	June — July 1971
ORNL-TM-3736	August — December 1971
ORNL-TM-3845	January — March 1972
ORNL-TM-3917	April — June 1972
ORNL-TM-4058	July — September 1972
ORNL-TM-4089	October 1972 — March 1973

CONTENTS

Page

PREFACE v

SUMMARY AND STATUS vi

0. INTRODUCTION 1

1. MATERIAL BEHAVIOR TESTS 3

1.1. Characterization of Product Forms 3

1.2. Exploratory Testing to Identify Behavioral Features . . . 6

2. CONSTITUTIVE EQUATION DEVELOPMENT 20

2.1. Elastic-Plastic Behavior 20

2.2. Time-Dependent Behavior 31

3. FAILURE STUDIES 41

3.1. Study of the Effect of Biaxiality in Creep-Fatigue at Elevated Temperatures 41

3.2. Investigations of Creep Failure Under Uniaxial and Multiaxial Conditions 48

4. DEVELOPMENT, EVALUATION, AND DISTRIBUTION OF STRUCTURAL ANALYSIS METHODS AND TOOLS 58

4.1. Two-Dimensional Elastic-Plastic-Creep Finite-Element Computer Program CREEP-PLAST 58

4.2. General Three-Dimensional Thick Shell Elastic-Plastic-Creep Finite-Element Computer Program EPACA 72

4.3. Simplified Inelastic Piping System Analysis Computer Program PIRAX 83

5. INELASTIC STRUCTURAL TESTS 89

5.1. Elastic-Plastic-Creep Tests and Analyses of Simply Supported Beams 89

5.2. Elastic-Plastic-Creep Tests of Simply Supported Circular Plates 98

5.3. Weldment Creep-Rupture Studies 114

5.4. High-Temperature Moire Strain Analysis of an In-Plane Loaded Finite-Width Plate with a Circular Hole 124

5.5. Elevated-Temperature Test of Stiffened Shear-Lag Panel . 125

5.6. Pipe Thermal Ratchetting Tests 130

CONTENTS (continued)

Page

6. DESIGN CRITERIA 161

6.1. Studies of Shakedown and Ratchetting of Structures . . . 161

6.2. Examination of K Factor Used in Code Case 1331 and Recommended Modifications 172

7. CORE STRUCTURES DESIGN CRITERIA AND DATA 180

REFERENCES 186

PREFACE

This is the sixth of a series of formal progress reports summarizing accomplishments in the ORNL program to develop high-temperature structural design methods for LMFBR vessels, components, and core structures. This report covers the period of March 1973 through June 1973. The technical activities of the program are comprehensively reported in the text of these reports under seven major headings which correspond to the major sections of the program plan document. A section, which is entitled "Summary and Status," precedes the text and gives a short synopsis of the reported progress and the status of each area. This section provides the reader with an opportunity to survey the contents of the report prior to reading the technical sections. The Summary and Status section also includes brief discussions of pertinent program management and liaison activities.

The program has as its goal the development of a verified high-temperature design technology applicable to the long-term operating conditions expected for LMFBR systems. Although the ultimate objective is to develop verified methods and criteria for reliably designing for high temperatures and long lives, efforts are also concentrated on establishing and validating methods and criteria to be used, on an interim basis, for FFTF and LMFBR Demonstration Plant designs. The overall program is divided into a number of tasks which are being carried out with the participation and cooperation of industrial groups, universities, and design code bodies.

SUMMARY AND STATUS

W. L. Greenstreet

ORNL staff members participated in a number of ASME, Pressure Vessel Research Committee (PVRC), and other meetings during the April through June 1973 period. The PVRC meetings attended were those of the Subcommittee on Plastic Fatigue Strength (April 18 and May 21, 1973) and of the Subcommittee on Elevated Temperature Design (April 18 and May 22, 1973). The ASME meetings were those of the Boiler and Pressure Vessel Code groups (Task Force on Creep Analysis, Task Force on Creep-Fatigue, and Subgroup on Elevated Temperature Design); these were held on May 22-23, 1973, and on June 19-20, 1973. Proposed guidelines for examining propensity for ratchetting and estimating accumulated strains were prepared for the May meetings of the ASME code groups. Also prepared was a write-up on factors to be used to account for plasticity and/or creep related reductions in bending stresses from those calculated on elastic bases; this latter write-up was accepted for use.

The high-temperature design standard, F9-4, continued to receive considerable attention. Three meetings in connection with this standard were attended; one meeting (April 3, 1973) was devoted to constitutive equations, while the remaining two (April 4 and June 21, 1973) were addressed to more general considerations.

Staff members also participated in a finite-element design application meeting, where they gave presentations on the use of finite-element methods in structural analyses. This meeting was held by the U.S. Atomic Energy Commission in Germantown, Maryland, on May 3-4, 1973. The purpose was to exchange information on the use of finite elements in nuclear physics and in solid mechanics applications.

ORNL assisted Westinghouse Advanced Reactors Division in the design analysis of the FFTF In-Vessel Handling Machine (IVHM) by performing a structural evaluation of the under-plug shielding assembly, including support cylinder and suppressor plate. Seismic and thermal loadings were considered; the latter were those associated with U1 and U2/N4 transients, which represent the most severe thermal events. Static and dynamic analysis

techniques were used in examining the seismic loadings. Results of the analysis showed that all but one of the regions investigated were adequate as designed. Minor changes were suggested for the shielding and suppressor plate supports. An informal technical report on the ORNL structural evaluation was transmitted to Westinghouse for use in preparing the overall design analysis report on the IVHM.

Under material behavior studies, tests are being continued to characterize the mechanical, metallurgical, and chemical properties of each product form of the type 304 stainless steel reference heat (9T2796); 1.0-in.-thick plate was added to those forms which are being examined on a priority basis. Room temperature stress-strain curves to 2% strain show that differences observed for as-received material (yield stress range from 26,500 to 34,400 psi) were greatly reduced by reanneal (yield stress range of 26,000 to 27,700 psi). Stress rupture data, which were obtained using reannealed specimens from seven product forms, do not indicate large differences in rupture life associated with product form or with specimen location and orientation relative to the stock material. The minimum creep rates for these seven product forms differed by only small amounts.

A machine to be used in performing creep-plasticity interaction studies was made operational and preliminary experiments were initiated. In addition, a new 50,000-lb electro-hydraulic testing machine was commissioned during this quarter.

Special stress-strain tests were performed on specimens from the reference heat (9T2796) to allow careful exploration of inelastic behavior at relatively low strains. It was again shown that deviations from linearity begin at low stresses and develop gradually at stresses below 10,000 psi. The nonlinearity causing mechanisms at low stresses remains to be studied and identified.

Studies on the influences of thermo-mechanical variables on creep rupture of the type 304 reference heat material have been deemphasized. Reannealing at temperatures in the range from 1850 to 2050°F did not produce discernible changes. In addition, cooling rate was found to be unimportant, except in the case of a very slow rate.

Effects of cyclic deformation on subsequent creep behavior at 1100°F is being examined. Results obtained suggest that small amounts of cold

work have very little influence on subsequent creep response. In the case of cyclic creep loading, the creep rates were lower than indicated by monotonic-loading test results. The cumulative creep curve for one cycled tubular specimen paralleled that for a second monotonically-loaded tubular specimen, but both curves were below that for a monotonically-loaded rod specimen.

Results from a multiply loaded relaxation specimen show that relaxation hardening is a gradual process. Each reloading to the original stress produced a relaxation curve which was slightly above the previous curve. In another study, it was shown that the hardening influences of creep strains are about the same as in the case of plastic strains. Although this is in agreement with other observations, additional testing is needed to clearly establish this suggested equivalency.

Constitutive equation development work in the elastic-plastic behavior category included completion of two additional experimental studies of deformation response and yield surface behavior. Nonradial loading histories were imposed in each case. Development work was also carried out on a differential-capacitance type strain measuring device. This device has potential for providing strain measuring precision at high temperatures that will allow us to improve our investigative ability, especially as related to details of elastic-plastic deformations and to creep- and plastic-deformation interactions.

We are also pursuing improvements for inelastic analysis guidelines by investigating formulations which will give quasi-continuous changes in the size of the yield surface, as measured by κ. These formulations are to include temperature and plastic strain as variables and are to apply for arbitrary loadings. A promising expression for isothermal loadings was derived and applied in the analysis of beam test B6; the cyclic elastic-plastic behavior results from this test have been employed in several comparisons. The latest predictions overestimated the strains for the second half of the first cycle, but reasonably good agreement was obtained for the second cycle.

Preparations were made to reinstate studies at Yale University. These studies are to deal with thermomechanical behaviors of structural materials and mathematical representations of these behaviors. As the planned theoretical studies progress, test recommendations will be provided to ORNL on a

continuing basis for possible incorporation into experimental activities of the overall program.

At Brown University, a multiaxial stress (tension-torsion) creep test (test No. 7) on a thin-walled tubular specimen (No. 4-304-16) was completed. After the stresses were removed, the specimen exhibited an elastic recovery followed by a slight time-dependent recovery.

Although the conditions for test No. 7 were similar to those for an earlier test (test No. 2), the creep rate for No. 7 was in better agreement with results from other tests at the effective stress of about 15,000 psi. The creep rate was an order of magnitude higher at 120 hours in test No. 2. Generally, the overall 120-hr creep rate results for an effective stress of 15,000 psi indicate that the strain rate vector decreases in magnitude as the stress state is changed from pure tension to pure torsion. This observation along with consideration of the directions of the strain rate vectors indicate that an ellipse associated with creep differs somewhat from a von Mises ellipse.

Fabrication was completed on four additional specimens at Brown University. Two of these have been prepared for testing. In addition, equipment is being prepared for creep testing in compression.

As a part of failure studies, fatigue tests were completed at Pennsylvania State University on 15 specimens at 1200°F and 6 specimens at 1000°F. This brings the total number of specimens tested to 91; 10 were tested at room temperature, 21 at 1200°F, and 6 at 1000°F. In the room temperature and the 1200°F tests, the torsional shear strain range to axial strain range ratios were 0.5, 1.0, and 2.0; they were 0.5 and 1.0 in the 1000°F tests. The number of cycles to failure ranged from 1,075 to 11,550 at room temperature, from 100 to 12,800 at 1200°F, and from 680 to 3,178 at 1000°F.

Using the octahedral shear strain as an index, the room temperature biaxial data show a linear correlation on a log-log plot of strain vs number of cycles to failure. Pure torsional data fall above the axial and biaxial test data in this case. A linear relationship is also exhibited by the 1000°F results, but the 1200°F results indicate a bilinear correlation with a transition at about 10^3 cycles. For a life of less than 10^3 cycles at 1200°F, the reduction from that given by the room temperature data is about 10. At 1000°F the reduction factor is about 4.

Uniaxial-constant and step-load tests are being continued by Babcock and Wilcox. The five constant load tests that were in progress during the last reporting period remain in test, with no failures having occurred. The total test times range to 9000 hours. Similarly, the six step-load tests under way during the last period are still in progress; each specimen has undergone two load changes.

New tests were initiated on three specimens in the so-called "interrupted" constant-load series. The objective for this series is to obtain information on material degradation as a function of creep exposure through destructive examinations.

Investigations are underway to identify sources for differences between results from creep and from rupture machines. A test now in progress indicates that differences between strains determined from measurements over the load train and those from measurements over the specimen gage length do not account for the overall discrepancies. The influences of specimen bending remain to be determined.

The first tubular rupture specimen was loaded in simple tension. Creep testing was delayed due to a minor failure in the loading system.

Structural analysis methods development and evaluation work resulted in notable advances during this period. The computer program CREEP-PLAST has undergone further improvements in the form of user-oriented operational modifications to improve versatility, lower computational costs, and to overcome minor limitations. The heat conduction analysis capability, which was developed by General Electric under ORNL subcontract, is being incorporated into the ORNL version of the program. Since incorporation of this expanded capability will be completed in the immediate future, release and distribution of the expanded version is announced in this report, and request forms are provided.

Verification and qualification examinations have included continued studies of elastic-plastic test results from thin-walled cylinders. These studies highlight the very close and interwoven relationships between stress and plastic strain increments during plastic loading, yield surface size, motion of the yield surface, and the direction of the plastic strain increment vector. Because of these interrelationships, directions for modification of the stress-plastic strain equations must be considered carefully and

in broad terms. Again, these studies show that bilinear stress-strain representations better approximate experimental results than the nonlinear representations used.

Debugging of EPACA is continuing; sources for errors, as noted in the last progress report, were identified and eliminated. An elastic analysis of an elbow subjected to an in-plane bending moment was completed and the results compared with experimental data. Agreement between the two sets of results is very good.

Although much additional debugging remains and only the two quadrilateral elements from the eight-element library can be used at this time, the current version of EPACA is being offered to the public. It is expected that experiences by other users will be very helpful in the remaining debugging and verification processes.

During this period, a mathematical representation for isochronous stress-strain behavior was selected and used in pseudo-elastic-plastic type analyses of sample problems at Battelle Columbus Laboratories. Incorporation of this analysis feature into the basic spatially three-dimensional computer program, PIRAX, for treating piping systems will be done in the near future. All of the components for the elbow and straight pipe test assembly are on hand and are being carefully examined before final annealing and welding.

In the structural test area, six types of specimens are presently being employed. These are simply-supported beams, simply-supported circular plates, capped cylindrical shells, finite-width plates with circular holes, stiffened shear-lag panels, and straight pipes subjected to thermal transient conditions.

Two beam tests, B7 and B8, which were deflection controlled, have been completed. These tests were conducted at 1100°F and the specimens were made from the reference heat of type 304 stainless steel. In the second test, B8, ten short-time cycles were imposed both before and after the creep loading period, while for B7 short-time cyclic loading was applied only at the end of the creep loading period. Deflection and strain measurements were made using DCDT's, dial gages, and Ailtech SG-425 strain gages.

Calculated and experimental results for test B7 were compared. Good comparisons were found in the case of elastic-plastic response, and the time-dependent responses were in good agreement. The agreement between

measured results and predictions is markedly better than for previous load-controlled tests. This is as expected and is significant because inelastic loadings in practice are largely deformation controlled.

Another pair of beam specimens is being prepared for load-controlled tests B9 and B10. These tests will duplicate previous load-controlled tests B5 and B6.

Two deflection-controlled circular plate tests, CP3 and CP4, were also completed during this period. The test temperature was 1100°F and the specimens again were made from reference heat material. In the first of these, CP3, ten short-time cycles were imposed at the beginning of the test and after the creep test period; for the second, short-time cyclic loading was imposed only after the creep period.

Two of the cylindrical specimens from the second series of weldment creep-rupture tests were inspected after reaching a total test time of 2000 hours. The deformation-time histories, as established by periodic measurement results, show continuously increasing circumferential strains in the base metal portions of the cylinders. Those regions made from pipe material continue to exhibit larger strains than those made from bar.

Accumulated strains for the weld material of both specimens inspected are very small in comparison to those for the base metal. Further, no trends are discernible for the weld material strains.

One specimen failed during this period after being under test conditions for about 1140 hours. The failure was in the weld region. Following dimensional inspection, this specimen is to be sectioned for visual and metallographic examination.

Detailed data reductions for the weldment creep-rupture test specimens are being continued. Refinements were made in the mathematical descriptions of the deformed specimens to achieve improved results.

At Catholic University, a trial stainless steel specimen was tested in the furnace which was fabricated as a part of the project being carried out. The test temperature and the loading cycle used were the same as those specified for the actual investigation. Photographs were taken at intervals to provide preliminary results for moire method analysis and study.

Improvements in contrast relative to the 500-lines-per-inch gratings at 1100°F continue to be pursued. Efforts have been made to minimize oxidation in the furnace and control of interline changes by the introduction of various substances is being studied.

Good progress is being made on the Boeing Aerospace Co. project to test shear-lag panels. Machining, straightening, and annealing of a second shear-lag specimen was completed; tensile tests were conducted and grain size determinations were made. The heating system was subjected to preliminary checkout and modified to achieve the desired temperature distribution control. Similarly, quasi-final modifications were made to the loading system. Finally, the first specimen was instrumented for room temperature, 500°F, and 1100°F load tests, and the signal conditioning and control equipment was set up.

An important achievement during this period was successful completion of the pretest runs on the Thermal Transient Test Facility (TTTF) and operation through the first ten thermal transient cycles on the first test specimen. Each cycle consisted of a ramp reduction in the sodium temperature from 1100°F to 800°F in about ten seconds, restoration of the sodium temperature to the 1100°F level after a short hold period at 800°F, and 160 hr of sustained operation under 700 psi internal pressure at 1100°F. Facility performance was very good throughout, and markedly good strain data were obtained from the Boeing capacitance strain gages.

Subsequent to this reporting period, the specimen was subjected to four additional cycles to complete the test sequence. Data from the Boeing capacitance gages were obtained for the first three of these cycles.

Inelastic ratchetting analyses were made on the basis of measured temperature and pressure histories and the ORNL-recommended constitutive equations for elastic-plastic and creep behavior. Very good agreement was found between the calculated and measured results. Further, it was shown that these calculated results compared better with the experimental data than those obtained when other selected elastic-plastic behavior representations were used.

Cycle conditions for the second specimen were selected. These are: a downshock rate of 23°F per second, 400 psi internal pressure, and a 328 hr hold time. Minor test section and system modifications are planned for ease of service and improved operations. Fabrication of the second test piece was completed.

In the design criteria area, analytical studies of ratchetting were continued. Comparisons were made between results obtained using rigorous inelastic analysis methods and those from calculations based on two simplified methods. For the 51 cases considered, it was found that the two simplified methods gave conservative results. In addition, comparison with experimental results from LMEC beam tests further substantiated that conservative predictions are given by the two methods.

A second study involved the shape, or section, factor, κ, used in ASME Code Case 1331. This study further identified the role of the shape factor and yielded numerical values to be used.

Compilation and development of design criteria for core structure components are being continued. Correlations of mechanical properties data for types 304 and 316 stainless steel are presently central parts of these on-going efforts. Application of data and correlations to the development of such items as strain limits and fatigue data adjustment factors is also underway.

0. INTRODUCTION

This is one of a continuing series of progress reports describing work under the LMFBR program task to develop a structural design technology and associated design criteria applicable to LMFBR system components. This is the sixth quarterly progress report (previously reports were issued on a monthly or bimonthly basis) and it covers the period April through June 1973.

The purpose of the high-temperature structural design methods program is to develop a verified structural design technology applicable to LMFBR components and core structures, excluding fuel elements. Included in the components category are such items as pressure vessels, piping, heat exchangers, pumps, and valves. This technology, which is to embrace the areas of materials properties and behavior, mathematical analogs for the description of material response, structural analysis methods, and design criteria, is to be developed on theoretically consistent, rational bases and experimentally verified.

In the development of this design technology, careful assessments are to be made of both elastic and inelastic structural behavior under conditions of elevated temperatures and, in the case of core components, high neutron exposure. Responses of interest are stress and strain behavior, dynamic response, structural instability (buckling), brittle failure, and failure through creep rupture, fatigue, creep-fatigue interaction, or crack propagation. Therefore, the structural analysis methods and design criteria are to be capable of reflecting or including the environmental and loading condition influences and lead to rational assessments of the consequences of the resultant effects on structural behavior and integrity.

Two objectives are to be served by the program. In addition to the development of the required technology as an end product, interim needs for structural design guidance, methods, and criteria are to be met on a continuing basis. In the initial phases of the program, existing knowledge and data concerning material behavior, existing constitutive theories and structural analysis methods, and existing design rules and criteria were thoroughly exploited to meet design requirements and to help establish bases for identification and pursuit of program activities aligned with the twofold objective. Thus, the activities established for the near-term lead naturally toward those for the long-term.

The overall program is currently comprised of seven major tasks. These are:

1. Material Behavior Tests
2. Constitutive Equation Development
3. Failure Studies
4. Development, Evaluation, and Distribution of Structural Analysis Methods and Tools
5. Inelastic Structural Tests
6. Design Criteria
7. Core Structures Design Criteria and Data

Starting with this issue, these major task headings are adopted for use in the progress reports; the organization will, therefore, be similar to that of the program plan document. The task numbers shown above will be maintained for the indicated tasks regardless of whether or not all tasks are reported in a given report. These reports include work performed under subcontracts as well as work performed at the Oak Ridge National Laboratory. The reader is referred to the preceding reports for background information.

1. MATERIAL BEHAVIOR TESTS

R. W. Swindeman
H. E. McCoy
W. R. Martin

1.1. Characterization of Product Forms

H. E. McCoy

Tests to characterize the mechanical, metallurgical, and chemical properties of each product form of the reference heat (9T2796) of type 304 stainless steel have been outlined in Ref. 1. Further, Ref. 1 assigned an item number to each product form of the reference heat, and testing priorities given for eleven product forms. Previous reports of status and test results are given in Refs. 1, 2, and 3. Testing and data consolidation are continuing.

Table 1.1 lists some of the properties for ten of the product forms. The 1 in. plate has been added to the previously cited eleven priority product forms, and characterization testing has just begun on the 3/8 in. and 1 in. plates (items numbered 4 and 7, respectively, in Ref. 1). The grain sizes of these ten products varied from ASTM 1 to 7, with some of the products having a wide variation within themselves. Tensile tests have been run at 25°C for 5 of the product forms in the as-received and reannealed conditions. The stress-strain curves to 2% strain are shown in Fig. 1.1 for the as-received material and in Fig. 1.2 for the reannealed material. The yield stress of the as-received products varied from 26,500 to 34,400 psi, but the work-hardening rates appear the same after a few tenths of percent strain. The yield stress of the reannealed material varied from 26,000 to 27,700 and the curves to 2% strain almost superimpose (Fig. 1.2).

The results of chemical analyses for C, O, and N are given in Table 1.1. The carbon content varied from 0.050 to 0.056% and the nitrogen content from 0.040 to 0.051%. The quoted reproducibility for each analysis is ±5%; the carbon analyses fall within this range and the values for nitrogen have a span of about ±10%. The oxygen analyses varied from 0.0046 to 0.0089 for eight of the products and values of 0.018 and 0.011 were noted for two products. Check analyses indicated concentrations of 0.019 and 0.014%,

Table 1.1. Information on several product forms of type 304 stainless steel, heat 9T2796

Product form	Item number	Specification	Hardness, R_B		Initial ASTM grain size	Yield Stress[b] at 25°C ksi		Chemical Composition, %[c]		
			Initial	Annealed[a]		Initial	Annealed	C	O	N
Pipe, 8-in. Schedule 80	11	A-376	73	69	5–6	30.3	26.0 26.5	0.056	0.018 0.019	0.042 0.042
Pipe, 4-in. Schedule 160	10	A-376	73	63	5–6	31.7 32.3	26.7 26.5	0.052	0.0089	0.051
Bar, 4 1/2-in.-diam	22	A-479	67	67	2–3[d] 3–5[e]	30.8	26.5 26.1	0.051	0.0062	0.049
Bar, 2-in.-diam	21	A-479	89	65	5–6[d] 6–7[e]			0.053	0.0049	0.048
Bar, 1 3/4-in.-diam	20	A-479	81	65	5–6			0.052	0.0062	0.048
Plate, 1/2 in. thick	5	A-240	73	66	5–6			0.052	0.0075	0.046
Plate, 3/4 in. thick	6	A-240	65	65	5–6	34.4	26.0	0.051	0.011 0.014	0.048 0.044
Plate, 2-in. thick	8	A-240	59	66	1–3	27.7 26.6	27.7	0.055	0.0086	0.040
Tube, 2 1/2-in.-O.D. × 5/8 in. W (H.R.)	51	A-479	88	65	6–7			0.051	0.0053	0.050
Tube, 2 1/2-in.-O.D. × 5/8 in. W (C.D.)	15	A-376	74	67	3–6			0.050	0.0046	0.047

[a] 1/2 hr at 1093°C (2000°F).

[b] Strain rate of 0.004 min^{-1}. All samples parallel with the primary forming direction.

[c] Four product forms were analyzed for trace elements and the following levels apply to all four forms: <.01% Ag, 0.05% Al, <0.01% B, <0.01% Ba, <0.005% Be, <0.02% Bi, <0.1% Ca, <0.1% Cb, <0.1% Cd, 0.3% Co, 0.3% Cw, 0.01% Mg, 0.02% Pb, <0.05% Pt, <0.02% Sn, <0.1% Sr, 0.05% Ta, <0.02% Ti, 0.03% V, <0.1% W, <0.2% Zr, <0.05% Zr, <0.05% Ge, 0.05% Ga. The concentrations of other alloying additions are 1.22% Mn, 0.029% P, 0.012% S, 0.47% Si, 18.5% Cr, 9.58% Ni, 0.10% Mo.

[d] Longitudinal plane.

[e] Transverse plane.

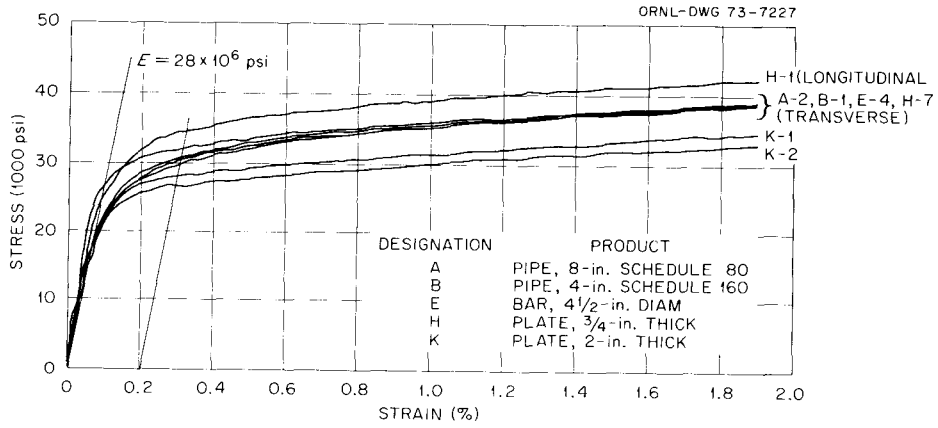

Fig. 1.1. Room temperature stress-strain properties for several product forms of type 304 stainless steel (heat 9T2796) in as-received condition.

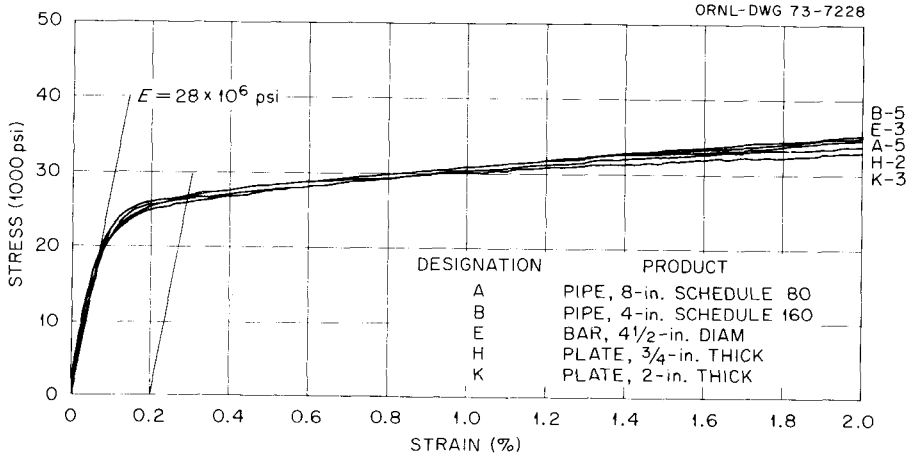

Fig. 1.2. Room temperature stress-strain properties for several product forms of type 304 stainless steel (heat 9T2796) reannealed 1/2 hour at 2000°F.

respectively. Thus, the oxygen concentrations in the product forms indicate variations far outside the ±5% reproducibility of the analysis. Metallographic studies in progress should indicate whether the inclusion count is significantly different for the product forms.

Stress-rupture properties at 1100°F for reannealed samples are shown in Fig. 1.3 for seven product forms. Three stress levels were involved and samples were taken from several locations and orientations within each product. The results obtained to date do not indicate a large difference in the rupture life due to variables of product form, specimen location, or specimen orientation. The rupture life of the 2 in. plate does seem to be slightly shorter, but the difference is not large.

The minimum creep rates for these same products are shown in Fig. 1.4. The differences among different product forms seem quite small and random in nature. The 2 in. plate, that seemed inferior based on the short-time rupture tests shown in Fig. 1.3, does not appear different from the other products on the basis of minimum creep rate.

1.2. Exploratory Testing to Identify Behavioral Features

R. W. Swindeman

1.2.1. Stress-strain testing

Progress was made in the development of laboratory testing facilities. A machine to perform creep-plasticity interaction studies was placed in operation. The first testing involved a number of strain-cycling experiments to check the capability relative to the servo-controlled electro-hydraulic machine. Results are summarized in Fig. 1.5 which plots the stress range against strain range for the tenth cycle of fixed strain range cycling at three temperatures. The performance was satisfactory and we are now in a position to begin interspersing creep and cyclic plasticity over time periods extending to at least 2000 hr.

A new 50,000 lb electro-hydraulic testing system was commissioned during the last quarter. We are currently investigating different specimen, grip, and extensometer designs.

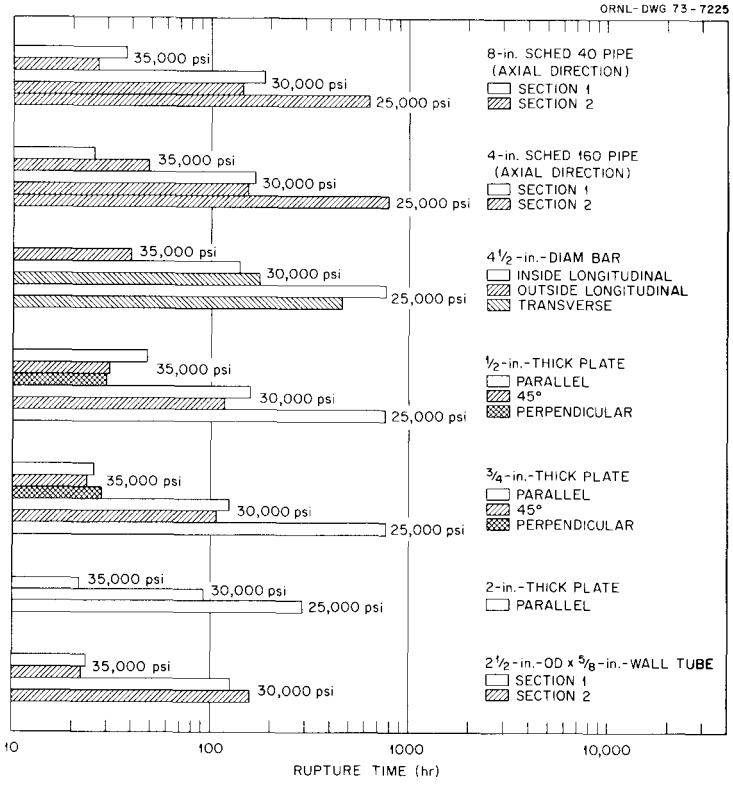

Fig. 1.3. Stress-rupture properties at 1100°F of several product forms of type 304 stainless steel (heat 9T2796) reannealed 1/2 hour at 2000°F.

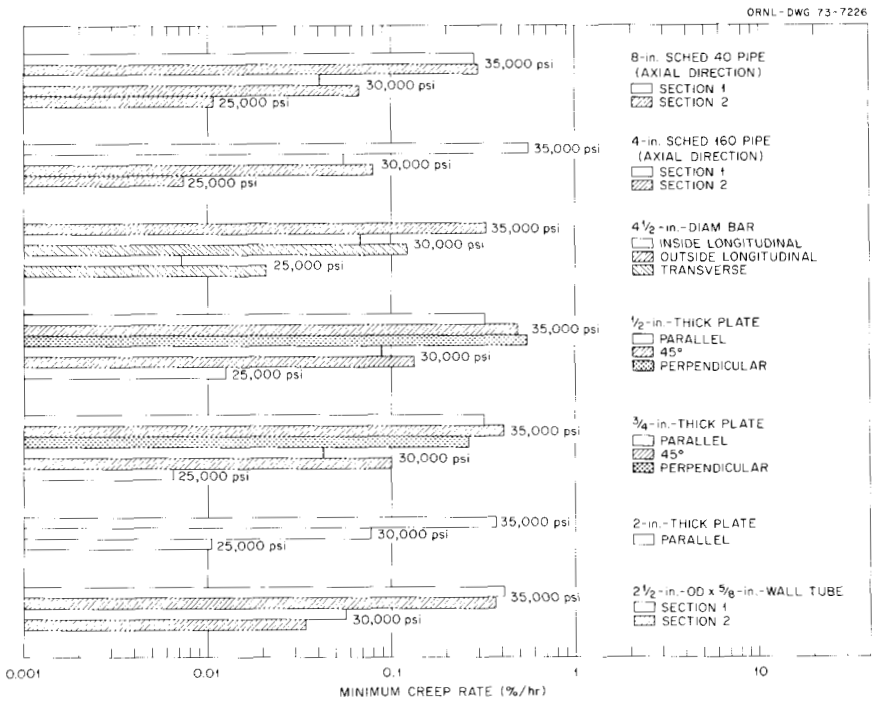

Fig. 1.4. Minimum creep rates at 1100°F for several product forms of type 304 stainless steel (heat 9T2796) reannealed 1/2 hour at 2000°F.

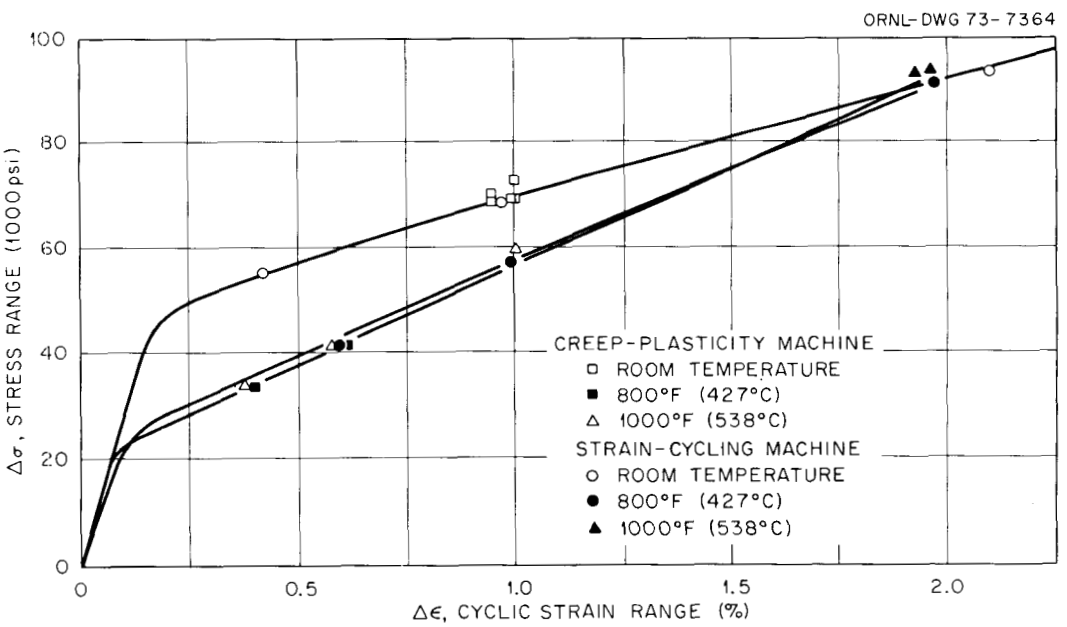

Fig. 1.5. Comparison of tenth cycle hardening data obtained on different machines for type 304 stainless steel (heat 9T2796 1 in. plate Item 7) reannealed for 1/2 hour at 2000°F (1093°C).

Several tensile tests were performed on the reference heat type 304 stainless steel (heat 9T2796, 1" plate) for the purpose of exploring the inelastic behavior at relatively low strains. It has been reported earlier[4,5] that, between the 0.1 percent inelastic offset strain and the uniform strain at the ultimate, the Ludwik equation provides an excellent representation of the true stress-true strain behavior for laboratory re-annealed material. Not included in this representation were inelastic offset strains in the zero to 0.1 percent range and these, of course, are often the most commonly experienced strain levels in design analysis. A tracing of a stress-strain curve obtained at 1100°F is shown in Fig. 1.6. This curve is shown along with three other stress-strain curves which cover temperatures ranging from 800 to 1100°F in Fig. 1.7. All tests were performed under servo-controlled conditions at a strain rate of 0.005/min. Low load cycling showed that the extensometer turn-around error and sensitivity corresponded to strain values less than 10^{-5}. We observed that the elastic limit of the curves was difficult to detect. Assuming the static moduli values provided in the ASME Code Case 1331 to be correct, we found as indicated in Fig. 1.6 that the 10^{-5} offset stresses were between 5,000 and 8,000 psi. Deviations from linearity developed gradually at all temperatures as shown in Fig. 1.7. Above a strain value of approximately .0005 in./in., the strain hardening rate (tangent modulus) rapidly changed and approached a near constant value which was maintained for several percent strain. The deviation from linearity below the knee of the stress-strain curve could be the result of several causes. Among them are the usual anelastic strain, which is recoverable, and true microyielding which is not recoverable. Causes of microyielding could result from eccentric loading, residual stress due to handling of the specimens, or the movement of favorably oriented mobile dislocations. At the present time available data are not sufficient to identify which of these causes of microyielding may have been operative, however, it does appear that the associated strains do not exceed the elastic components.

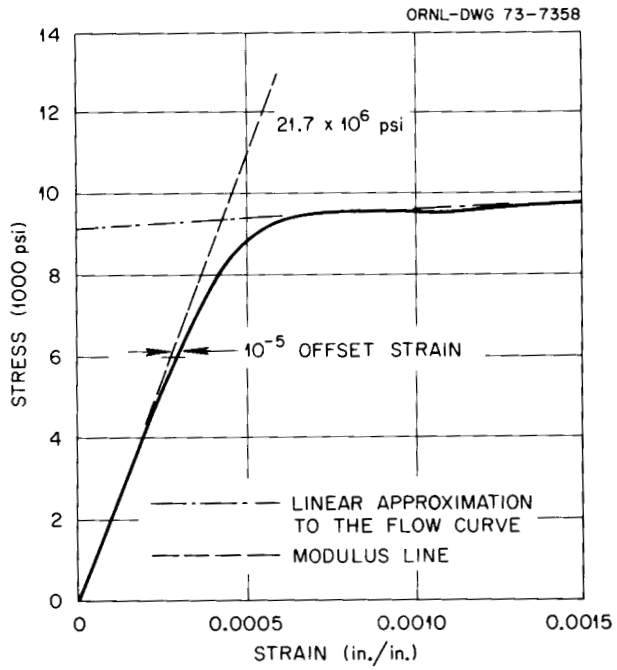

Fig. 1.6. Tensile stress-strain curve for type 304 stainless steel at 1100°F. Heat 9T2796 (1 in. plate, Item 7) reannealed servo-control. Specimen 7RP-131.

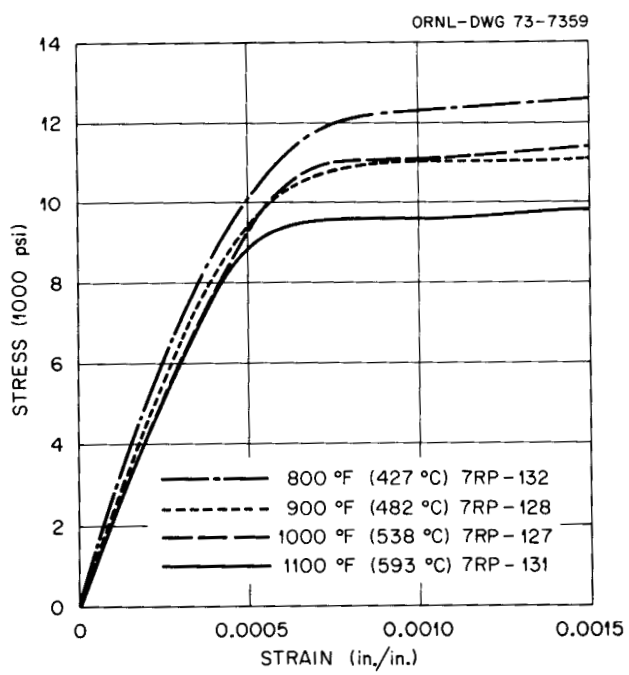

Fig. 1.7. Tensile stress-strain curves for type 304 stainless steel at 800, 900, 1000, and 1100°F. Heat 9T2796 (1 in. plate, Item 7) reannealed at 2000°F for 1/2 hour and tested at 0.005/min under servo-control.

1.2.2. Creep testing

Testing to examine the influence of thermo-mechanical variables on the creep-rupture response of the reference heat of type 304 stainless steel (9T2796) is continuing. It was reported earlier[6] that the reannealing temperature did not have an important effect on the creep behavior of 1 in. plate (Item 7), especially when the reannealing temperature was in the 1850 to 2050°F range. Likewise, the cooling rate effect was not pronounced except for a very slow rate, which greatly improved the ductility and the rupture life. Studies on the effects of heat treatment are continuing, with a reduced emphasis, and are to include two other product forms [5/8-in.-diam bar, HRAP (Item 18) and 5/8-in.-diam bar, cold drawn (Item 23)].

Currently, attention is being given to the influence of cyclic deformation on subsequent creep behavior at 1100°F. Several specimens reannealed at 2000°F were subjected to ten cycles at room temperature over a one percent strain range. This treatment raised the yield strength from a nominal 26,000 psi to about 35,000 psi, which is more typical of type 304 stainless steel plate in the A-240 condition. Creep tests were then initiated at 1100°F and over the stress range from 15,000 to 35,000 psi. The results obtained to date are summarized in Fig. 1.8 where they are compared to the minimum-creep-rate and rupture-life trend curves developed from tests on reannealed material. The data suggest that small amounts of cold work do not greatly influence the subsequent creep behavior. The significant difference in the loading strains is, of course, not shown here. The reannealed material, for example, had a yield stress near 11,000 psi at 1100°F, while the precycled material had a yield stress near 17,500 psi at 1100°F. The similarity in creep properties of the two conditions may, in fact, be due to the influence of loading strains. We have seen that the "warm-work," which is associated with the loading of reannealed specimens to very high stresses (greater than or equal to 30,000 psi), actually depresses initial creep rate for a short period.[7] We have also observed that the insertion of a large plastic strain pulse in a creep test being conducted at a very high stress (greater than or equal to 30,000 psi) also depresses the creep rate for a short while. Conversely, we have found in these present investigations that small precycling strains increase the primary creep at high and intermediate stresses.

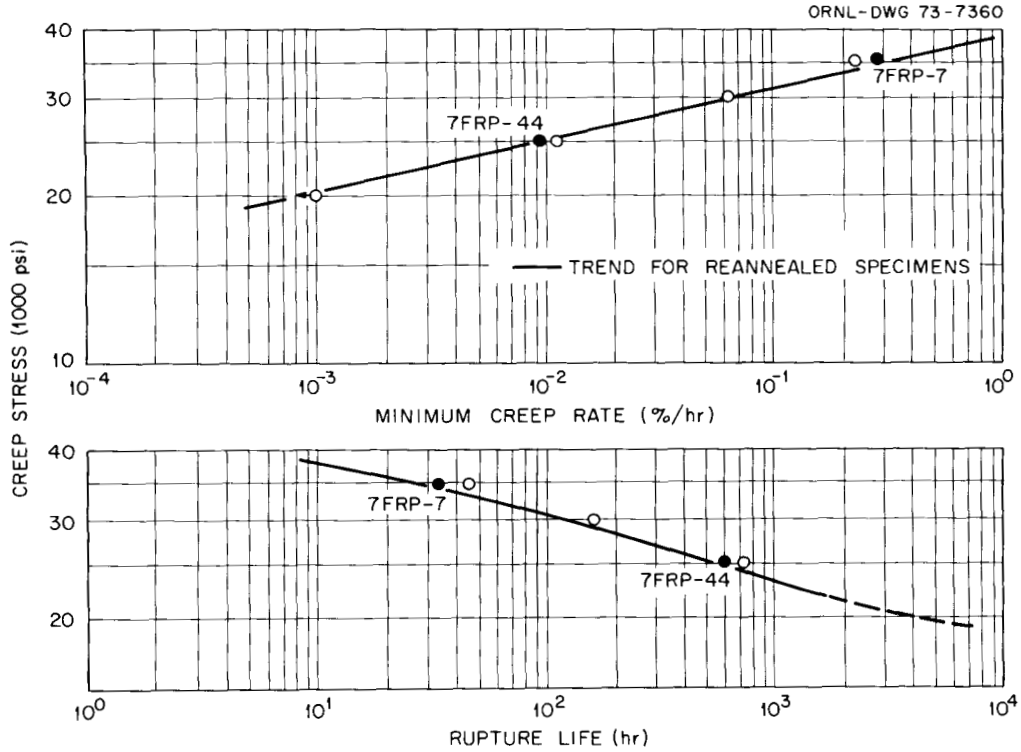

Fig. 1.8. Influence of cyclic deformation on the minimum creep rate and rupture life of type 304 stainless steel at 1100°F (593°C). Heat 9T2796 (1 in. plate, Item 7) reannealed at 2000°F (1093°C). Open symbols for specimens pre-cycled at room temperature and 1% strain range, closed symbols for specimens pre-cycled at 1100°F (593°C); specimen 7FRP-7 at 2% and specimen 7FRP-44 at 0.6% strain range.

Similarly, small plastic strain pulses can also accelerate creep at intermediate stresses (15,000 — 20,000 psi), at least for a short time.[7] Two data points are included in Fig. 1.8 which show that the influence of precycling at 1100°F is similar to precycling at room temperature.

Two of the cyclic creep tests described in the last quarterly[6] were discontinued recently. Specimen 7CRP12 (+22,000/—20,000 psi) was stopped after 9 1/2 cycles (3192 hr) and exhibited about 6% accumulated strain. Specimen 7CRP9 (+24,500/—22,500 psi) ruptured after 11 1/4 cycles (3723 hr) with 20 percent accumulated strain. We have observed, even during the initial constant load hold period, lower creep rates in these cyclic creep tests than we expected from our monotonic test results. Post test load, temperature, and extensometer calibrations eliminated apparatus error as a reason for these differences. Two other possibilities are that cold work was introduced into these tubular specimens during extensometer attachment and at the large strain levels of some tests, the Poisson's contraction was restrained by the specimen shoulders and this set up a stress condition that retarded the axial creep rate. In Fig. 1.9 a comparison is made between two monotonic curves and the cumulative creep curve constructed from the cyclic creep test. Specimen 7RP155 was a conventional monotonic creep-rupture specimen, 1/4 in. diam and 2.25 in. gage length. Specimen 7CRP13 was a tubular specimen identical to the cyclic test specimen 7CRP9 (0.6 in. diam, 0.06 in. wall, and 0.5 in. gage length). The creep behavior of the monotonic tubular specimen parallels the cumulative creep curve of the cyclic specimen. Both are below the curve produced by a conventional test of the rod specimen. The most significant difference is in the time for tertiary creep and rupture. These are greater for tubular geometry. Cyclic creep test data for all tests performed are summarized in Fig. 1.10 which plots the log cyclic creep strain component against log stress for the first, second, and fourth cycles. These data are compared to monotonic trend curves.

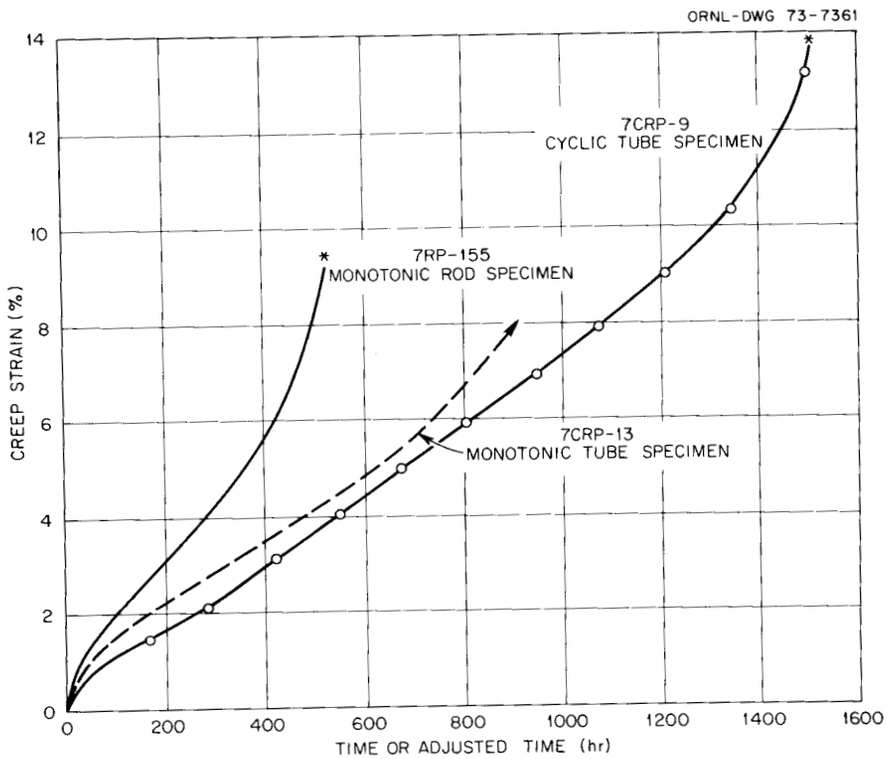

Fig. 1.9. Comparison of monotonic creep curves with cumulative creep curve constructed from cyclic creep test data. Type 304 stainless steel heat 9T2796 (1 in. plate, Item 7) tested at 1100°F. Specimens 7RP155 and 7CRP13 tested at 25,000 psi, specimen 7CRP9 tested at +24,500/−22,500 psi with a two weeks cycle period. The line segments between the open symbols represent the creep strains in excess of the reversal strains.

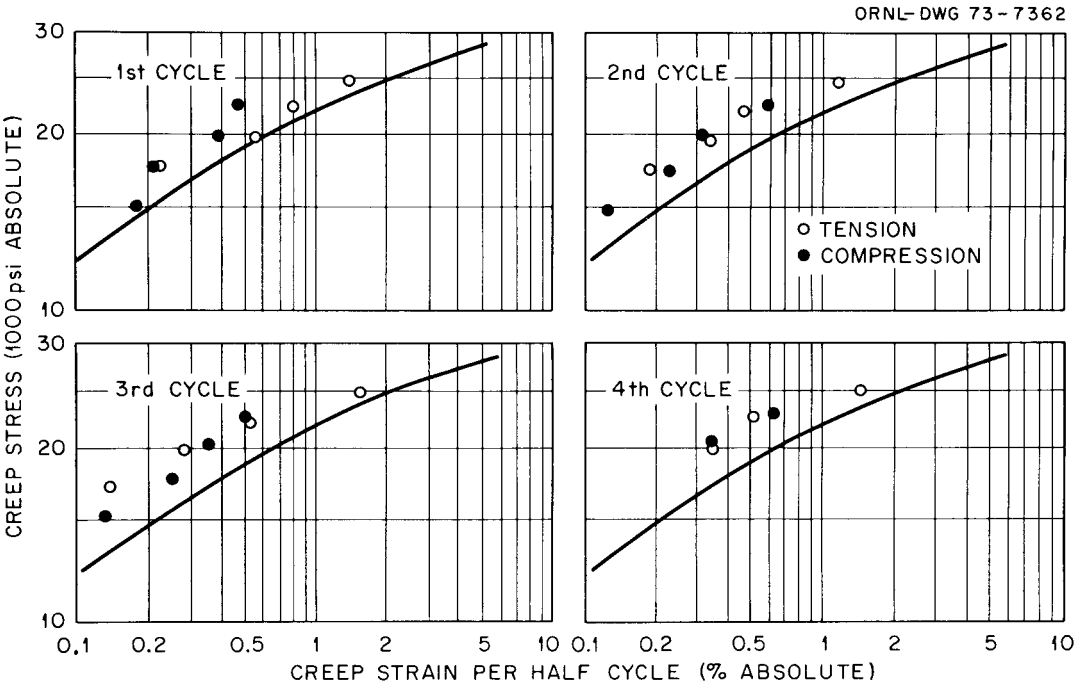

Fig. 1.10. Comparison of monotonic and cyclic creep strains for type 304 stainless steel heat 9T2796. The smooth line represents the trend for monotonic data at 168 hours, open symbols are for strains produced in the tension half of the creep cycle, and filled symbols are for compression. The cycle time was 336 hours. Only the creep strain components are included.

1.2.3. Relaxation testing

No relaxation tests were performed in the last quarter. The results obtained from earlier testing periods are still being studied. Some previously unreported results of interest involve multiple loadings and plots of behavior patterns at 1100°F are included in Fig. 1.11. Our findings were that the relaxation hardening was fairly gradual for this heat of type 304 stainless steel (heat 9T2796). In other words, each reloading to the original stress, after a period of relaxation, produced a curve which was slightly above the previous curve. Such behavior, of course, was expected. The slow increase in the resistance to relaxation implied by these results is in qualitative agreement with the relatively slow rate of hardening we have observed under monotonic creep conditions for this heat of type 304 stainless steel. Some checks were also made to see if relaxation rates after reloadings which included a large plastic strain (about .2%) were different than when the reloading plastic strains were small (less than .1%). We observed no meaningful trend. At first glance, this behavior conflicts with our previous observation, based on creep data, that plastic strain pulses accelerate creep rates for a short interval at intermediate stresses.[7]

1.2.4. Creep-plasticity testing

The first results obtained from creep-plasticity interspersion tests are summarized in Fig. 1.12. As indicated, about 1.13 percent strain range was introduced in the first cycle. After the specimen had yielded in the second tensile loading, the specimen was placed under a creep condition. This occurred near a strain of minus 0.2 percent strain. The creep stress was held at 15,000 psi for 165 hours (approximately one week). This produced about 0.2 percent creep strain. A second plastic loop was then introduced. We observed a small strain aging peak, which is quite typical for these testing conditions, then the flow curve returned to a pattern which we expected for continuous cycling. These data suggest that the hardening influence of creep strains is about the same as plastic strains for these very specific conditions. This is in qualitative agreement with the results we obtained from tests which were reloaded after relaxation periods around 100 hours. The step load creep tests, on the other hand,

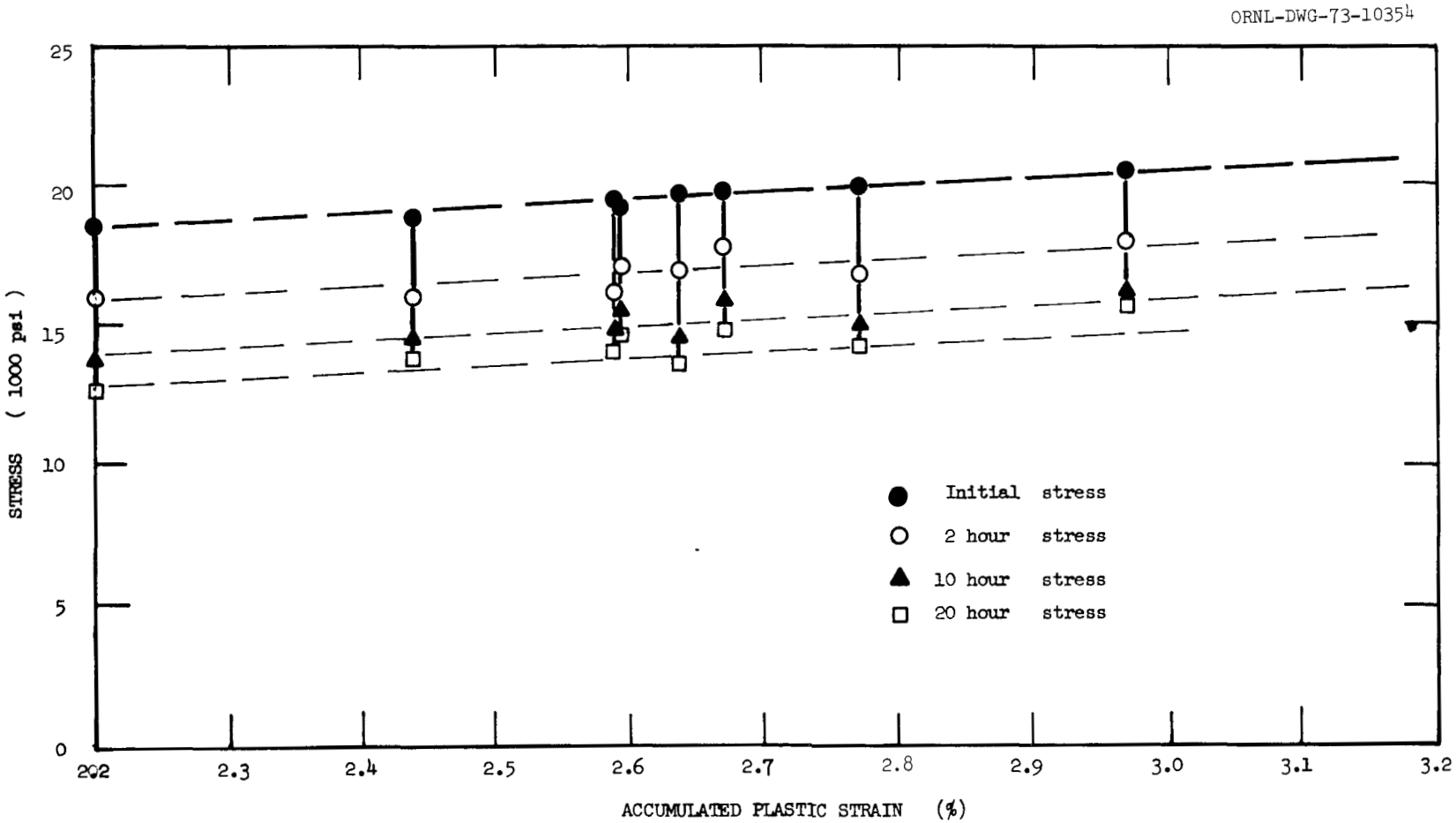

Fig. 1.11. The influence of repetitive loading into the plastic strain range on the relaxation strength of type 304 stainless steel at 1100°F (593°C), heat 9T2796 (1 in. plate, Item 7) reannealed for 1/2 hour at 2000°F (1093°C). Specimen 7RPT-8.

ORNL DWG 73-10355

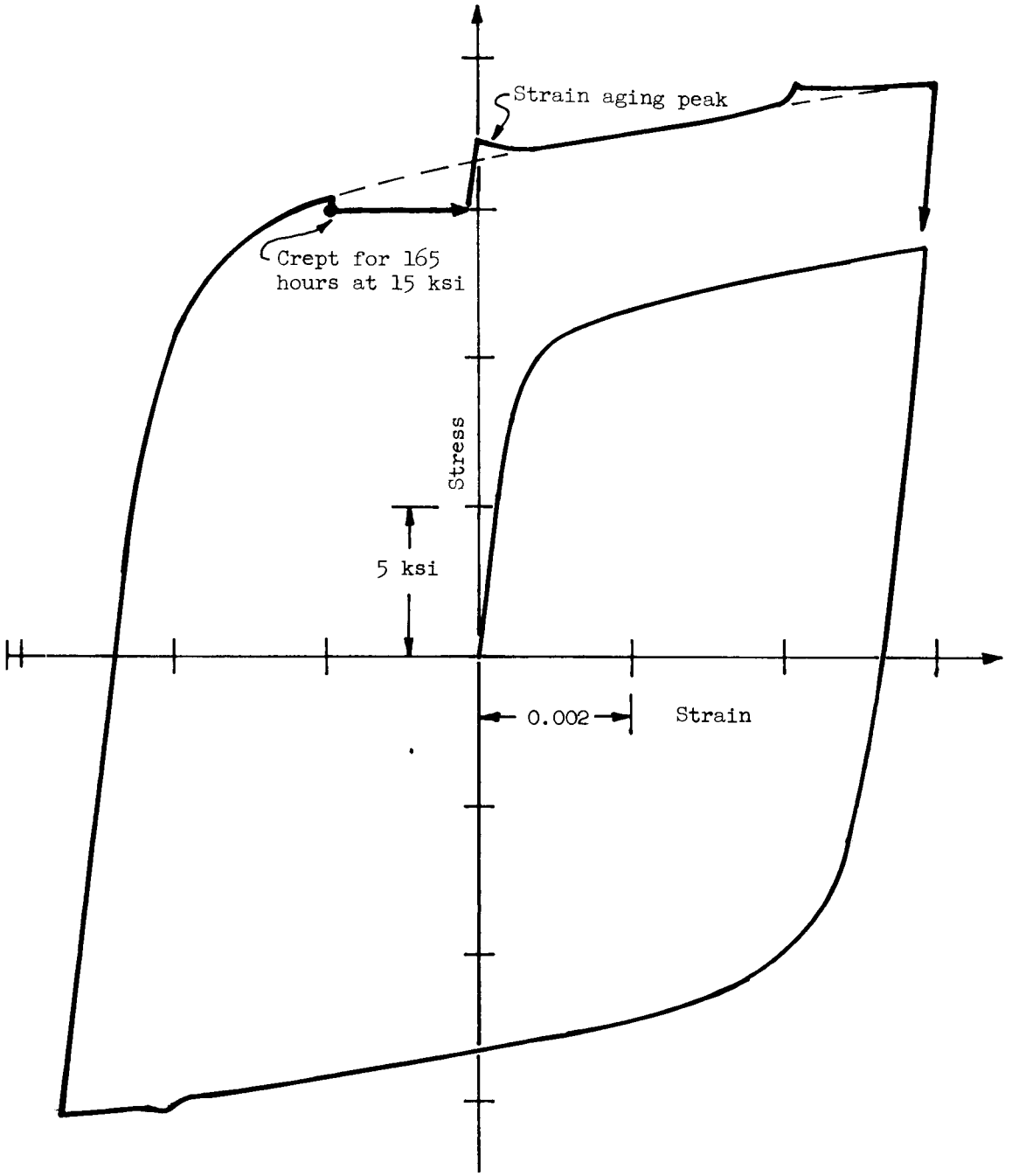

Fig. 1.12. Influence of a creep strain introduced in a strain cycle on the subsequent hardening curve for type 304 stainless steel. Heat 9T2796 plate (Item 7) reannealed for 1/2 hour at 2000°F. Specimen 7FRP68. Tested at 1100°F.

often showed the creep strains are more hardening than plastic. The creep strains were accumulated over longer testing times, however (three weeks).

2. CONSTITUTIVE EQUATION DEVELOPMENT

2.1. Elastic-Plastic Behavior

K. C. Liu

2.1.1. Experimental tests

Experimental elastic-plastic deformation and yield surface behavior studies at room temperature were continued as a part of a concerted effort to obtain key information on type 304 stainless steel behavior under general biaxial stress loadings within a relatively short period of time. The results obtained will form the basis for improved hardening law development. Two sets of programmed nonradial biaxial stress tests at room temperature were performed during this reporting period.

The tests are best described by referring to the diagram of Fig. 2.1. This diagram shows loading path directions which must be examined to permit meaningful characterization of subsequent loading response for a specimen that has been preloaded along a path such as $\overline{OP}$. The reasons are as follows.

Consider proportional, or radial, loading of a specimen from the virgin state at point O to the stress state at point P in the plastic region of the biaxial stress space shown in Fig. 2.1. The classical kinematic hardening theory assumes that the initial yield surface translates rigidly in the stress space as the stress point is moved along loading path No. 5 to point P. Any subsequent unloading from point P within the yield surface through that point will not alter the shape or position of the surface. The linear hardening hypothesis of the classical theory results in a flow rule, or an incremental stress-strain relation, which gives the same increment of plastic strain for a given increment of stress in the normal direction, regardless of the location of the stress point on the subsequent yield surface. Further, the motion of the surface is determined in all cases by a constant which relates the translation of the yield surface and the plastic strain. Consequently, any radial loading from the center, O', of the subsequent yield surface toward the outside, such as loadings along paths Nos. 1, 5, 6, 7, and 8, will yield stress-strain responses which do not depend upon direction with respect to the prestraining path $\overline{OP}$.

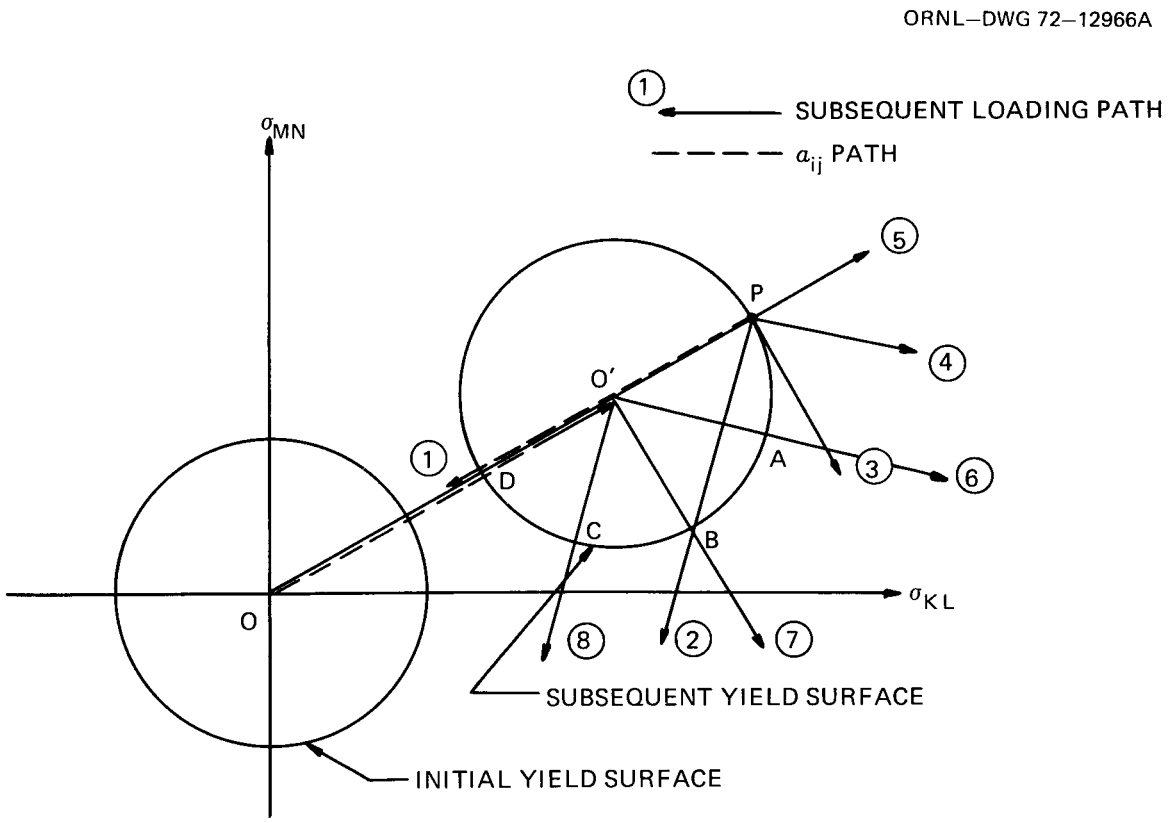

Fig. 2.1. Schematic of loading paths.

Directional invariance can be considered only as a first approximation. This is shown by the results of our previous tests[8] for cyclic loadings in biaxial stress space. Proportional loading from the origin in the direction of path No. 5 in Fig. 2.1 followed by completely reversed loading from point P along path No. 1 is a typical combined stress cyclic loading history. Results from this type loading show that the plastic strain rate at point P in the direction of path No. 5 is much higher for a given stress rate than the strain rate at point D in the direction of loading path No. 1 for the same stress rate. A continuous change in plastic strain rate for a given stress rate would be expected to occur with direction of loading between these two extremes when the loadings are radial with respect to the current surfaces. However, the plastic strain rate dependencies for radial paths through points along the yield locus other than points D, P, and B are virtually unknown. [The test results for loading path No. 7 (passing through B) were reported in the last progress report.[9]] Hence, plastic deformation behavior data corresponding to other directions are to be obtained by exploring loading paths Nos. 6 and 8, which were selected to give coverage at 45 deg intervals.

The first of the two room temperature tests was programmed to study yield surface behavior as well as stress-strain response along loading path No. 6. Details of the loading program used in this test are shown in Fig. 2.2. After an initial prestraining to point P, the specimen was partially unloaded and the subsequent yield surface was investigated. The dashed-line circle in the diagram indicates the configuration based on the classical kinematic hardening rule. The second major segment of the loading path was along a straight line running from near the center of the surface through the point P to the point Q. Again, a subsequent yield surface was investigated following partial unloading from point Q. Since the position of the subsequent yield surface determined from experiment and that calculated from theory were not the same, the third and fourth segments of the loading path were chosen to initiate from point T and from point U, respectively. These points were close to the centers of the experimentally determined subsequent yield surface configurations. In every case, the direction of the loading path was rotated 45 deg clockwise with respect to the immediate prior direction, as shown in Fig. 2.2. The test data obtained

ORNL-DWG-73-10356

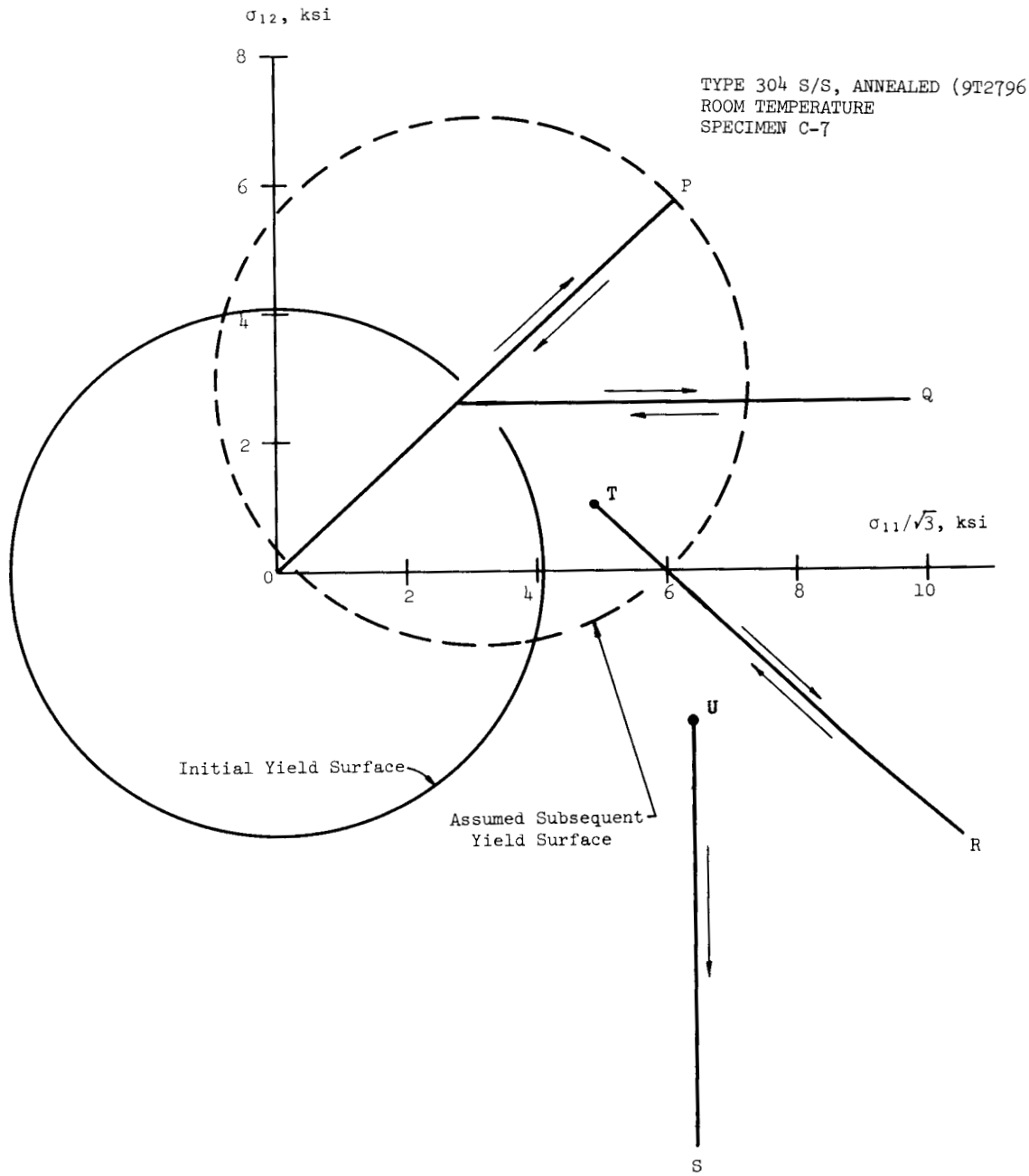

Fig. 2.2. Loading path diagram.

provide additional information on surface translation and change in shape as functions of plastic deformation history. Because of the complexities of the inelastic stress-strain responses, a significant amount of work remains in processing and digesting the information obtained.

In the last progress report we gave the results for nonradial biaxial stress tests[9] along paths corresponding to Nos. 3 and 7 in Fig. 2.1. The stress-strain responses obtained from these tests were also subjected to analytical studies, which were discussed in Section 4.1.2 (Ref. 10) in the last progress report. This study indicated discrepancies between the experimental data and results obtained from kinematic hardening theory. Therefore, the second of the two yield surface experiments carried out was programmed to investigate the stress-strain relation along loading path No. 4 (Fig. 2.1), which bisects the angle between paths No. 3 and No. 5, and to determine subsequent yield surfaces relative to this type of loading. Portions of the data taken along path No. 4 as well as along subsequent loading paths were not very satisfactory due to unstable instrument control. Therefore, detailed discussion of the test results must be deferred until data processing is completed.

In connection with high-temperature testing, we have initiated design, fabrication, and testing work on a high-temperature biaxial capacitive transducer which will give strain measuring precision at elevated temperature as required by our yield surface tests. This is an important project because the presently used extensometer devices for high-temperature tests do not measure strain directly from a specimen. Of course, the use of such devices is acceptable for investigations of yield surfaces, but greater accuracy is required for the necessarily detailed examinations of inelastic stress-strain responses associated with elastic-plastic deformation and with plasticity and creep deformation interactions at elevated temperatures. Therefore, the development of a new high-temperature extensometer which can provide direct measurement of biaxial strains at elevated temperature is required, and the preliminary design of such an extensometer is being prepared.

2.1.2. Theoretical studies

The study of bilinear cyclic stress-strain relations discussed in the last progress report[9] is continuing. In order to achieve a smooth transition from κ_0 to κ_1 for structural analysis use, a set of bilinear stress-strain relations, which were determined in accordance with the rule discussed in Ref. 10, was given in the last progress report and used in beam analyses. That particular set of curves (shown in Fig. 2.3) was constructed from the results of an ORNL cyclic test at 1100°F with a constant cyclic strain range of 0.6% strain, obtained by R. W. Swindeman. Two more bilinear stress-strain curves shown in Figs. 2.4a and 2.4c were constructed from later cyclic test data for 0.4% and 1% total strain range by the same method. It is seen that κ is a function of cyclic strain range and other variables.

In order to include hardening behaviors, as shown in Fig. 2.4, in inelastic structural analyses, an analytical expression for κ in terms of related variables that will give a single quasi continuous-type function has been actively sought. Because the elements of real structures are often subjected to a variety of time varying loading and temperature loadings in service applications the function derived must be applicable for any range of expected condition. An attempt to formulate a useful mathematical expression to represent the bilinear curves of Fig. 2.4 is described here.

Since suitable available data at the time of this study were limited to those obtained at room temperature and 1100°F, the temperature variable was not included in this first formulation. The expression given below was derived for 1100°F cyclic loadings.

$$\kappa = A(II_0^*)^{-B}\left[D \sum_{i=0}^{n} II_i^p/(II_0^*)^{3/2} + E\right]^{G(II_0^p)^{1/2}} \tag{2.1}$$

in which

$$II^p = \frac{1}{2}\,\varepsilon_{ij}^p\,\varepsilon_{ij}^p \tag{2.2}$$

ORNL-DWG-73-5961

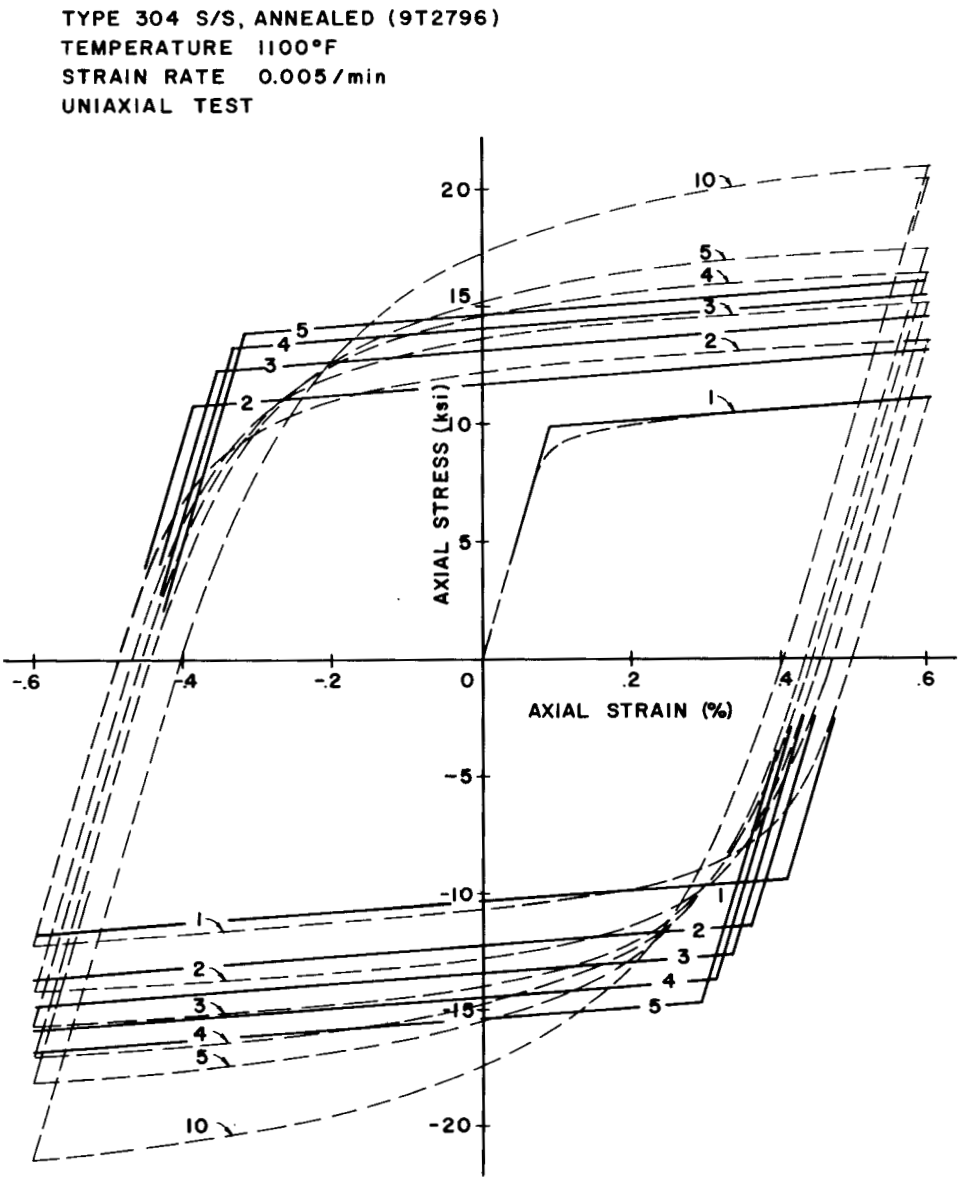

Fig. 2.3. Nonlinear and bilinear stress-strain relations.

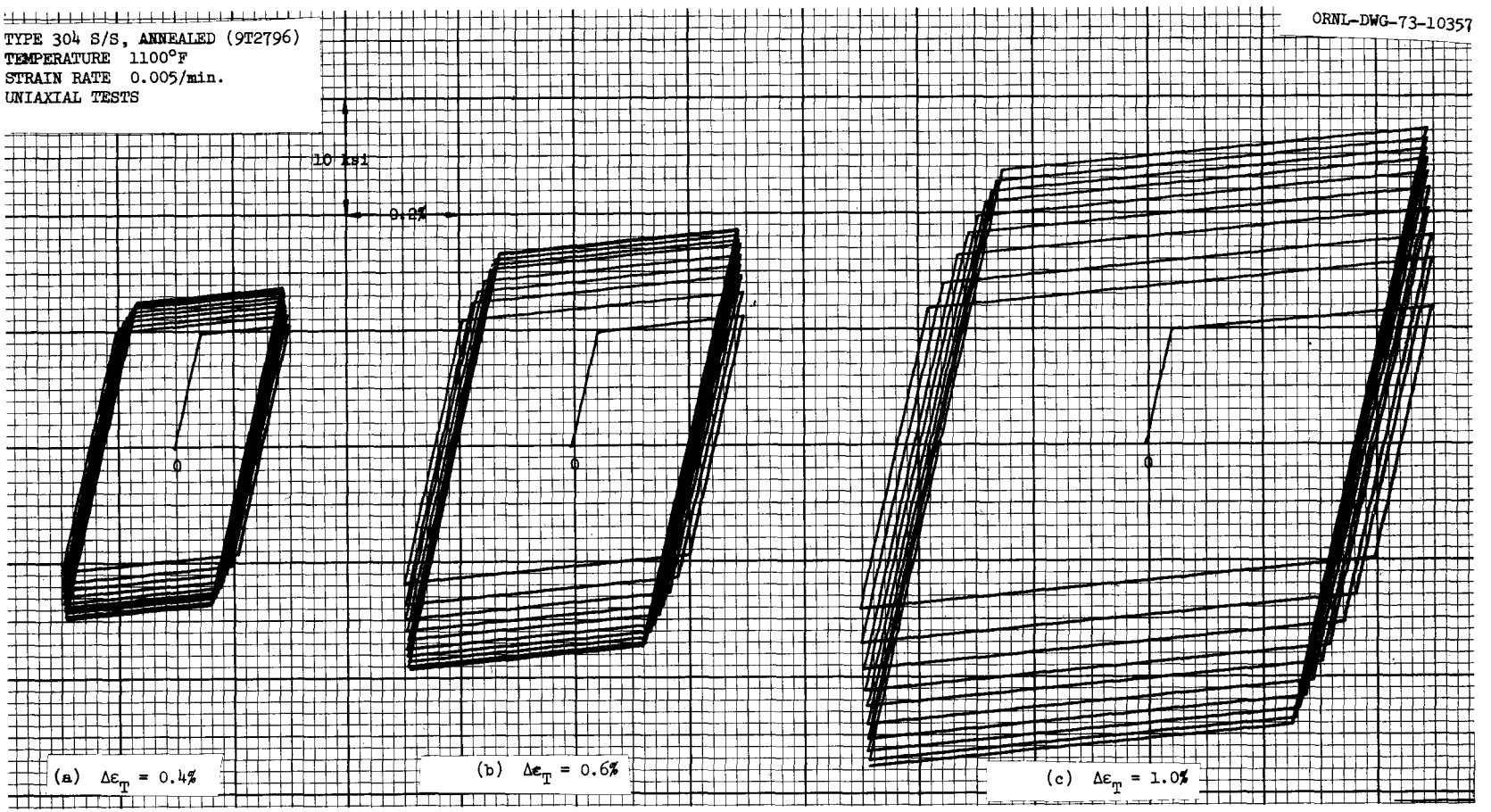

Fig. 2.4. Uniaxial bilinear stress-strain curves.

and other II's are defined analogously. Here, the subscripts "i" denotes the last previous point of loading reversal. All points of loading reversal are sequentially numbered, with i=0 being the virgin state. The terms A, B, D, E, and G are constants, while the other symbols are defined in Fig. 2.5.

Equation (2.1) is intended to represent cyclic hardening behavior of the material over three constant strain ranges from 0.4% to 1% strain. However, due to discrete changes of the reference variables in the cyclic loading process, as shown in Fig. 2.5, the equation is capable of representing salient features of random cyclic loading behavior as well as that of constant range cyclic loading. This is illustrated in Fig. 2.6 by a set of cyclic bilinear stress-strain curves calculated from Eq. (2.1). Significant reduction material hardening for decreases in plastic strain range during a test is a typical phenomenon for this type of cyclic loading test.

When κ takes the form of Eq. (2.1), the expression for function C which relates the tensor describing the translation of the yield surface, α_{ij}, and the plastic strain tensor, ε^p_{ij}, by

$$d\alpha_{ij} = C d\varepsilon^p_{ij} \tag{2.3}$$

is derived as follows for bilinear stress-strain representation.

$$C = S - \frac{1}{\sqrt{2\kappa}} \frac{d\kappa}{d\varepsilon^p_{ij}} \gamma_{ij} \tag{2.4}$$

where

$$\gamma_{ij} = \frac{1}{\sqrt{2\kappa}} (\sigma'_{ij} - \alpha_{ij}) \tag{2.5}$$

and

$$S = \gamma_{ij}\, d\sigma'_{ij} / \gamma_{k\ell}\, d\varepsilon^p_{k\ell} \ , \tag{2.6}$$

and σ'_{ij} is the deviatoric stress tensor.

The expression (2.1) is not a final form and is only for current use in performing analyses of simple structures, such as beams, being tested in other parts of this program. Development work associated with the derivation of a suitable general function form is being continued.

ORNL-DWG-73-10358

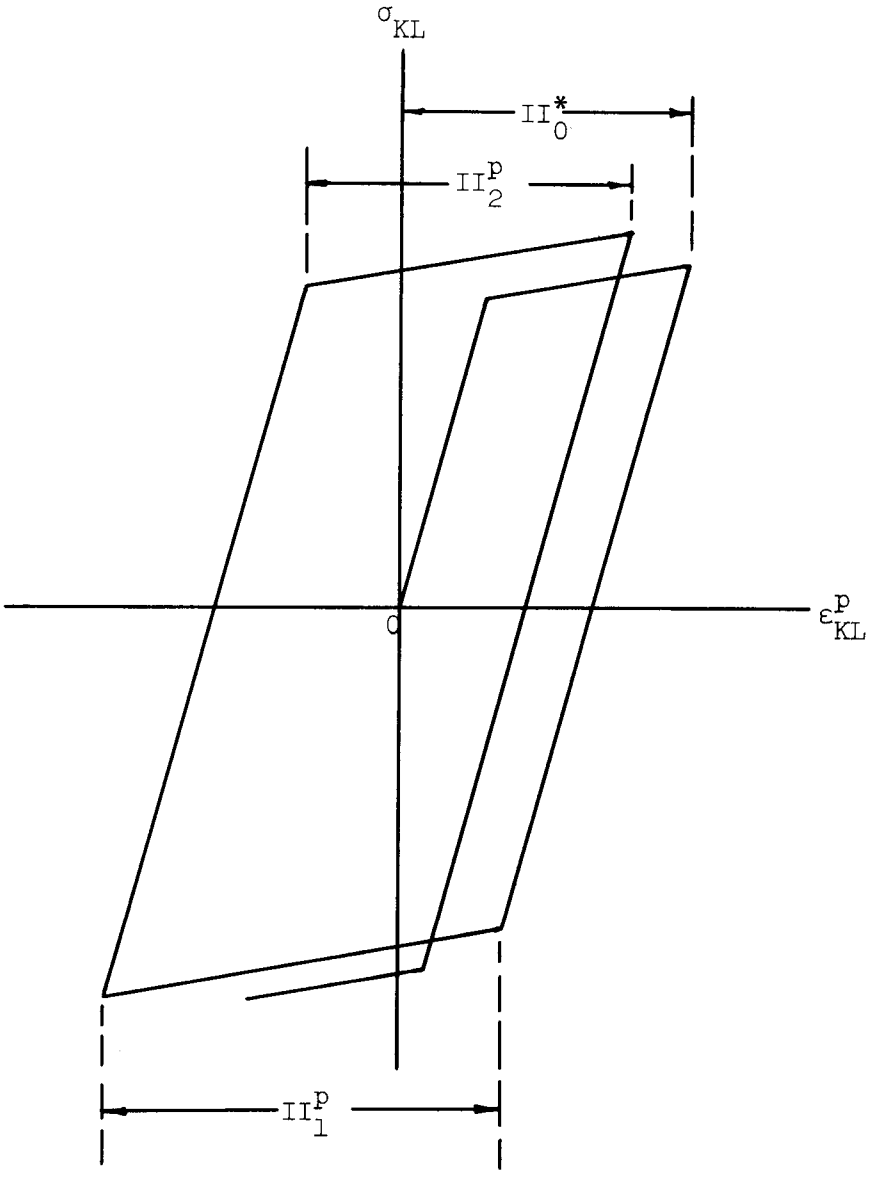

Fig. 2.5. Schematic of bilinear stress-strain curves.

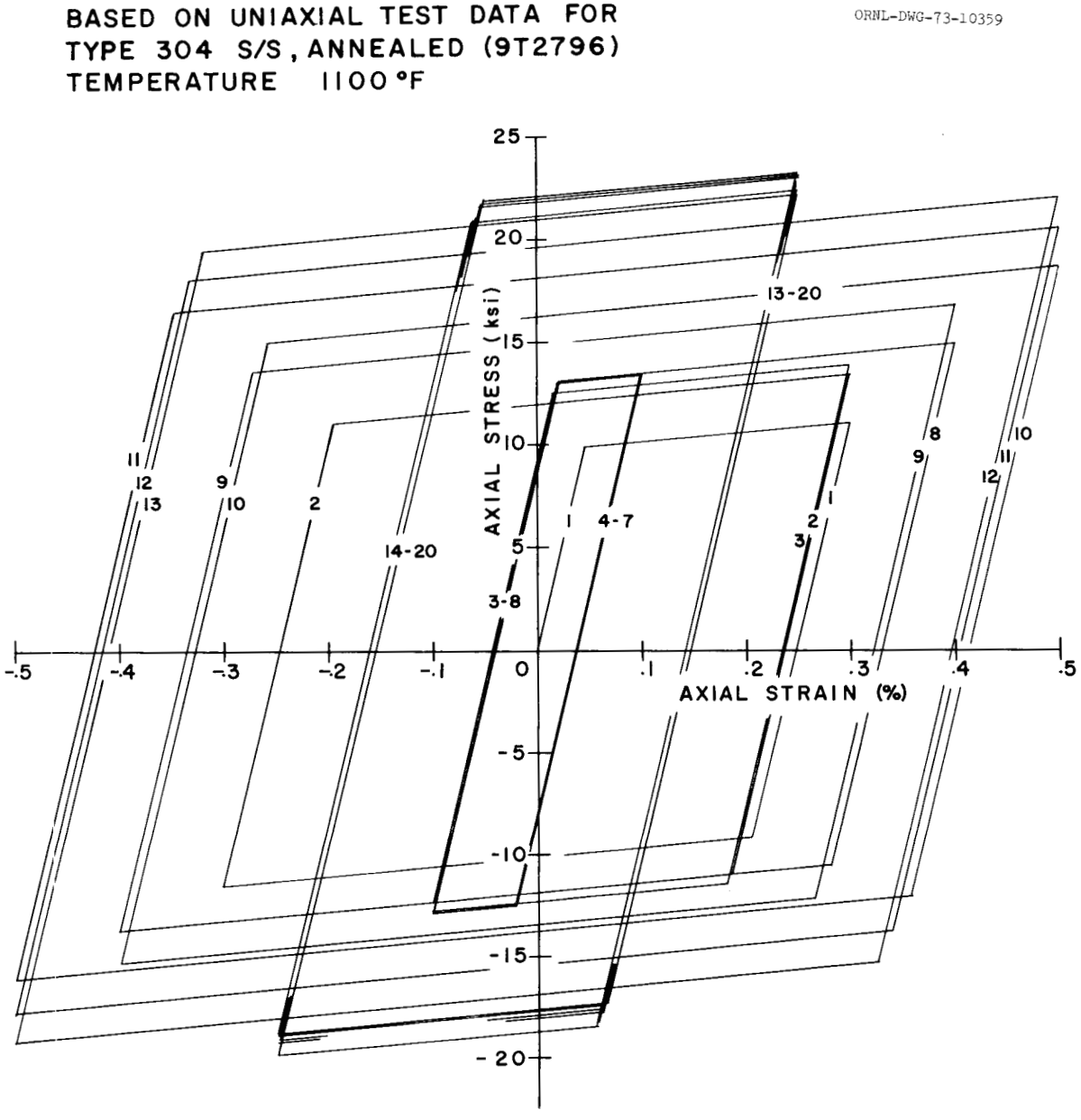

Fig. 2.6. Random cyclic stress-strain curves.

2.2. Time-Dependent Behavior

C. E. Pugh

2.2.1. Representation of nonlinear hereditary behavior of materials

The knowledge of thermomechanical behavior of structural materials and the mathematical representation of this knowledge are of fundamental importance in the analysis and design of LMFBR components. A final proposal has been received from Yale University to provide contributions to the development of applicable theories as a part of ORNL's overall efforts in this area. The principal investigator is Professor E. T. Onat, and an initiation of a subcontract in early FY-1974 is being sought.

Available experimental and theoretical knowledge will be reviewed, including constitutive equations that are being recommended and candidate equations for design use. The following questions will be examined: Are these constitutive equations capable of representing, with sufficient accuracy, the essential and significant features of the observed behavior? How can these equations be modified so that their accuracy is increased and their ability to represent significant features is enhanced? The examination of these questions will embrace the ideas in Ref. 11 and involve extensions to the work reported in Ref. 11 in the areas of multiaxial stressing, thermodynamic aspects, and microscopic studies. As the theoretical work progresses, test recommendations will be provided to ORNL on a continuing basis for possible incorporation into experimental activities of the overall program.

2.2.2. Multiaxial creep studies (Professor W. N. Findley, Brown University)

1. Test No. 7 using Specimen 4-304-16 was performed with the same stress ratio, σ/τ, as Test No. 2 but with a Mises stress of 15 ksi instead of the 15.170 ksi used in Test No. 2. The initial stresses were σ = 13,819 psi, τ = 3,369 psi and were held fixed for 1006.9 hours. The load was removed, and the creep strain recovery was recorded for 319.4 hr. The average temperature was 1117.2°F.

Results for this test are given in Figs. 2.7 through 2.10, and some limited comparisons with Test No. 2 are shown in Table 2.1. Comparisons with Test No. 2 (see Ref. 12) show that both the tension and torsional creep rates were significantly less in Test No. 7 than in Test No. 2. Initial and one-hour strain readings were larger in tension and smaller in torsion for Test No. 7 than Test No. 2. The direction of the strain rate vector for Test No. 7 (shown in Fig. 2.11 and 2.12) moved somewhat farther away from the Mises equivalent than Test No. 2. The creep rate at 120 hr in Test No. 7 was about 1/10 that in Test No. 2.

It appears from Fig. 2.12 that there is, for stress states on the Mises surface, a trend for the strain rate vector to decrease in magnitude as the stress state moves from pure torsion toward pure tension. This observation is in agreement with the direction of the strain rate vectors. Both suggest that the creep surface ellipse may have a somewhat shorter shear axis than the Mises ellipse.

After the stresses were removed in Test No. 7, the specimen exhibited an elastic response followed by a slight time-dependent recovery as shown in Figs. 2.8 and 2.10. The only known differences between Test No. 7 and Test No. 2 are the following: (a) the effective stress was slightly lower in Test No. 7 than in Test No. 2, and (b) the specimen in Test No. 2 was finished by machining, whereas the specimen in Test No. 7 was finished by honing the bore and grinding the outside diameter.

Circumferential strains observed during Test No. 7 are shown in Figs. 2.9 and 2.10. Strains during the early part of the test are not available due to a circuitry error, which also affected the zero reading. Thus the strains shown are approximations which were computed by selecting a zero reading which would yield the same ratio of axial to circumferential strain at 300 hr in Test No. 7 as observed in the pure tension creep test at 300 hr in Test No. 6.

2. Two additional specimens have been finished by honing and grinding, specimens Nos. 8 and 11, and two others have been finished by machining, specimens Nos. 7 and 10. The honed and ground specimens will be used for a series of creep tests at an effective stress of 10 ksi, while the two finished by machining will be used for a pure torsion and a pure tension creep test at 15 ksi effective stress.

Table 2.1. Comparison of results from tests Nos. 2 and 7, type 304 stainless steel specimens

	Test 2	Test 7
Stress state (σ,τ) (psi)	(13975,3407)	(13819,3369)
Effective stress (psi)	15,170	15,000
ε_{11}, axial strains (%)		
Initial	0.6248 (50 secs)	0.8254 (50 secs)
1 hour	0.8786	0.9669
120 hours	2.9140	1.4206
ε_{12}, shear strains (%)		
Initial	0.3381 (42 secs)	0.2964 (30 secs)
1 hour	0.4332	0.3512
120 hours	1.1730	0.5454
Strain rates at 120 hr (%/hr)		
$\dot{\varepsilon}_{11}$, axial	0.0167	0.0015
$\dot{\varepsilon}_{12}$, shear	0.0051	0.0007
$\dot{\bar{\varepsilon}}$, effective	0.0126	0.0013

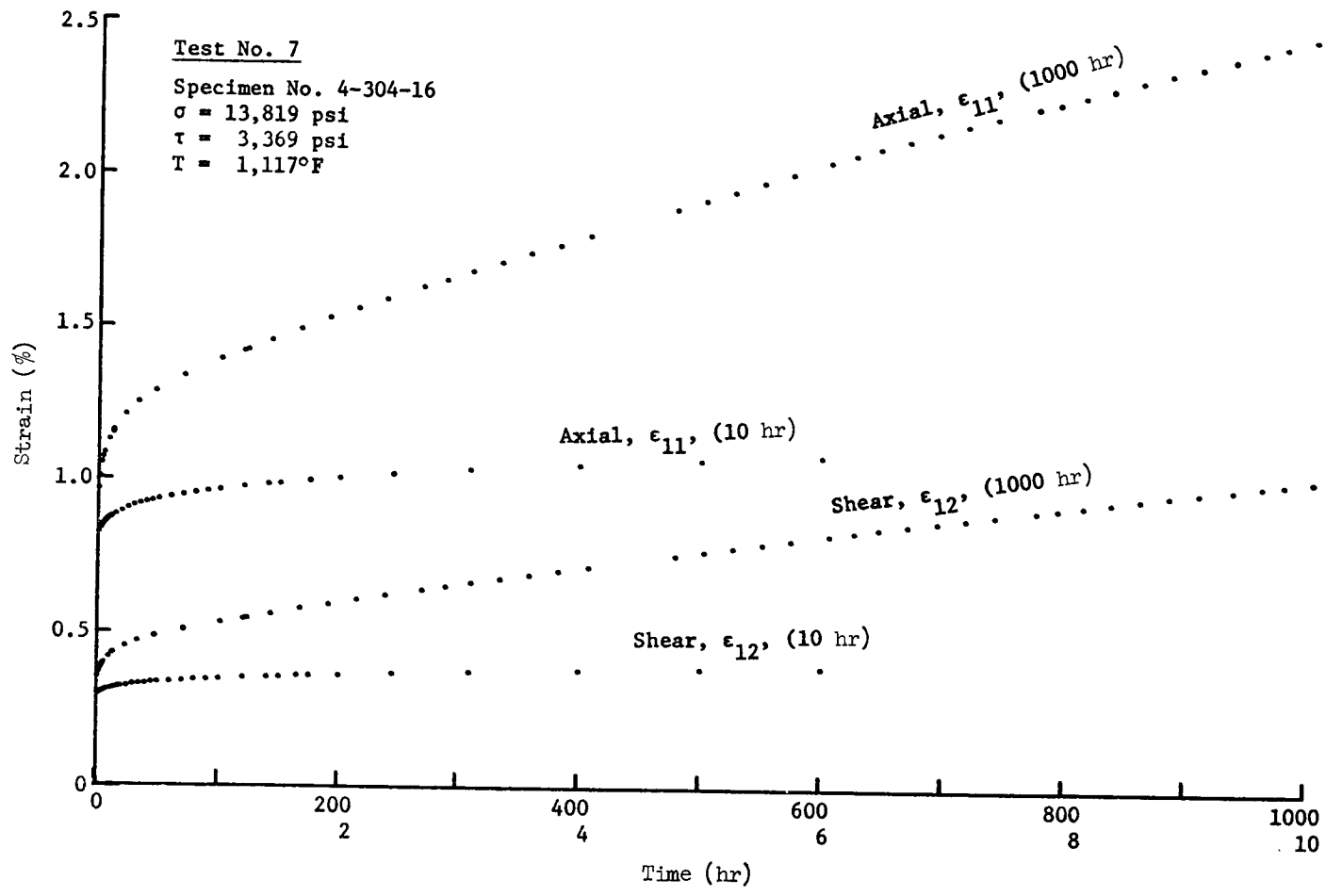

Fig. 2.7. Short-time and long-time creep strains versus time for test No. 7 conducted with the same stress-ratio as test No. 2. Type 304 stainless steel (heat 9T2796) specimen from nominal 2-in. bar stock.

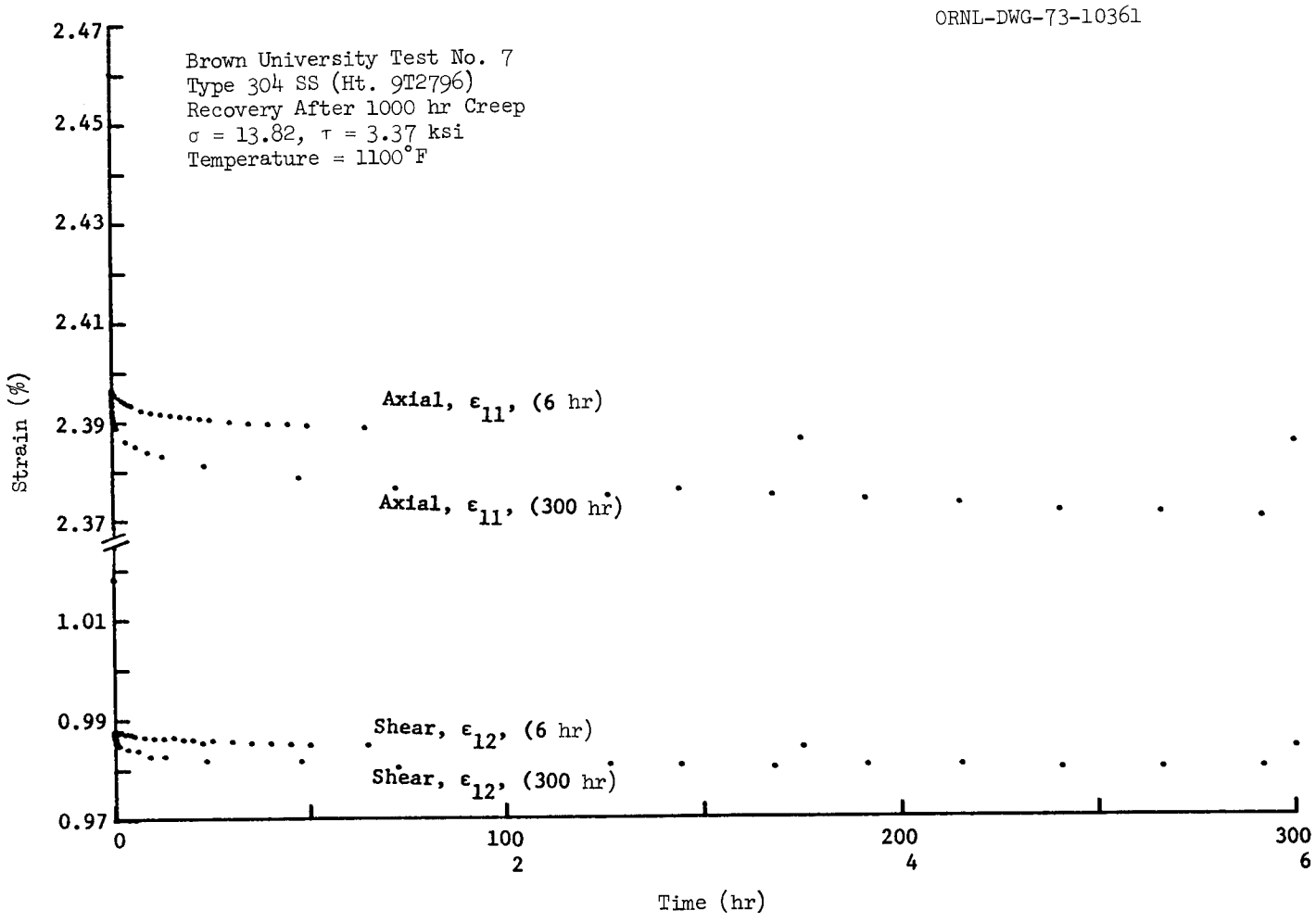

Fig. 2.8. Creep strains versus time during unloaded, or recovery, interval following 1007 hours of creep at constant load, test No. 7. Type 304 stainless steel (heat 9T2796) specimen from nominal 2-in. bar stock.

ORNL-DWG-73-10362

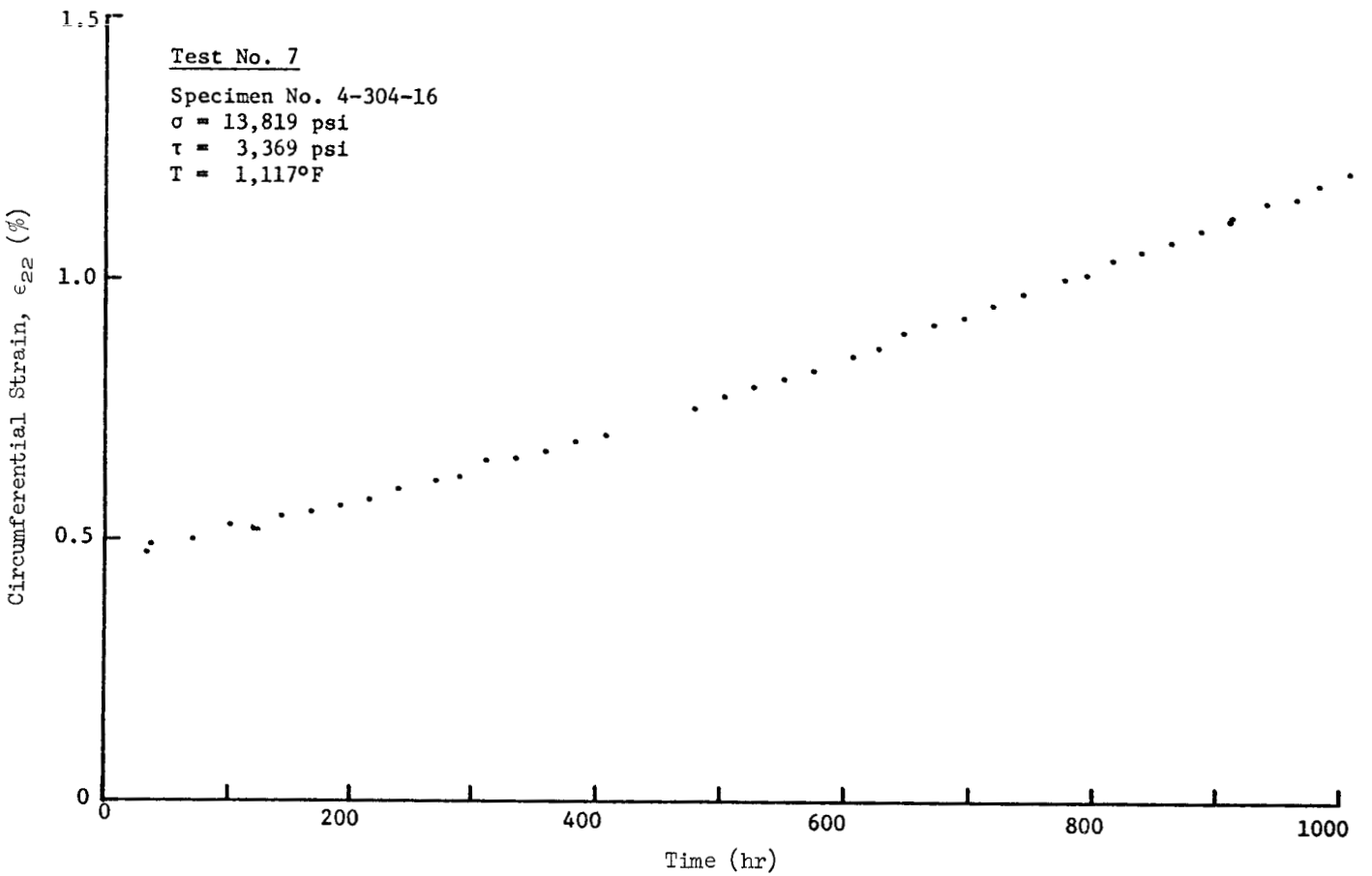

Fig. 2.9. Circumferential strain versus time during sustained loading portion of test No. 7. Type 304 stainless steel (heat 9T2796) specimen from nominal 2-in. bar stock.

ORNL-DWG-73-10363

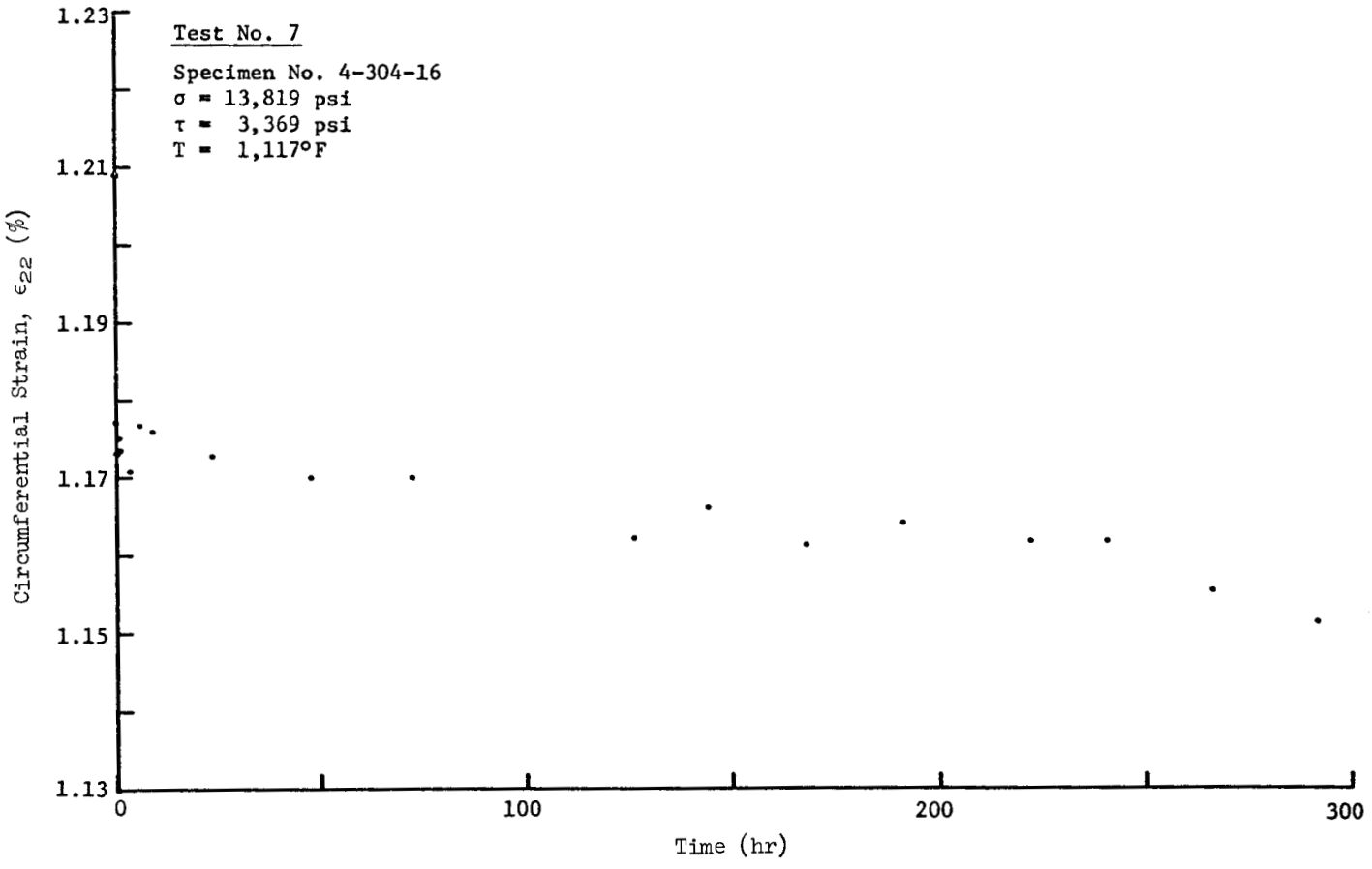

Fig. 2.10. Circumferential strain versus time during unloaded, or recovery, interval of test No. 7. Type 304 stainless steel (heat 9T2796) specimen from nominal 2-in. bar stock.

ORNL-DWG-73-10364

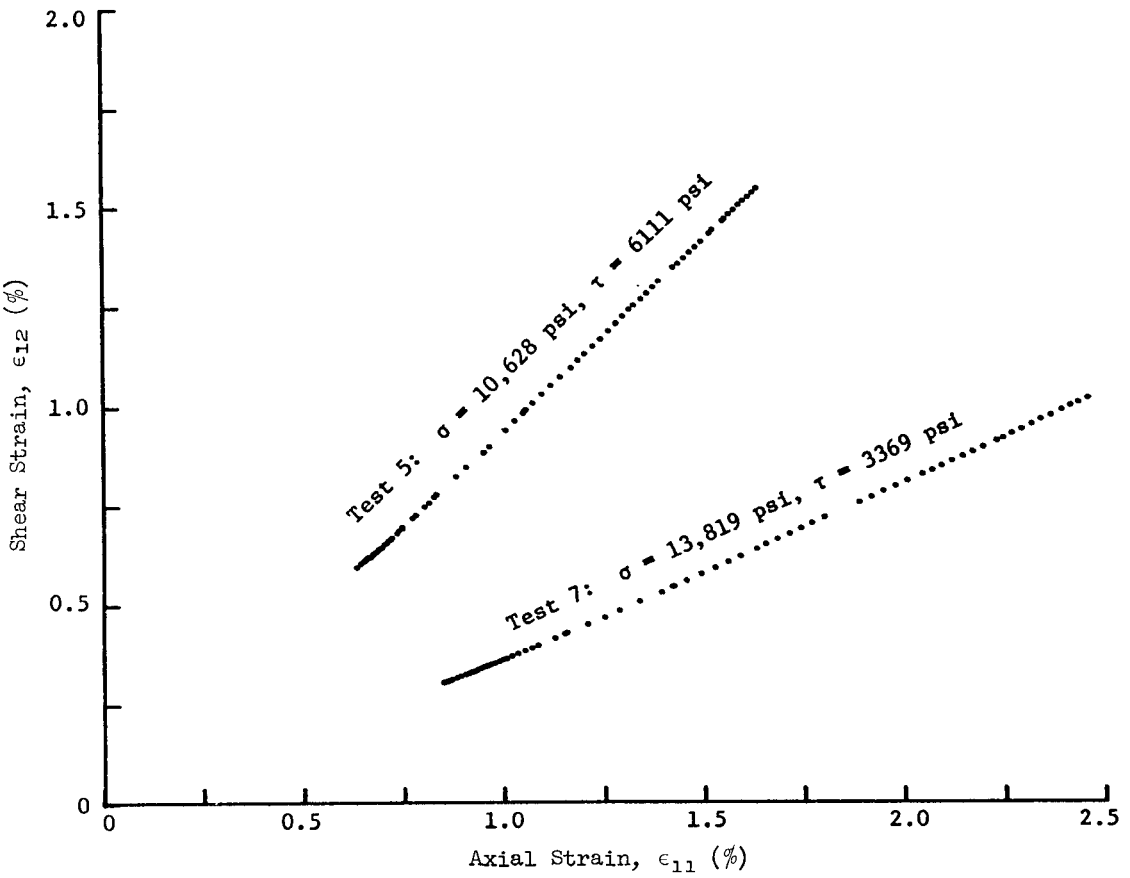

Fig. 2.11. Shear strain-axial strain trajectories for tests Nos. 5 and 7. Type 304 stainless steel (heat 9T2796) specimen from nominal 2-in. bar stock.

ORNL-DWG-73-10365

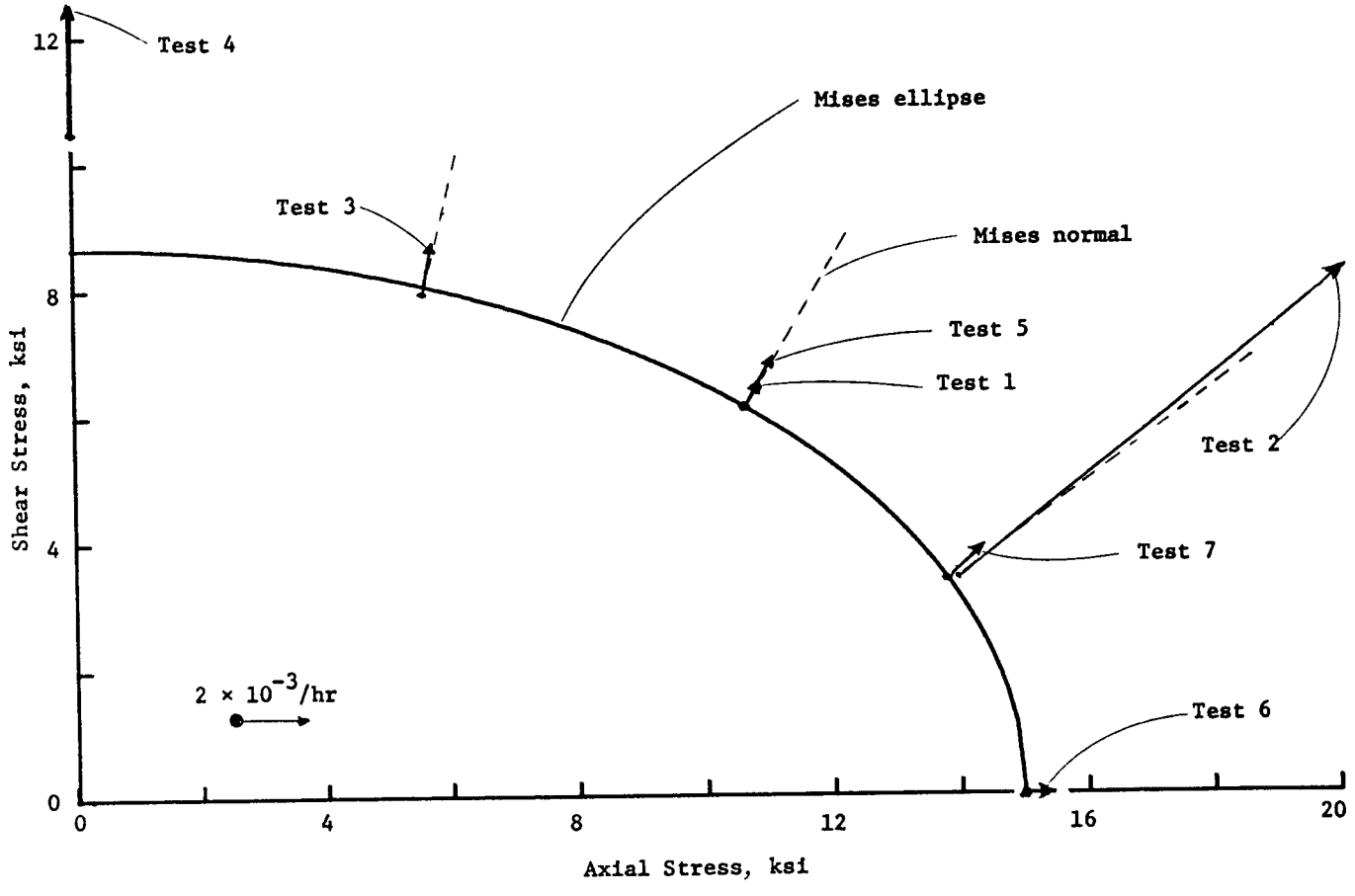

Fig. 2.12. Effective strain rate vectors in tension-torsion stress space at 120 hours and 1100°F for tests Nos. 1 through 7. Type 304 stainless steel (heat 9T2796) specimens from nominal 2-in. bar stock.

3. Specimen No. 11, Test No. 8, is ready for test in pure torsion at a stress of 5,772 psi and a temperature of 1100°F. This is an effective stress of 10 ksi.
4. Specimen No. 8, Test No. 9, is ready for test in pure tension at a stress of 10,000 psi and a temperature of 1100°F.
5. Six additional high temperature lamps have been received.
6. The possibility of shortening the compression specimen system to minimize the chance of buckling is being explored. A short (8-13/16 in.) heating lamp was obtained. This was mounted in an old specimen with suitable end fittings, end heaters, thermocouples and heat reflector and a test was made to determine whether it would be possible to use this lamp in tests at 1100°F. Results indicate that the lamp has sufficient wattage. So this method appears possible. Some preparations have been made toward performing a compression load test at temperature to determine whether buckling is likely at stresses up to 15 ksi.

3. FAILURE STUDIES

3.1. Study of the Effect of Biaxiality in Creep-Fatigue at Elevated Temperatures

Professor S. Y. Zamrik
Pennsylvania State University

3.1.1. Fatigue tests

Biaxial strains are imposed on type 304 stainless steel tubular specimens as a result of simultaneous push-pull and torsional loadings. Biaxial tests were conducted at 1200°F, 1000°F, and room temperatures. The loading system is sinusoidal at a frequency of 25 cpm.

3.1.2. Experimental results

Twenty-one biaxial specimens have been tested at 1200°F and six at 1000°F. The biaxial strain ratio of torsional shear strain range, $\Delta\gamma_{x\theta}$, to axial strain range, $\Delta\varepsilon_x$, varied from 1/2 to 5. Experimental data are presented in Table 3.1, which also shows the applied biaxial strain range in terms of maximum principal strain range, $\Delta\varepsilon_1$, effective strain range, $\Delta\bar{\varepsilon}_e$, and octahedral shear strain range, $\Delta\gamma_{oct}$. The three are interrelated in the form of:

$$\Delta\gamma_{oct} = \sqrt{2}\,\Delta\bar{\varepsilon}_e \tag{3.1}$$

$$\Delta\bar{\varepsilon}_e = \frac{2}{\sqrt{3}}\,\Delta\varepsilon_1\,\sqrt{1 + \phi + \phi^2} \tag{3.2}$$

or

$$\Delta\bar{\varepsilon}_e = \frac{2}{\sqrt{3}}\left[\frac{\Delta\varepsilon_1}{0.5 + \sqrt{2.25 + R^2}}\right][3 + R^2]^{1/2} \tag{3.3}$$

where $\phi = \Delta\varepsilon_2/\Delta\varepsilon_1$ and $R = \Delta\gamma_{x\theta}/\Delta\varepsilon_x$.

In deriving the preceeding equations, it is assumed that the volume remains constant and Poisson's ratio is 1/2. As a result of this assumption, the data can be presented in terms of any of these three measures since they deviate by a constant. This can be observed in examining Table 3.2

Table 3.1. Biaxial fatigue test results for 304 stainless steel (heat 9T2796)

Specimen No.	Axial Strain Range $\Delta\varepsilon_x$ (%)	Torsional Shear Strain Range $\Delta\gamma_{x\theta}$ (%)	$\frac{\Delta\gamma_{x\theta}}{\Delta\varepsilon_x}$ (R)	Temp. (°F)	Principal Strain Ranges $\Delta\varepsilon_1$ (%)	$\Delta\varepsilon_2$ (%)	$\Delta\varepsilon_3$ (%)	Total Strain Range $\Delta\varepsilon_T$ (%)	Effective Strain Range $\Delta\varepsilon_e$ (%)	Octahedral Shear Strain Range $\Delta\gamma_{oct}$ (%)	# of Cycles To Failure (N)
G 14	2.00	1.00	0.5	Room	2.08	-1.08	-1.00	2.55	2.08	2.94	1075
G 17	1.50	0.75	0.5	Room	1.56	-0.81	-0.75	1.91	1.56	2.21	1700
G 18	0.50	0.25	0.5	Room	0.52	-0.27	-0.25	0.64	0.52	0.74	11550
G 15	2.00	2.00	1.0	Room	2.30	-1.30	-1.00	2.82	2.30	3.26	1160
G 20	0.80	0.80	1.0	Room	0.921	-0.521	-0.40	1.13	0.92	1.30	4100
H 1	1.00	2.00	2.0	Room	1.50	-1.00	-0.50	1.87	1.53	2.16	2780
H 2	0.75	1.50	2.0	Room	1.125	-0.75	-0.375	1.40	1.14	1.62	4300
H 3	0.60	1.20	2.0	Room	0.90	-0.60	-0.30	1.12	0.91	1.30	6000
H 4	0.50	1.00	2.0	Room	0.75	-0.50	-0.25	0.94	0.77	1.08	6900
G 16	1.00	5.00	5.0	Room	2.86	-2.36	-0.50	3.74	3.05	4.32	1100
H 6	0.50	0.25	0.5	1200	0.52	-0.27	-0.25	0.64	0.52	0.74	2452
H 7	1.50	0.75	0.5	1200	1.56	-0.81	-0.75	1.91	1.56	2.21	150
I 6	0.80	0.40	0.5	1200	0.832	-0.432	-0.40	1.02	0.83	1.17	164
H 18	1.20	0.60	0.5	1200	1.248	-0.648	-0.60	1.53	1.25	1.77	110
H 16	0.60	0.30	0.5	1200	0.62	-0.32	-0.30	1.12	0.62	0.88	1074
I 3	0.72	0.72	1.0	1200	0.83	-0.47	-0.36	1.02	0.83	1.18	100
I 2	0.60	0.60	1.0	1200	0.69	-0.39	-0.30	0.847	0.69	0.98	700
I 4	0.90	0.90	1.0	1200	1.04	-0.59	-0.45	1.133	1.04	1.47	152
I 5	0.40	0.40	1.0	1200	0.46	-0.26	-0.20	0.565	0.46	0.65	1121
I 15	0.40	0.40	1.0	1200	0.46	-0.26	-0.20	0.565	0.46	0.65	2390
I 16	0.70	0.70	1.0	1200	0.81	-0.46	-0.35	0.995	0.81	1.15	865
H 8	0.60	1.20	2.0	1200	0.90	-0.60	-0.30	1.12	0.91	1.30	693
H 9	0.75	1.50	2.0	1200	1.125	-0.75	-0.375	1.40	1.14	1.63	400
H 11	0.50	1.00	2.0	1200	0.75	-0.50	-0.25	0.94	0.77	1.08	830
H 13	0.30	0.60	2.0	1200	0.45	-0.30	-0.15	0.56	0.46	0.65	4045
H 14	0.40	0.80	2.0	1200	0.60	-0.40	-0.20	0.75	0.61	0.86	2612
H 15	0.60	1.20	2.0	1200	0.90	-0.60	-0.30	1.12	0.91	1.30	800
H 19	0.28	0.56	2.0	1200	0.42	-0.28	-0.14	0.52	0.43	0.60	7800
H 17	0.25	0.50	2.0	1200	0.375	-0.25	-0.125	0.47	0.39	0.55	12800
I 7	0.2	1.00	5.0	1200	0.572	-0.472	-0.10	0.748	0.61	0.86	6200
I 8	0.6	3.00	5.0	1200	1.716	-1.416	-0.30	2.24	1.83	2.59	215
I 13	1.2	0.60	0.5	1000	1.248	-0.648	-0.60	1.529	1.248	1.764	1187
I 14	1.6	0.80	0.5	1000	1.664	-0.864	-0.80	2.039	1.664	2.353	680
I 9	0.8	0.80	1.0	1000	0.921	-0.521	-0.40	1.131	0.923	1.31	1698
I 10	0.6	0.60	1.0	1000	0.691	-0.391	-0.30	0.848	0.692	0.978	3178
I 11	1.2	1.20	1.0	1000	1.381	-0.781	-0.60	1.697	1.385	1.958	835
I 12	1.0	1.00	1.0	1000	1.151	-0.651	-0.50	1.414	1.154	1.632	955

Table 3.2. Strain range measures expressed in terms of the maximum principal strain range for various strain ratios

$R = \frac{\Delta\gamma_{x\theta}}{\Delta\varepsilon_x}$	$\phi = \frac{\Delta\varepsilon_2}{\Delta\varepsilon_1}$	Effective strain range $\Delta\bar{\varepsilon}_e$	Total strain range $\Delta\varepsilon_T$ [a]	Octahedral shear strain range $\Delta\gamma_{oct}$
0 (uniaxial)	−0.500	1.0000 $\Delta\varepsilon_1$	1.2247 $\Delta\varepsilon_1$	1.4142 $\Delta\varepsilon_1$
0.5	−0.5194	1.0002 $\Delta\varepsilon_1$	1.2251 $\Delta\varepsilon_1$	1.4145 $\Delta\varepsilon_1$
1.0	−0.5657	1.0028 $\Delta\varepsilon_1$	1.2283 $\Delta\varepsilon_1$	1.4182 $\Delta\varepsilon_1$
2	−0.6666	1.0181 $\Delta\varepsilon_1$	1.2469 $\Delta\varepsilon_1$	1.4399 $\Delta\varepsilon_1$
3	−0.74053	1.0378 $\Delta\varepsilon_1$	1.2710 $\Delta\varepsilon_1$	1.4677 $\Delta\varepsilon_1$
4	−0.7904	1.0547 $\Delta\varepsilon_1$	1.2917 $\Delta\varepsilon_1$	1.4916 $\Delta\varepsilon_1$
5	−0.8252	1.0681 $\Delta\varepsilon_1$	1.3082 $\Delta\varepsilon_1$	1.5105 $\Delta\varepsilon_1$
6	−0.8504	1.0787 $\Delta\varepsilon_1$	1.3211 $\Delta\varepsilon_1$	1.5255 $\Delta\varepsilon_1$
7	−0.8694	1.0871 $\Delta\varepsilon_1$	1.3314 $\Delta\varepsilon_1$	1.5374 $\Delta\varepsilon_1$
8	−0.8842	1.0940 $\Delta\varepsilon_1$	1.3399 $\Delta\varepsilon_1$	1.5471 $\Delta\varepsilon_1$
9	−0.8961	1.0996 $\Delta\varepsilon_1$	1.3467 $\Delta\varepsilon_1$	1.5550 $\Delta\varepsilon_1$
10	−0.9057	1.1043 $\Delta\varepsilon_1$	1.3525 $\Delta\varepsilon_1$	1.5617 $\Delta\varepsilon_1$
∞ (pure torsion)	−1.0000	1.1547 $\Delta\varepsilon_1$	1.4142 $\Delta\varepsilon_1$	1.6330 $\Delta\varepsilon_1$

[a] $\Delta\varepsilon_T = \sqrt{2}\,\Delta\varepsilon_1[1 + \phi + \phi^2]^{1/2}$

where, for example, the deviation of $\Delta\bar{\varepsilon}_e$ from $\Delta\varepsilon_1$ for R = 0 to R = 4 is negligible.

To simplify the evaluation of data obtained thus far for room, 1000°F, and 1200°F temperatures under axial, torsional and biaxial tests, the octahedral shear strain theory will be used as a reference. Thus, the converted data of all tests are shown in Figs. 3.1 through 3.3.

In Fig. 3.1, the upper bound for the room temperature data is represented by the pure torsional data and the lower bound by the axial data. The biaxial data varies between the two bounds, for example, the biaxial test data for a strain ratio of 0.5, low shear strain component, fall near the axial data, and data approach the upper bound of pure torsional data as the shear strain increases. The lower bound can be considered as a conservative design base line if the classical octahedral shear strain theory is used as an interpretative method to biaxial room temperature data. It is related to the number of cycles to failure in a power law relationship in the form of:

$$\Delta\gamma_{oct} \, N^{\alpha} = C \tag{3.4}$$

However, this approach is not valid if one examines Fig. 3.2 where the temperature is 1200°F. The data do not follow the room temperature observation despite the fact that an upper bound is still the torsional data. The 1200°F environment shows a considerable detrimental factor on the life of the material under biaxial loading, since the biaxial test data fall below the axial data (a lower bound at room temperature). The most critical scatter and deterioration in life takes place at $N \leq 10^3$ cycles. This behavior is not noticeable in the 1000°F data shown in Fig. 3.3. The life at 1000°F was reduced by a factor of 4 while at 1200°F by a factor of 10. It is suspected that at 1200°F, a drastic drop in the mechanical properties of type 304 stainless steel takes place.

It is also observed that two life regions have developed at 1200°F with 10^3 cycles as a transition mode. Although no definite explanation can be forwarded for this transition at this time, attention should be drawn to the left side region where to some extent the slope of the line is the same as that drawn for room and 1000°F data lines. Also the reduction in life is severe when compared to room temperature. To check

ORNL-DWG-73-10366

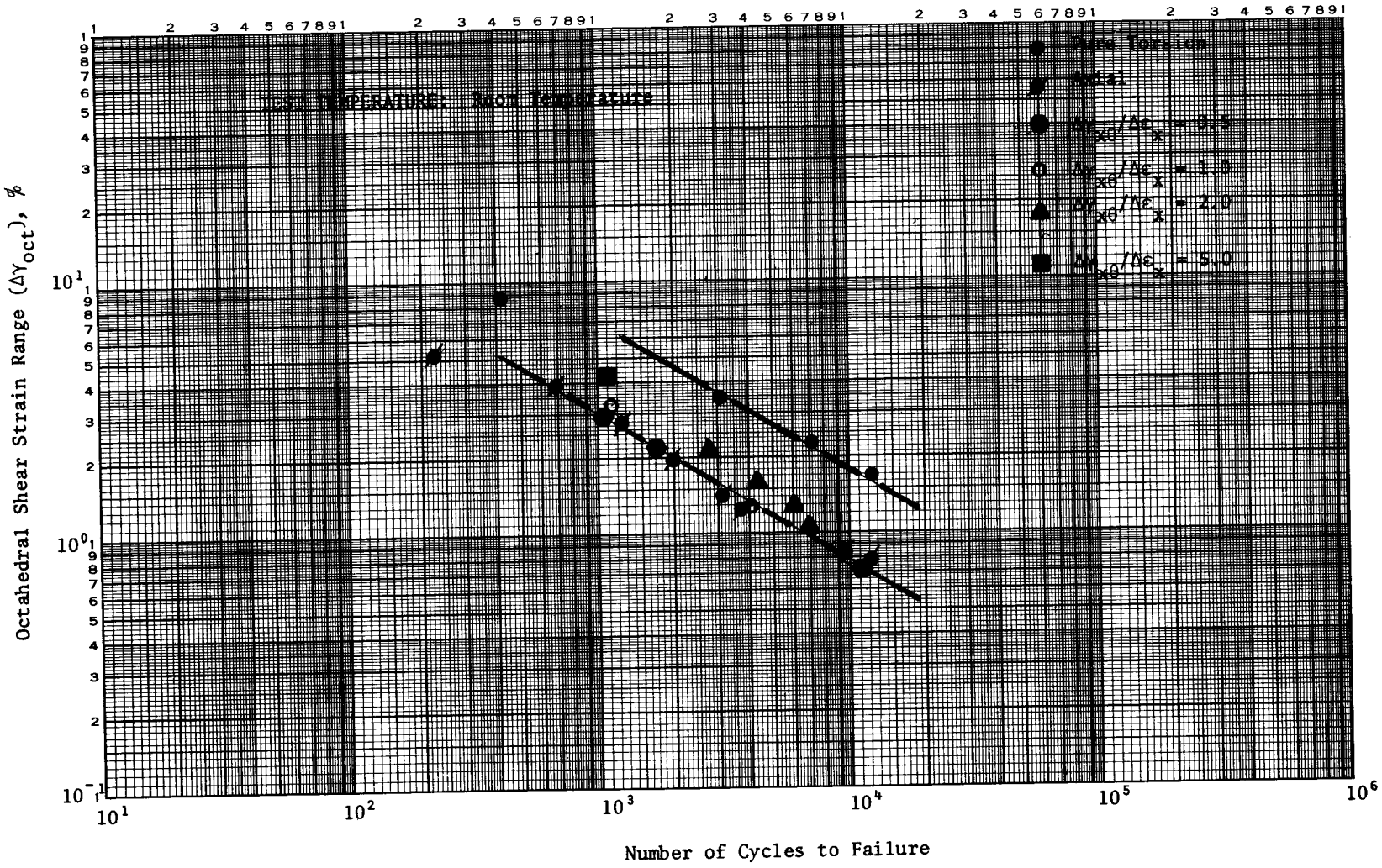

Fig. 3.1. Comparison of axial to biaxial fatigue data from room temperature tests. Type 304 stainless steel (heat 9T2796).

ORNL-DWG-73-10367

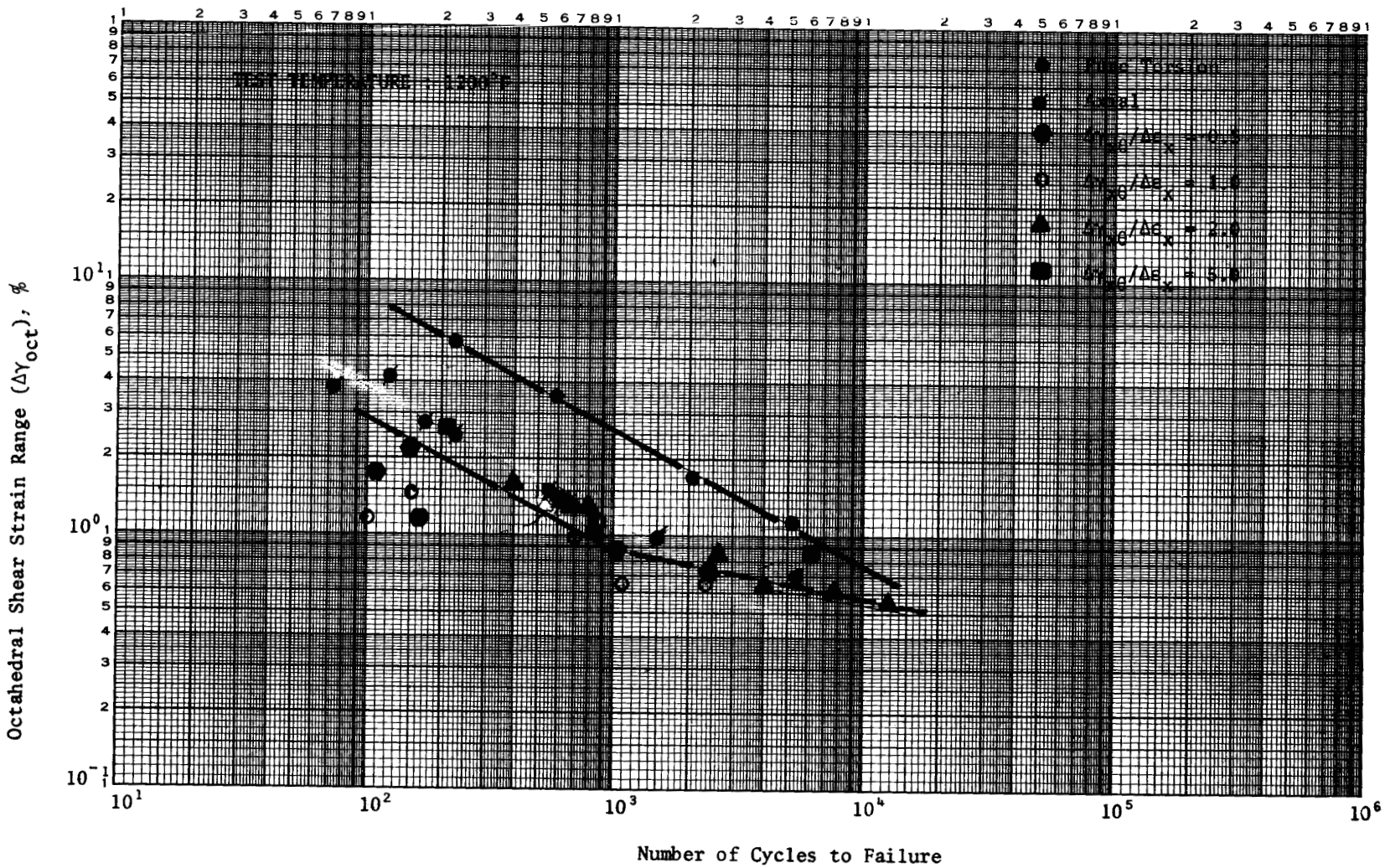

Fig. 3.2. Comparison of axial to biaxial fatigue data from 1200°F tests. Type 304 stainless steel (heat 9T2796).

ORNL-DWG-73-10368

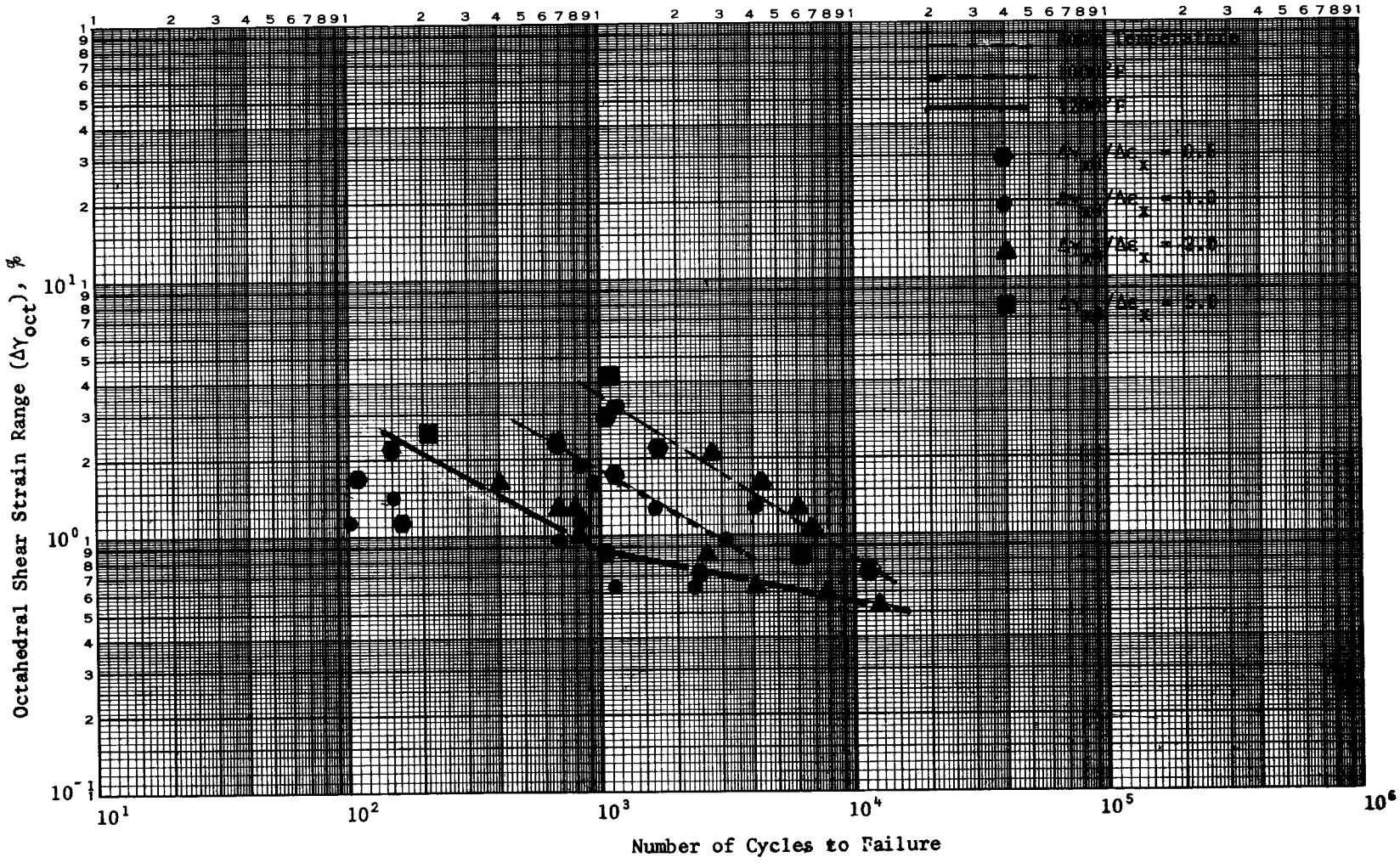

Fig. 3.3. Temperature effect on biaxial fatigue tests. Type 304 stainless steel (heat 9T2796).

this observed transition region and to determine the effect of temperature range on the mechanical properties of the material tested in biaxial fatigue, monotonic tension tests at 1000°F, 1100°F, and 1200°F are in progress.

The specimen chart shown in Table 3.3 identifies each test specimen taken from bar No. 35 of the ORNL reference heat (9T2796) of type 304 stainless steel, along with specimen dimensions.

3.2. Investigations of Creep Failure Under Uniaxial and Multiaxial Conditions

C. C. Schultz
Babcock and Wilcox

The status as of June 30 of the constant load, step load, and interrupted uniaxial tests are shown in Tables 3.4, 3.5, and 3.6, respectively.

The first three specimens for the interrupted uniaxial tests (19.5 ksi) have been loaded. These tests are identified as BWI-1, BWI-2, and BWI-3. The progress of these tests is shown in Fig. 3.4. Tests BWI-1 and BWI-3 both experienced unexplained steps between the final load increment and the initial creep data point (time, 2 hours). The data as shown in Fig. 3.4, have been adjusted so that the creep strain at a time of 2 hours is zero.

The initial tubular rupture specimen was loaded in simple tension. During loading an oil seal in the axial load system failed. Repairs have been made and the specimen will be reloaded as the specimen should not have incurred damage.

The progress of test BWC-5B (20 ksi) is shown in Fig. 3.5. This specimen, which was originally anticipated to rupture in 2,000 to 4,000 hours, has finally begun tertiary creep. Consideration of more recent data led to an estimate of 7,500 hours for rupture at 20 ksi.

A B&W sponsored program was initiated to rectify the apparent difference in creep strain data as obtained from the two types of testing machines being used. A threaded rupture machine specimen (9R-2A) is being tested with four DCDT's over the 2-in. gage length and a single DCDT and dial gage over the full load train. Figure 3.6 shows the creep strain as measured by all six transducers. It can be concluded that the strain

Table 3.3. Chart giving numbers and dimensions of specimens taken from 1-in. diam bar type 304 stainless steel (heat 9T2796)

Specimen number[a]	Inside diameter	Outside diameter
I 1	0.337 in.	0.457 in.
I 2	0.336 in.	0.456 in.
I 3	0.339 in.	0.459 in.
I 4	0.340 in.	0.460 in.
I 5	0.344 in.	0.464 in.
I 6	0.340 in.	0.460 in.
I 7	0.342 in.	0.462 in.
I 8	0.342 in.	0.462 in.
I 9	0.342 in.	0.462 in.
I 10	0.340 in.	0.460 in.
I 11	0.345 in.	0.465 in.
I 12	0.346 in.	0.466 in.
I 13	0.347 in.	0.467 in.
I 14	0.346 in.	0.466 in.
I 15	0.348 in.	0.468 in.
I 16	0.347 in.	0.467 in.
I 17	0.343 in.	0.463 in.
I 18	0.349 in.	0.469 in.
I 19	0.344 in.	0.464 in.
I 20	0.342 in.	0.462 in.
I 21	0.347 in.	0.467 in.

[a]The letter I refers to specimens taken from bar No. 35.

Table 3.4. Status of uniaxial rupture tests — type 304 stainless steel (heat 9T2796) 1100°F

Test No.	Specimen No.	Stress (ksi)	Total strain on loading[a] (%)	Time to secondary creep (hrs)	Minimum creep rate (%/hr)	Time to tertiary creep (hrs)	Intercept creep strain (%)	Test time[d] (hrs)	Fracture elongation[e] (%)	Reduction in area (%)
BWC-1	7-15	30	4.7					187 R	19.0	30.5
BWR-1	7-1	30	---					138 R	21.5	32.9
BWC-2	2-22	28	5.8	40	0.016	195	0.50	227 R	13.0	20.4
BWR-2	2-1	28	---	40	0.022	230	0.65	368 R	16.5	29.0
BWR-13	7-13	28	---	60	0.023	215	0.88	276 R	16.5	18.9
BWC-9	7-25	28	3.8	85	0.021		1.16	415 R	18.3	25.2
BWC-3[h]	7-28	25	3.8	80	0.0065	500	0.45	667 R	12.7	12.0
BWR-3	7-8	25	---	100	0.0079	585	0.71	948 R	17.0	23.2
BWC-4	2-28	22	3.7	175	0.0014	1,400	0.60	2,130 R	10.7	13.7
BWR-4	7-7	22	---	160	0.0030	1,170	0.72	2,026 R	12.5	16.6
BWC-5[f]	2-15	20	---					--- D		
BWC-5B	2-16	20	1.8					8,800 I		
BWR-5[i]	2-14	20	---					4,842 D		
BWR-6	7-14	19	---					9,000 I		
BWR-9	7-11	18	---					8,000 I		
BWR-11[g]	2-12	17	---					94 D		
BWR-11	2-10	17	---					8,200 I		
BWR-7	2-4	16	---					8,700 I		

[a]All specimens were step-loaded at 1.87 ksi increments, except test BWC-5B, which was step-loaded at 1.49 ksi increments. Loading curves on BWR series include load train displacements, thus not reported.

[b]Time to tertiary creep based on the 0.2% offset from the minimum rate line.

[c]Intercept creep strain does not include the elastic and initial plastic components.

[d]R = rupture; D = discontinued; I = in test.

[e]Elongation over 3 inches in BWC series; over 2 inches in BWR series.

[f]Temperature excursion to 1300°F prior to loading. Replaced by Test No. BWC-5B.

[g]Temperature excursion at 1300°F at 94 hours. Replaced by Test No. BWR-11B.

[h]Failure occurred near end of gage length.

[i]Temperature excursion to 1380°F at 4,842 hours. Terminated.

Table 3.5. Status of uniaxial step load rupture tests — type 304 stainless steel (heat 9T2796) 1100°F

Test No.	Specimen No.	Stress (ksi)	Total strain on loading (%)	Time to secondary creep (hrs)	Minimum creep rate (%/hr)	Time to tertiary creep[a] (hrs)	Intercept creep strain[b] (%)	Time at load[c] (hrs)	Fracture elongation[d] (%)	Reduction in area (%)
BWC-6	2-17	16						3,871		
		25						136		
		20						4,660 I		
BWR-10	2-11	16						3,871		
		25						136		
		20						4,660 I		
BWC-7	2-18	17						3,699		
		25						136		
		20						4,660 I		
BWR-8	2-5	17						3,703		
		25						136		
		20						4,660 I		
BWLF-5	2-25	20						503		
		25						198		
		20						4,050 I		
BWC-8	7-16	18						5,071		
		25						136		
		20						2,800 I		
BWR-12	7-12	18						5,071		
		25						136		
		20						2,800 I		

[a]Time to tertiary creep based on the 0.2% offset from the minimum rate line.

[b]Intercept creep strain does not include the elastic and initial plastic components.

[c]R = rupture; D = discontinued; I = in test.

[d]Elongation over 3 inches in BWC series; over 2 inches in BWR series.

Table 3.6. Status of uniaxial interrupted tests — type 304 stainless steel (heat 9T2796) 1100°F

Test No.	Specimen No.	Stress (ksi)	Time at load (hrs)
BWI-1	4-6	19.5	1,780
BWI-2	5-6	19.5	1,780
BWI-3	6-6	19.5	1,780

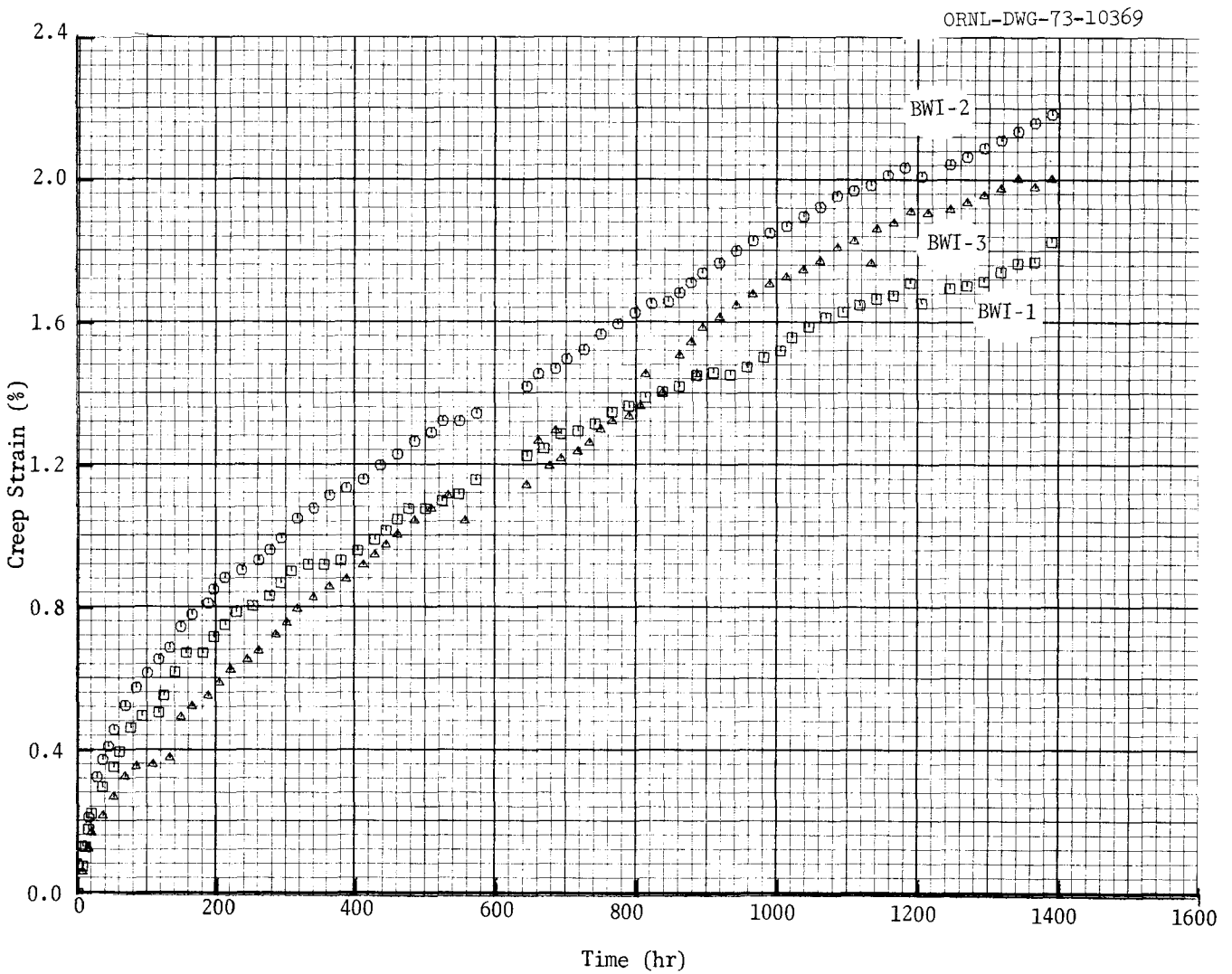

Fig. 3.4. First three constant load uniaxial tests (in progress) in the Interrupted Test Series. Loaded at 19.5 ksi at 1100°F. Type 304 stainless steel (heat No. 9T2796), 5/8-in. rod.

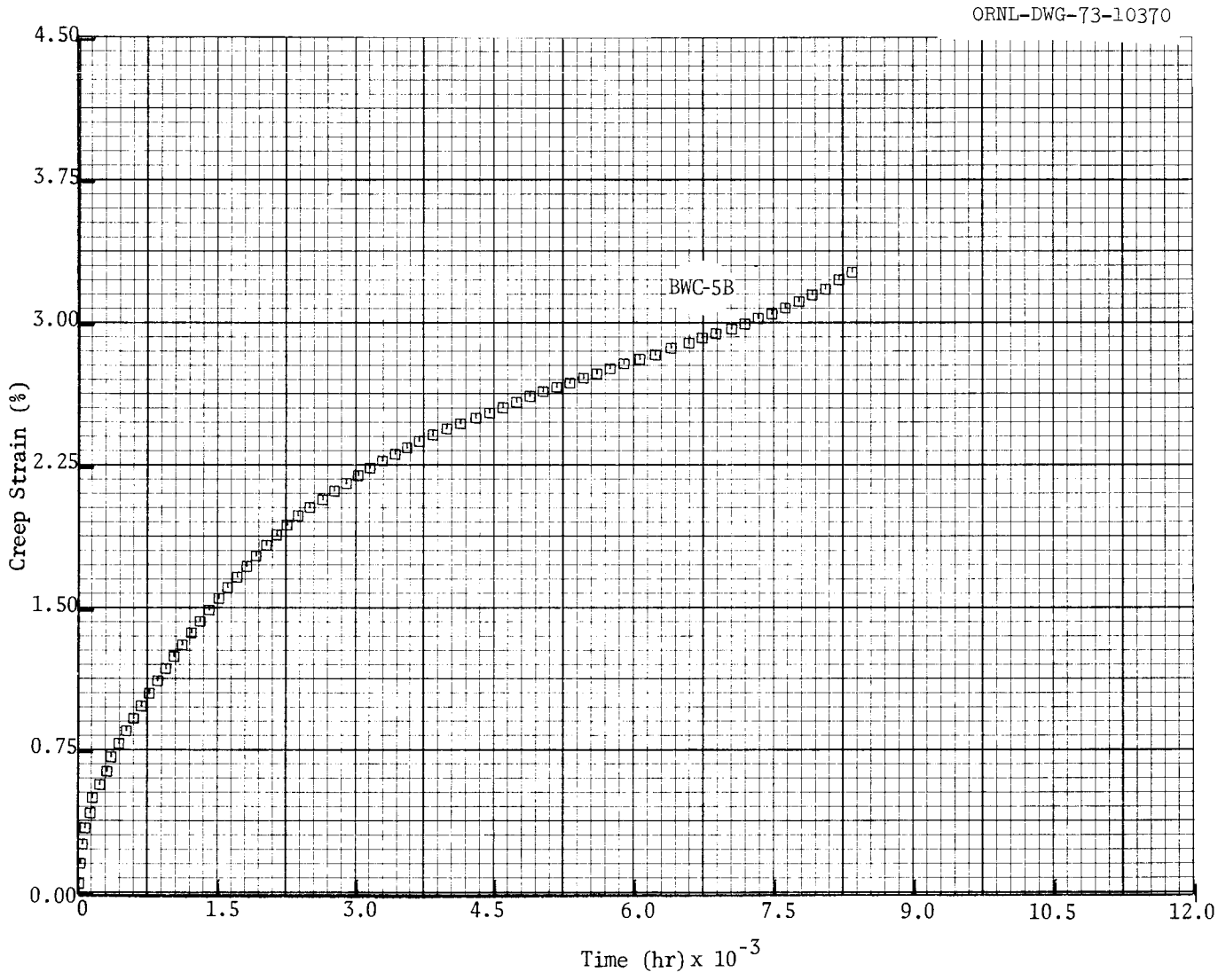

Fig. 3.5. Constant load uniaxial rupture test (in progress). Loaded at 20 ksi at 1100°F. Type 304 stainless steel (heat No. 9T2796), 5/8-in. rod.

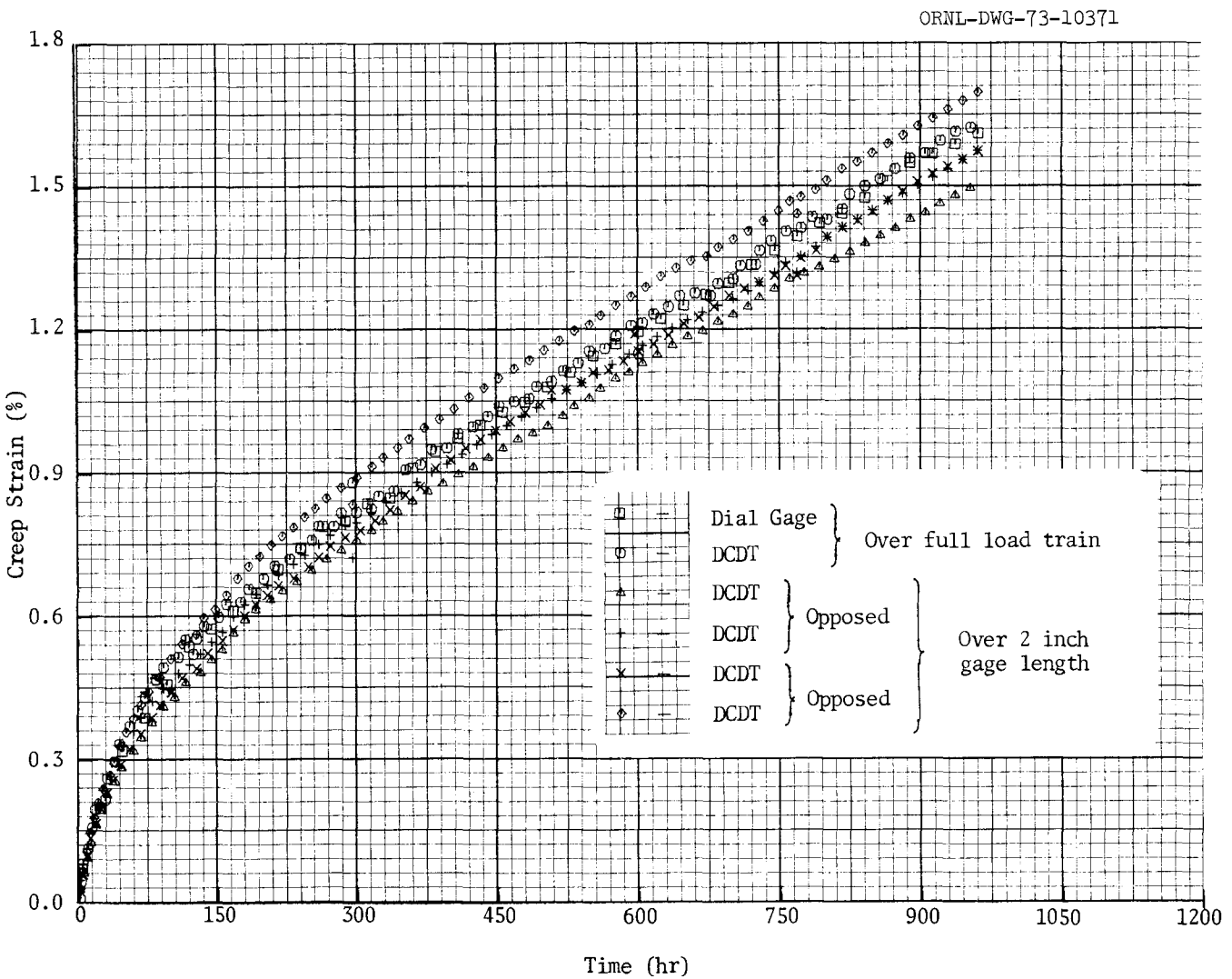

Fig. 3.6. Special constant load uniaxial test to evaluate differences in the two types of testing machines. Loaded at 20 ksi at 1100°F. Type 304 stainless steel (heat No. 9T2796), 5/8-in. rod. Specimen 9R-2A.

occurring outside of the gage length is not sufficient to explain the differences seen thus far between the two types of machines. No conclusion can be reached with respect to specimen bending, which will be the next area of consideration. Figure 3.7 compares the four tests that have been started at 20 ksi, one of which is specimen 9R-2A. Tests BWC-5B and BWLF-5 are being conducted in a creep machine while test BWR-5 is being conducted in a rupture machine.

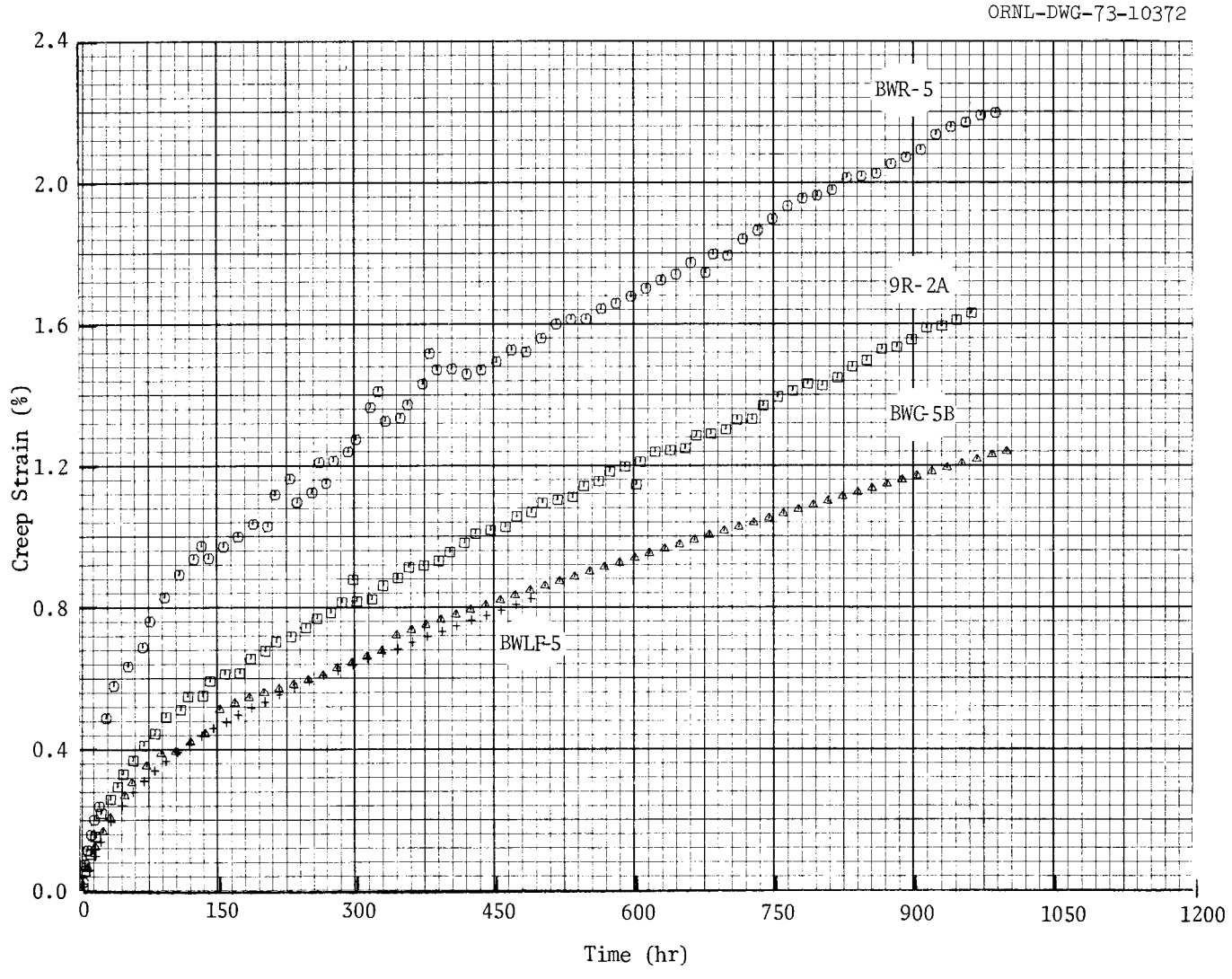

Fig. 3.7. Comparison of four constant load uniaxial tests loaded at 20 ksi at 1100°F. Type 304 stainless steel (heat No. 9T2796), 5/8-in. rod.

4. DEVELOPMENT, EVALUATION, AND DISTRIBUTION OF STRUCTURAL ANALYSIS METHODS AND TOOLS

J. M. Corum

4.1. Two-Dimensional Elastic-Plastic-Creep Finite-Element Computer Program CREEP-PLAST

4.1.1. Program development (J. A. Clinard)

Further improvements have been made to the ORNL in-house version of CREEP-PLAST. These improvements are user-oriented operational modifications which do not significantly alter the overall scope of the program or the computing strategy. The modifications are aimed primarily at improving the versatility of the program, lowering the cost of computation, and overcoming minor limitations known to exist in the earlier versions of the program. The following is a summary of the improvements which have been implemented in the ORNL version of CREEP-PLAST during the last two quarters and which are currently being employed for in-house applications. Some of these improvements will become available for general distribution by ORNL as soon as they are verified completely and the adequacy of the modifications is determined. The modifications which produce severe machine dependency are not likely to be made available for general distribution since it is hoped that the ORNL distributed version of CREEP-PLAST can be maintained as a virtually machine-independent program.

1. The program has been modified for solution of a limited constrained degree of freedom structural problem. The displacement history of a maximum of 100 nodes can be specified by the user through a single displacement multiplier array similar to the pressure multiplier arrays which are available to vary the pressure and concentrated nodal loads.

2. Vector storage of data has been implemented so that the core requirements can be easily varied by the user on a problem-to-problem basis. The dimensions of two arrays control the storage requirements for a problem. One array is the storage area of the system equations, both during the formulation in the STIFF link and during the solution procedure in the SOLVE link. This area also serves as the temporary storage area for plotting information in the CREEP link. The other array is the storage area for element and nodal

information, some of which previously appeared in the BLANK and CREEP1 common blocks. With vector storage, small problems have been run on the ORNL IBM 360 computer system in less than 200K bytes (including buffers). Previously, all problems required about 500-540K bytes. It should be further noted that if the dimension of the array for storage of the system equations is large enough to accommodate the entire system, the equations are maintained in memory during formulation and solution, and no I/O is required. This completely eliminates the use of scratch storage units 21 and 22. Coupled with other improvements to the program this has lowered the I/O ratio for "core-maintained" problems below 2:1 on the ORNL computer.

3. The I/O procedures have been improved by implementation of KBSAM IBM/360 buffering for units 17, 18, 21, and 22. Both the CPU and wall-clock times for execution have been significantly reduced so that the I/O ratio of about 3:1 for moderate size problems has remained unchanged. The reduction in execution time has reduced the cost of computation by about 40% compared to the version of CREEP-PLAST currently available for general distribution. This reduction is due in part to KBSAM I/O and in part to maximum utilization of core through vector storage and through an improved overlay. There are secondary benefits from KBSAM I/O. No system I/O buffers are allocated for direct access devices under KBSAM control. Therefore, memory which was previously allocated as buffers for standard FØRTRAN I/O on units 17, 18, 21, and 22 (64-150K bytes, depending on the DCB parameters) is now employed to increase the work space available to the solution routines, thus increasing the efficiency of the solution technique. Also, the NOTE and POINT facilities of KBSAM have reduced execution time by eliminating the back spacing of unit 21 during back-substitution.

4. Program logic has been changed so that element calculations in the STIFF and CREEP links are looped in 100-element blocks instead of 50-element blocks as in the previous version. This means that units 17 and 18, the scratch storage units for element information, must be accessed only one-half as many times during program operations, thus providing a savings in wall-clock time with a minimal (12K byte) increase in storage requirements. Also, the logic has been modified so that if the number of elements for the problem is less than 100, element information is maintained in core and units 17 and 18 are completely eliminated. This requires no increase in storage requirements.

5. A routine has been added to calculate and print the maximum effective incremental strain and stress for equation-of-state creep problems, so that the user can quickly check the adequacy of his time-step selection. Automatic stops can easily be included if maximum allowable incremental changes are exceeded.

In addition to the above user-oriented modifications, several errors pertaining to nonisothermal problems have been identified and corrections have been made. These corrections are available in the new version of CREEP-PLAST that is being made available to the public as described in the next subsection.

4.1.2. Program distribution (J. M. Corum and J. S. Crowell)

As described in the previous progress report,[13] work was completed at General Electric, under ORNL subcontract, to develop a heat conduction analysis capability for CREEP-PLAST. The new subroutines and modifications were received by ORNL in April. Several errors in the new program were discovered during implementation. Some of the errors were machine-dependent (or operating-system-dependent) and would not have been apparent in the UNIVAC version at General Electric. Enough corrections have been made to enable us to run the small sample problem sent by General Electric and we have obtained good agreement with the results from the UNIVAC version. We are making additional corrections and plan to incorporate the thermal analysis capability fully into the ORNL version of CREEP-PLAST in the immediate future.

Since the heat conduction analysis capability is essentially ready for use and since numerous other modifications and corrections have been made to the basic CREEP-PLAST program that was initially distributed, a new version is now being offered to the public and can be obtained by using the order forms included in this report. The new version will have the thermal analysis capability incorporated into the basic structural analysis program. Those prior recipients of the structural analysis portion of CREEP-PLAST who have adapted the program to their own machine may want to implement the thermal analysis capability as a separate program. The temperature history calculated by the thermal analysis program could then be used as input to the user's CREEP-PLAST program. In this case, the entire program should

still be ordered. Instructions will be included for using the thermal analysis protions of the new ORNL version and creating a temperature history tape for later use.

As was previously done, the new program is being released with the agreement and understanding that any changes and modifications will be coordinated with ORNL. In this way everyone will benefit from any corrections, modifications, or extensions made to the program, and a current updated version will always be available.

A formal request form and agreement document are provided on the following two pages for the reader's convenience. If you desire a copy of the new version of CREEP-PLAST, which includes thermal analysis capability, remove the forms, fill them out, and send both to the ORNL Computer Librarian:

Computer Librarian
Room A228, Building 4500-N
Oak Ridge National Laboratory
P. O. Box X
Oak Ridge, Tennessee 37830

The agreement document must be signed by a person in your organization with appropriate authority. Since AEC regulations require that we recover the costs of disseminating computer software, we are charging approximately $25.00 for materials, handling, and mailing. The signed agreement document serves as our authority to bill your organization.

4.1.3. Verification and qualification of CREEP-PLAST by benchmark problem calculations (J. A. Clinard and J. M. Corum)

One type of benchmark problem being used to verify and qualify the CREEP-PLAST program consists of thin-walled tubular specimens subjected to nonproportional tension-torsion loadings at room temperature. Experimental data of this type have been obtained by Liu,[9] and some elastic-plastic analysis results were reported in the previous progress report.[10] One of the problems previously examined is depicted again in Fig. 4.1. Additional elastic-plastic analyses have been carried out for this particular case, and the results are summarized here.

Two analyses of the problem in Fig. 4.1 were previously reported. First, a nonlinear analysis, which used a piecewise linear representation of the monotonic stress-strain curve, was performed, and second, a bilinear

REQUEST FORM FOR CREEP-PLAST THERMAL AND STRUCTURAL ANALYSIS COMPUTER PROGRAM

Return form to: Computer Librarian
Room A228, Building 4500-N
Oak Ridge National Laboratory
P. O. Box X
Oak Ridge, Tennessee 37830

The source program, in card image form, will be sent to you on a magnetic tape. The tape will be a 600 ft mini-tape which you may keep.

Please check the option below which comes closest to meeting your system's requirements as to tape format. Tapes will be prepared in advance in these two standard formats. Your request for the program can be met more quickly if you can accept one of these standard formats.

_____ Option 1: 7-track tape
BCD card code
556 bpi density
Unblocked records (84 characters per physical record, with last four characters blank)

_____ Option 2: 9-track tape
EBCDIC card code
800 bpi density
Blocked records (800 characters, or ten cards, per physical record)

If you require modifications to the option checked above, please indicate them below.

character code _____ BCD _____ EBCDIC

density _____ 200 _____ 556 _____ 800

physical record size _____

Note: Our 9-track tape drives are all 800 bpi density.

What type of computer will be used to read the tape? _____

On what type of computer will the program be executed? _____

Name and address of requester: _____

_____

_____

_____

_____

Phone number of requester: _____

Signed: _____ Date: _____

AGREEMENT FOR
USE OF THERMAL AND STRUCTURAL ANALYSIS
COMPUTER PROGRAM CREEP-PLAST

WHEREAS, Union Carbide Corporation, acting under its Prime Contract W-7405-eng-26 with the United States of America (Government) as represented by the United States Atomic Energy Commission (Commission), in operating and managing the Government-owned facility identified as the Oak Ridge National Laboratory entered into Subcontract No. 3511 with the General Electric Company for the development of a special elastic-plastic-creep structural analysis computer program identified as CREEP-PLAST; and

WHEREAS, it is one of the objectives of the Commission to provide the liquid-metal fast-breeder reactor component manufacturers and other interested Commission approved parties with a well-documented, non-proprietary structural analysis computer program to be used by said recipients on their own computers; and

WHEREAS, it is a further objective that all corrections, changes, and modifications should be incorporated in an up-to-date master computer program to be made available by the Oak Ridge National Laboratory to all interested aforementioned manufacturers and other Commission approved parties;

NOW, THEREFORE, in consideration of Union Carbide Corporation making the Computer Program CREEP-PLAST available to _____(Recipient) on a non-exclusive, royalty-free basis, the recipient agrees to furnish the Oak Ridge National Laboratory with any changes, corrections, modifications or updating the recipient makes to the Computer Program, for incorporation in a current master computer program to be made available by the Oak Ridge National Laboratory to all Commission approved parties.

The recipient further agrees not to withhold or classify as proprietary any of said corrections, changes, modifications and alterations to the Computer Program and hereby grants to the Government an irrevocable, non-exclusive, royalty-free license to use the same for any purpose whatsoever.

It is understood the recipient will be billed for a handling and mailing charge of approximately Twenty Five Dollars ($25.00) due Union Carbide Corporation for the account of the Government. The exact cost will be determined by Commission cost recovery guidelines applicable at the time of the request.

Date_____ Name_____

Title_____

Representing_____

Address_____

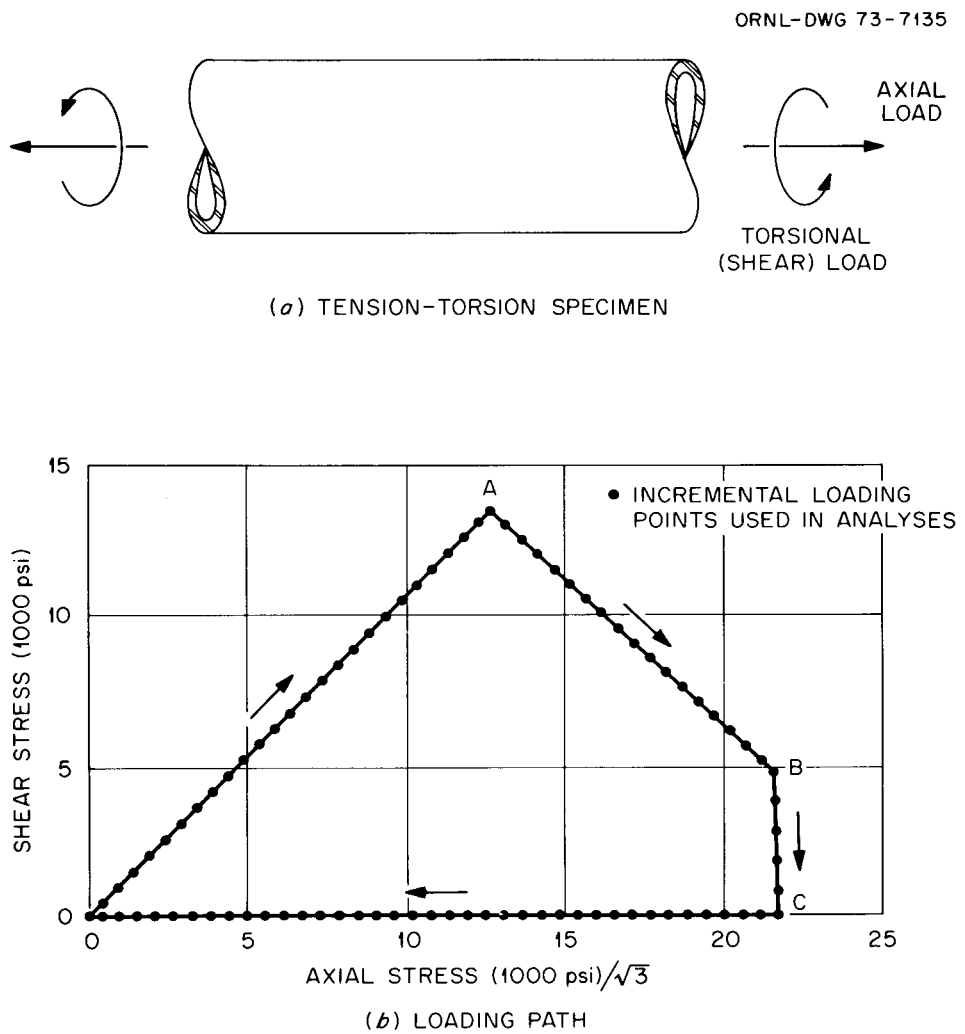

Fig. 4.1. Loading path for tension-torsion test of thin-walled tubular specimen.

analysis was carried out. In both cases, representations of the tenth-cycle cyclic stress-strain curve were used for reversed loading.* The proportional limit for the bilinear stress-strain curve was 27,000 psi, while 15,000 psi was used for the nonlinear curve.** The bilinear analysis predictions agreed reasonably well with the measured response. The nonlinear analysis predictions agreed well with the measured response for the proportional loading to point A (see Fig. 4.1) but not for the nonproportional loading path from A to C. The latter disagreement is believed attributable to the kinematics of the nonlinear kinematic hardening theory of CREEP-PLAST and not to the nonlinear representation of the stress-strain curve employed for the problem. This observation seems valid since between A and C the effective stress level always falls within the bounds of the final segment of the piecewise linear curve. This segment has the same slope as the plastic portion of the bilinear curve employed in the previously reported companion analysis.

To further investigate the sources of the disagreement, three additional nonlinear analyses of the problem have been performed. Each used the same piecewise linear stress strain curve, which was shown in the previous report,[10] and cyclic hardening was neglected in all three. As before, the finite-element model consisted simply of two plane-stress triangular elements forming a square, and the loading steps depicted in Fig. 4.1 were used. The only difference in the three analyses was the value used for the proportional limit, and consequently the size of the yield surface. The three cases were:

Case 1. Proportional limit of 21,500 psi. This is the apparent value of the proportional limit for the representative monotonic stress-strain curve used in the analyses.

---

*In the nonlinear analysis, the shape of the tenth-cycle curve was assumed to be adequately described by the shape of the initial monotonic curve with an appropriate increase in the proportional limit to account for hardening.

**The 15,000 psi value agrees reasonably well with the initial departure from linearity which has been very precisely measured by Liu.[9] However, the representative curve used in the nonlinear analysis would appear, by visual inspection, to have a proportional limit of about 21,500 psi.

Case 2. Proportional limit of 15,000 psi. This is the value used in the previous nonlinear analysis, and it agrees reasonably well with the initial small departure from linearity precisely measured by Liu.[9]

Case 3. Proportional limit of 10,000 psi. This fictitiously low value was used as an extreme case.

It should be emphasized that all three analyses used exactly the same stress-strain curve. The different proportional limit values determined only the size of the yield surface as used in the mathematical formulation.

The results are typified in Fig. 4.2, where the plastic strain trajectories predicted by the three analyses are compared with the measured trajectory. In all cases the analyses over predict the axial strain and under predict the shear strain. The larger the yield surface, the more realistic the predictions. Case 1, which used the observed proportional limit of 21,500 psi, still does not agree as well with experiment as did the bilinear predictions which were presented in the previous progress report[10] and which utilized a proportional limit of 27,000 psi.

The influence of the size of the yield surface is further illustrated by the plots shown in Figs. 4.3 to 4.5. Here, the calculated stress points along the loading path are shown together with the corresponding centers of the yield surface and the outlines of the surface in the tension-torsion space for each analysis. Vectors representing the direction and relative magnitude of the plastic strain increment associated with each stress point on the loading path are also shown.* Analogous plots for the two earlier analyses were included in the previous progress report.[10]

The yield surface movement exhibited in Figs. 4.3 to 4.5 is markedly different, depending on the size of the surface. Careful comparison of the yield surfaces and associated plastic strain increments with the measured and predicted plastic strain trajectories in Fig. 4.2 helps to explain why, in this particular problem, the larger yield surfaces result in more realistic predictions.

---

*The plastic strain increment at each point is that associated with the subsequent load step.

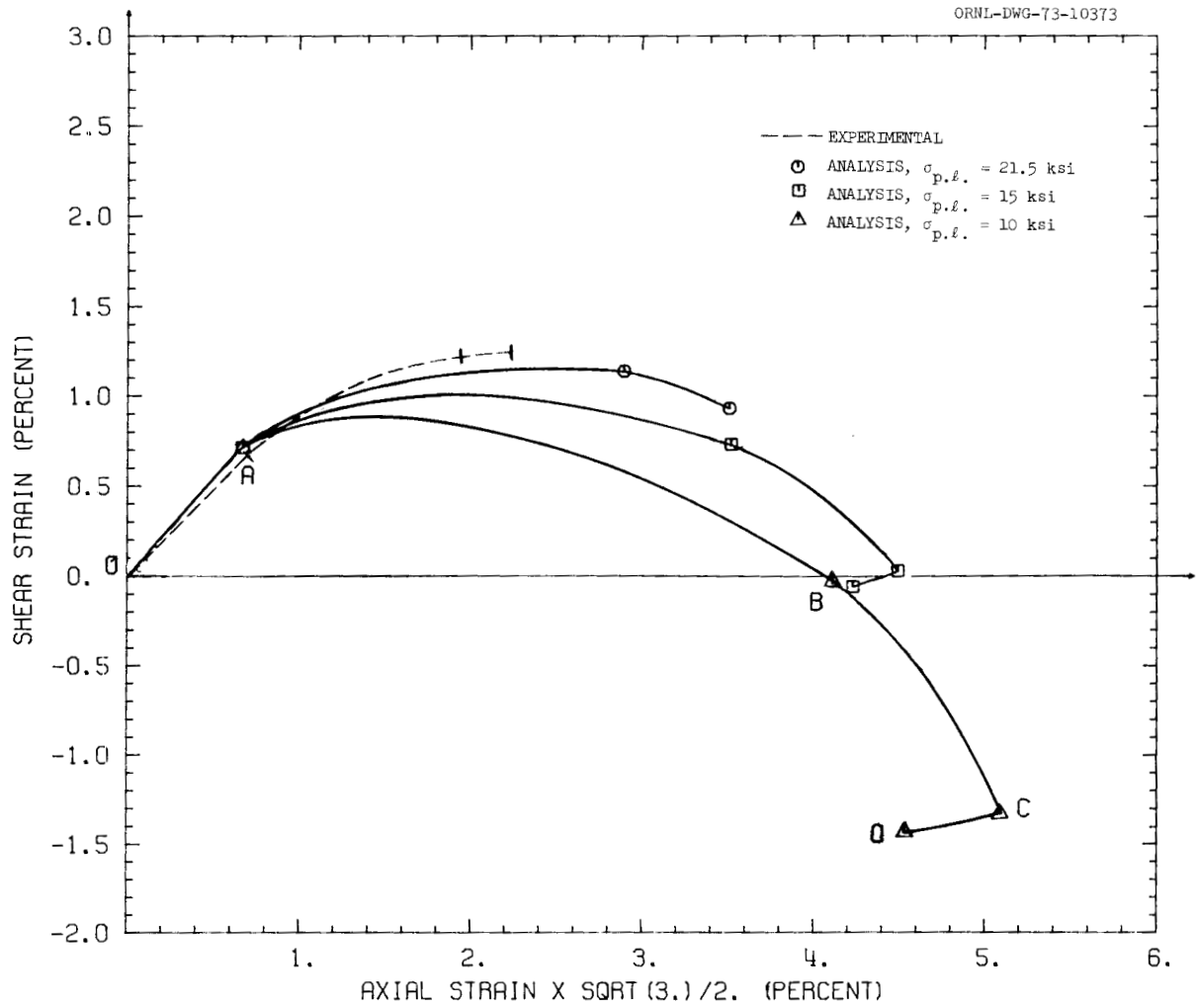

Fig. 4.2. Comparison of measured and predicted plastic strain trajectories for tension-torsion test. The shear strain shown in this figure is the Lagrangian strain ($\varepsilon_{12} = \frac{1}{2}\gamma_{12}$, where γ_{12} is engineering shear strain).

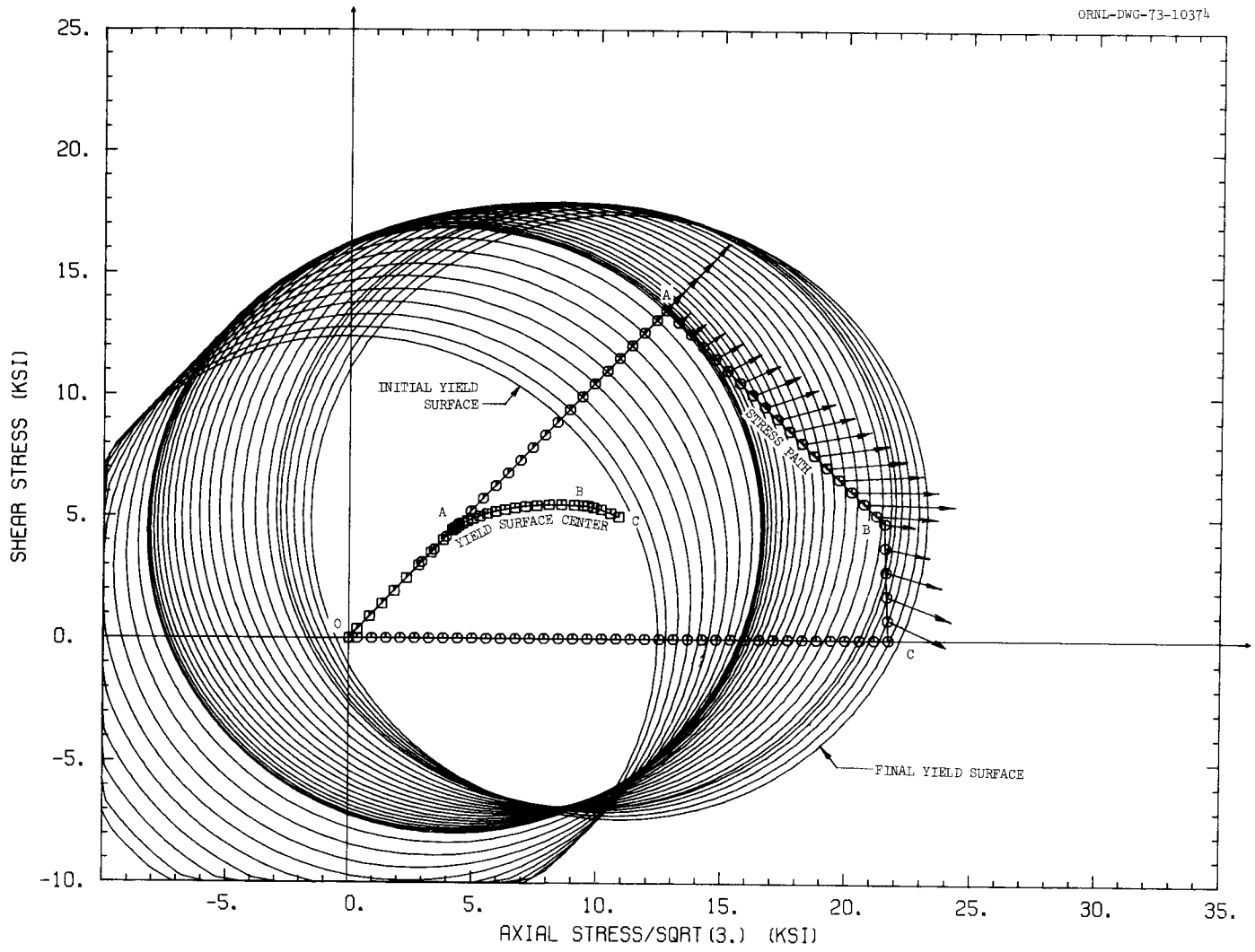

Fig. 4.3. Predicted yield surfaces for each load step in the Case 1 analysis ($\sigma_{p.\ell.}$ = 21,500 psi) of the tension-torsion test. The vectors show the direction and relative magnitude of the plastic strain increment at each stress point along the loading path.

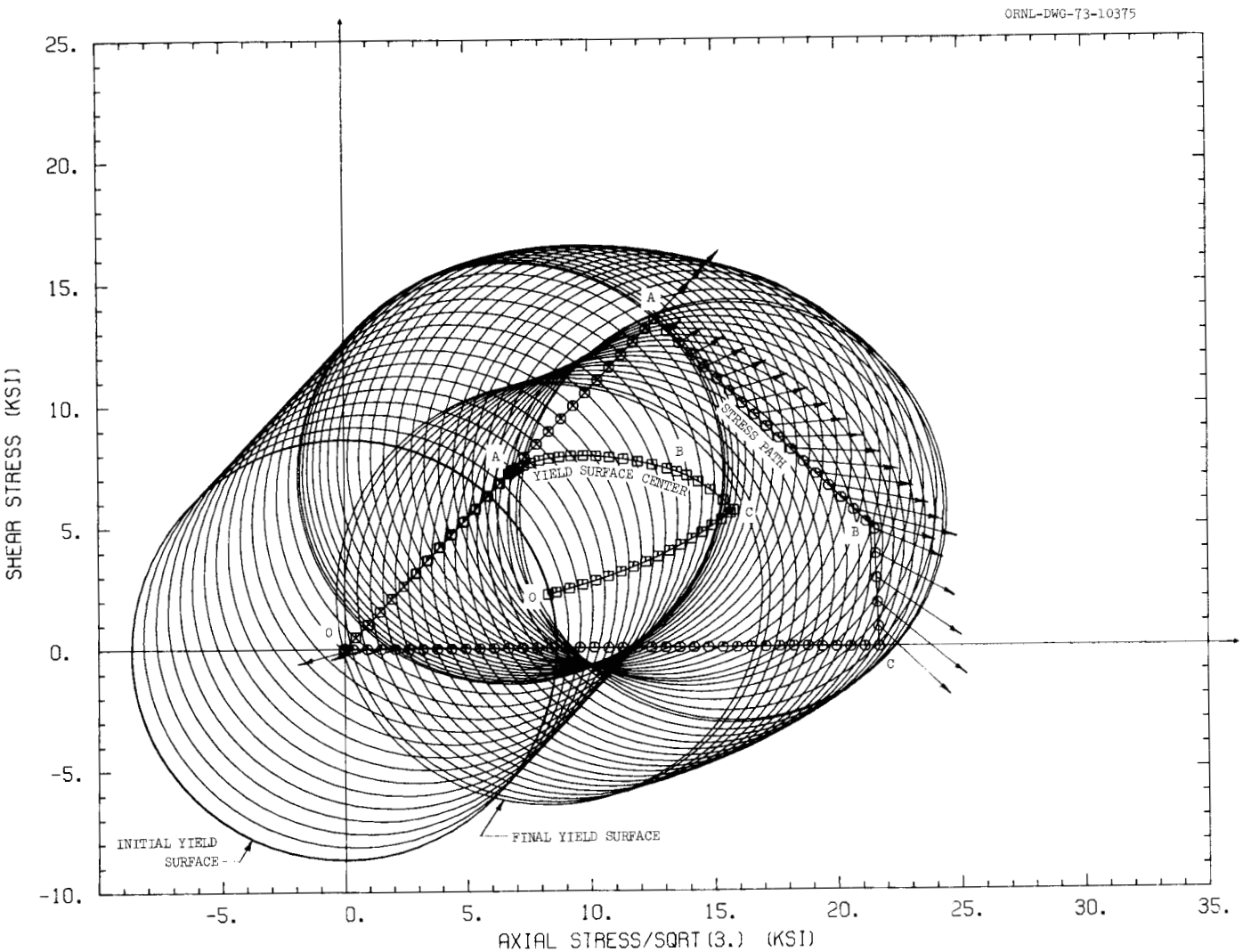

Fig. 4.4. Predicted yield surfaces for each load step in the Case 2 analysis ($\sigma_{p.\ell.}$ = 15,000 psi) of the tension-torsion test. The vectors show the direction and relative magnitude of the plastic strain increment at each stress point along the loading path.

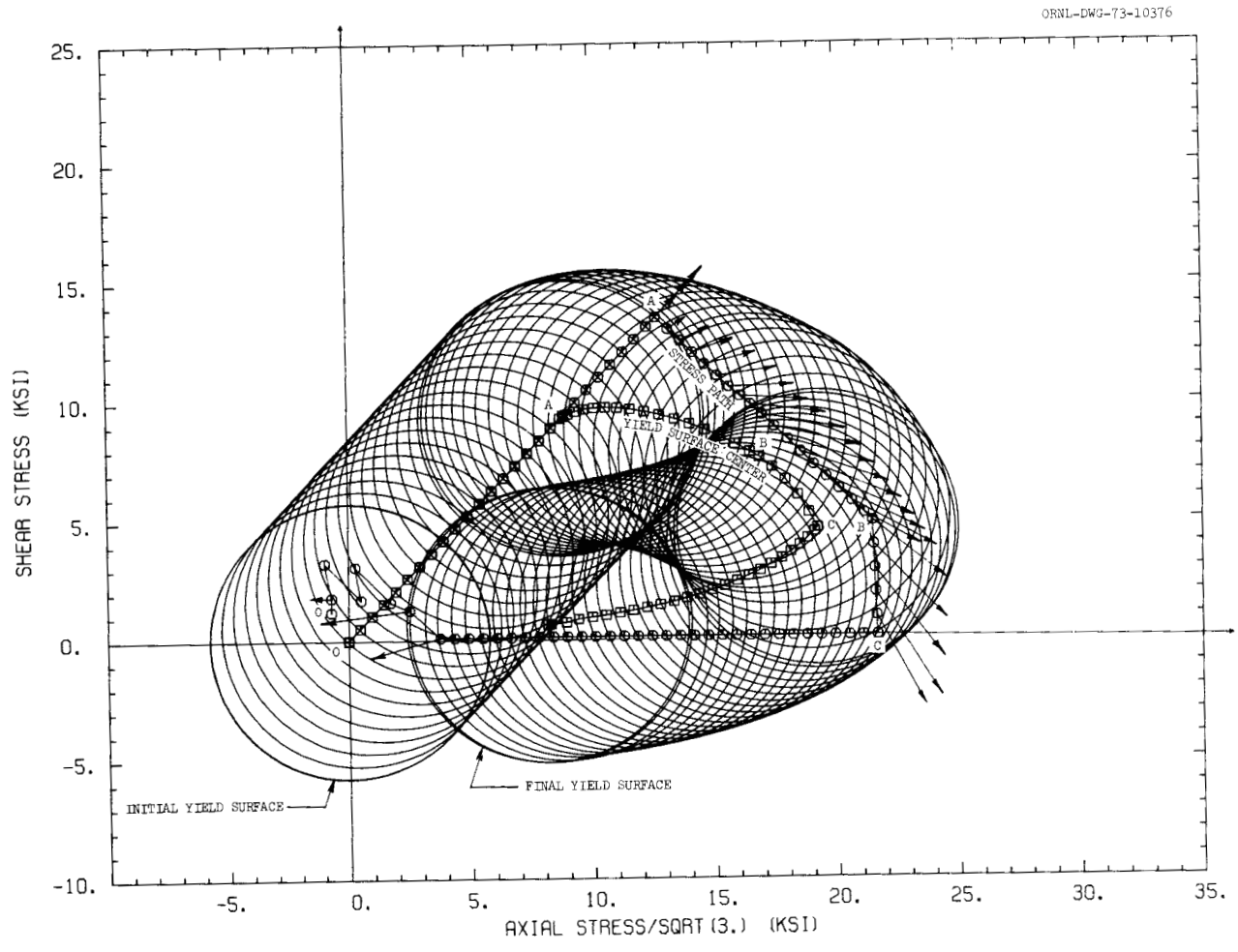

Fig. 4.5. Predicted yield surfaces for each load step in the Case 3 analysis ($\sigma_{p.\ell.}$ = 10,000 psi) of the tension-torsion test. The vectors show the direction and relative magnitude of the plastic strain increment at each stress point along the loading path. Note that the analysis has become unstable near the end of the load path. This can be attributed to the gradual drift of the stress state from the yield surface, a numerical problem related to the discrete load steps used and the extreme nonradiality of the load path.

4.2. General Three-Dimensional Thick Shell Elastic-Plastic-Creep Finite-Element Computer Program EPACA

4.2.1. Program development, verification, and qualification
(S. K. Iskander and J. S. Crowell)

In this quarter several additional errors in the EPACA computer program causing inaccurate results have been identified and corrected. Several of these errors will be discussed briefly here, and some results of the elastic analysis of a practical elbow problem and the comparison of the results with experimental data will be presented. Progress in other areas will also be summarized.

Figure 4.18 on p. 105 of the previous progress report[14] showed the deterioration of stresses along the top fibers of a small thick-walled tube subjected to a bending moment as compared with beam theory. This seems to have been the culmination of several causes.

The EPACA code uses a dynamic vector storage scheme. Accordingly, the location of each element of the stiffness matrix has to be assigned within this vector. Moreover, limitations of available core storage during both the formation of the stiffness array as well as later during the solution of the system necessitate the external storage of the stiffness array as "blocks." During the formation of the stiffness of each element, tests are carried out to determine whether enough core is available for the system formation in progress, as well as verifying that enough core will be available to solve the resulting block of equations when it is later read back into core from external storage. Should either test fail, the stiffnesses that were already fully formed are written out on external storage.

During this phase, for certain combinations of the amount of storage allocated and nodal numbering schemes, these tests have proved to be inadequate. One manifestation of this was that, although the program wrote out a block of equations onto external storage and freed the space they originally occupied, the available space at this stage was still not sufficient, and the program did not recognize this situation. As a result, the stiffnesses of the structure were summed incorrectly. The first few blocks of the stiffness formation were formed correctly. It is during the later stages of formation and solution that this situation came into play. Hence the results for the first portions of the structure to be handled by

the program appeared to be correct, while the latter solution progressively deteriorated. This problem necessitated the complete revision of the portions of the code that were involved in these operations.

Another source that contributed to erroneous results arises in cases where flat elements are used to model structures and there exists some angle between the element meeting at a single node. During coordinate transformation of the stiffness of the element from a system of axes normal to the element to a system with one axis whose direction is the average of the normals of all the elements meeting at this node, there is generally a small resultant component of rotational "stiffness" about the common normal, and consequently some decision has to be made regarding whether or not to include it in the total stiffness matrix. In cases in which all the elements at a node are in a single plane, this rotational stiffness would theoretically be zero but in practice could be some small number arising from general computational errors. Hence the resulting matrix might be either singular or ill-conditioned, and consequently the rotational stiffness should not be included for such locations. Also, in cases where there is an angle between flat elements meeting at a node, the rotational stiffness is insignificant. Hence some judgment is necessary during the preparation of the input as to whether or not to take this rotational stiffness into account at an individual node.

The small thick-walled tube problem previously mentioned above was reanalyzed after all the above corrections and considerations were taken into account. The new results are within 2% of simple beam theory if the local perturbations due to the introduction of the end forces are neglected.

As a further check on this and other problems (for which no theoretical solution exists) a capability of calculating the reactions has been implemented instead of the old "residue" calculations. These reactions facilitate an equilibrium check. This is now functional and has been used successfully in the above problem as well as in the example described below.

The elastic analysis of a piping elbow that was described in the previous progress report[14] has been redone, and the predictions now agree reasonably well with experimental data. The problem analyzed is depicted in Fig. 4.6 and consisted of a 10-in. sched-40, long-radius, 90° elbow with 12-in. and 18-in. straight pipe extensions. The material was carbon

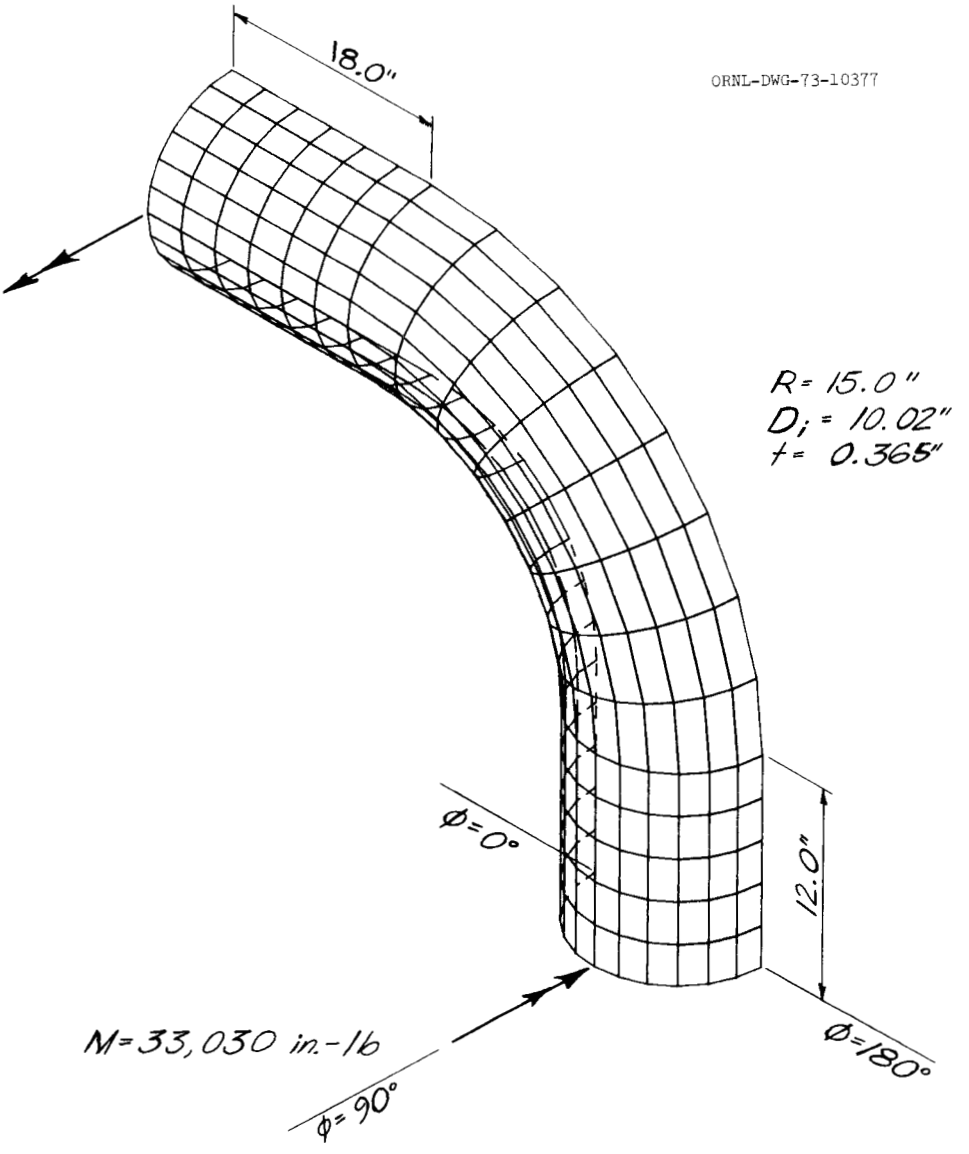

Fig. 4.6. Finite-element idealization of elbow assembly analyzed.

steel, and the experimental model was strain gaged and tested at room temperature. An in-plane bending moment of 33,030 in.-lb was applied in the case reported here.

The finite-element idealization that was used is shown for one-half of the assembly in Fig. 4.6. Actually the full model was represented in the analysis. A total of 456 flat quadrilateral elements (NKØD=6) were used in the total representation. Representative results are presented and compared with strain-gage data in Figs. 4.7 through 4.9.* Figures 4.7 and 4.8 show the variation of circumferential and longitudinal stresses along the length of the assembly for the circumferential angles, Ø, of 90 and 180°, respectively (see Fig. 4.6). Figure 4.9 shows the variation of circumferential and longitudinal stresses around the circumference of the elbow at the center of the bend.

Although these results are presented only as an indication of the present state of the program, the reasonably good agreement between theory and experiment indicates that the program gives elastic results within tolerable accuracy. Moreover, the accuracy may be improved by refining the mesh, particularly within areas of steep stress gradients.

A small improvement to facilitate input preparation for users of EPACA has also been made. The format fields have all been tentatively standardized to five and ten. Furthermore, the plotting capability of the program for both the undeformed and deformed mesh is now operational, although the plotting capability for the deformed mesh needs some modification to improve the interpretation of the results. Figure 4.6 was produced using this plotting capability.

4.2.2. Program distribution (J. M. Corum and J. S. Crowell)

The following minimal amount of basic verification work has now been completed on EPACA:

1. The two flat quadrilateral elements have been used in very simple inelastic analyses and in realistic elastic analyses. They appear to be

---

*The experimental model was tested as a part of the ORNL Piping Program — Design Criteria for Piping, Pumps, and Valves. Acknowledgment is due W. G. Dodge for providing the experimental data as well as the plots presented here.

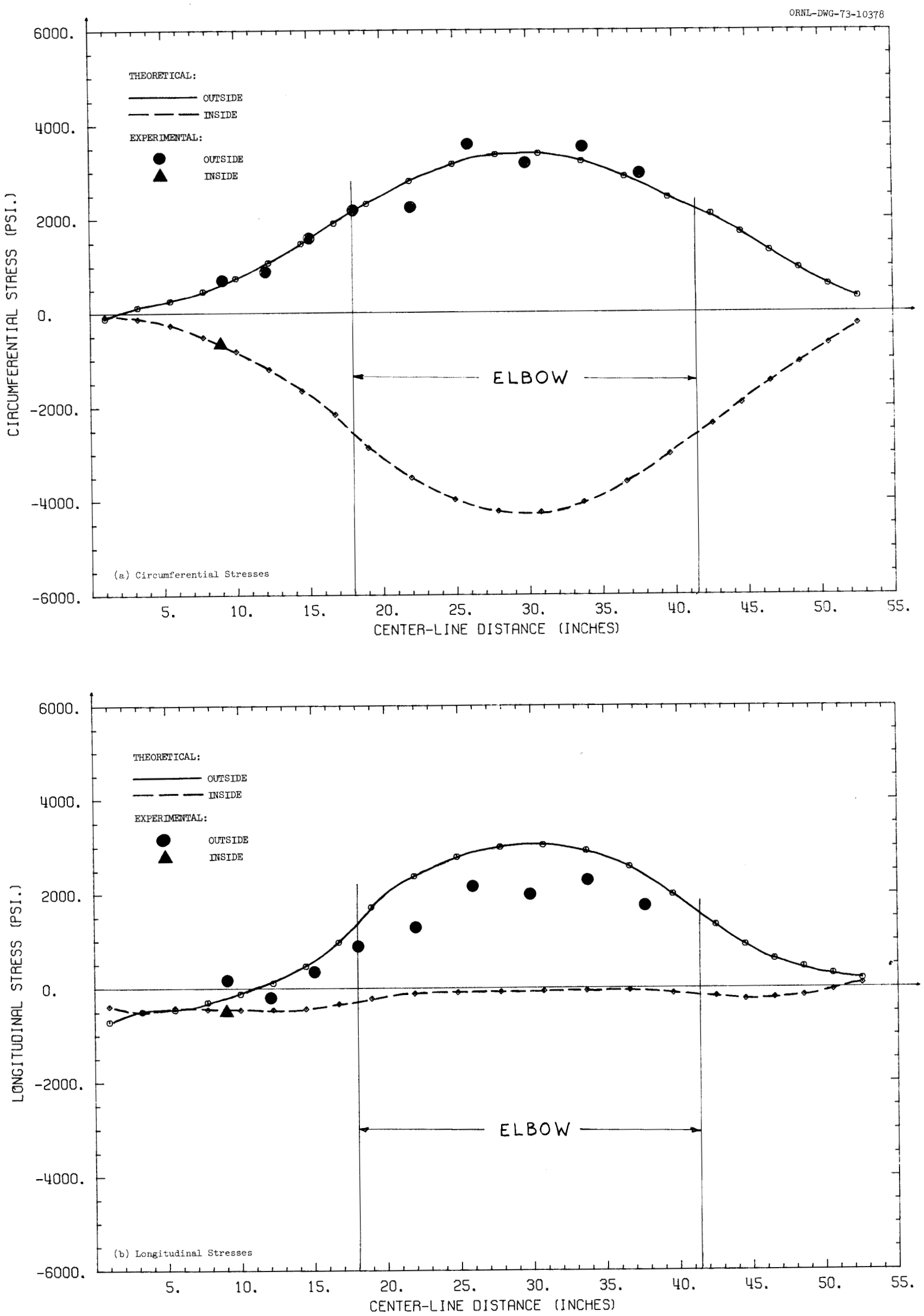

Fig. 4.7. Comparison of predicted and measured stresses along line corresponding to $\phi = 90°$ (see Fig. 4.6). Note that the predictions shown are actually the values at the element centers, 7.5° from $\phi = 90°$.

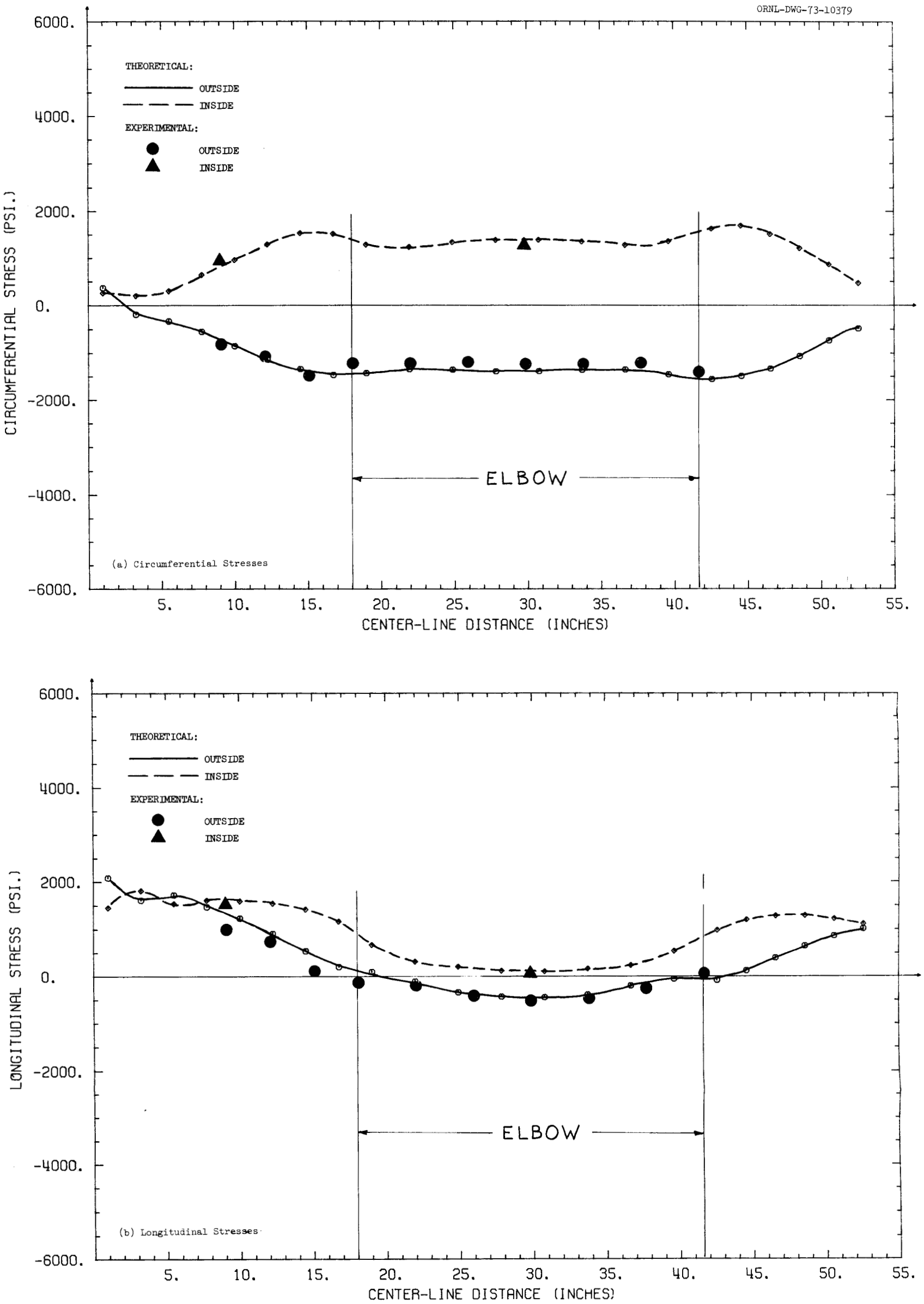

Fig. 4.8. Comparison of predicted and measured stresses along line corresponding to $\phi = 180°$ (see Fig. 4.6). Note that the predictions shown are actually the values at the element centers, 7.5° from $\phi = 180°$.

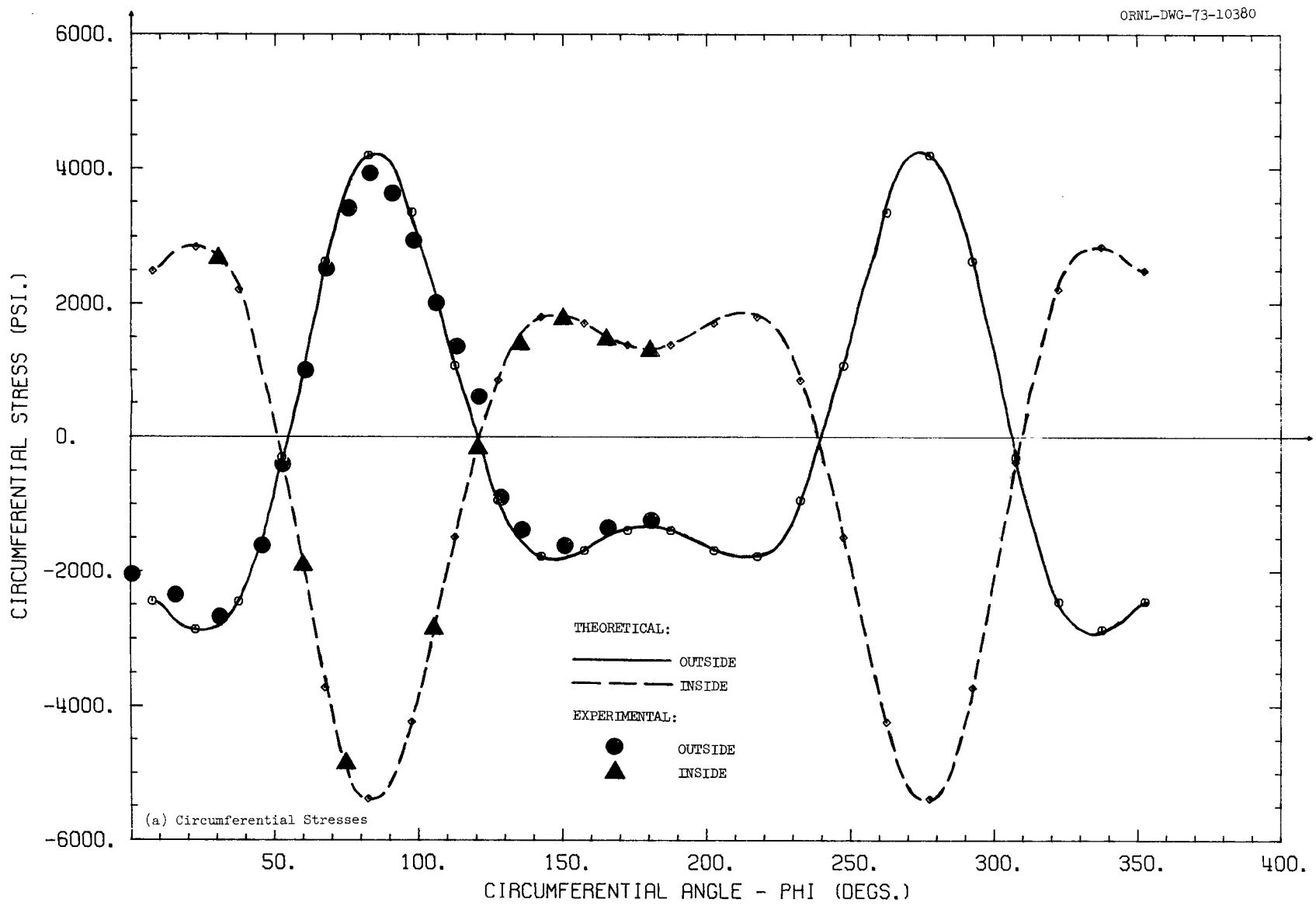

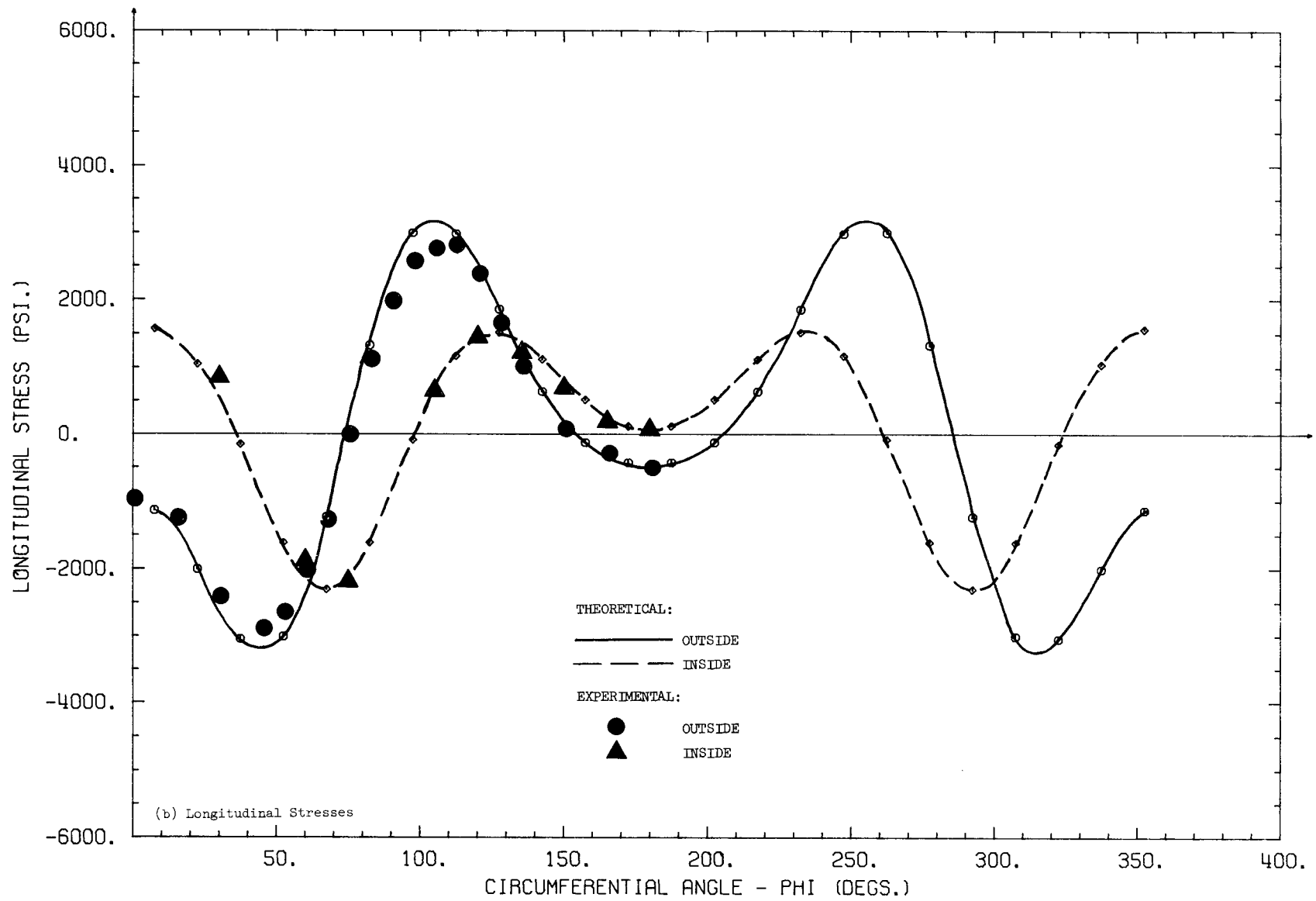

Fig. 4.9. Comparison of predicted and measured stresses around circumference at midsection of elbow bend.

adequately formulated and working correctly. The triangular elements are not yet adequate, in a practical sense, because of inconvenient coordinate systems used for each element. The isoparametric elements are not adequately debugged and verified.

2. The program has been used for large elastic problems, and does appear to give good results, as evidenced by the elbow results given in the previous subsection.

3. Simple uniaxial elastic-plastic and elastic-creep analyses indicate that the basic features of inelastic constitutive equations are correctly formulated and handled.

Much additional debugging and verification work remains before all of the major features of the program and the eight available elements can be adequately checked out. Nonetheless, the decision has been made to offer the current version of the program to the public with the anticipation that it can now serve as a useful design analysis tool and that feedback from users will hasten the remaining debugging and verification process.

The program is being released under the same arrangement as that for the two-dimensional program CREEP-PLAST. That is, the recipient must agree that any changes and modifications will be coordinated with ORNL, so that everyone will benefit from corrections, modifications, or extensions made to the program, and a current updated version will always be available.

A formal request form and agreement document are provided on the following two pages. Both forms should be filled out and sent to the ORNL Computer Librarian:

Computer Librarian
Room A228, Building 4500-N
Oak Ridge National Laboratory
P. O. Box X
Oak Ridge, Tennessee 37830

Note that a cost of <u>approximately</u> $40.00 will be charged to recover the costs of materials, handling, and mailing. The signed agreement document serves as our authority to bill your organization. This will be done after the program is mailed to you.

REQUEST FORM FOR EPACA COMPUTER PROGRAM

Return form to: Computer Librarian
Room A228, Building 4500-N
Oak Ridge National Laboratory
P. O. Box X
Oak Ridge, Tennessee 37830

The source program, in card image form, will be sent to you on a magnetic tape.

Please check the option below which comes closest to meeting your system's requirements as to tape format. Tapes will be prepared in advance in these two standard formats. Your request for the program can be met more quickly if you can accept one of these standard formats.

_____ Option 1: 7-track tape
BCD card code
556 bpi density
Unblocked records (84 characters per physical record, with last four characters blank)

_____ Option 2: 9-track tape
EBCDIC card code
800 bpi density
Blocked records (800 characters, or ten cards, per physical record)

If you require modifications to the option checked above, please indicate them below.

character code _____ BCD _____ EBCDIC

density _____ 200 _____ 556 _____ 800

physical record size _____

Note: Our 9-track tape drives are all 800 bpi density.

What type of computer will be used to read the tape?_____

On what type of computer will the program be executed?_____

Name and address of requester:_____

_____

_____

_____

_____

Phone number of requester: _____

Signed:_____ Date:_____

AGREEMENT FOR
USE OF STRUCTURAL ANALYSIS
COMPUTER PROGRAM EPACA

WHEREAS, Union Carbide Corporation, acting under its Prime Contract W-7405-eng-26 with the United States of America (Government) as represented by the United States Atomic Energy Commission (Commission), in operating and managing the Government-owned facility identified as the Oak Ridge National Laboratory entered into Subcontract No. 3535 with The Franklin Institute for the development of a special elastic-plastic-creep structural analysis computer program identified as EPACA; and

WHEREAS, it is one of the objectives of the Commission to provide the liquid-metal fast-breeder reactor component manufacturers and other interested Commission approved parties with a well-documented, non-proprietary structural analysis computer program to be used by said recipients on their own computers; and

WHEREAS, it is a further objective that all corrections, changes, and modifications should be incorporated in an up-to-date master computer program to be made available by the Oak Ridge National Laboratory to all interested aforementioned manufacturers and other Commission approved parties;

NOW, THEREFORE, in consideration of Union Carbide Corporation making the Computer Program EPACA available to _____(Recipient) on a non-exclusive, royalty-free basis, the recipient agrees to furnish the Oak Ridge National Laboratory with any changes, corrections, modifications or updating the recipient makes to the Computer Program, for incorporation in a current master computer program to be made available by the Oak Ridge National Laboratory to all Commission approved parties.

The recipient further agrees not to withhold or classify as proprietary any of said corrections, changes, modifications and alterations to the Computer Program and hereby grants to the Government an irrevocable, non-exclusive, royalty-free license to use the same for any purpose whatsoever.

It is understood that the recipient will be billed for a handling and mailing charge of approximately Forth Dollars ($40.00) due Union Carbide Corporation for the account of the Government. The exact cost will be determined by Commission cost recovery guidelines applicable at the time of the request.

Date_____ Name_____

Title_____

Representing_____

Address_____

4.3. Simplified Inelastic Piping System Analysis Computer Program PIRAX

G. H. Workman
E. C. Rodabaugh
Battelle-Columbus Laboratories

A specialized computer program to be known as PIRAX is being developed to perform inelastic flexibility analyses of piping systems. A primary objective of this effort is to develop a method which is simple enough to be used in routine design work on critical high-temperature piping systems. The program is to be based on simplified, but understood, descriptions of the elastic-plastic and creep behavior of the material and on somewhat less than a completely rigorous inelastic analysis treatment of critical piping components such as elbows and tees. The program will permit a quantitative, but approximate, assessment of piping deflections and reactions to be made on an economical basis. As a part of the development program, a simple piping system is to be tested at elevated temperatures to provide data for comparison with predictions of the computer program.

During this reporting period, the form of the mathematical representation of the isochronous stress-strain behavior has been tentatively fixed. This representation is:

$$\varepsilon = \frac{\sigma}{E} + k_p \left\{ \frac{\sigma}{\sigma_{op}} \right\}^m \tag{4.1}$$

where

ε = strain

σ = stress

E = elastic modulus

k_p = nominal plasticity strain

σ_{op} = nominal plasticity strength

m = plasticity exponent.

The present plan is for the form of the creep/relaxation behavior to remain as described previously. That is, only secondary creep will be explicitly represented.

This assumed behavior allows most of the development for the creep/relaxation solution to be transferred directly to a psuedo elastic-plastic type analysis by using isochronous stress-strain curves. Also, this representation is similar to that given by the well-known Ramberg-Osgood[15] formulation:

$$\frac{\varepsilon}{\varepsilon_y} = \frac{\sigma}{\sigma_y}\left\{1 + \left|\frac{\sigma}{\sigma_y}\right|^{r-1}\right\} \tag{4.2}$$

where

ε = strain

σ = stress

ε_y, σ_y, r = material and temperature dependent coefficients.

Equations (4.1) and (4.2) are directly related through the following relationships:

$$E = \frac{\sigma_y}{\varepsilon_y}$$

$$k_p = \varepsilon_y$$

$$\sigma_{op} = \sigma_y$$

$$m = r \ .$$

An example of the application of Eq. (4.1) along with the creep/relaxation solution already formulated for a cantilever beam with a constant end displacement (relaxation) and a constant end force (creep) is given to demonstrate the techniques to be followed for the completion of this phase. First assume the material is type 304 stainless steel at a temperature of 1100°F. Figure 4.10, a reproduction of Fig. 7A-7 from Code Case 1331-7, Interpretations of ASME Boiler and Pressure Vessel Code,[16] contains the pertinent isochronous stress-strain relationships. If it is assumed that the application of the load/displacement will require 100 hours, then the proper curve can be approximated. The resulting elasto-plastic equation is also given in Fig. 4.10, along with its plot to show its approximation to the actual curve. The secondary creep parameters for the creep/relaxation behavior were taken from data given by U.S. Steel Corporation.[17]

ORNL-DWG-73-10381

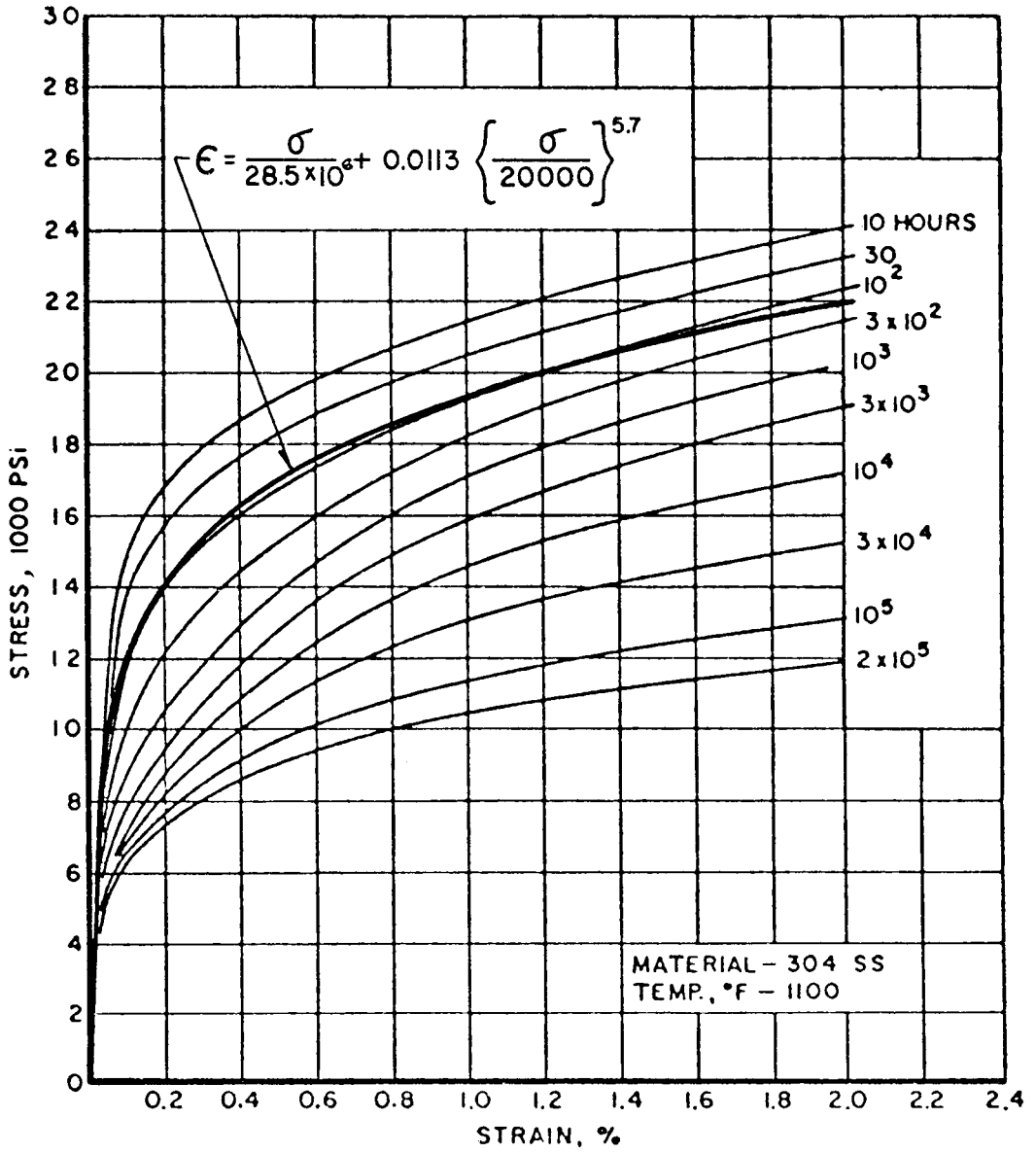

Fig. 4.10. Stress-strain curves for type 304 stainless steel at 1100°F.

Utilizing small deflection-beam bending assumptions, a solution can be formulated. These solutions are illustrated in Fig. 4.11 for the relaxation analysis and Fig. 4.12 for the creep analysis. Within each analysis, two cases were evaluated. One corresponded to an end displacement/end force ratio for a maximum elastic stress of 10,000 psi, while the other was for a maximum elastic stress of 20,000 psi. The cantilever beam was assumed to be 4-in., sched-40, pipe with a length of 100 in.

The elasto-plastic portion is plotted as a fraction of the applied end displacement for the relaxation analysis and as a fraction of the applied end force for the creep analysis. Note that the time-dependent portion of the plot really begins at 100 hours in these cases.

The incorporation of the elasto-plastic behavior into the basic spatially three-dimensional digital computer program will begin next month and it is estimated that it will require the rest of this calendar year to complete. It is anticipated that within a month the mathematical formulation will have progressed to the point where strain accumulations are predicted within the formulation.

In the experimental phase, definite progress has been made within the last month. All of the parts of the test specimen (including the elbow) have been completed and are now being carefully measured before final annealing and welding. The annealing will be performed by ORNL.

ORNL-DWG-73-10382

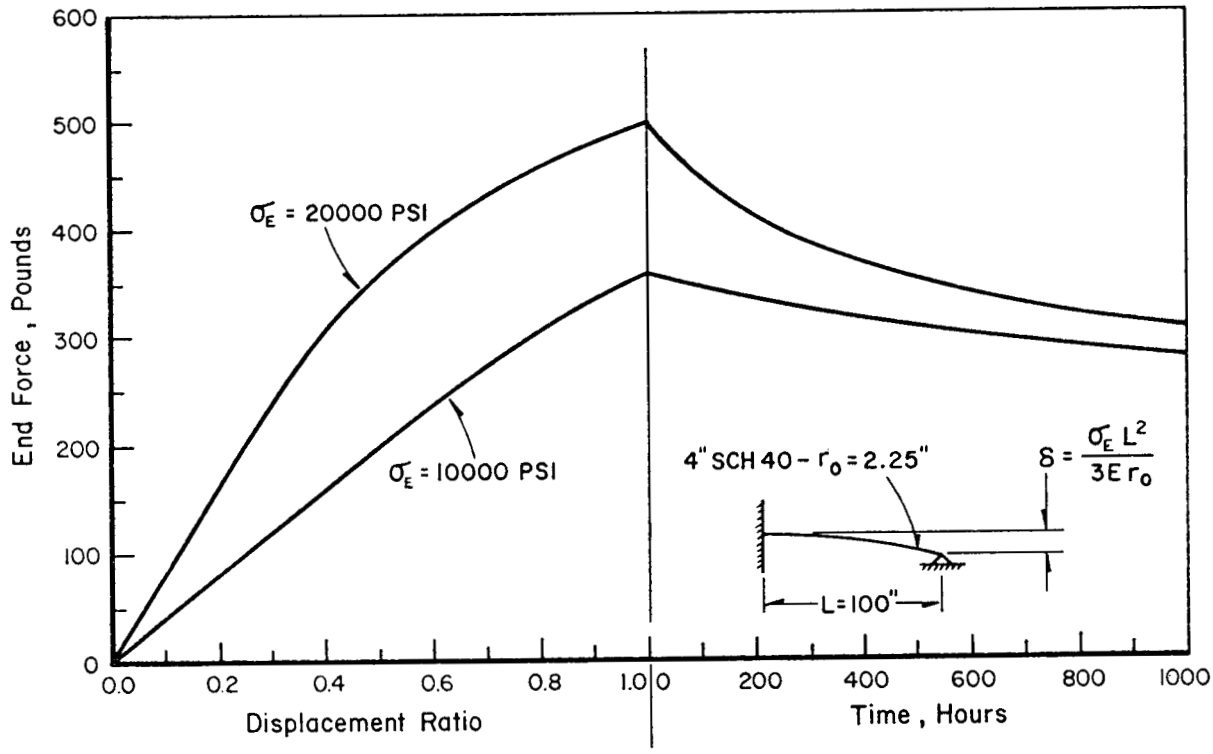

Fig. 4.11. Cantilever-beam relaxation analysis results.

ORNL-DWG-73-10383

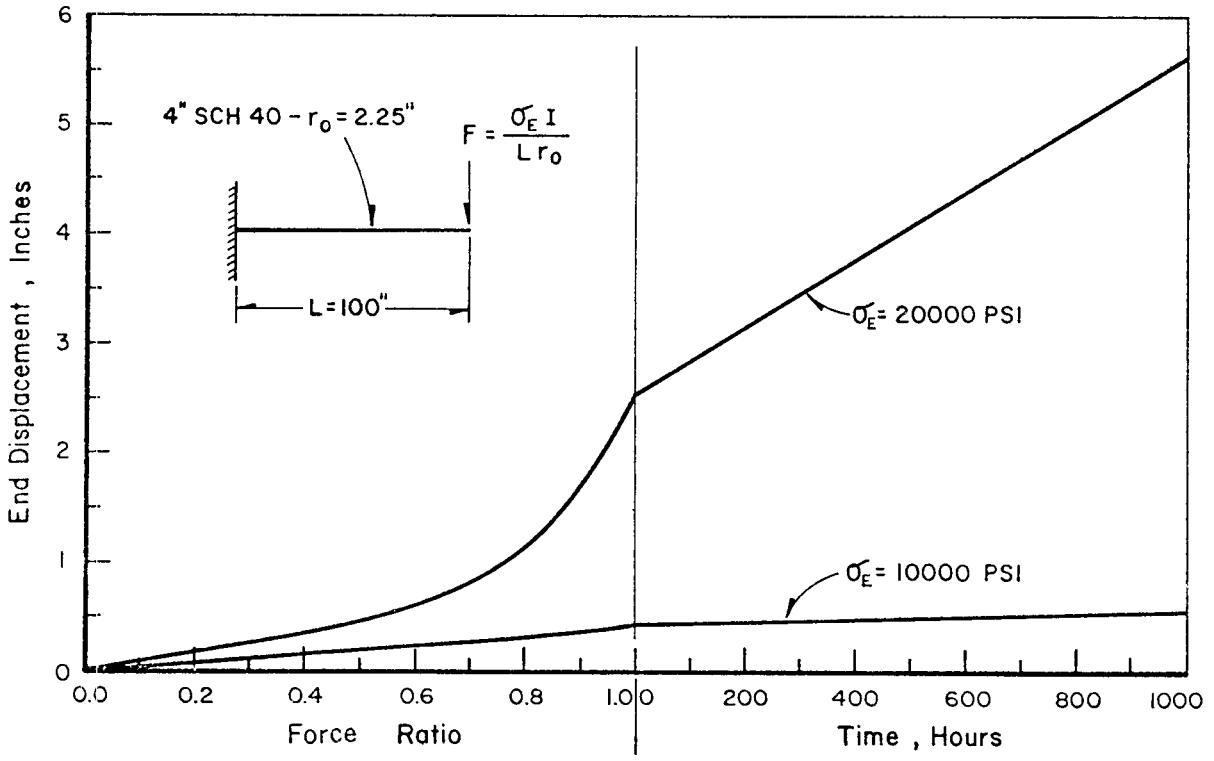

Fig. 4.12. Cantilever-beam creep analysis results.

5. INELASTIC STRUCTURAL TESTS

J. M. Corum

Elevated-temperature inelastic structural tests, or preparations for tests, are currently underway for six different types of simple structures: simply supported beams, simply supported circular plates, capped circular-cylindrical shells, finite-width plates with a circular hole, stiffened shear-lag panels, and straight pipes subjected to thermal ratchetting conditions. Results and/or progress on each of these six types of tests are reported in the following sections. Included, in some cases, are discussions of inelastic analyses of the structures and comparisons of predicted behavior with test results.

5.1. Elastic-Plastic-Creep Tests and Analyses of Simply Supported Beams

5.1.1. Status of test work (J. M. Corum, M. Richardson)

Two beam tests, B7 and B8, which were deflection controlled, have been completed. These tests were conducted at a temperature of 1100°F and they used beams from the reference heat (9T2796) of type 304 stainless steel. The beams were each 1 in. thick, 2 in. high, and 26 in. long. They were simply supported on 24 in. centers and loaded at the midpoint. Typical test results are given in the following subsection.

Preparations for the next two tests, B9 and B10, are currently underway. These tests will be load controlled and will be exact duplicates of tests B5 and B6. The purpose of these two duplicate tests is to examine the reproducibility of the structural test data. The two load controlled tests, B9 and B10 (or B5 and B6), and the two deflection controlled tests, B7 and B8, will provide a useful package of test results with which the design analyst can evaluate his inelastic analysis techniques. Complete results from these four tests will be presented in a topical report.

In our load-controlled tests, the load is maintained during the creep portion of the test using dead weights. Mechanical friction build up and random sudden release has been a source of difficulty during these extended

test periods. Consequently, a load trimming device has been added to the control system. The trimmer senses a change in the output from the load cell and, by means of a current-to-air converter, adjusts to the correct load using a small pneumatic ram. With this device, the load can be maintained to ±10 lb.

Some effort has been made to determine the reliability of the sheathed chromel-alumel thermocouples which have been used in all of our beam and plate tests. New, calibrated couples used for each test produce the most reliable data. It was found that the inherent inhomogeneity of the thermocouple leads precludes reuse of the couples once they have been at 1100°F for extended periods of time and then removed. To date, reannealing of the used thermocouples has not produced satisfactory results. Currently we are investigating the possibility of using platinum-rhodium thermocouples as a more economical means of measuring temperature.

5.1.2. Results of beam tests B7 and B8 and comparison with analytical predictions (J. M. Corum, M. Richardson, and J. A. Clinard)

The loading histories for beams B7 and B8 are shown in Fig. 5.1. Both beams were subjected to an imposed center deflection of 0.10 in. during the initial creep, or relaxation, period; this was followed by a step decrease in center deflection to −0.10 in. for the second creep period. Both beams were subjected to a short-time cyclic loading, between fixed deflection limits, at the end of the creep test. The significant difference in the two tests was that beam B8 was subjected to ten short-time cycles, between fixed deflection limits prior to the initial creep period while beam B7 was not. A saw-tooth deflection pattern with a period of 2 min. was used for the short-time cyclic loadings. All of the remaining deflection changes were applied in 30 sec per quarter cycle and followed a ramp pattern.

Instrumentation for beams B7 and B8 consisted of seven DCDT's and seven dial gages for transverse deflection measurements, ten thermocouples, and four Ailtech (Microdot) SG425 strain gages.

The measured temperature ranges, over the middle 16 in. of the beam length, are shown in Figs. 5.2 and 5.3 for various times during beam tests B7 and B8, respectively. The temperatures during test B7 very nearly met our

ORNL-DWG-73-10385

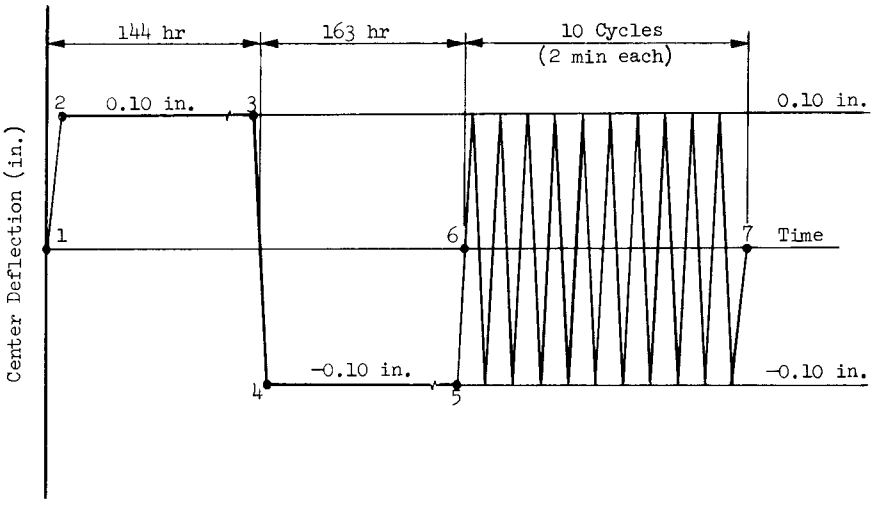

(a) BEAM TEST B7

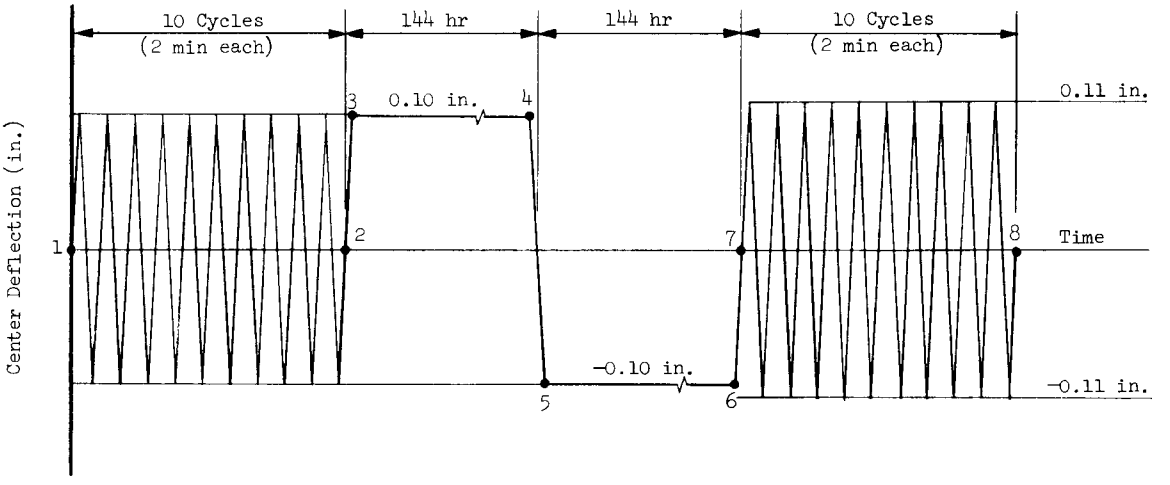

(b) BEAM TEST B8

Fig. 5.1. Loading histories for elevated-temperature beam tests B7 and B8.

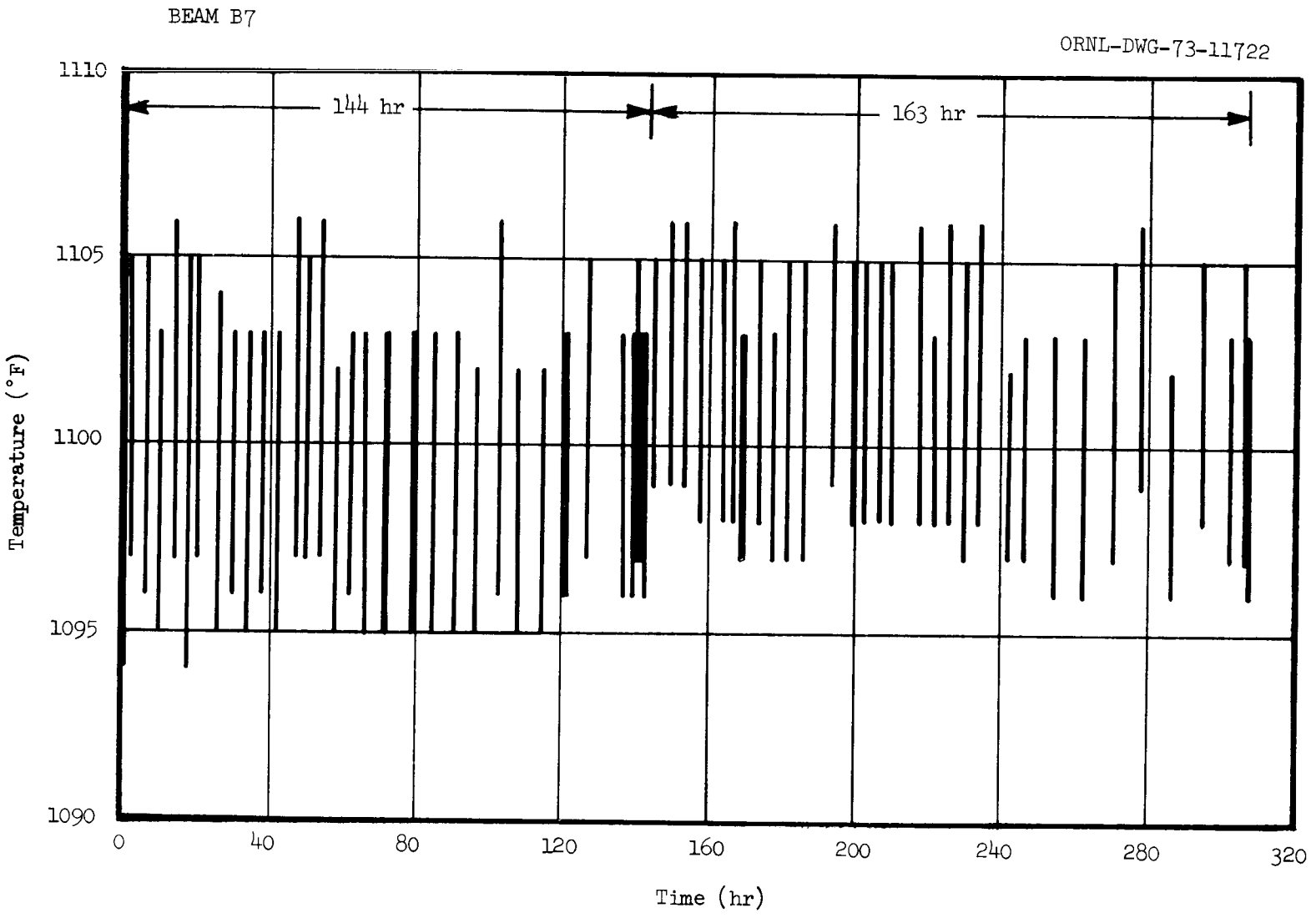

Fig. 5.2. Measured temperature range over middle 16 in. of beam B7 during 1100°F test.

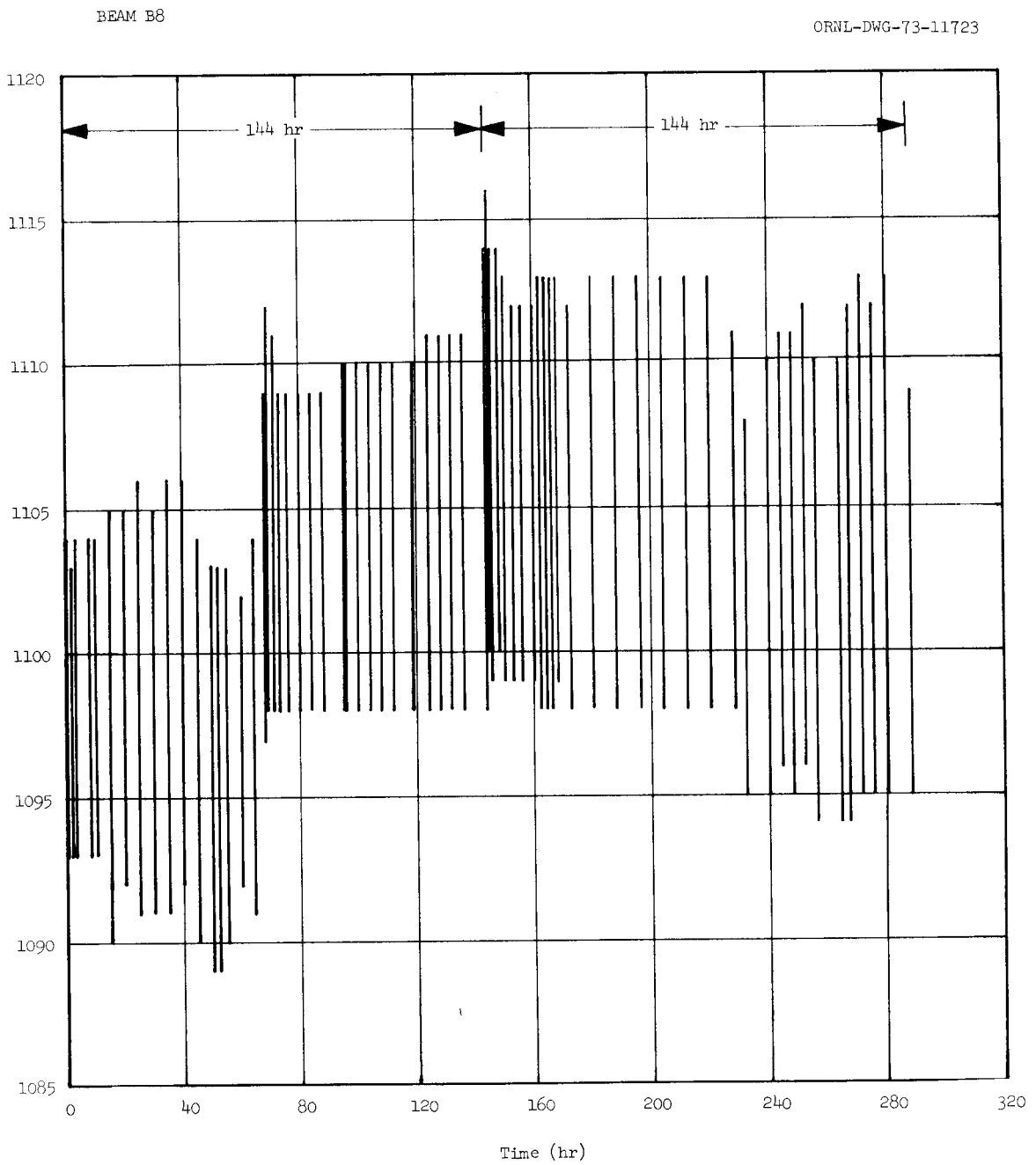

Fig. 5.3. Measured temperature range over middle 16 in. of beam B8 during 1100°F test.

ultimate goal for temperature control. We are striving for temperature variations in our structural tests of less than ±5°F both spatially and with time.

The results of test B7 are typified by the plots of measured center load versus center deflection shown in Figs. 5.4, 5.5, and 5.6 for the various portions of the loading history. Each figure also contains, for comparison, the predictions of an elastic-plastic-creep finite element analysis using the CREEP-PLAST computer program. The finite element mesh used was the same as in previous beam analyses that have been reported (see, for example, Ref. 18). A bilinear representation of the cyclic stress-strain curve for a strain range of 0.4% was used, and for all plastic loadings subsequent to the first, the tenth cycle representation was used. The material properties used were identical to those used for the bilinear analysis of plate CP1, as described in Refs. 19 and 20.

The measured center load is shown as a function of deflection in Fig. 5.4 for the initial loading to a center deflection of 0.10 in. (points 1 to 2), for the hold period at constant deflection (points 2 to 3), for the reversed loading to −0.10 in. (points 3 to 4), for the subsequent hold period at constant deflection (points 4 to 5), and finally for the loading back to zero deflection (points 5 to 6). In this deflection controlled situation, the agreement between measured results and predictions is good.

Figure 5.5 shows the load relaxation as a function of time during the hold periods at constant center deflection. Here the total load relaxation is reasonably well predicted by the analysis, although the predicted drop in load is not initially as large as the measured drop. This disagreement is due in part to the fact that the uniaxial creep law underpredicts the very steep initial portions of the actual measured uniaxial creep response of the material (see, for example, Fig. 4.15 of Ref. 19).

Figure 5.6 shows the results of the ten post-creep cycles between the fixed center deflection limits of ±0.1 in. The analysis results shown are for one partial post-creep cycle. The prediction represents the measured data reasonably well.

The agreement between the measured results and the predictions shown in Figs. 5.4, 5.5, and 5.6 is noticeably better than in previous load-controlled tests. This was not unexpected, and it is significant because

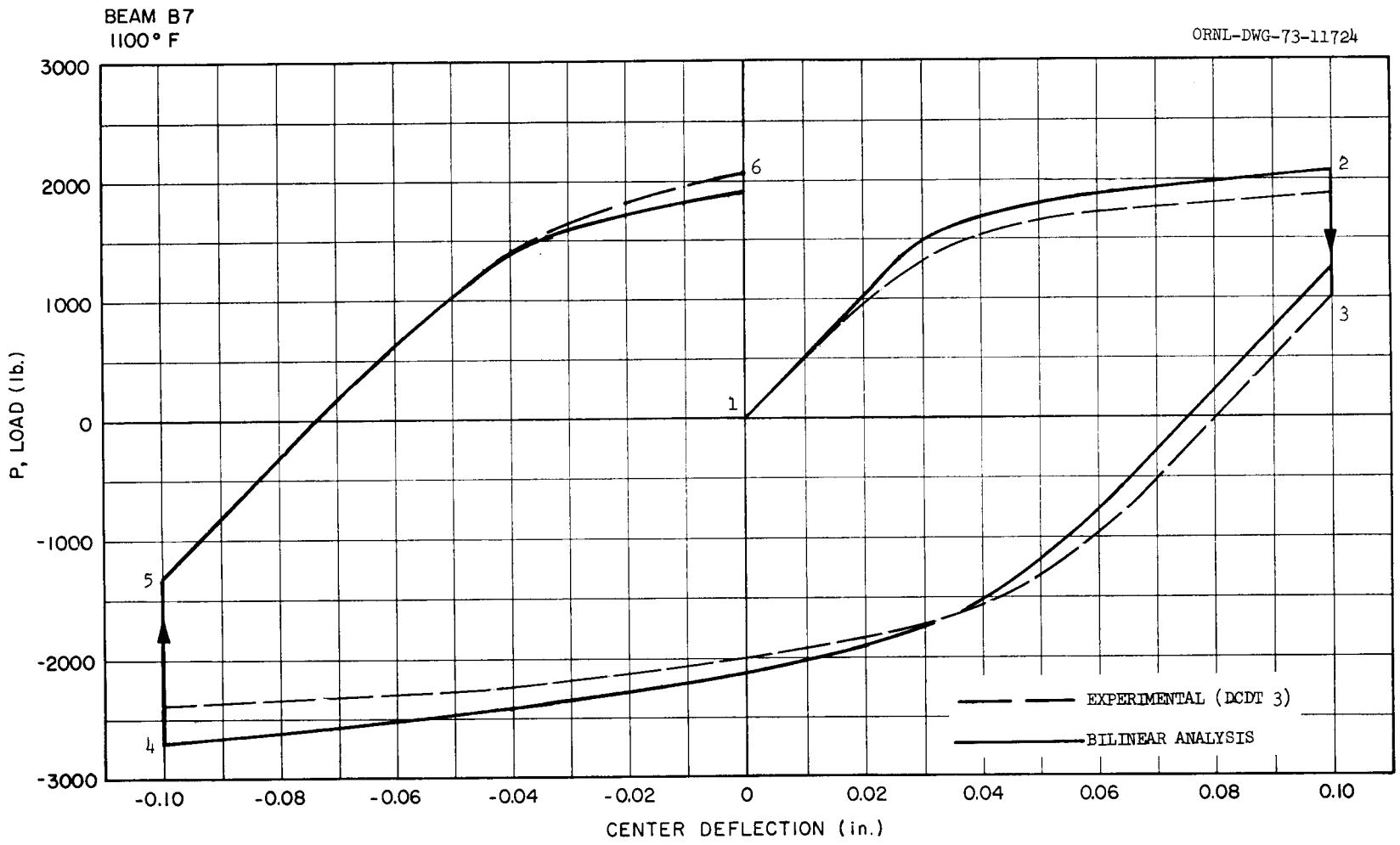

Fig. 5.4. Comparison of measured and predicted load-deflection behaviors for deflection changes associated with relaxation portions of beam B7 test. Numbered points correspond to points numbered on loading history diagram (Fig. 5.1a).

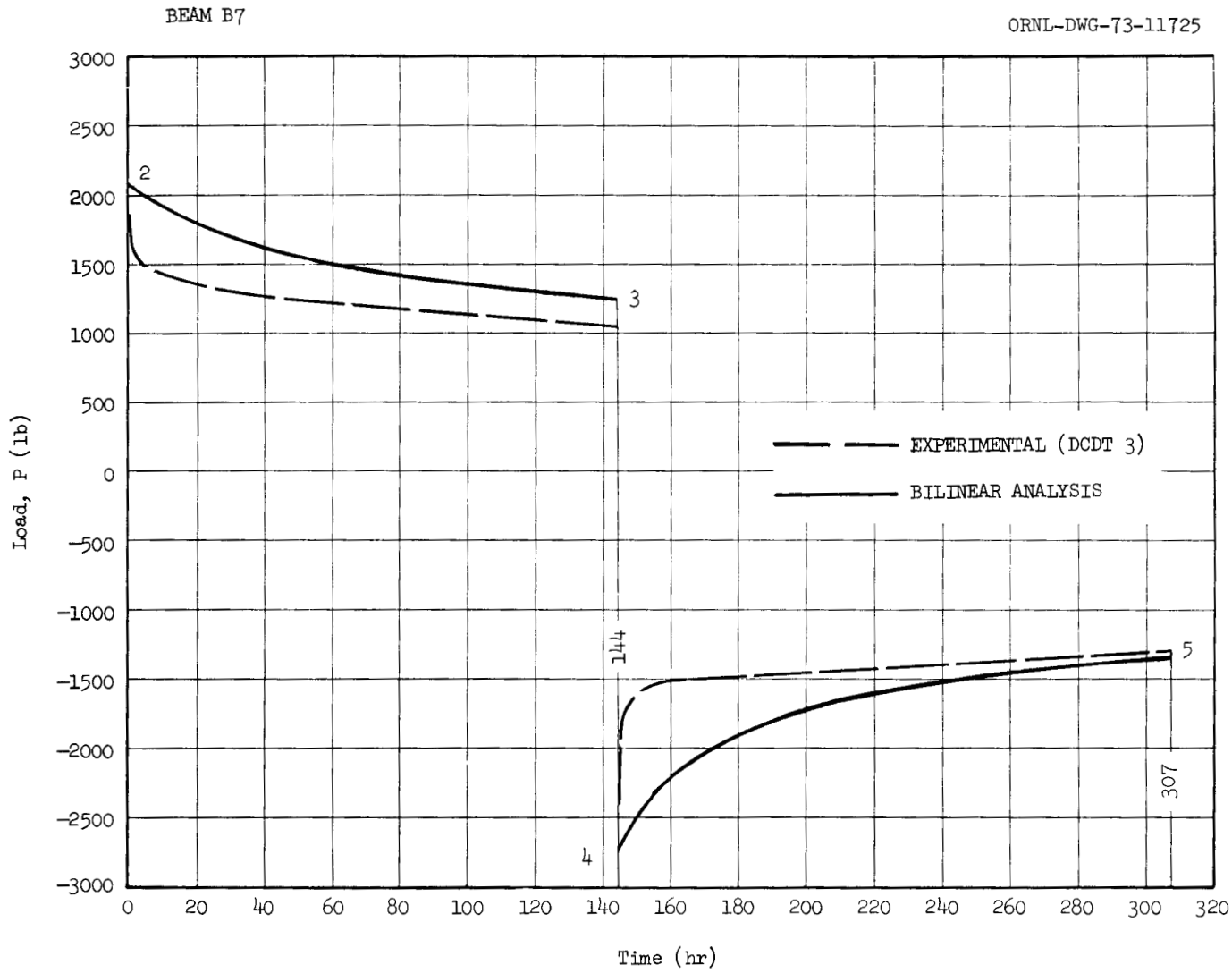

Fig. 5.5. Comparison of measured and predicted load relaxation versus time for beam B7. Numbered points correspond to points numbered on loading history diagram (Fig. 5.1a).

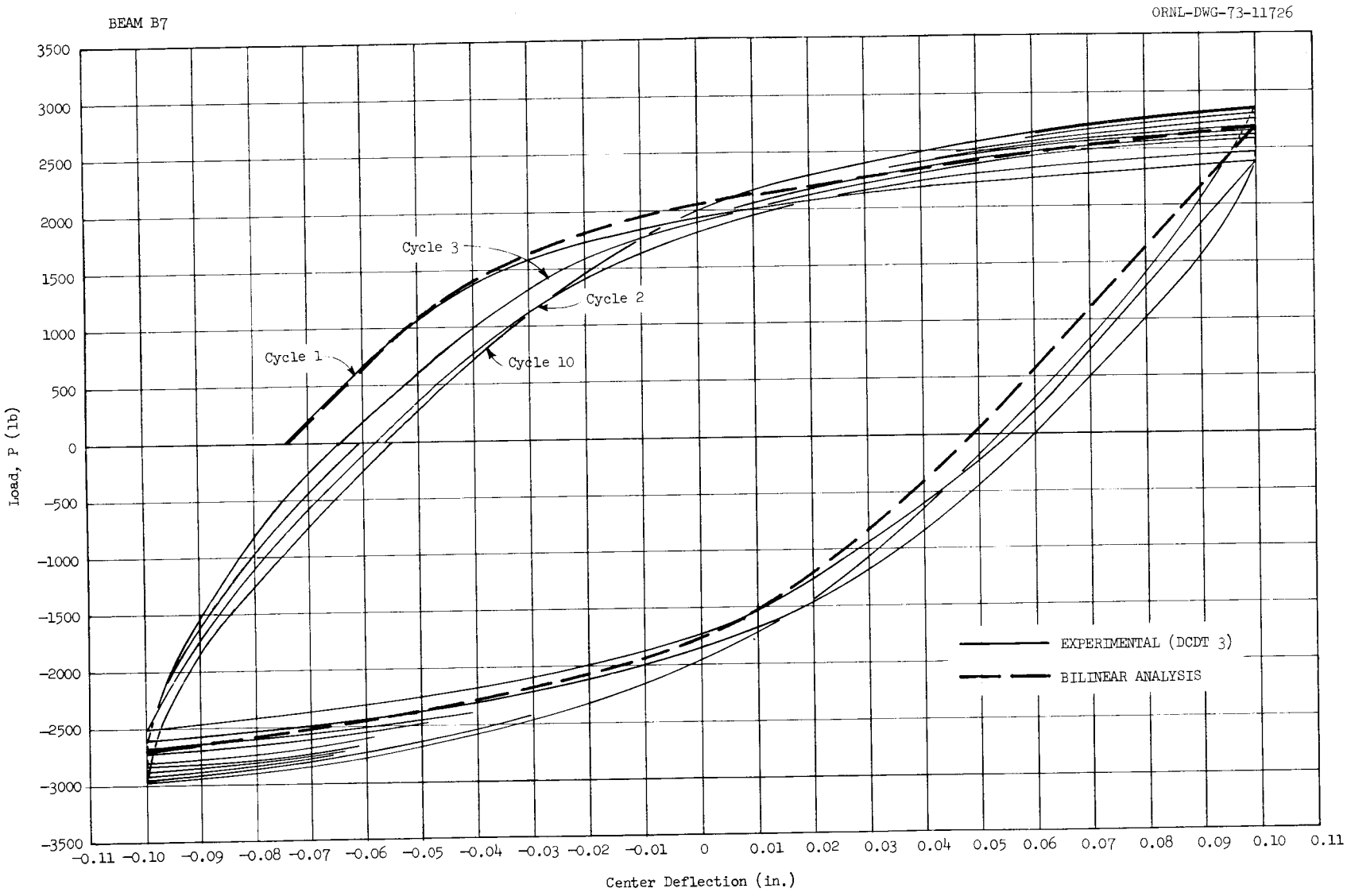

Fig. 5.6. Measured load-deflection behavior during ten short-time post-relaxation cyclic loadings of beam B7. Analytical predictions are shown for a part of the first cycle. Note that this plot overlaps the plot shown in Fig. 5.4.

most inelastic loadings in actual structural situations are largely deformation controlled. Note that the analytical predictions were based exactly on the methods recommended in Appendix A of RDT Standard F9-1T.[21]

The test results for beam B8 are typified by the load-center deflection plots in Figs. 5.7 through 5.10. Figure 5.7 shows the results for the ten pre-creep cycles between the fixed center deflection limits of ±0.1 in. Note the significant cyclic hardening that occurs. Figures 5.8, 5.9, and 5.10 for beam B8 are analogous to Figs. 5.4, 5.5, and 5.6 for beam B7. Comparison of the corresponding figures in the two sets shows the effects of the prior cyclic hardening in beam B8.

5.1.3. Cyclic hardening bilinear analysis of beam B6 (W. K. Sartory)

In the preceding progress report[22] the experimentally determined behavior of the cyclicly loaded beam B6, which was tested at 1100°F, was compared with the results of a number of elastic-plastic analyses. An additional analysis of beam B6 has now been carried out using a new cyclic hardening bilinear representation of the plastic behavior which was described in Section 2.1 of this report. A typical uniaxial cyclic curve obtained using this representation is shown in Fig. 5.11. The behavior predicted for beam B6 for the first and second cycles of loading between ±2000 lb is shown in Figs. 5.12 and 5.13. The beam appears to be harder than predicted for the first reverse loading, but otherwise the agreement is reasonably good.

5.2. Elastic-Plastic-Creep Tests of Simply Supported Circular Plates

J. M. Corum
M. Richardson

Two deflection controlled elevated-temperature elastic-plastic-creep circular plate tests CP3 and CP4, have been completed. These two tests were very similar to beam tests B7 and B8 described in the previous section. They were conducted at a temperature of 1100°F and they used plates from the reference heat (9T2796) of type 304 stainless steel. The plates were each

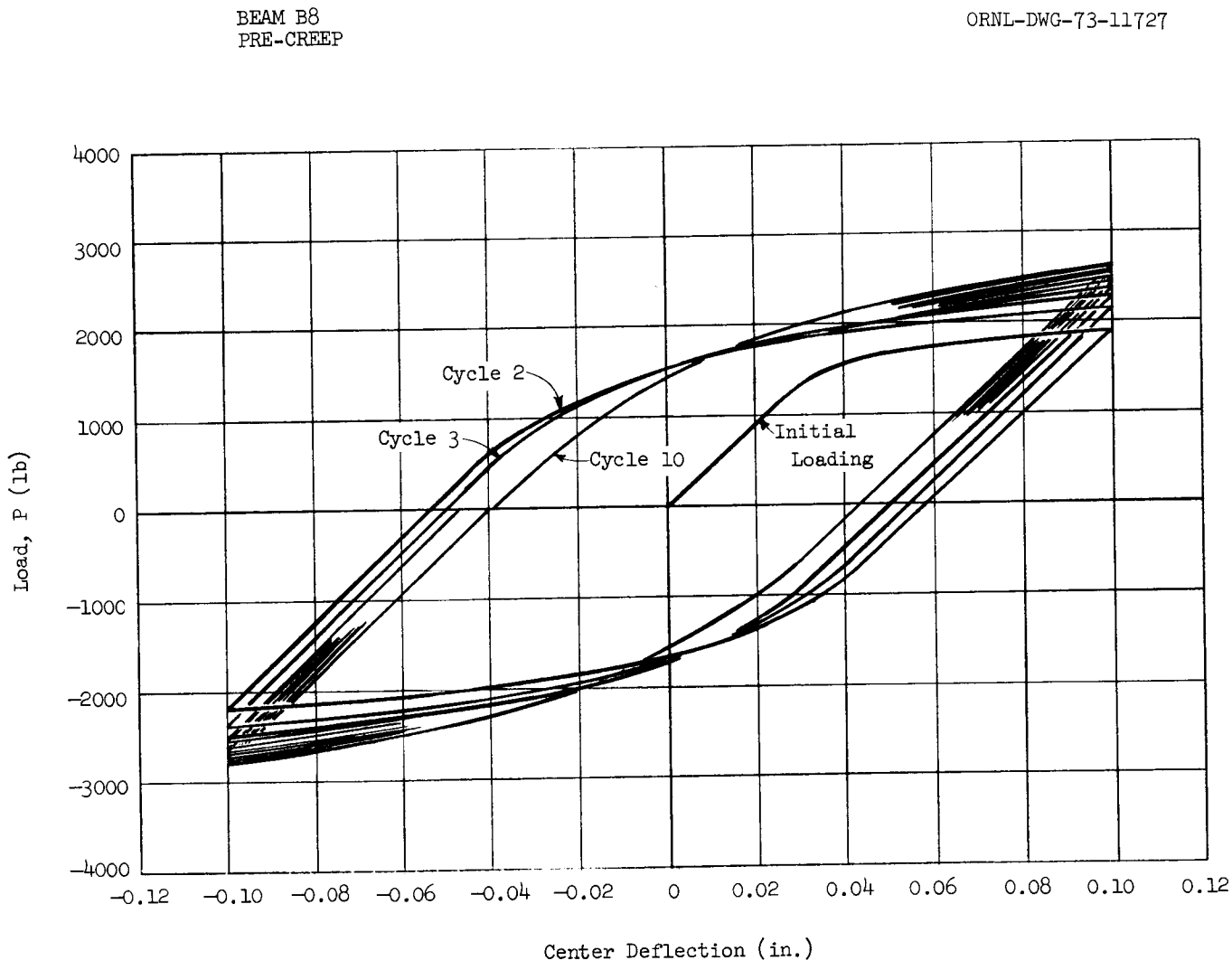

Fig. 5.7. Measured load-deflection behavior during ten short-time pre-relaxation cyclic loadings of beam B8.

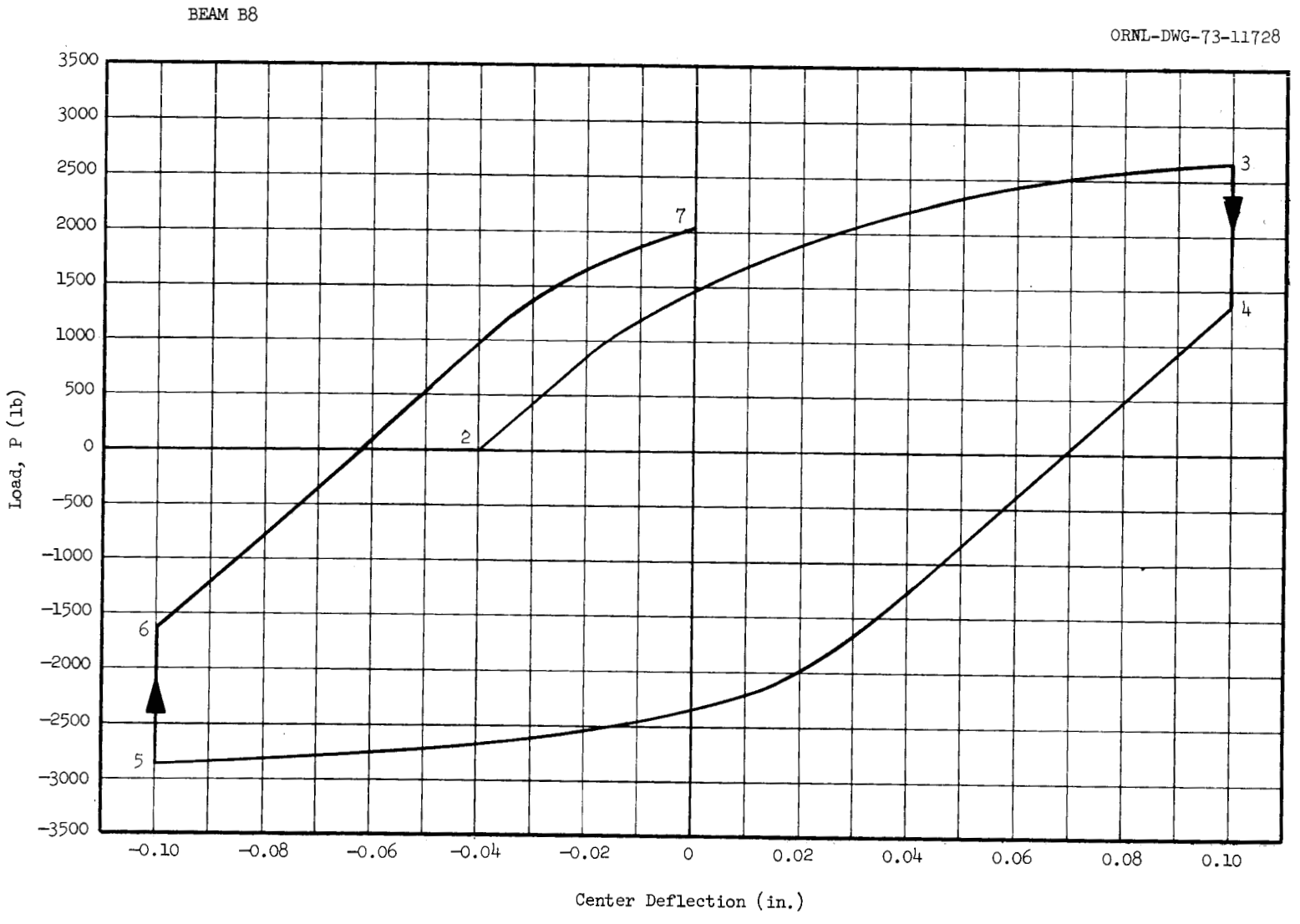

Fig. 5.8. Measured load-deflection behavior for deflection changes associated with relaxation portions of beam B8 test. Numbered points correspond to points numbered on loading history diagram (Fig. 5.1b).

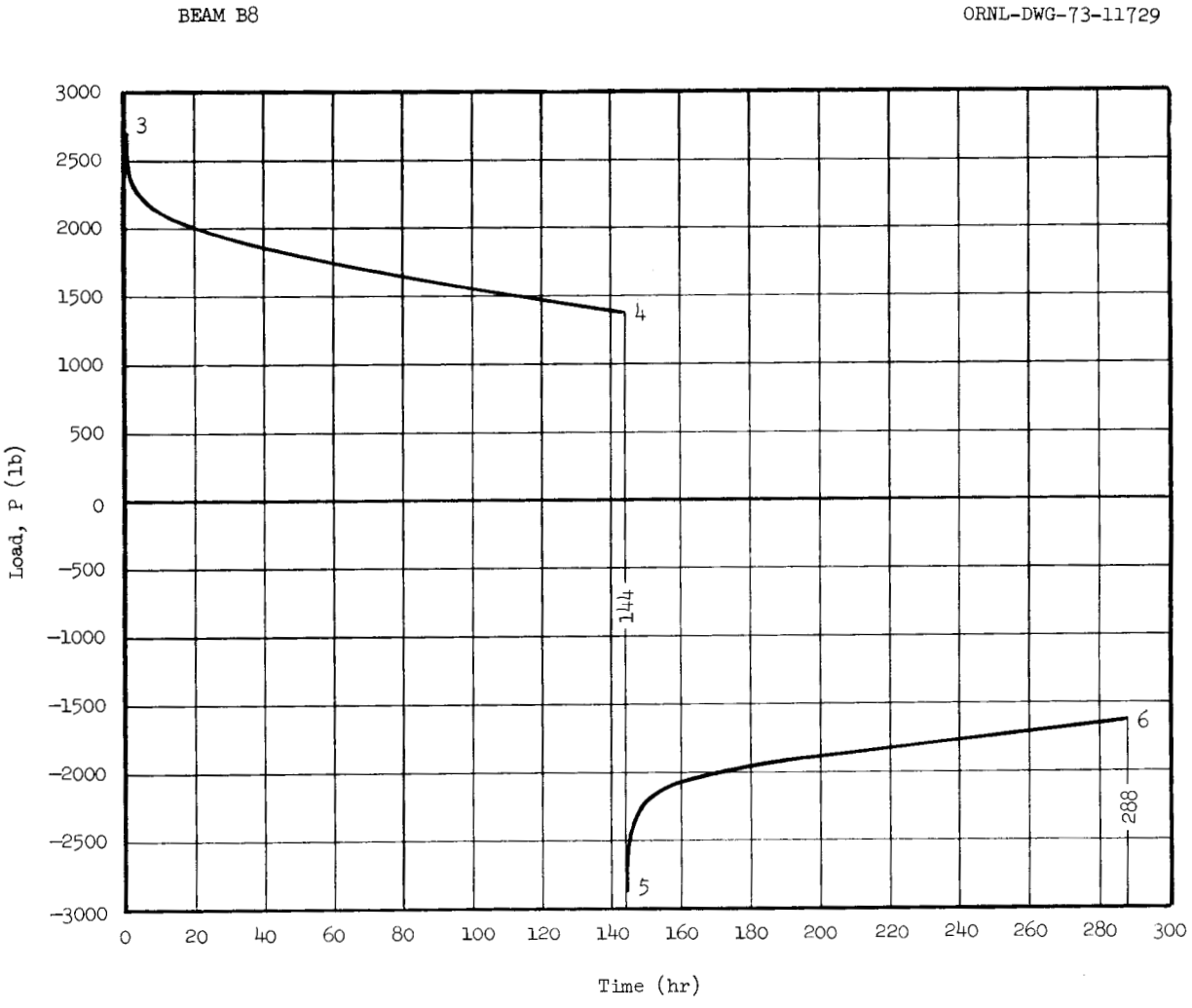

Fig. 5.9. Measured load relaxation versus time for beam B8. Numbered points correspond to points numbered on loading history diagram (Fig. 5.1b).

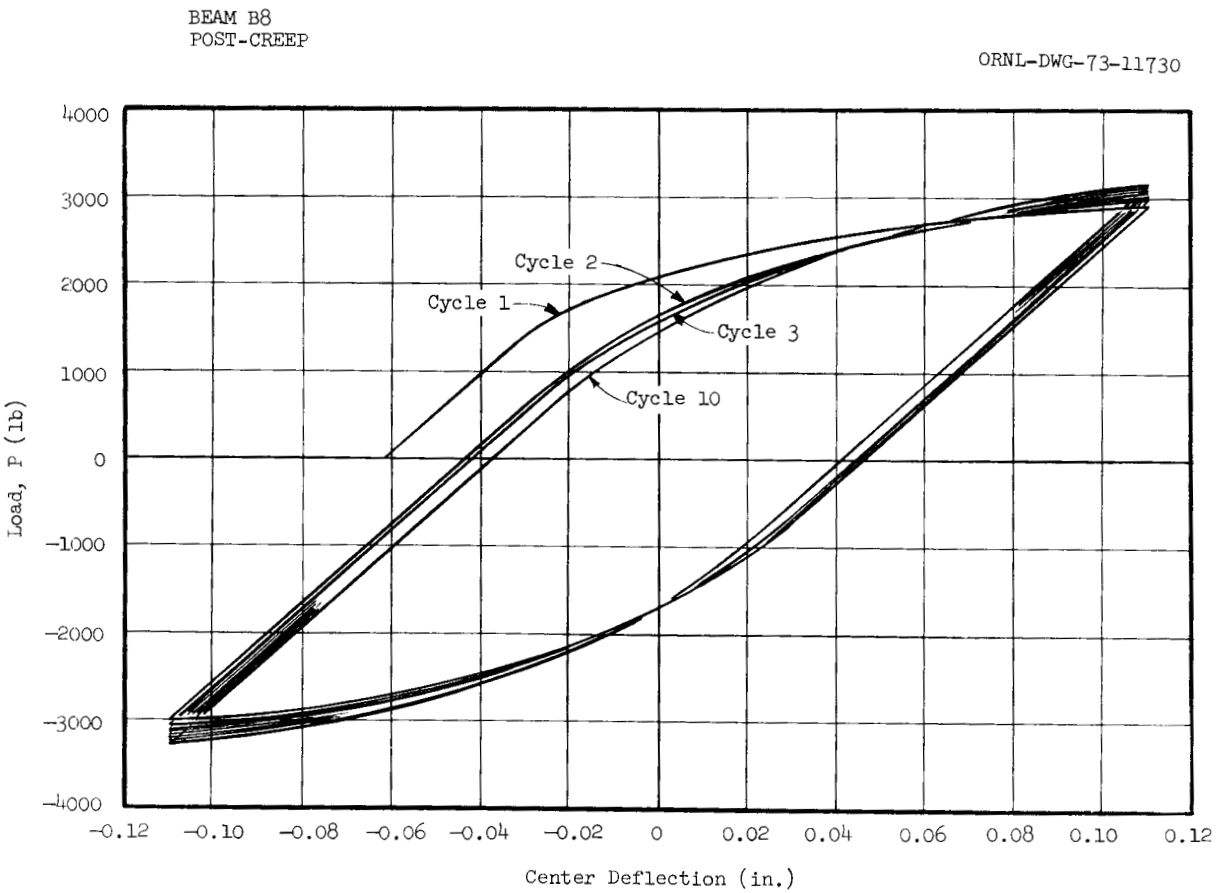

Fig. 5.10. Measured load-deflection behavior during ten short-time post-relaxation cyclic loadings of beam B8.

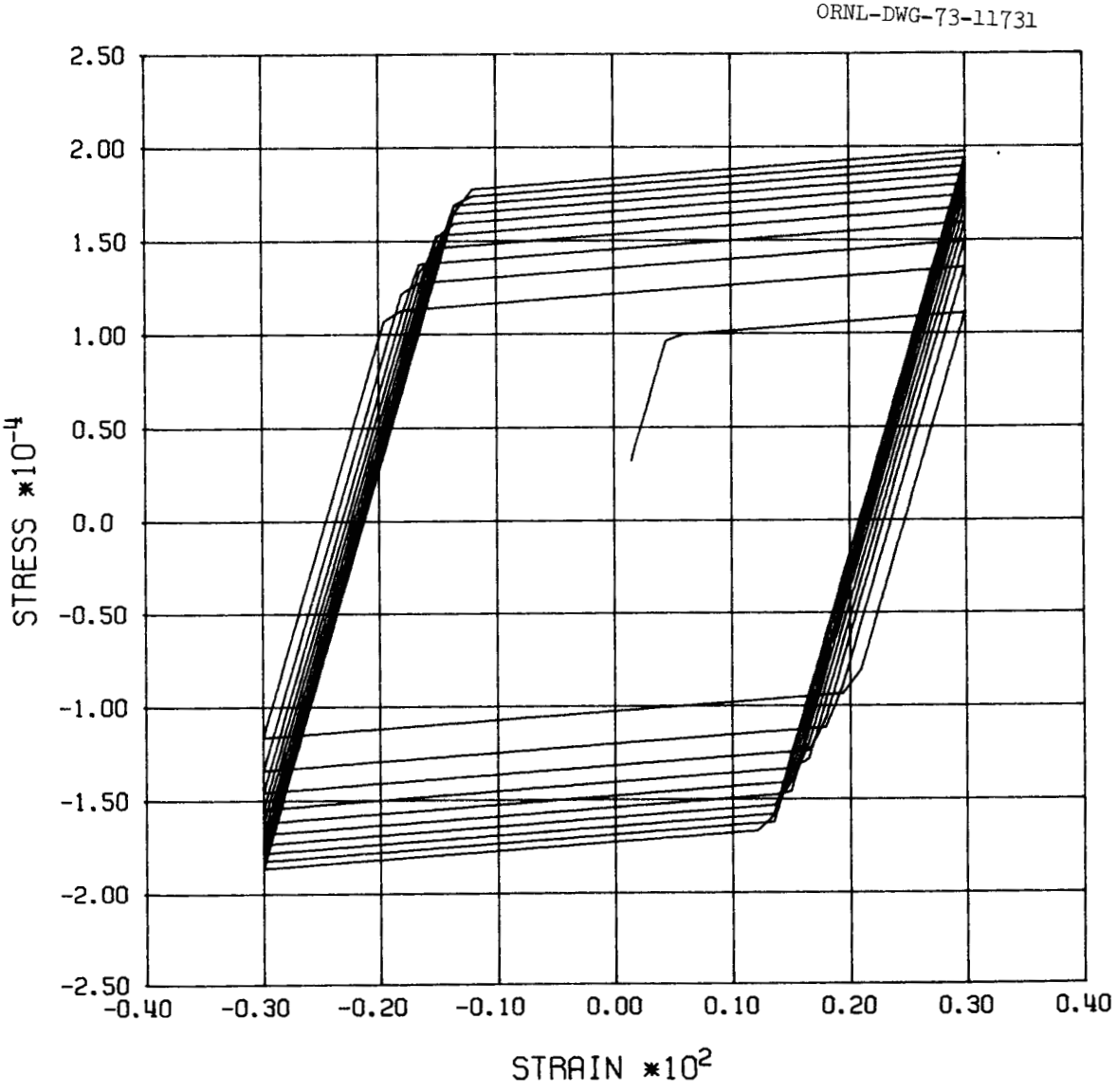

Fig. 5.11. Typical uniaxial cyclic stress-strain curve bilinear plasticity representation.

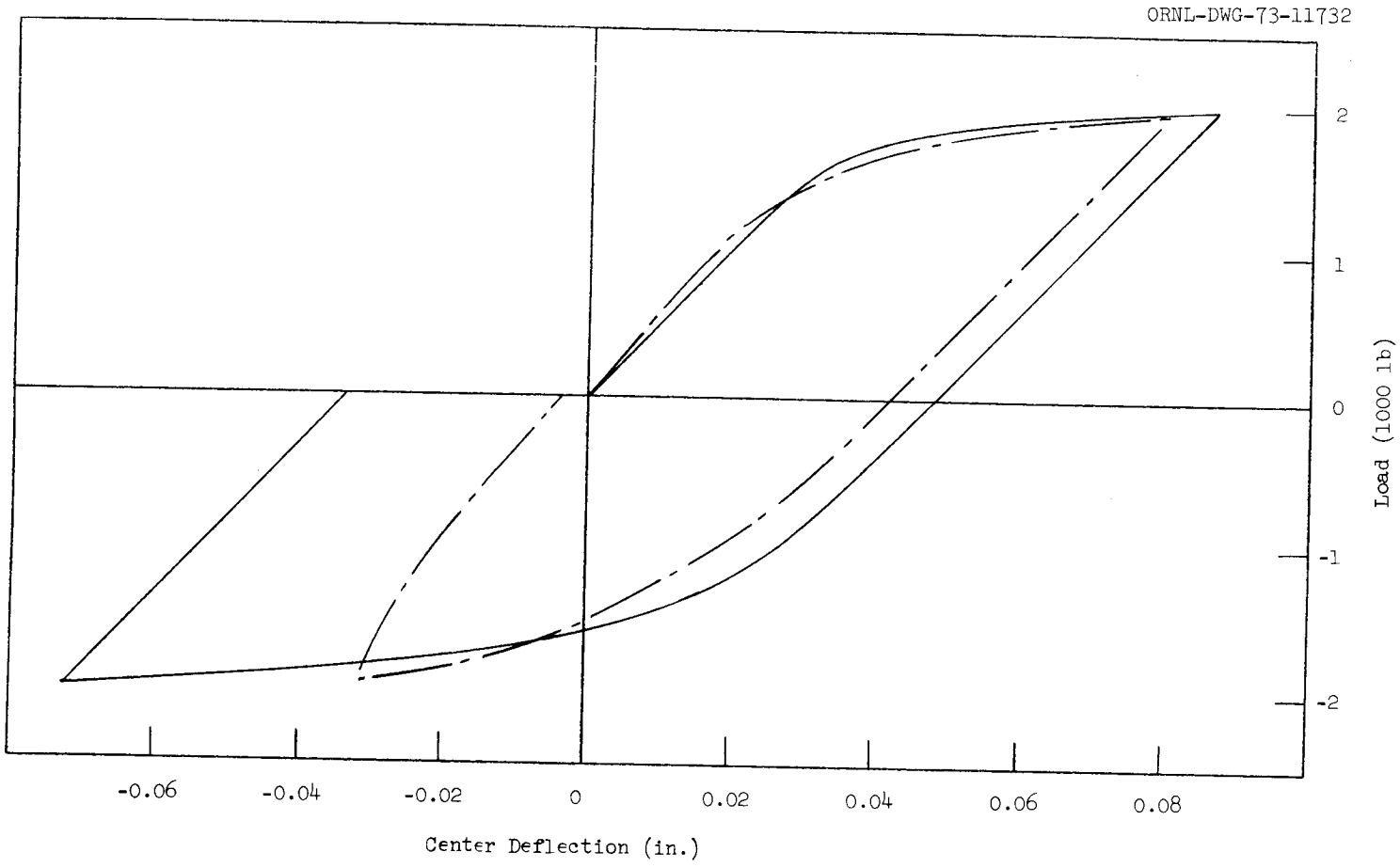

Calculated with cyclic hardening bilinear plasticity

Experimental

Fig. 5.12. Comparison of measured and predicted load versus center deflection response for the first elastic-plastic loading cycle of beam B6 at 1100°F.

ORNL-DWG-73-11733

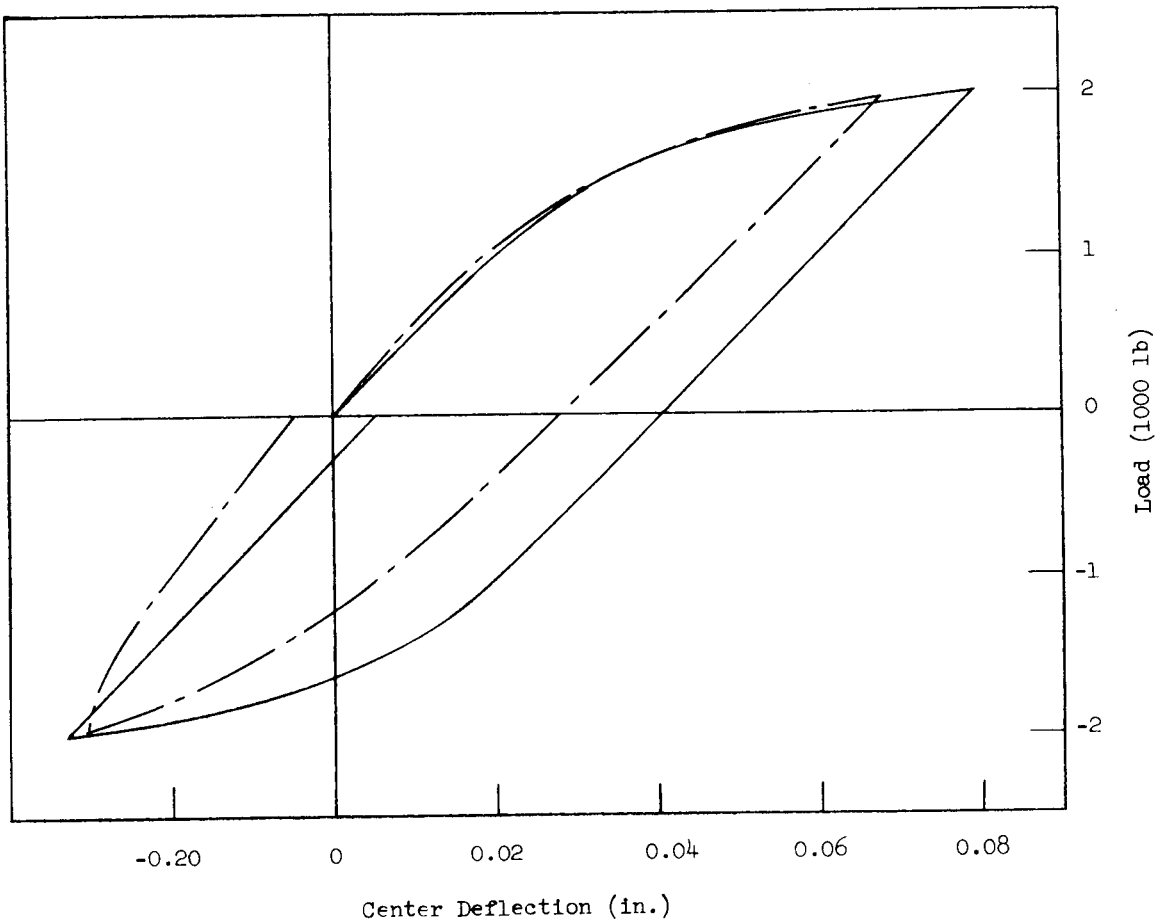

——— Calculated with cyclic hardening bilinear plasticity

— — — Experimental

Fig. 5.13. Comparison of measured and predicted load versus center deflection response for the second elastic-plastic loading cycle of beam B6 at 1100°F.

20.75 in. in outside diameter and 0.50 in. thick. They were loaded at the center through a bass, and they were simply supported on a 20.0 in. diameter circle. The geometry of the plates and the instrumentation used is identical to that shown in Fig. 5.12 of Ref. 23.

The loading histories for plates CP3 and CP4 are shown in Fig. 5.14. Both plates were subjected to an imposed center deflection of 0.11 in. during the initial creep, or relaxation, period; this was followed by a step decrease in center deflection to −0.11 in. for the second creep period. Both plates were subjected to a short-time cyclic loading, between fixed deflection limits, at the end of the creep test. The significant difference in the two tests was that plate CP3 was subjected to ten short-time cycles, between fixed deflection limits, prior to the initial creep period while plate CP4 was not. A saw-tooth deflection pattern with a period of 2 min. was used for the short-time cyclic loadings. All of the remaining deflection changes were applied in 30 sec per quarter cycle and followed a ramp pattern.

The measured temperature ranges over the middle 13.5 in. of a single diameter are shown in Figs. 5.15 and 5.16 for various times during plate tests CP3 and CP4, respectively. The temperatures in test CP3 were well within our goal of 1100 ± 5°F, while the temperature in test CP4 occasionally became locally hotter than 1105°F by 2 or 3°F.

The results of tests CP3 and CP4 are typified by plots of the measured center load versus center deflection analogous to those presented in the previous section for beams B7 and B8. The results for CP3 are shown in Fig. 5.17 through 5.20. Figure 5.17 shows the results for the ten pre-creep cycles between the fixed center deflection limits of ±0.11 in. The measured center load is shown as a function of deflection in Fig. 5.18 for the initial loading to a center deflection of 0.11 in. (points 2 to 3), for the hold period at constant deflection (points 3 to 4), for the reversed loading to −0.11 in. (points 4 to 5), for the subsequent hold period at constant deflection (points 5 to 6), and finally to the loading back to zero deflection (points 6 to 7).

Fig. 5.19 shows the load relaxation as a function of time during the hold periods at constant center deflection. Finally Fig. 5.20 shows the measured results for the ten post-creep cycles between the fixed center deflection limits of 0.11 in.

ORNL-DWG-73-11734

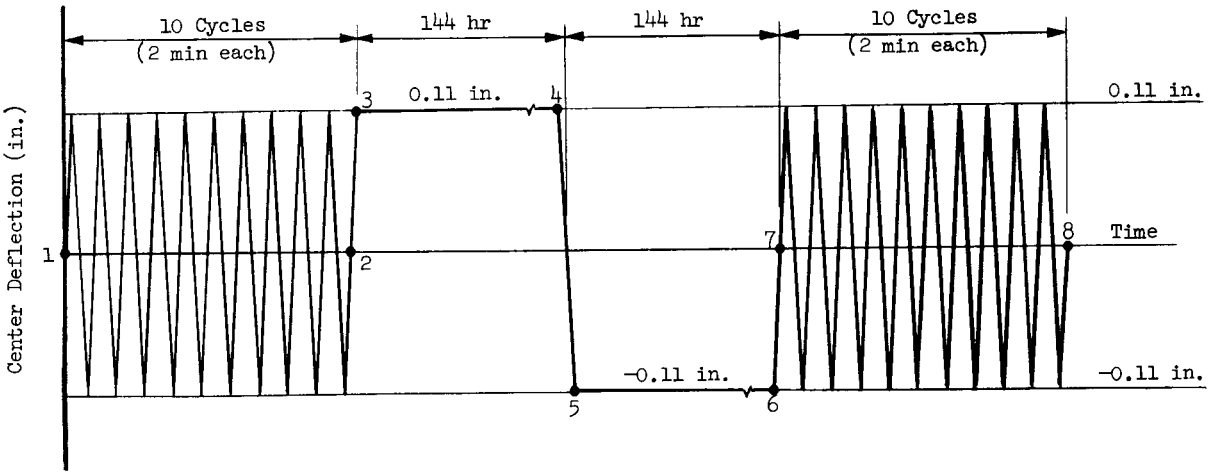

(a) PLATE TEST CP3

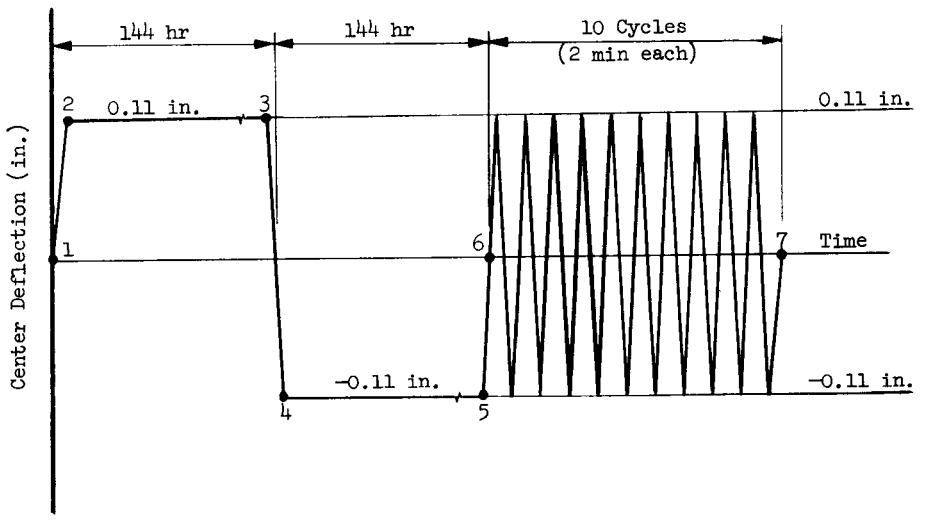

(b) PLATE TEST CP4

Fig. 5.14. Loading histories for elevated-temperature circular plates tests CP3 and CP4.

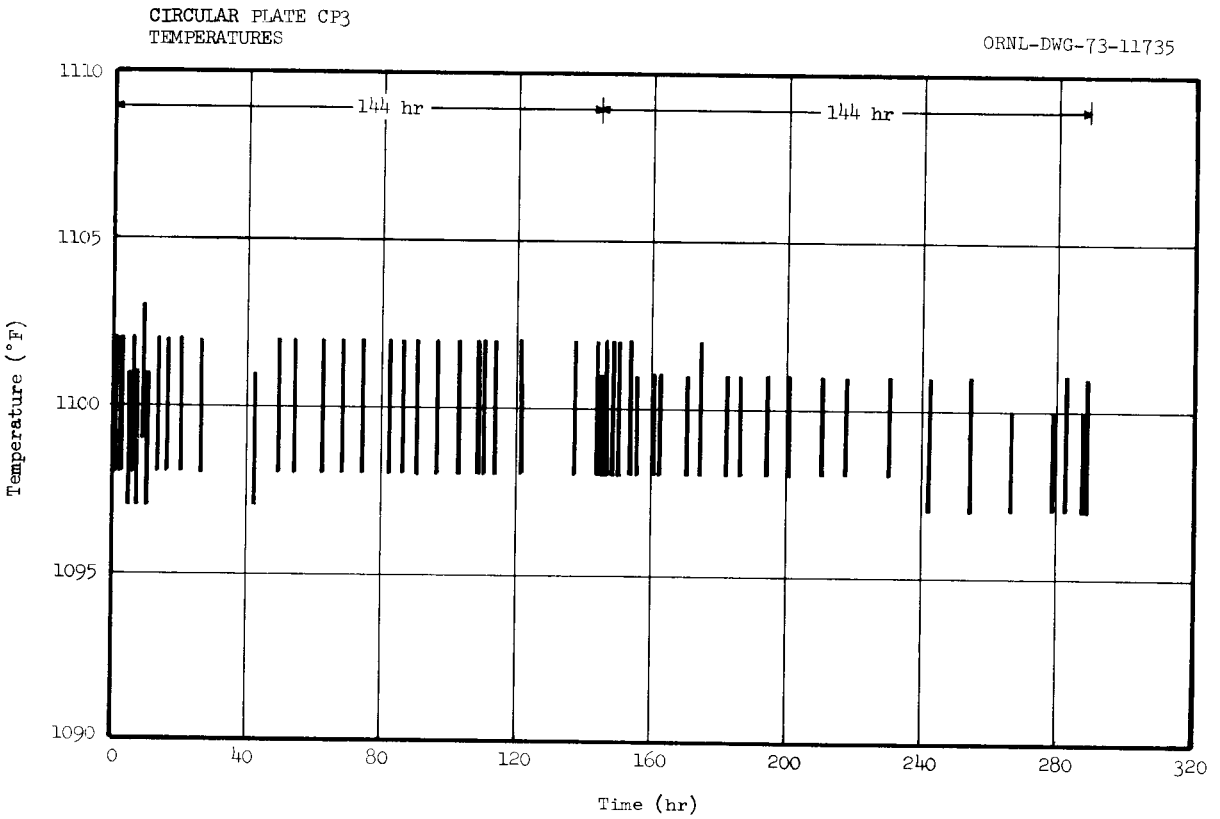

Fig. 5.15. Measured temperature range over middle 13.5 in. of a single diameter of plate CP3 during 1100°F test.

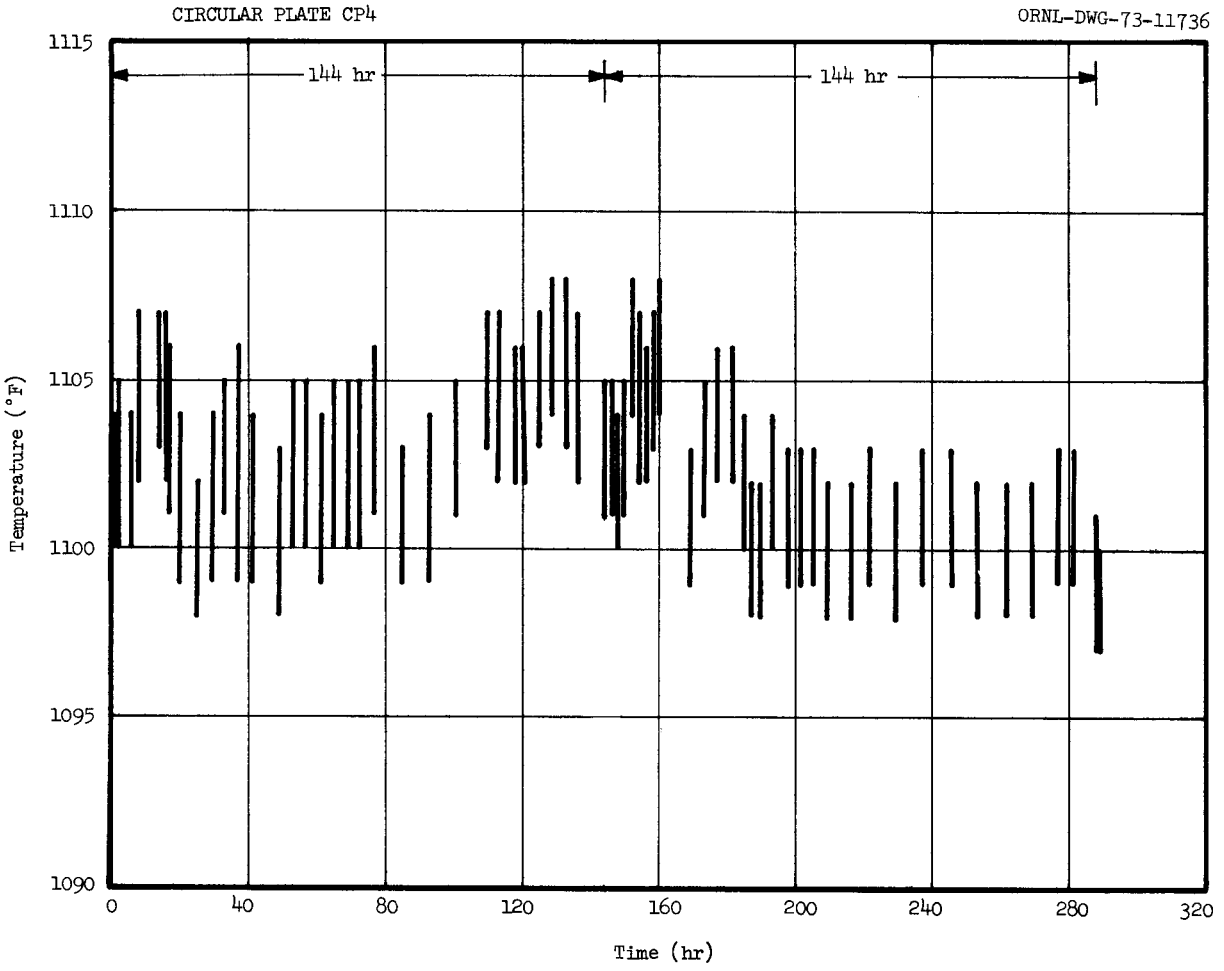

Fig. 5.16. Measured temperature range over middle 13.5 in. of a single diameter of plate CP4 during 1100°F test.

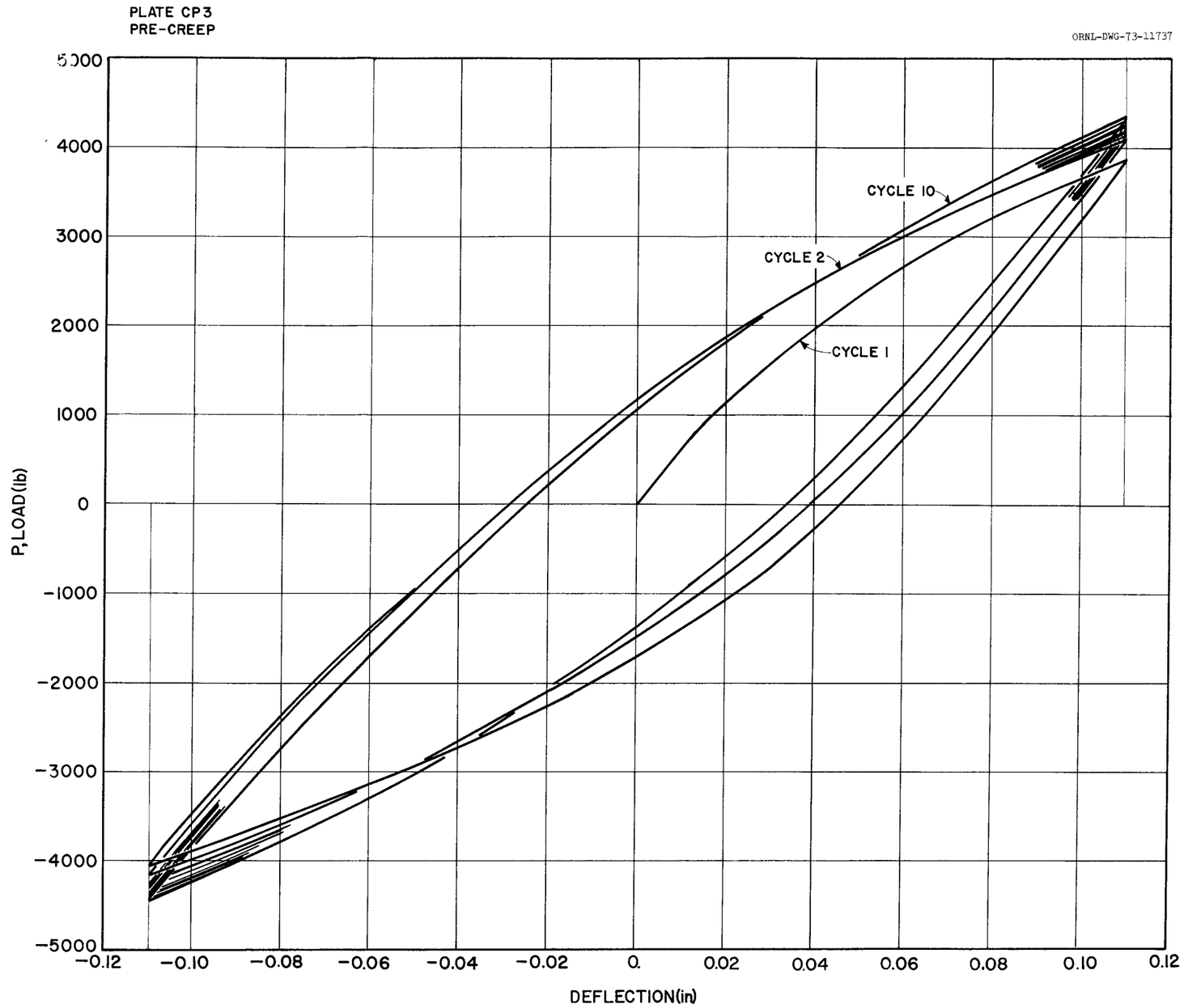

Fig. 5.17. Measured load-deflection behavior during ten short-time pre-relaxation cyclic loadings of plate CP3.

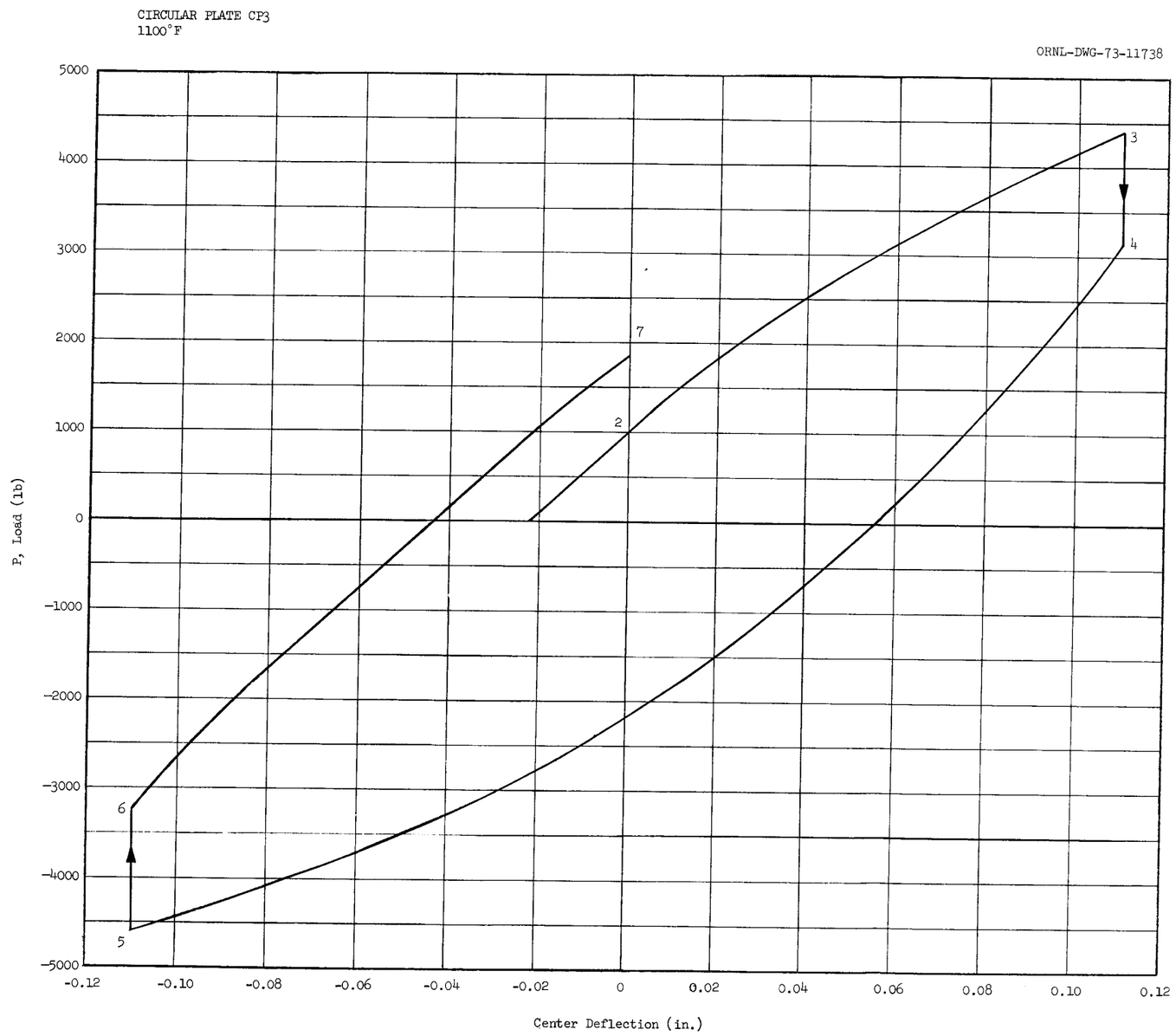

Fig. 5.18. Measured load-deflection behavior for deflection changes associated with relaxation portions of plate CP3 test. Numbered points correspond to points numbered on loading history diagram (Fig. 5.14a).

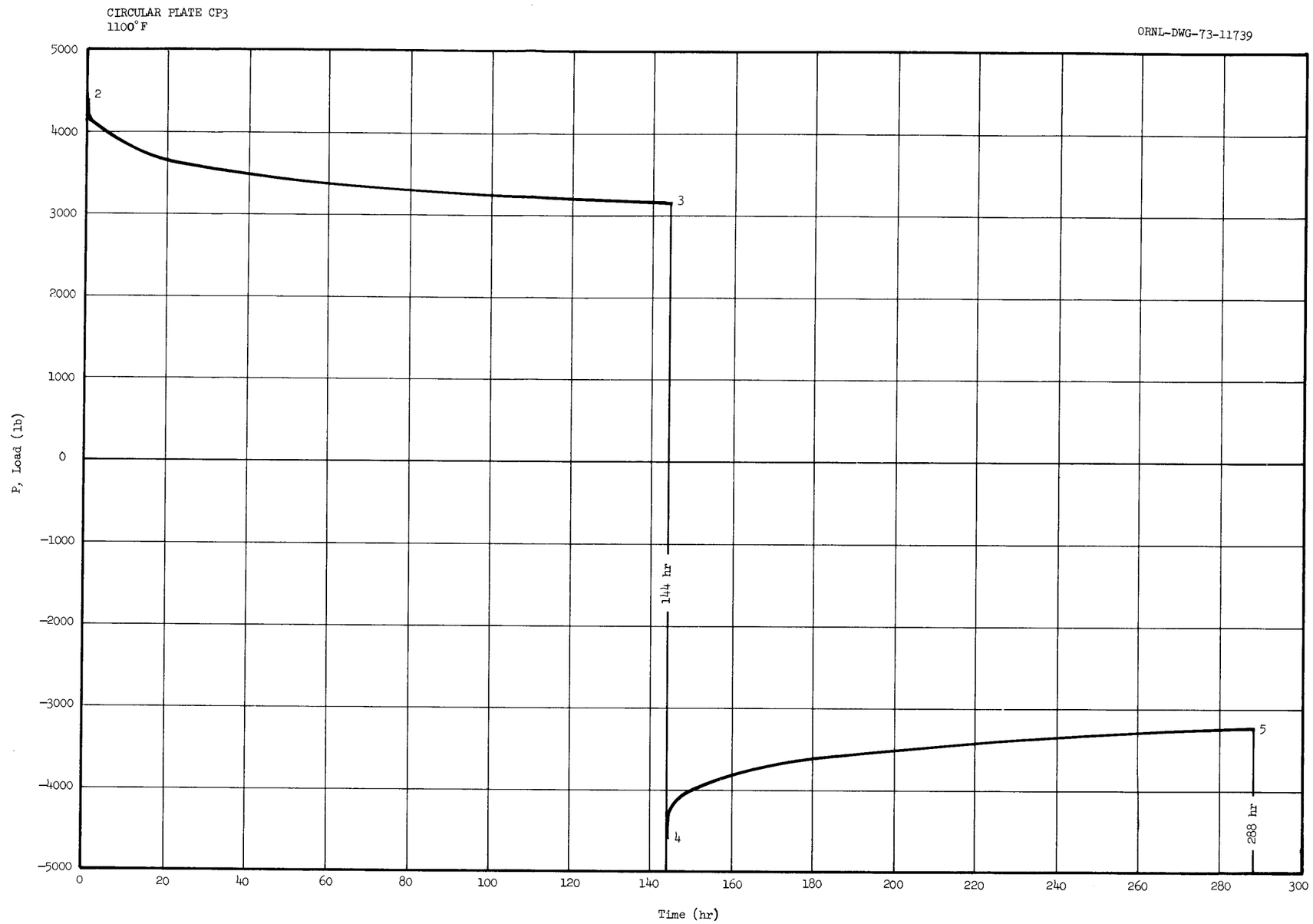

Fig. 5.19. Measured load relaxation versus time for plate CP3. Numbered points correspond to points numbered on loading history diagram (Fig. 5.14a).

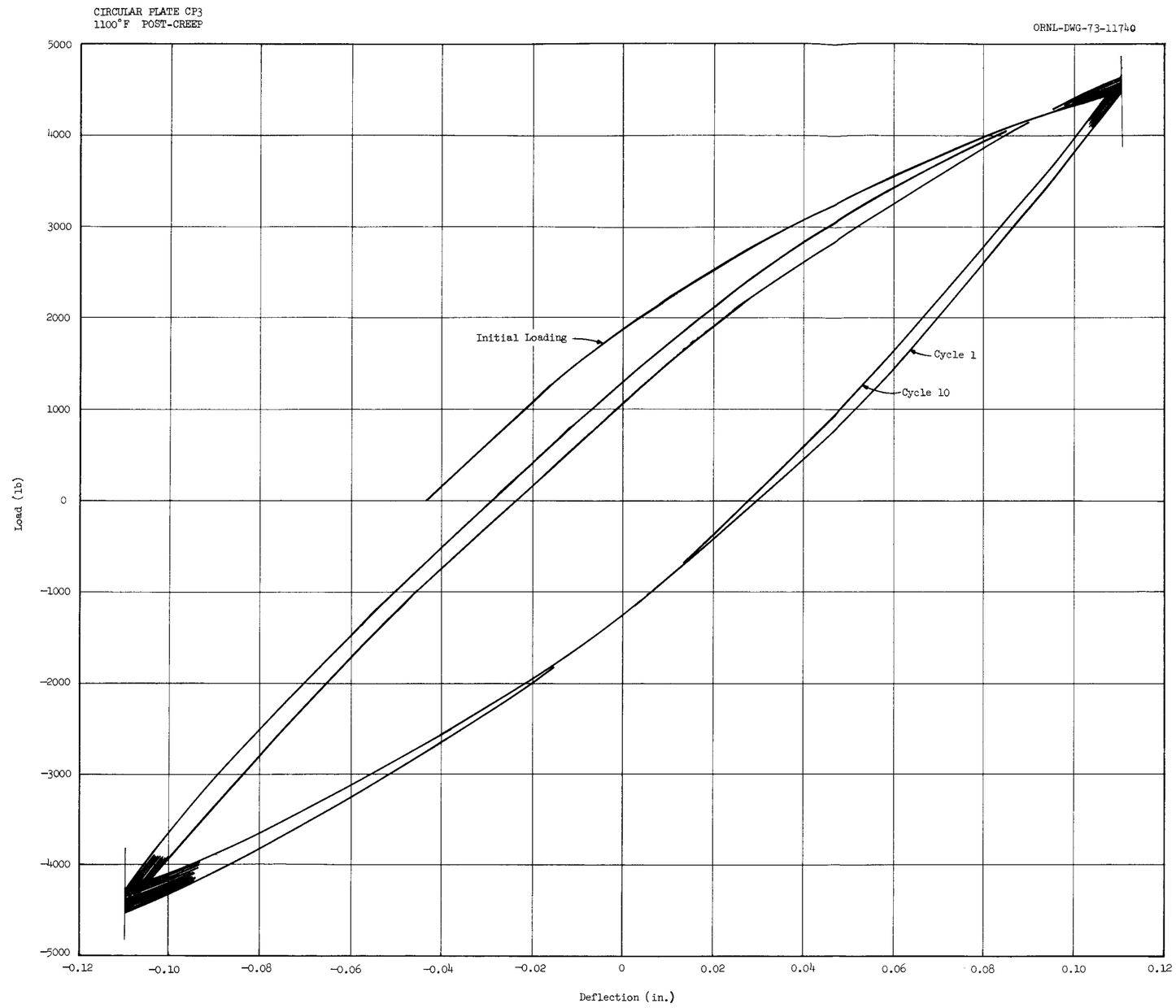

Fig. 5.20. Measured load-deflection behavior during ten short-time post-relaxation cyclic loadings of plate CP3.

The test results for plate CP4 are shown in Figs. 5.21, 5.22, and 5.23, which are analogous to Figs. 5.18, 5.19, and 5.20 for plate CP3. Comparison of the corresponding figures in the two sets shows the effects of the prior cyclic hardening in plate CP3.

Inelastic analysis results for plates CP3 and CP4 will be presented and compared to test data in the next progress report. Those readers wishing to make their own analytical comparisons with the experimental results should use the material properties data for the reference heat discussed in connection with beams B7 and B8 in the previous section of this chapter.

5.3. Weldment Creep-Rupture Studies

W. J. McAfee
M. Richardson
W. K. Sartory

5.3.1. Experimental program

Testing and inspection of the tubular WCR specimens is continuing on schedule. During this reporting period two specimens were inspected after reaching a total test time of 2000 hrs. The deformation measurements obtained were used to calculate comparative time dependent strains for selected points of interest in each specimen. These results are shown in Table 5.1 and in Fig. 5.24. Both the table and the figure include previous data.[24] The base metal of each specimen continues to accumulate significant creep strain. The general deformation trends, as established by previous inspection data, are being continued with one exception. This exception is that cylindrical segment of Spec. 3-M2 that is made of bar material. Preliminary calculations indicate that approximately 0.1% maximum circumferential creep strain was accumulated in this cylindrical portion of Spec. 3-M2 during the time interval 1000—2000 hrs. The cylindrical segment of this specimen made of pipe material, during this same time interval, accumulated approximately 0.5% maximum circumferential creep strain. This difference in creep behavior is shown graphically in Fig. 5.24.

In comparison to the base metal, the weld material of both the specimens inspected has accumulated very small circumferential strains. No definite trends in weld deformation behavior have been established as yet.

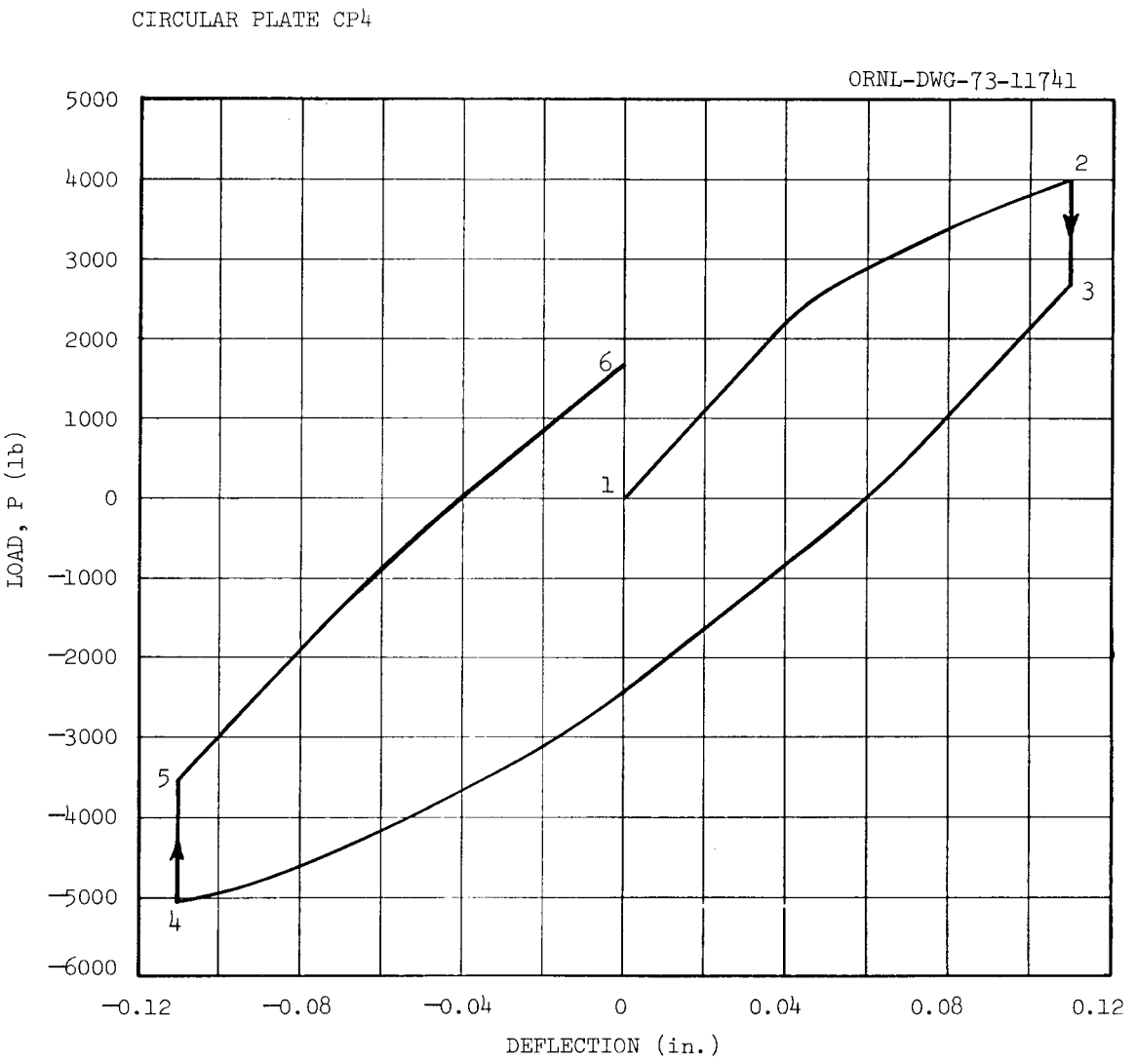

Fig. 5.21. Measured load-deflection behavior for deflection changes associated with relaxation portions of plate CP4 test. Numbered points correspond to points numbered on loading history diagram (Fig. 5.14b).

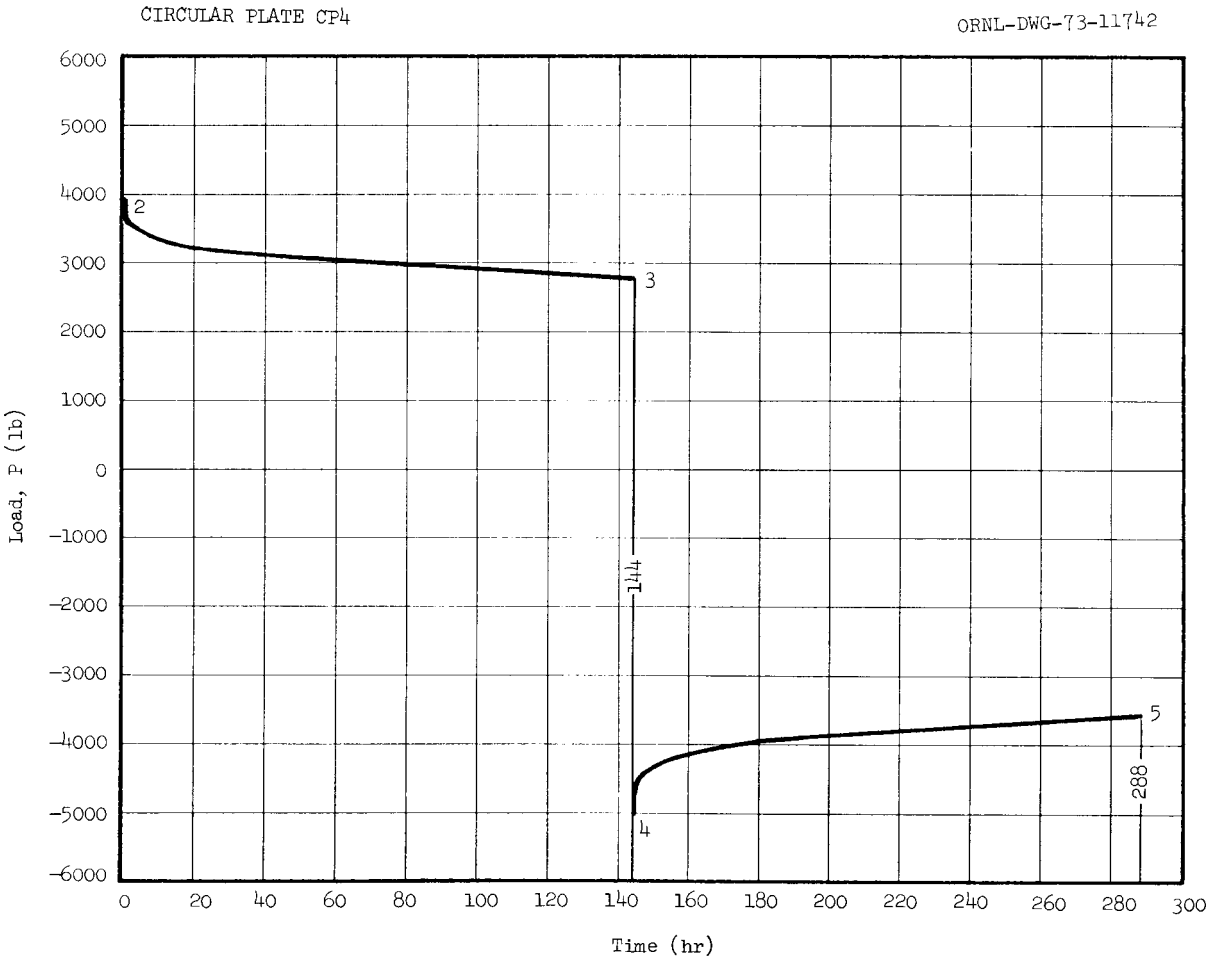

Fig. 5.22. Measured load relaxation versus time for plate CP4. Numbered points correspond to points numbered on loading history diagram (Fig. 5.14b).

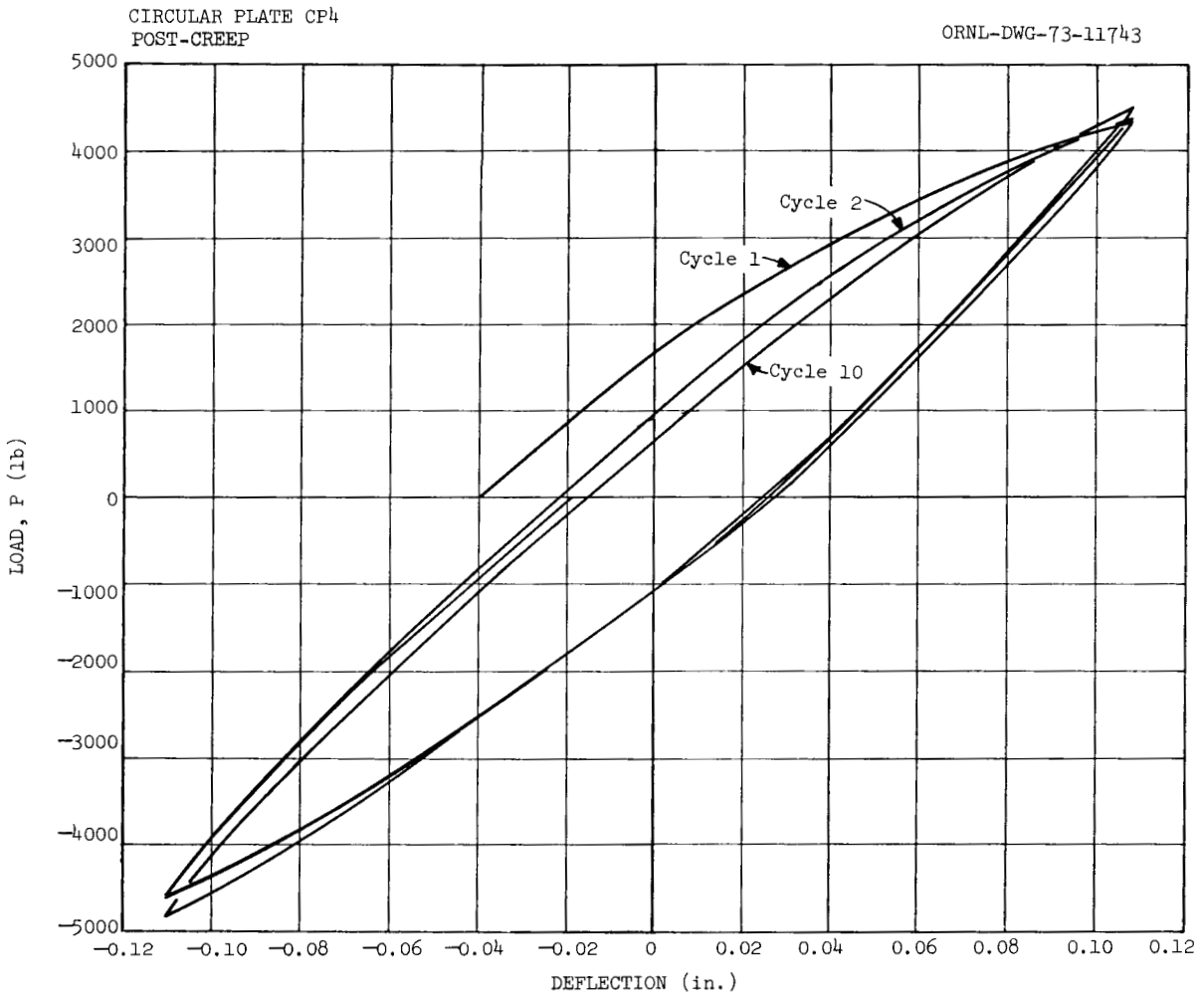

Fig. 5.23. Measured load-deflection behavior during ten short-time post-relaxation cyclic loadings of plate CP4.

Table 5.1. WCR creep deformation

Specimen No.	Material	Total test time (hr)				Stress[a] (ksi)
		500	1000	1500	2000	
		Average circumferential strain (%)				
1-M2	Base metal (pipe)	1.693				17.0
2-M2	Base metal (pipe)	1.477		2.013	2.433	17.0
	Base metal (bar)	1.036		1.427	1.687	17.0
	Weld	0.205		0.060	0.185	17.0
3-M2	Base metal (pipe)	1.508	2.069		2.580	17.0
	Base metal (bar)	0.952	1.759		1.870	17.0
	Weld	−0.225	0.216		−0.005	17.0
4-M2	Base metal (pipe)	1.939	2.563	7.977[b]		19.8
	Weld	0.285	0.270	2.302[b]		19.8
	Weld	0.315	0.230	2.464[b]		19.8

[a]Von Mises

[b]Strain after temperature increase.

Failure time = 1136 hrs.

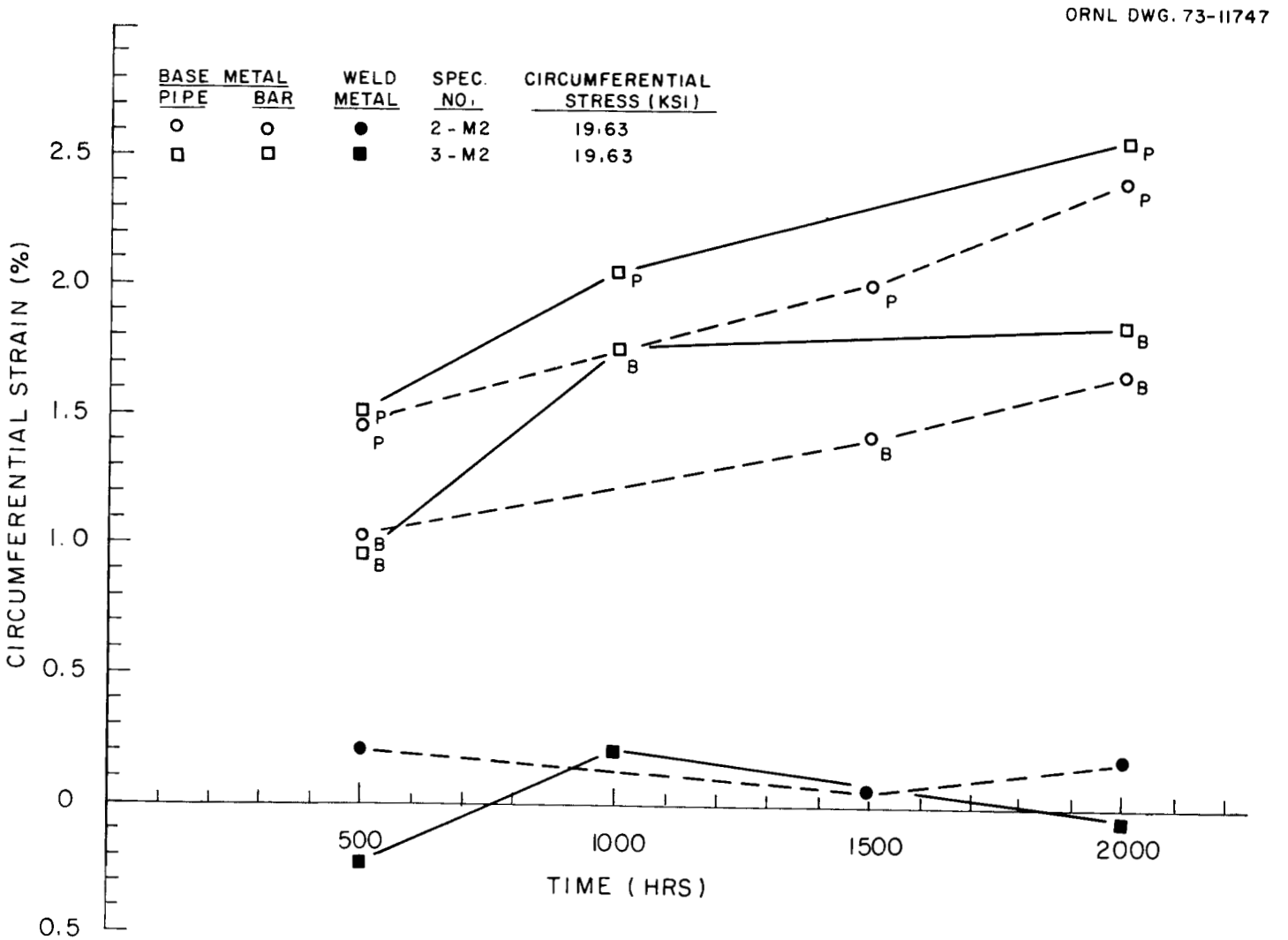

Fig. 5.24. Comparison of circumferential strain in base metal and welds of WCR specimens.

One specimen failed during this period; this was Spec. 4-M2. The design life of this specimen was 1000 hrs. It had accumulated 1136 hrs in test when failure occurred during a period of increased furnace temperature. It is estimated that the specimen reached 1400°F before failure occurred. Thus the failure data shown in Table 5.1 present difficulties in interpretation since significant creep strain could have accumulated in a very short time at the higher temperatures. The ruptures in this specimen were in the weld region and were small fissures. This is unlike previous specimens that ruptured in the base metal. A complete dimensional inspection is to be performed after which the specimen will be sectioned for visual and metallographic inspection.

5.3.2. Test data reduction

Data reduction for the weldment creep-rupture specimens has been described in an earlier report.[25] Further work has now been carried out in fitting equations to the cylinder and cap deformations to determine the strain.

Material particles are identified by considering the specimen to be in a hypothetical reference state in which its geometry is a perfect cylinder. A cylindrical coordinate system is then set up and each particle is identified by the reference coordinates $(\bar{r}, \bar{\theta}, \bar{z})$.

The deformed location of a particle is given by its Cartesian coordinates (x, y, z), and the undeformed location is given by the Cartesian coordinates $(\hat{x}, \hat{y}, \hat{z})$. To interpolate between measured points, the series

$$x(\bar{\theta}, \bar{z}) = P_1(\bar{z}) + P_2(\bar{z})\cos\bar{\theta} + P_3(\bar{z})\sin\bar{\theta} + P_4(\bar{z})\cos 2\bar{\theta} + P_5(\bar{z})\sin 2\bar{\theta} + P_6(\bar{z})\cos 3\bar{\theta} ,$$

where P_1,——,P_6 are polynomial spline functions, is used. The spline functions are continuous and have two continuous derivatives across the scribe rings. Interpolation equations of the same form are used for y, z, $\hat{x}$, $\hat{y}$, $\hat{z}$.

For a hemispherical cap the reference state is a perfect hemisphere, and the interpolation equation is

$$x(\bar{\theta}, \bar{\phi}) = P_1(\cos\bar{\phi}) + \sin\bar{\phi}\, P_2(\cos\bar{\phi})\cos\bar{\theta} + \sin\bar{\phi}\, P_3(\cos\bar{\phi})\sin\bar{\theta} + \sin^2\bar{\phi}\, P_4(\cos\bar{\phi})\cos 2\bar{\theta} + \sin^2\bar{\phi}\, P_5(\cos\bar{\phi})\sin 2\bar{\theta} + \sin^3\bar{\phi}\, P_6(\cos\bar{\phi})\cos 3\bar{\theta} ,$$

where $\bar{\phi}$ is the reference angle measured from the pole.

For a disc cap, the reference state is a perfect disc, and the interpolation function is

$$x(\bar{r}, \bar{\theta}) = P_1(\bar{r}^2) + \bar{r}P_2(\bar{r}^2)\cos\bar{\theta} + \bar{r}P_3(\bar{r}^2)\sin\bar{\theta} + \bar{r}^2P_4(\bar{r}^2)\cos 2\bar{\theta} + \bar{r}^2P_5(\bar{r}^2)\sin 2\bar{\theta} + \bar{r}^3P_6(\bar{r}^2)\cos 3\bar{\theta} .$$

The form of the cap equations is chosen so as to force the deformation to be analytic at the center point.

Using index notation, the strain tensor is defined as

$$e_{mn} = \frac{1}{2}\left(\frac{\partial x_i}{\partial \bar{x}_m}\frac{\partial x_i}{\partial \bar{x}_n} - \frac{\partial \hat{x}_j}{\partial \bar{x}_m}\frac{\partial \hat{x}_j}{\partial \bar{x}_n}\right)$$

where $x_1 = x$, $x_2 = y$, $x_3 = z$

$\hat{x}_1 = \hat{x}$, $\hat{x}_2 = \hat{y}$, $\hat{x}_3 = \hat{z}$

$\bar{x}_1 = \bar{r}$, $\bar{x}_2 = \bar{\theta}$, $\bar{x}_3 = \bar{z}$ for a cylinder or disc

$\bar{x}_1 = \bar{r}$, $\bar{x}_2 = \bar{\theta}$, $\bar{x}_3 = \bar{\phi}$ for a hemisphere

Because it follows the conventions of tensor analysis which emphasize simplicity of transformation, the strain tensor e_{mn} does not reduce to engineering strain in the infinitesimal limit. The alternative strain measure

$$e_{mn} = \frac{1}{2}\left(\frac{\partial x_i}{\partial \bar{x}_m}\frac{\partial x_i}{\partial \bar{x}_n} - \frac{\partial \hat{x}_j}{\partial \bar{x}_m}\frac{\partial \hat{x}_j}{\partial \bar{x}_n}\right) \Big/ \sqrt{\frac{\partial \hat{x}_k}{\partial \bar{x}_m}\frac{\partial \hat{x}_k}{\partial \bar{x}_m}\frac{\partial \hat{x}_\ell}{\partial \bar{x}_n}\frac{\partial \hat{x}_\ell}{\partial \bar{x}_n}}$$

(no summation on m, n)

sometimes referred to as the "physical components" of the tensor, is not itself a tensor but does reduce to engineering strain (except for a factor of 2 in shear) and is therefore easier in interpret.

Figure 5.25 shows the radial and hoop physical strain components for a disc cap. Figure 5.26 shows the axial and hoop strain for a cylinder with two welds.

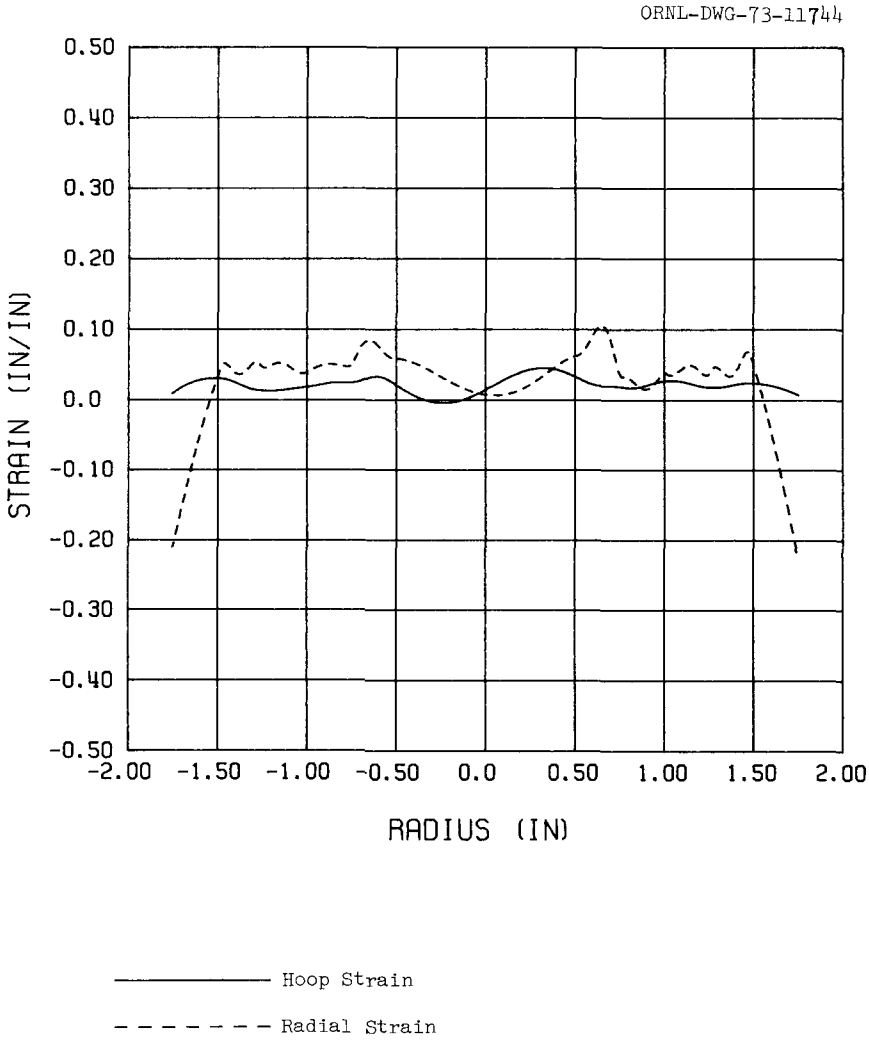

Fig. 5.25. Inelastic strain (plastic plus creep) at outer surface of flat cap versus radial position in cap for Spec. 1-M1 (see Ref. 25).

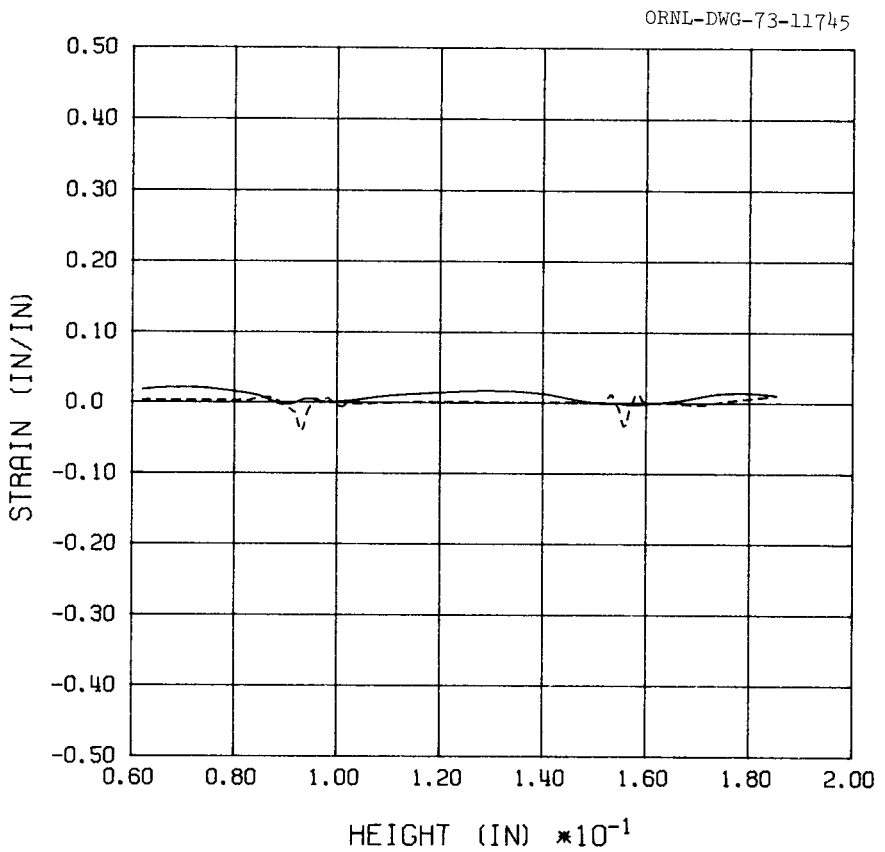

——————— Hoop Strain

- - - - - - - Axial Strain

Fig. 5.26. Inelastic strain (plastic plus creep) at outer surface of cylinder versus axial position along cylinder for Spec. 4-M2.

5.4. High-Temperature Moire Strain Analysis of an In-Plane Loaded Finite-Width Plate with a Circular Hole

A. J. Durelli
The Catholic University of America

The object of the research reported here is to strain analyze a finite-width stainless steel plate with a circular hole when it is subjected, at 1100°F, to an in-plane, unidimensional, reverse loading that produces elastic-plastic and creep deformations. In the investigation an attempt will be made to provide high temperature structural test data for comparison with independently obtained theoretical predictions and also to demonstrate the applicability of moire to analyze, at elevated temperatures, structures exhibiting elastic-plastic-creep behavior.

To conduct the test, a special loading frame, a special furnace, and special measuring equipment are required.

a) In the first three months, preliminary work was conducted to build the equipment and prepare the plate for application of the measuring technique.

b) In the second quarter period the building of the loading frame was started, the design of the furnace was well advanced and a new temperature recorder was obtained.

c) In the third quarter period the loading frame components were assembled and a plate tested in the frame, under tension and compression, for proper application of loading. The furnace was built and the desired temperature attained.

d) In the fourth quarter period the techniques to apply gratings to the surface of the plate were developed. Appreciable time has been spent to obtain sufficient contrast between lines and interlines of the grating, when the photograph is obtained at 1100°F.

e) In the fifth quarter, which is reported here, a preliminary stainless steel test specimen, provided by ORNL, was tested in the furnace following the specified loading cycle, at the specified temperature. Photographs were taken at periodic intervals. These preliminary results will be evaluated in the next quarter.

Efforts are still underway to improve the contrast in photographs of the 500-lines-per-inch grating at 1100°F. To minimize oxidation effects, etc., the furnace has been made almost leak proof and nitrogen and later argon, were fed in continuously during the test of the preliminary specimen. Argon seems to give better results. Experiments are being conducted to fill the interlines with temperature resistance materials that will increase the contrast. Several fillers have been tried: graphite, calcium carbonate, manganese dioxide and titanium dioxide, some of them mixed with sodium silicate. So far none of them seem to be completely satisfactory. The use of sodium silicate had to be discarded.

These studies are being continued. A small asbestos box with infrared lamps and quartz tubes has been built to test gratings, etching procedures, and photography techniques on small specimens. The specimens, to be supplied by ORNL, will come from the same heat of type 304 stainless steel (9T2796) as the actual structural test specimen.

5.5. Elevated-Temperature Test of Stiffened Shear-Lag Panel

R. L. Egger
D. R. Harting
Boeing Aerospace Company

This effort is in progress at the Boeing Aerospace Company in Kent, Washington. The program, consisting of a series of tests that are based on the use of a stiffened shear-lag panel specimen design, has two purposes: first, to provide elevated temperature structural test data for comparison with elastic-plastic-creep structural analysis predictions, and second, to further develop and demonstrate the applicability and potential of the Boeing high temperature capacitive strain gage as an accurate, long-term stable measuring device for liquid-metal fast-breeder reactor structural applications.

This is the third quarterly progress report. Accomplishments during this period are summarized below and elaborated upon in the remainder of this section.

- Machining, straightening, and annealing of shear-lag specimen No. 2 was completed. Tensile specimens were made and tests performed to determine the yield stress of specimen No. 2 and the grain sizes of both specimens No. 1 and No. 2.
- Specimen No. 1 was instrumented for the thermal survey testing.
- Thermal survey testing was completed. During the survey, the heating system was modified to reduce specimen temperature gradients.
- The loading system was proof-tested and the guide bearing support structure was modified to improve the alignment of the specimen buckling restraints.
- Shear-lag specimen No. 1 was instrumented for the room temperature, 500°F and 1100°F load tests. Signal conditioning and control equipment was set up and is ready for these tests.

One temperature cycle to 2000°F (with slow cooling) was used to both anneal and straighten shear-lag specimen No. 2 (as reported in the last quarterly report,[26] the panel sections of specimen No. 2 distorted when the picture frames were removed). Based on the tests of four tensile coupons, the room temperature 0.2% yield strength of specimen No. 2 was found to be 27,000 psi. The ASTM grain size of specimen No. 1, which was subjected to three annealing/straightening cycles to 2000°F, was between 0 and +1. The ASTM grain size of specimen No. 2, which was subjected to only one annealing/straightening cycle, was between +2 and +3.

The primary purpose of the thermal survey tests was to verify that the temperature of the shear-lag specimen could be held uniform at 1100°F. Included as part of the thermal survey tests were functional tests of the oven, heating equipment, temperature measuring instrumentation, and fail-safe systems. Load cell environmental effects were also monitored. Shear-lag specimen No. 1 was instrumented with nineteen response thermocouples (plus control and fail-safe thermocouples) for the survey tests.

The thermal survey testing began with the heating oven divided into two temperature control zones; this configuration, however, could not control the specimen temperature gradients within the desired tolerances. The oven was subsequently modified so as to be divided into six control zones, after which another thermal survey test was performed. The specimen was maintained at 1100°F ± 5.5°F for over twenty-four hours.

Functional tests of the fail-safe and redundant heat control systems demonstrated that the redundant systems would switch on automatically and control the specimen temperature to within the same tolerance as the primary systems. Transient perturbations during the transition were less than 40°F. No load cell environmental effects were observed.

Using a bar to simulate a shear-lag specimen, the load control system was proof-tested to demonstrate that tension and compression loads of up to 16,000 lb could be applied at rates of up to 600 lb per second. The guide bearing support structure was modified so that it would be self-aligning, thus eliminating the necessity for precision shimming each time a specimen was installed in the load fixture.

The thermocouples installed on specimen No. 1 for the thermal survey tests were removed. Twenty-five bonded resistance strain gages, one capacitive strain gage, and ten response thermocouples were installed in preparation for the preliminary room temperature, 500°F, and 1000°F load tests of specimen No. 1. The bonded resistance strain gages were selected and installed for operation at 500°F. Nineteen of the bonded resistance strain gages have 1-in. gage lengths (to simulate the capacitive strain gages to be used on specimen No. 2); the other six bonded resistance strain gages have 1/8-in. gage lengths and will be used to correct for the high transverse sensitivity of the 1-in. gage length gages. Figures 5.27 and 5.28 are photographs of the front and back sides (respectively) of specimen No. 1. The capacitive strain gage (without a cover) is shown installed at the mid-section of the specimen in Fig. 5.24. A second capacitive strain gage, with a cover, is shown installed at the far edge of the specimen in Fig. 5.27. This gage was installed earlier to establish that there were no oven power supply effects on the capacitive gage and its lead wires.

Load testing of specimen No. 1 is scheduled to begin the week of July 16. The room temperature and 500°F loads will be limited to the elastic range of the specimen. The bonded resistance strain gages will be removed for the 1100°F load tests and only the capacitive gage at the center of the specimen will monitor strain.

Specimen No. 2 will be instrumented for the 850 hr test at 1100°F, which is scheduled to begin the second week in September.

ORNL-Photo-2612-73

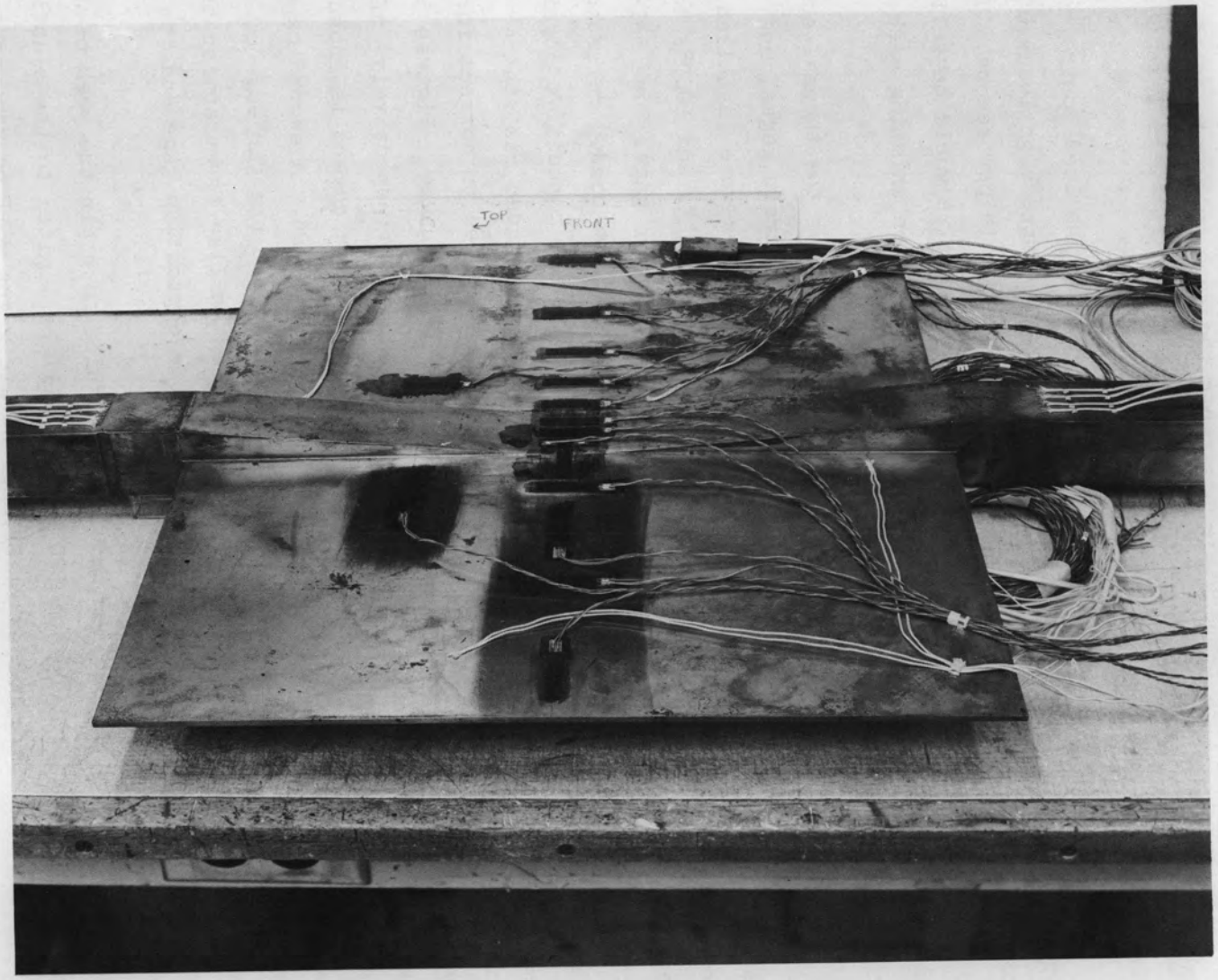

Fig. 5.27. Shear-lag specimen No. 1, front side.

ORNL-Photo-2613-73

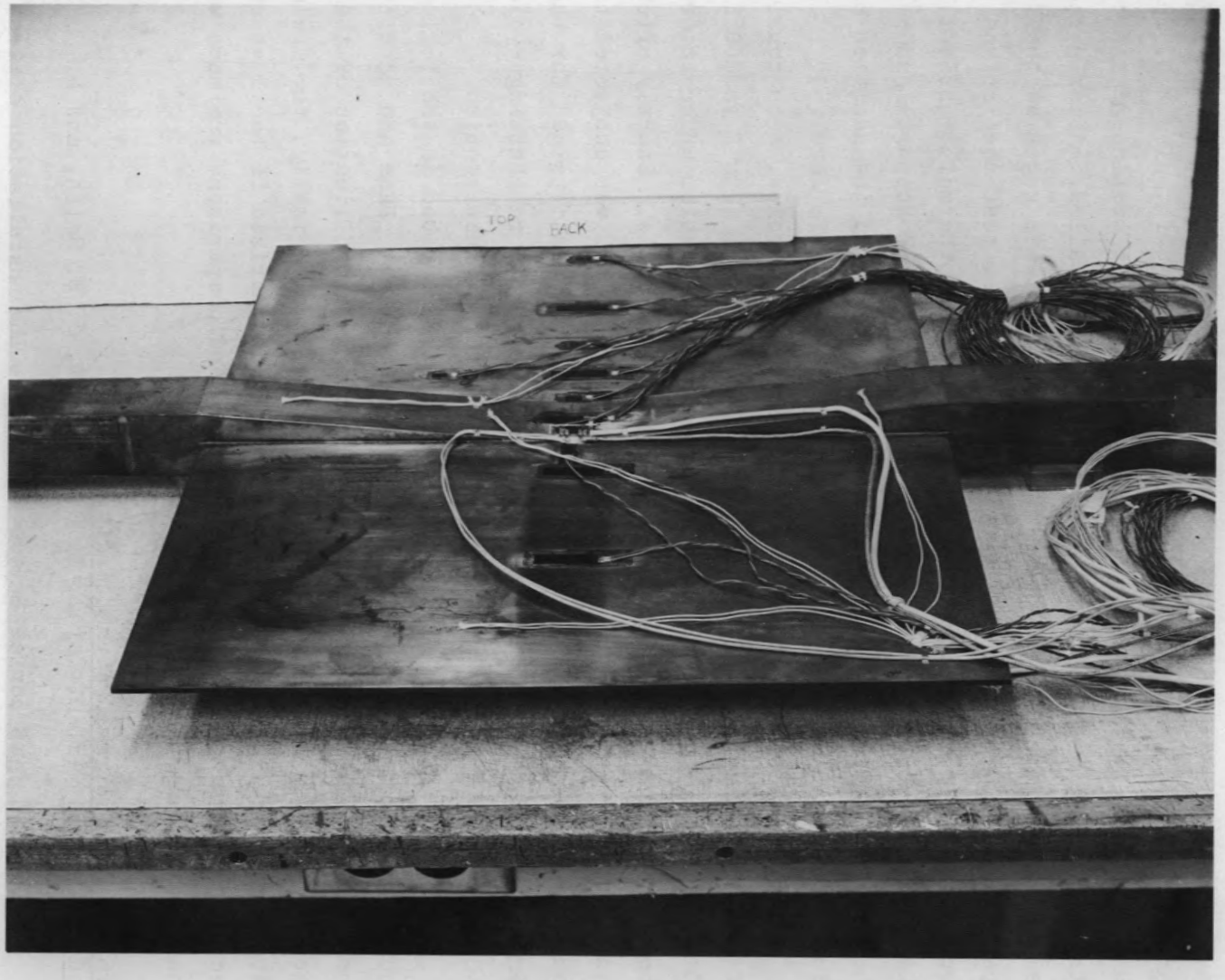

Fig. 5.28. Shear-lag specimen No. 1, back side.

5.6. Pipe Thermal Ratchetting Tests

At the beginning of this report period the dummy test section, which was used for shakedown testing of the Thermal Transient Test Facility (TTTF), had been removed, and the first fully instrumented 8-in.-diam × 0.375 in. wall pipe test section, which was designated as test section 3B and constructed of type 304 stainless steel, had been installed. After a room temperature calibration of the high-temperature strain gages at the 700 psi operating pressure, the facility was heated and the test section was subjected to one isothermal sodium flow transient (isothermal transient) at 800°F, which proved that the modification to the pipe supports had reduced the bending stresses to within an acceptable range and the addition of vibration dampers had reduced the vibration to an acceptable level.

Test section 3B was then subjected to 10 test cycles, each consisting of a thermal downshock in the sodium temperature from 1100°F to 800°F in 10 sec followed by a 160-hr period of sustained operation under internal pressure at 1100°F to obtain a 7-day ratchetting cycle. Shortly after the end of the current reporting period, the test section was subjected to four additional ratchetting cycles. Strain data were obtained for the first three of these and consequently results for 13 ratchetting cycles (13 weeks of operation) will be presented later in this section.

The testing of the first specimen (3B) is described in the following subsection together with a brief summary of the test plans and conditions for the second test specimen (3C). Operation and modification of the TTT Facility is then discussed in the next subsection. Finally, the inelastic ratchetting analyses that were performed are summarized in the last subsection and the test results are presented and comparisons are made with analytical predictions.

5.6.1. Pipe thermal ratchetting testing and test plans (J. M. Corum, A. G. Grindell, J. E. Smith, and H. C. Young)

5.6.1.1. Test series 1 (specimen 3B). The installation of test section 3B for the first pipe thermal ratchetting test series was nearly completed at the beginning of this report period. The test section was supported by the redesigned and strengthened pipe anchor and pipe guide.[27]

Automotive shock absorbers were installed at each of two locations, one near the inlet to the test section and the other at the midpoint in the orifice run. Three absorbers were placed orthogonally in the X, Y, and Z planes at each location. A number of room temperature strain gages were installed, and the test section and system piping were pressurized with argon to 700 psig at room temperature to calibrate the three Boeing capacitive strain gages, six Ailtech (Microdot) weldable strain gages, and two strain-gage-based, air-cooled, extensometers (the instrumentation for test section 3B was described in Ref. 37).

The system was then filled with sodium, and the test section was subjected to one isothermal flow transient with 800°F sodium during which the recorded outputs of three accelerometers mounted on the test section and the recorded rectilinear plots of the capacitive strain gage outputs were observed. These outputs indicated that the shock absorbers and the redesigned test section supports had been effective in satisfactorily reducing the vibration reported previously.[27] As the temperatures of the test section and the sodium system were being prepared for the first thermal transient, the capacitive strain gages indicated that the maximum stress induced in the test section by the thermal expansion of the interconnecting sodium piping system was less than 200 psi, a value which is acceptable.

The test section was then subjected to the first thermal transient, in which the sodium temperature in the test section was reduced from 1100 to 800°F in approximately 10 sec with a programmed flow of temperature graded sodium. During the transient the sodium static pressure was maintained within the range of 700 psig ±25 psi. Initially, we had planned to operate the test section at the creep test conditions of 1100°F and 700 psig ±5 psi for a duration of approximately 21 days to achieve a ratchetting cycle of 3 weeks; however, at the request of AEC-RRD, the duration of the creep test was reduced to approximately 160 hr to provide a ratchetting cycle of 1 week. The test section subsequently was subjected to ten 1-week ratchetting cycles as indicated in Table 5.2.

For ready reference, the *nominal* sodium temperature and pressure histories for the first test are depicted in Fig. 5.29. During the thermal transient (from points a to b in Fig. 5.29), temperature and strain data were recorded every 0.2 sec by a high-speed data acquisition system. During

Table 5.2. Ratchetting cycle operation test series 1 (test section 3B)

Thermal transient 1100°F to 800°F ∿29.5°F/sec (max)			7-day creep test 1100°F and 700 psig steady state		
Cycle No.	Time	Date	Cycle No.	Duration	Hours
1	13:10	4/24/73	1	22:40 on 4/24/73 to 11:54 on 5/1/73	156.3
2	11:54	5/1/73	2	21:10 on 5/1/73 to 11:48 on 5/8/73	158.5
3	11:48	5/8/73	3	22:31 on 5/8/73 to 11:27 on 5/15/73	157.0
4	11:27	5/15/73	4	20:15 on 5/15/73 to 12:03 on 5/22/73	159.8
5	12:03	5/22/73	5	21:25 on 5/22/73 to 11:26 on 5/29/73	158.0
6	11:26	5/29/73	6	20:55 on 5/29/73 to 10:46 on 6/5/73	157.8
7	10:46	6/5/73	7	19:50 on 6/5/73 to 10:45 on 6/12/73	158.9
8	10:45	6/12/73	8	20:20 on 6/12/73 to 10:53 on 6/19/73	158.5
9	10:53	6/19/73	9	20:15 on 6/19/73 to 10:48 on 6/26/73	158.5
10	10:48	6/26/73	10	20:00 on 6/26/73 to 10:30 on 7/2/73	158.5

ORNL-DWG-73-6741

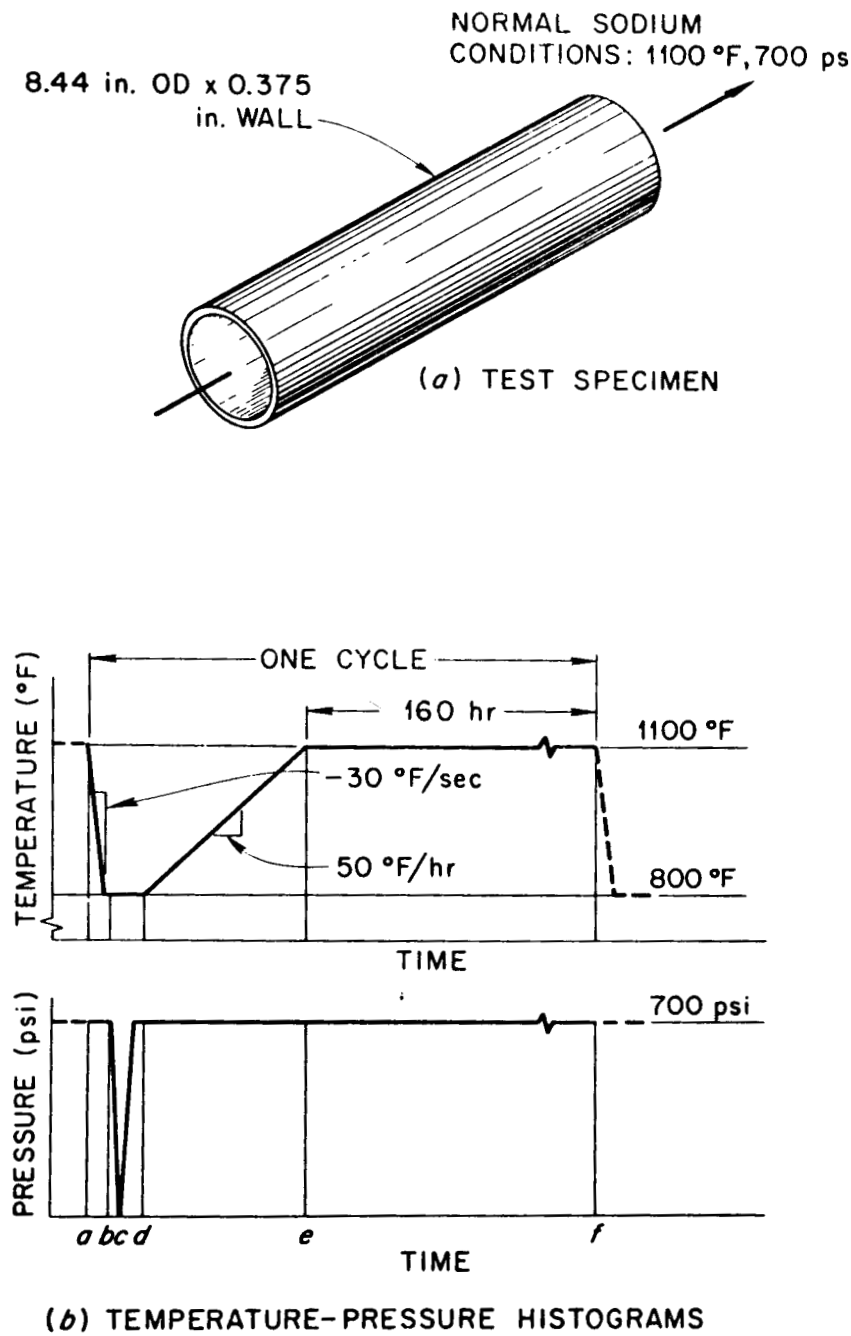

Fig. 5.29. Nominal test conditions for first pipe thermal ratchetting test.

the heat-up period (points d to e) and the 160 hr hold period (points e to f), data were recorded every 15 minutes.

After draining the sodium from the system, we plan to remove the test section oven to measure the absolute strain values on the circumferentially and axially oriented Demec gages. We then plan to refill the system with sodium and conduct five additional 1-week ratchetting cycles with this test section.*

For the next test, Test Series 2, to be performed with test section 3C, we plan to change the ratchetting test conditions to 400 psig with a thermal downshock of approximately 23°F per sec and to increase the duration of the creep test portion of the cycle to 2 weeks. Therefore, at the completion of the 15 scheduled ratchetting cycles with test section 3B and before removal of this test section, we plan to operate at these new conditions through several isothermal flow transients and one or more thermal transients to prove the facility capability for the lower sodium flow and thermal downshock rates as well as demonstrate the operation of the high-pressure gas control system at the revised conditions.

5.6.1.2. Plans for test series 2 (specimen 3C). The second 8-in.-diam by 30-in.-long test piece (designated test section 3C) was fabricated, and it is ready for final pressure and leak testing. The inlet end of the bladder in the test section was modified to provide better flow guidance in an attempt to reduce temperature fluctuations in the flowing sodium that were observed during the thermal transient operations with test section 3B. The butt weld end cap on the inlet end of the bladder was replaced with a 6-in. by 2 1/2-in., schedule-10 reducer and 2 1/2-in. butt weld cap as shown on Fig. 5.30. Also, the test section design was modified to provide a gas vent and a sodium drain. The configuration of the sodium piping causes gas to be trapped in the test section during sodium filling; the gas vent line will eliminate this operational problem. The sodium drain will permit removal of a small sodium heel at one end of the test piece and will ease the task of cleaning the interior of test sections in the event of either subsequent use or extensive metallurgical examination.

*Subsequent to the current reporting period, four additional ratchetting cycles were conducted. A temporary malfunction in the capacitive gage system precluded the obtaining of reliable strain data during the last of these.

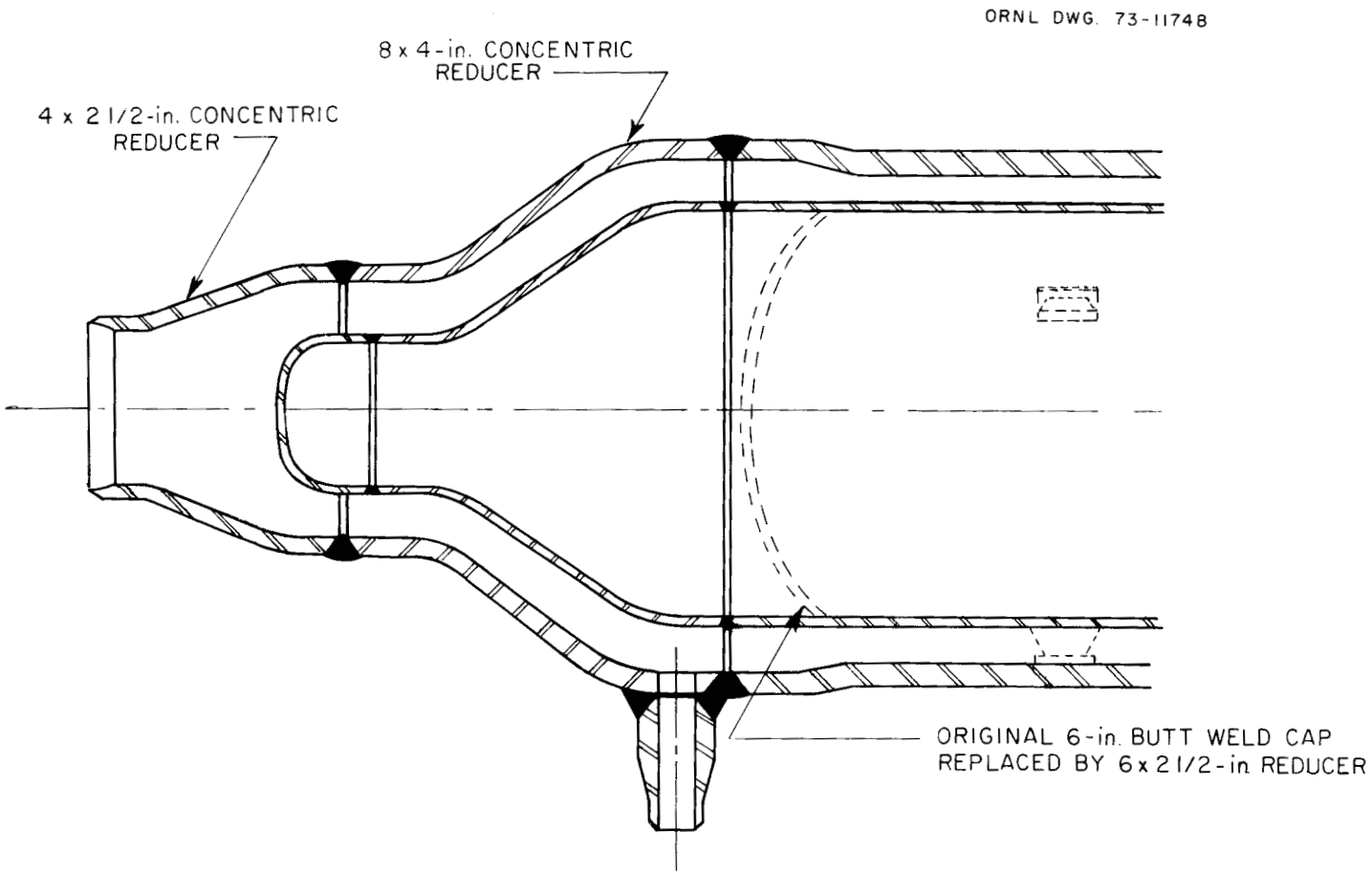

Fig. 5.30. Cross section of test section 3C, LMFBR-TTTF. Shows redesigned bladder to provide more flow guidance at inlet to test section. Original bladder termination shown with dotted lines.

The conditions for the first pipe thermal ratchetting test (test series 1, specimen 3B) were extreme in that the combination of primary (pressure) and secondary (thermal) stresses was in a region outside the range of normal LMFBR design, and the ratchetting phenomenon was dominated, at least initially, by plastic ratchetting relative to creep ratchetting. For the second test, we plan to relax the conditions sufficiently to put the test inside the normal design region.

The regions commonly identified in ratchetting evaluations are shown in Fig. 5.31. Regions R_1 and R_2 are dominated by plastic ratchetting, and are avoided in normal operation. As can be seen in the figure, our first test was in the R_2 region. The dashed line in Fig. 5.31 shows the approximate combinations of elastically calculated primary and secondary stresses which can currently be obtained in the TTTF without significant hardware modifications. The second test (specimen 3C) has been chosen to lie on this line, and is shown in the P region of Fig. 5.31.

The specific test conditions for test series 2 are:

Thermal downshock from 1100°F to 800°F	23°F/sec
Internal pressure	400 psi
Hold time (based on 2 week cycle)	328 hr
Total number of cycles	10–15

The sequence of events and procedures will be exactly the same as in the first test, and the nominal temperature and pressure histograms are the same except for the above changes.

The predicted outside circumferential strain versus time based on the above nominal conditions is shown in Fig. 5.32. Note that 15 cycles extend just past the knee of the curve. Beyond 15 cycles the predicted deformation in essentially time-dependent creep only. Note also that the total circumferential strain at the end of 15 cycles is predicted to be about 0.09%. This is approximately one-third of the strain in test series 1.

The test section instrumentation for test series 2, as indicated below, is to be identical to that used for test series 1 with the exception of the addition of four more active Boeing capacitive strain gages:

ORNL-DWG-73-11746

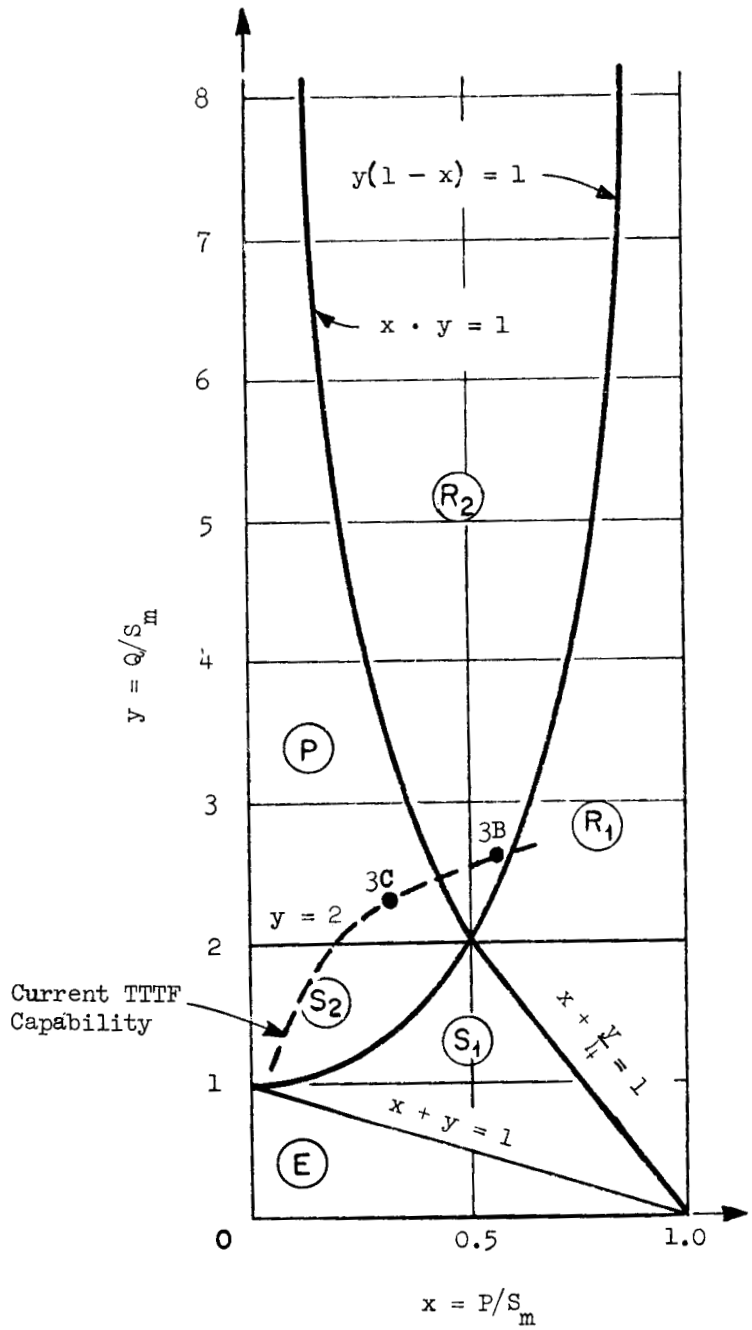

Fig. 5.31. Stress regimes for ratchetting evaluations using elastic calculations. The dashed line represents the combinations of primary and secondary (thermal) stresses that can be currently obtained in the TTTF. The points show the conditions for test series 1 (specimen 3B) and for test series 2 (specimen 3C).

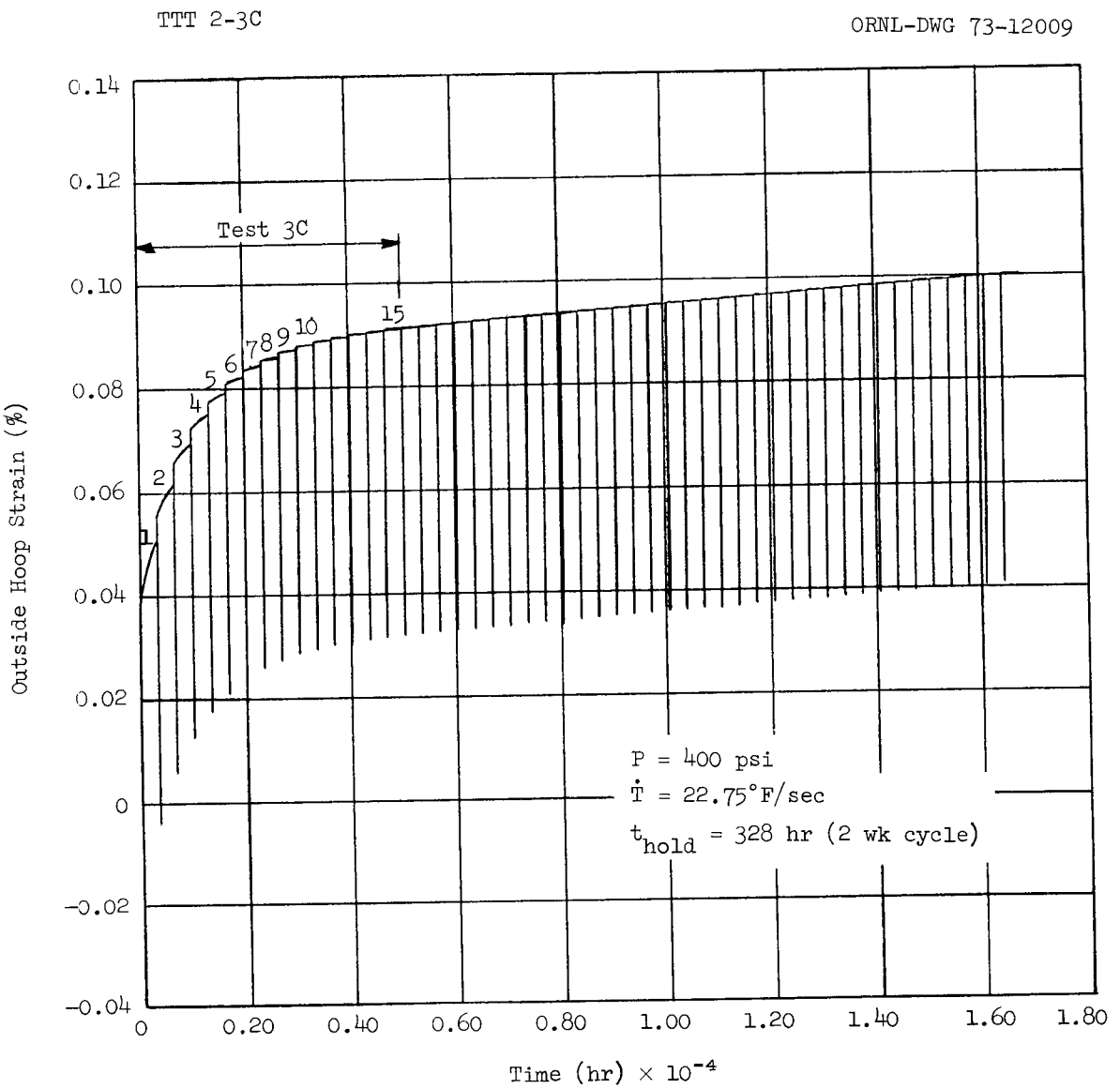

Fig. 5.32. Predicted outside hoop strain versus time for the second pipe thermal ratchetting test (test series 2, specimen 3C). Although 50 cycles are shown, 10–15 cycles are planned for the actual test.

Sodium thermocouples	5
Through-the-wall thermocouples (including the associated outside surface thermocouple)	6
Outside surface thermocouples	12
Microdot gages	6
Strain-gage-based extensometers	2
Boeing capacitive strain gages	6
Thermocouples associated with Boeing gages	14*
Source tank pressure	1
Source tank sodium level	1
Total	53

Three capacitive gages will be located in the circumferential direction, 90° apart at the middle of the test section; two capacitive gages will be located axially, 180° apart at the middle; and one will be located circumferentially on a weld at the end of the test section. The thermocouple locations will be unchanged. The mechanical extensometers and Prewitt scratch gages that were installed on test section 3B will not be installed on test section 3C. The Demec tabs will still be used.

The ANSCAN fast speed data acquisition system (FSDAS) that was used during the first four thermal transients in test series 1 is no longer available to the Thermal Transient Test Facility. The technical feasibility of using the FSDAS recently installed in the LMFBR-Fuel Failure Mockup (in the same building as the TTTF) was investigated. Two two-conductor shielded cables were installed to connect the TTT Facility to the FFM-FSDAS. The cable routing, approximately 350 ft long over a double crane-bay area, was selected to minimize the pickup of 60 Hz noise. Tests made with various signals from the TTTF indicated that the basic interconnection was feasible and a total of 60 of the two-conductor cables will be installed between the two facilities. The programmatic feasibility of coordinating and correlating thermal transient data, taken with a shared FSDAS, and creep test data taken locally remains to be proven.

---

*Both the rod connecting the two ends of each capacitive strain gage and the specimen surface directly underneath are instrumented with thermocouples to provide data for computing corrections required by any temperature differences between the two. On one of the gages to be used in test series 2, the gage rod will be instrumented with three thermocouples (one in the middle and one on each end) to provide information regarding the uniformity of the gage temperature.

5.6.2. Test facility operation and modification
(A. G. Grindell and H. C. Young)

Melting of the sodium in the sump tank was initiated December 15, 1972, and the system piping was filled with sodium on December 28, 1972. By the end of this report period the test facility had sustained 11 isothermal sodium flow transients (isothermal transient) and five thermal transients with the dummy test section and an additional isothermal transient and ten complete ratchetting cycles with test section 3B. The sodium system has been operated at 700 psig and at temperatures from 800 to 1100°F for approximately 2000 hr.

The high-pressure argon control system maintained the gas pressure in the sodium source tank during the creep test operation at 700 psig ±2 psi (allowable is ±5 psi) and during the thermal transient at 700 psig +15, −20 psi (allowable is ±25 psi).

The test section oven controller governs the output of a saturable reactor to four variable transformers that directly supply the oven heaters. This arrangement provides a nearly infinitely variable control of the oven power supply. The controller has consistently held the test section temperature within ±1°F of the set point during the creep test period (required temperature is 1100°F ±5°F). The test section temperatures are monitored on a panel mounted temperature indicator and are recorded by the Dextir data acquisition system. A 9°F difference, noted at one time, between the temperature indicator and the Dextir reading was traced to an error in the standard millivolt input signal used to calibrate the temperature indicator. Although the calibration of the standard was within the specified recalibration date, the voltage of the standard cell had dropped and the technique for rezeroing did not uncover the error. It is believed part of the error (as much as 7°F) was caused by use of an incorrect ice bath technique for the reference junction. Because the temperature indicator is critical to accurately setting up the pipe nest temperature gradient for the thermal transient, its calibration has since been routinely rechecked each week. The technique used for performing calibration checks was reviewed and improved.

The temperature at the inlet thermal sleeve on the thermal capacitance tank was monitored with a high-speed recorder during a thermal transient.

The results were superimposed in Fig. 5.33(a) on a prediction of temperature vs time used in an inelastic analysis reported previously.[28] The experienced thermal transient appears to be less severe than that used in the analysis. The sodium shutoff valve has continued to operate satisfactorily. The thermal capacitance tank effectively isolates the sodium valve during the thermal transient downshock. The valve body temperature changes only about 25°F in 60 sec.

A number of alarms and controls are provided for monitoring the test facility during unattended operation. Any one of about 50 fault conditions, all of which sound an alarm locally, will sound an alarm during unattended operation in the Plant Shift Superintendent's office (PSS). The PSS notifies the designated responsible test facility operating personnel whenever there is an alarm during unattended operation. Some of the fault conditions sound an alarm only, while others provide for automatically shutting off electrical power to all trace heaters and venting the high argon pressure in the sodium source tank. A limited number of fault conditions will drain the system. It is important that spurious signals or false alarms do not cause unwanted thermal transients or otherwise abort the test program. Since the system was first filled with sodium, the PSS has notified the operating personnel of alarm conditions on 34 occasions. None of these resulted in a change in pressure or temperature on the test section. Nine or ten alarms received on one high-temperature alarm that shuts off the system heaters occurred during shakedown prior to operation with test section 3B. This fault was traced to a defective temperature monitor. The pressure in the instrument air supply to the building twice fell below normal value for short periods; however, the facility continued to operate on a nitrogen bottle system that is piped in parallel with the instrument air supply but isolated from it by a check valve. Most of the other alarms occurred on temperature recorders that give an alarm on high temperature only for which the corrective action is performed manually. Although a few of the alarms could be traced to malfunction in temperature recorders, most were caused by a gradual increase in a temperature that had been set very close to the alarm point. A small voltage increase ($\sim$+1%) in the building electrical supply was enough to cause an alarm. There were no alarms during unattended operations for the final five of the ten pipe ratchetting cycles with test section 3B.

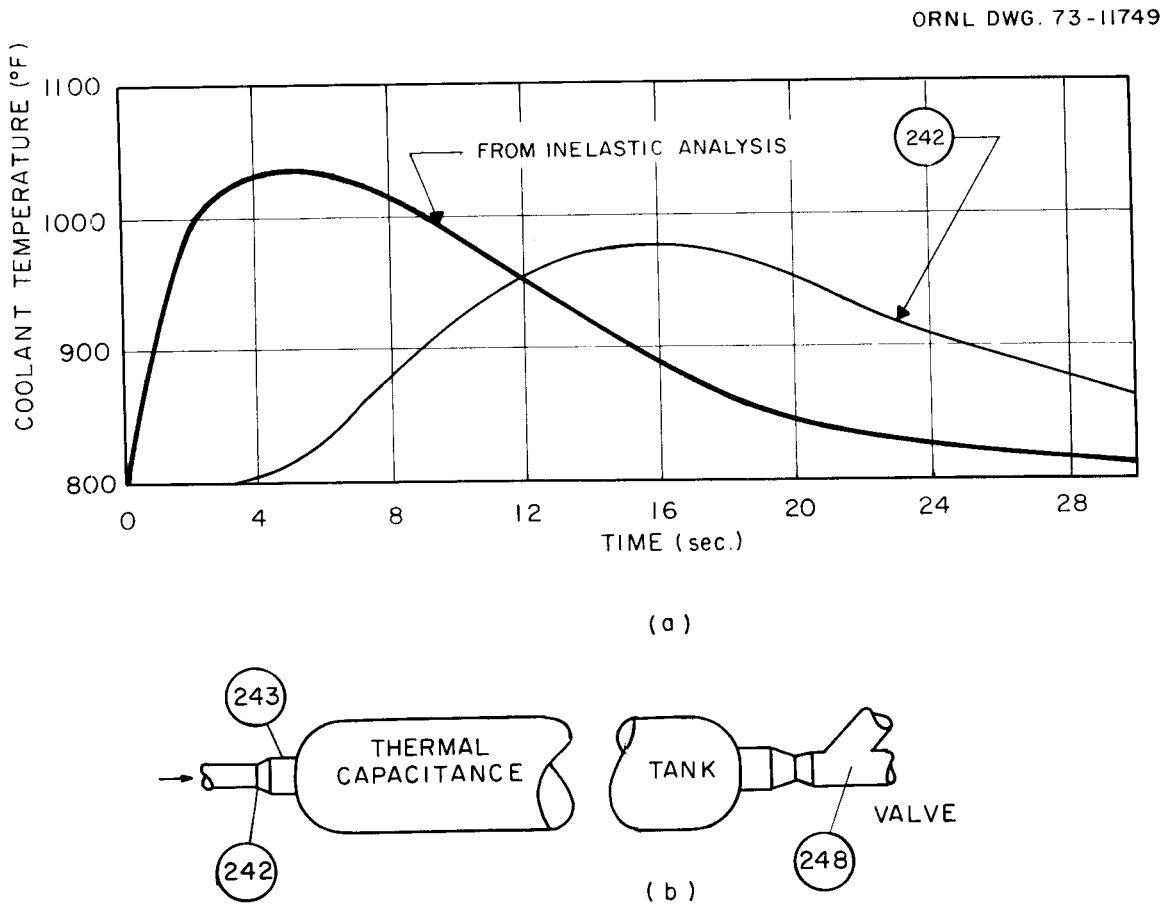

Fig. 5.33. Thermal transient temperature vs time for thermal capacitance tank in the LMFBR-TTTF.

a. Note comparison of thermal transient of the thermal sleeves at tank inlet as measured with TE-242 on high-speed recorder to the more severe transient used in the inelastic analysis of the sleeve.

b. Note locations of thermocouples on tank. TE-242 is plotted above in (a). TE-243 initially at 800°F reached a new equilibrium of 850°F in 67 sec. TE-248 initially at 750°F reached a new equilibrium of 773°F in 60 sec.

An unused cold trap and economizer, designed and fabricated for the Aircraft Nuclear Propulsion Project, was installed on the sump tank after upgrading to quality level II by appropriate tests and inspections. Initial operation using steam for heating and cooling the cold trap was not satisfactory. Building instrument air was substituted for steam and trace heaters were installed on the helically wrapped cooling coil mounted on the cold trap external surface. The cold trap, cooling coil, and heaters were then covered with thermal insulation. Although temperature control was improved greatly, some difficulty was experienced in establishing flow through either the cold trap or the parallel sample station. The sodium flow indication from an electromagnetic flow meter would respond to an increase in electromagnetic pump voltage only to decrease gradually to zero, suggesting that the system was gas bound rather than plugged. The sump tank was evacuated, the cold trap degassed, and satisfactory sodium flow was established. The cold trap had since operated at 290°F outlet temperature which is equivalent to an oxygen level of approximately 2 ppm. Earlier analysis of the sodium samples by the mercury amalgamation method indicated about 13 ppm. Results of the most recent sample analysis are not yet available.

The test facility design was modified by connecting a nozzle, installed at the bottom of the pipe nest during original facility construction, to the sump tank to provide a drain for the sodium trapped at the bottom of the pipe nest. After the initial sodium filling operation, the trapped sodium presented an operational problem during all subsequent refillings. It required the use of separate lines to evacuate the sodium system both upstream and downstream of the trap. The evacuation was further complicated because the only ingress into the downstream portion was through a syphon break line installed into the sump tank side of the sodium shutoff valve which separates the sodium system from the sump tank. This in turn required evacuation of the sump tank to avoid raising sodium into the system until the evacuation operation was completed. The trapped sodium also required protection against the intrusion of air and moisture during test section replacement or any maintenance or modification that required opening the sodium system.

5.6.3. Results from first pipe thermal ratchetting test and comparisons with analytical predictions (J. M. Corum and W. K. Sartory)

5.6.3.1. Inelastic analysis. The ratchetting analysis was carried out using the PLACRE computer program, which was developed primarily as a research tool at the Oak Ridge National Laboratory. PLACRE is a two-dimensional finite-element program for elastic-plastic-creep analysis of plane and axisymmetric structures. For plasticity analyses, it uses the modified stiffness method, with iterations within each load increment. For creep, the usual time-increment, initial strain approach is employed.

For general two-dimensional analyses, three-node triangular elements are used in PLACRE. However, since the ratchetting problem in a long, straight pipe can be considered one-dimensional, in the sense that temperature, stress, and strain are each dependent only on the radius, a special pipe-wall bending element was added to PLACRE to more efficiently perform pipe ratchetting analyses.[29] This element, which is shown in Fig. 5.34(a), is a three-node constant-strain axisymmetric rectangle. Nodes 1 and 2 have only a radial displacement degree of freedom. Node 3, which is common to all elements [see Fig. 5.34(b)], has two degrees of freedom, corresponding to rotation and axial displacement. Each element in the representation is connected by a roller to a rigid bar which, in turn, is attached to node 3. The associated heat transfer calculations are performed using a finite-difference procedure with a mesh point located at the center of each finite element. Sixteen elements across the wall were used for the ratchetting analysis reported here.*

The inelastic analysis required cyclic stress-strain data over the 800 to 1100°F temperature range and creep data at 1100°F. These data were obtained using uniaxial specimens from plate material of the same heat (9T2796) of type 304 stainless steel as the pipe ratchetting specimen. To assure that the data would be applicable, the material test specimens and the pipe specimen were given identical pretest heat treatments, consisting of a full anneal at 2000°F for 30 min followed by rapid cooling.

---

*It should be emphasized that the special finite element was employed only to improve the efficiency of the calculations. Comparative analysis have shown that a grid of 64 conventional triangles with constraints yields essentially identical results to those obtained with the 16 special elements.

ORNL-DWG 72-14161A

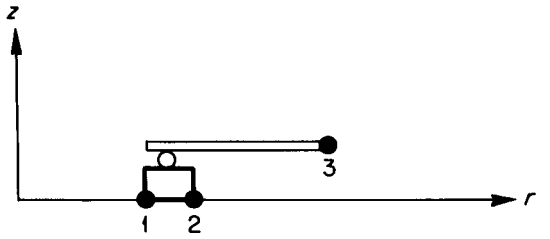

(*a*) SCHEMATIC DIAGRAM OF SINGLE ELEMENT

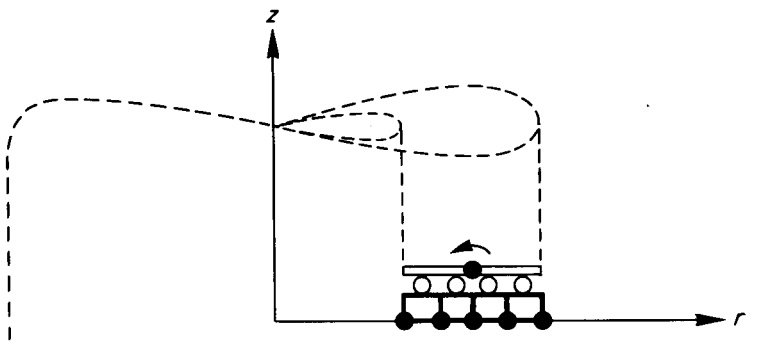

(*b*) SIMULATION OF A PIPE WALL WITH BENDING

Fig. 5.34. Special pipe-wall bending element for one-dimensional ratchetting analysis.

The cyclic stress-strain curves used in the analysis are shown in Fig. 5.35. These curves, one for 800°F and one for 1100°F, are each for ten cycles of loading between fixed strain limits of ±0.3%. The latter value corresponds approximately to the maximum elastic-plastic strains accumulated in the ratchetting test specimen in the 13 test cycles. Both curves were obtained at a strain rate of 0.005/min, which is of the same order as the maximum strain rate in the ratchetting specimen during the transients. Instead of the actual nonlinear stress-strain curves, the principal analysis, which will, in the following, be referred to as the "reference analysis," utilized bilinear equivalent curves, which were constructed by the procedure recommended in Ref. 21. The bilinear equivalents are depicted in Fig. 5.35 for each half cycle.

Uniaxial, constant-load creep curves have been obtained for heat 9T2796 at 1100°F for a variety of stress levels down to, and including, 7.5 ksi. Test times were generally to 5000 hr. On the basis of these data, the following creep law was developed to define the creep response at 1100°F[30]:

$$\varepsilon^C = A(\sigma)[1 - e^{-r(\sigma)t}] + K(\sigma)t \ ,$$

where

$$A(\sigma) = 5.436 \times 10^{-5}\ \sigma^{1.843} \ ,$$

$$r(\sigma) = 5.929 \times 10^{-5} \exp\ (0.2029\sigma) \ ,$$

and

$$K(\sigma) = 6.73 \times 10^{-9}\ [\sinh\ (0.1479\sigma)]^{3.0} \ .$$

Here, the creep strain ε^C is in in./in., σ is stress measured in ksi, and t is time measured in hours.

The predictions of the creep law are compared to typical measured uniaxial creep curves in Fig. 5.36. As can be seen, the above law, which was based on all the data, generally underpredicts the measured response for relatively short times. Consequently, a second law, of the same form, was developed on the basis of data only to 1000 hr.[30] The predictions of this law are also shown in Fig. 5.36. In addition to the reference analysis, which used the creep law developed on the basis of all the data, an analysis using the 1000 hr creep law was also performed.

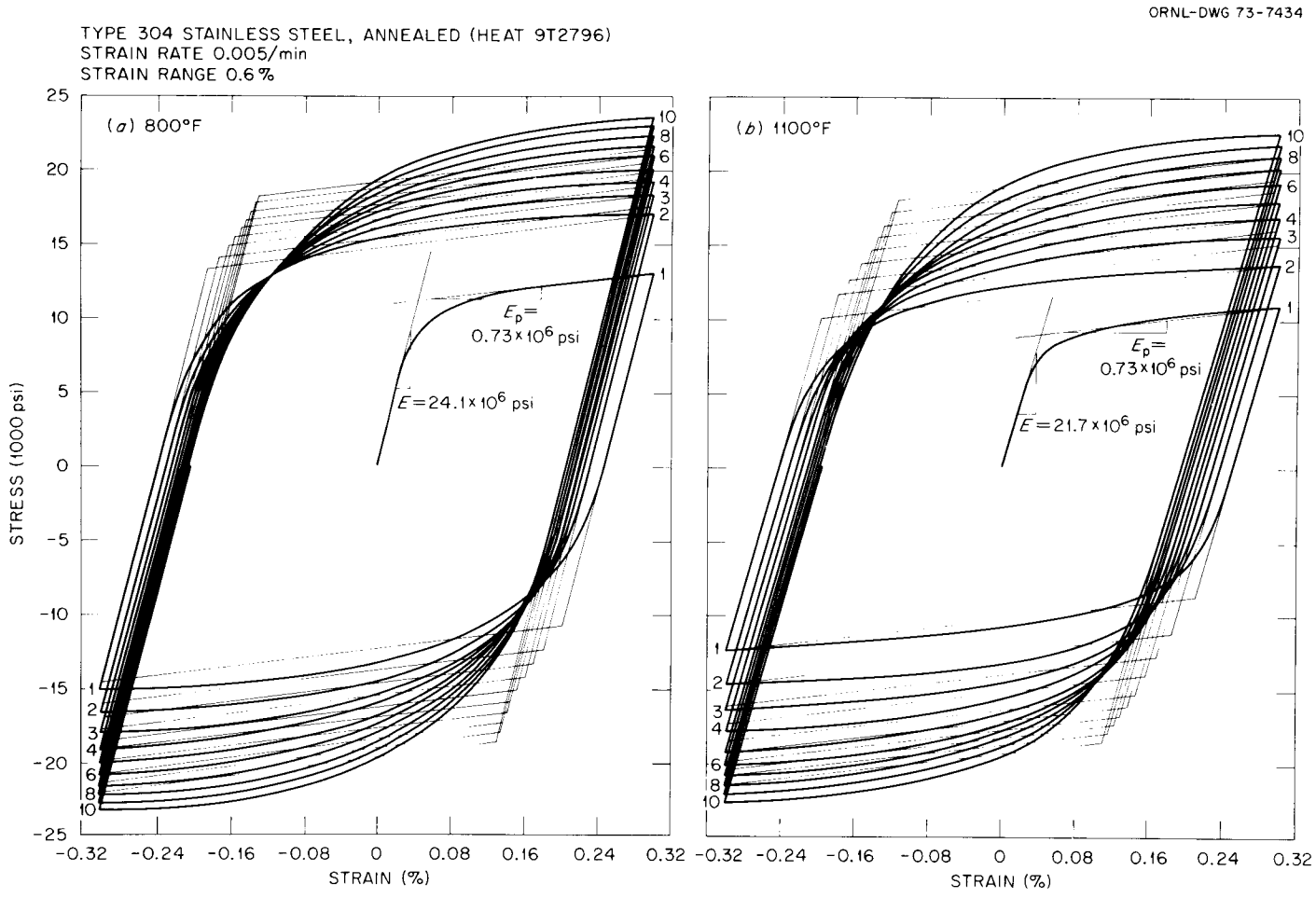

Fig. 5.35. Cyclic stress-strain curves for type 304 stainless steel (heat 9T2796) at 800°F and 1100°F. Bilinear equivalent curves are depicted for each half cycle.

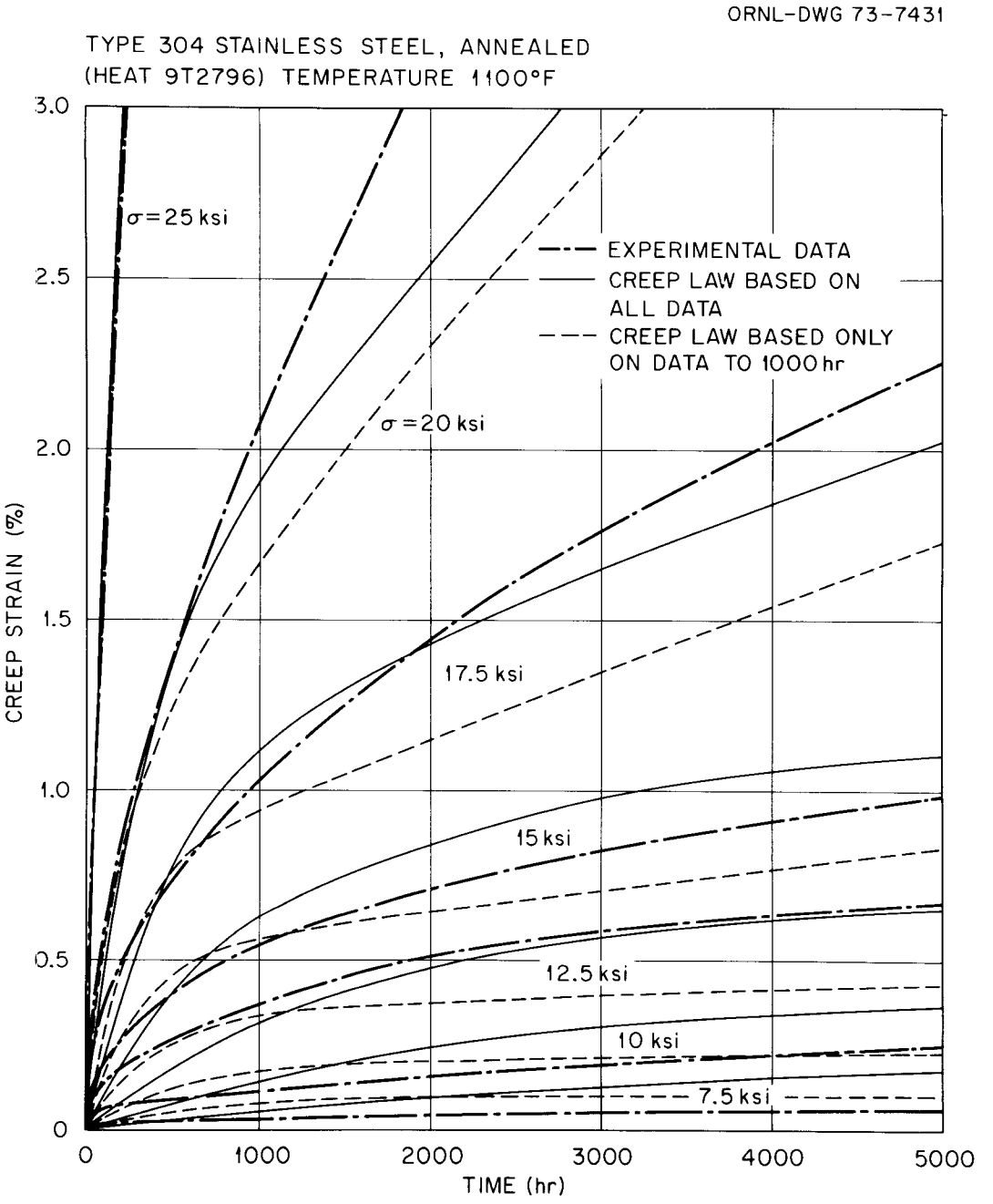

Fig. 5.36. Comparison of creep laws used in analyses with measured uniaxial creep curves for type 304 stainless steel (heat 9T2796) at 1100°F.

Other material properties were represented by fitting polynomials to the data in Table 5.3. Poisson's ratio was taken as 0.30 at all temperatures. The heat transfer coefficient during the thermal transients was taken to be 43.9 Btu/hr-in.^{2}-°F.*

Table 5.3. Properties of type 304 stainless steel

	Temperature (°F)			
	800	900	1000	1100
Modulus of elasticity (10^6 psi)	24.1	23.3	22.5	21.7
Instantaneous coefficient of thermal expansion (10^{-6} in./in./°F)	10.90	11.09	11.28	11.47
Thermal conductivity (Btu/hr-in.-°F)	0.9625	0.9917	1.0350	1.0750
Specific heat (Btu/lb-°F)	0.132	0.134	0.137	0.139
Density (lb/in.^{3})	0.284	0.283	0.282	0.281

In addition to the reference analysis, which adhered to the recommendations of Appendix A of RDT Standard F9-1T[21] and utilized belinear representations of the initial monotonic and tenth-cycle stress-strain curves, seven additional analyses were performed to study the sensitivity of the analysis predictions to variations in the material behavior representations. Also, an analysis was performed without creep to illustrate the influence of creep on ratchetting.

The eight ratchetting analyses that were performed are very briefly summarized below. Each is identical to the reference analysis except as noted.

*The sodium velocity through the annulus in the test piece was 3.1 ft/sec.

1. Reference analysis using classical kinematic hardening and the bilinear representation of the initial monotonic curve at each temperature for the initial plastic loading of each element and the bilinear representation of the tenth-cycle curve at each temperature for the first reversed plastic loading and all subsequent plastic loadings. The κ values for the initial monotonic curves and the tenth-cycle curves are denoted by $\kappa_0(T)$ and $\kappa_1(T)$, respectively. The creep law used was based on all of the data.

2. Analysis based on the 1000 hr creep law.

3. Analysis neglecting creep.

4. Analysis with no cyclic hardening ($\kappa_1/\kappa_0 = 1$).

5. Bilinear analysis in which κ was taken as a function of accumulated effective plastic strain (and temperature) and was changed for each element at each plastic loading reversal. The κ functions at 800 and 1100°F were obtained by plotting the half-cycle values from Fig. 5.35 as functions of accumulated plastic strain.

6. Bilinear analysis in which κ was varied according to the isotropic hardening model until the value corresponding to the tenth-cycle was reached; kinematic hardening was used thereafter.

7. Nonlinear analysis using the initial nonlinear monotonic curves for the initial plastic loading of each element and the nonlinear tenth-cycle curves for all subsequent plastic loadings.

8. Nonlinear analysis in which κ was taken as a function of accumulated effective plastic strain as in case 5 above. Here, the post-yield portion of the nonlinear tenth-cycle curve was used to represent the elastic-plastic response for all plastic loadings after the first, which was represented by the initial monotonic curve.

It should be emphasized that each of the above methods of representing elastic-plastic behavior is very approximate, even for the uniaxial case. For example, the tenth-cycle curves used in the nonlinear analyses properly describe the behavior only of specimens cycled exactly as those represented in Fig. 5.35. To properly describe, analytically, the nonlinear response of an arbitrarily cycled specimen requires that the entire past history be accounted for. This has not yet been accomplished for general temperature

and load changes,* and it is one of the reasons that the simpler bilinear representations of the uniaxial curves are currently recommended for analyses.

5.6.3.2. Test results and comparisons with analytical predictions. The idealized ramp transient shown in Fig. 5.29 is difficult to obtain in practice, and is unnecessary since the analysis procedure can readily accept any temperature-time response. The actual measured thermal transients imposed on the pipe specimen in the first four downshocks are shown in Fig. 5.37 along with the measured internal pressure response. The temperature-time history is consistent from cycle to cycle and agrees well with the expected transient predicted by design calculations. The transient used in the analysis is also shown in Fig. 5.37 and agrees with the average of the measured transients except that it was shifted upward to start exactly at 1100°F at time zero.

Figure 5.38 shows the measured and predicted temperature distributions through the wall of the specimen at various times after the initiation of the transient. Data for the first four cycles are shown. The agreement from cycle to cycle is good, and the measured response is in good agreement with the predictions considering that the transient used in the analysis was slightly displaced, timewise, from the measured transients (see Fig. 5.37).

Turning to the inelastic analysis results, the predicted circumferential stress-strain paths at the outside and inside surfaces are shown in Fig. 5.39 for 50 cycles. These results are from the reference analysis. Note that the lettered points shown for the first cycle correspond to the points labeled in the histograms of Fig. 5.29.

The gross ratchetting behavior of the pipe specimen is shown in Fig. 5.40, where the measured circumferential strain on the outer surface is compared with the predictions of the reference analysis, which used the creep law based on all the creep data, and again in Fig. 5.41, where the predictions are based on the 1000-hr creep law (analysis no. 2). The experimental data are from the two Boeing capacitive strain gages, which were located 90° apart near the midlength of the specimen. Data points are shown

---

*See Section 2.1 in this report for a discussion of efforts and progress in this area.

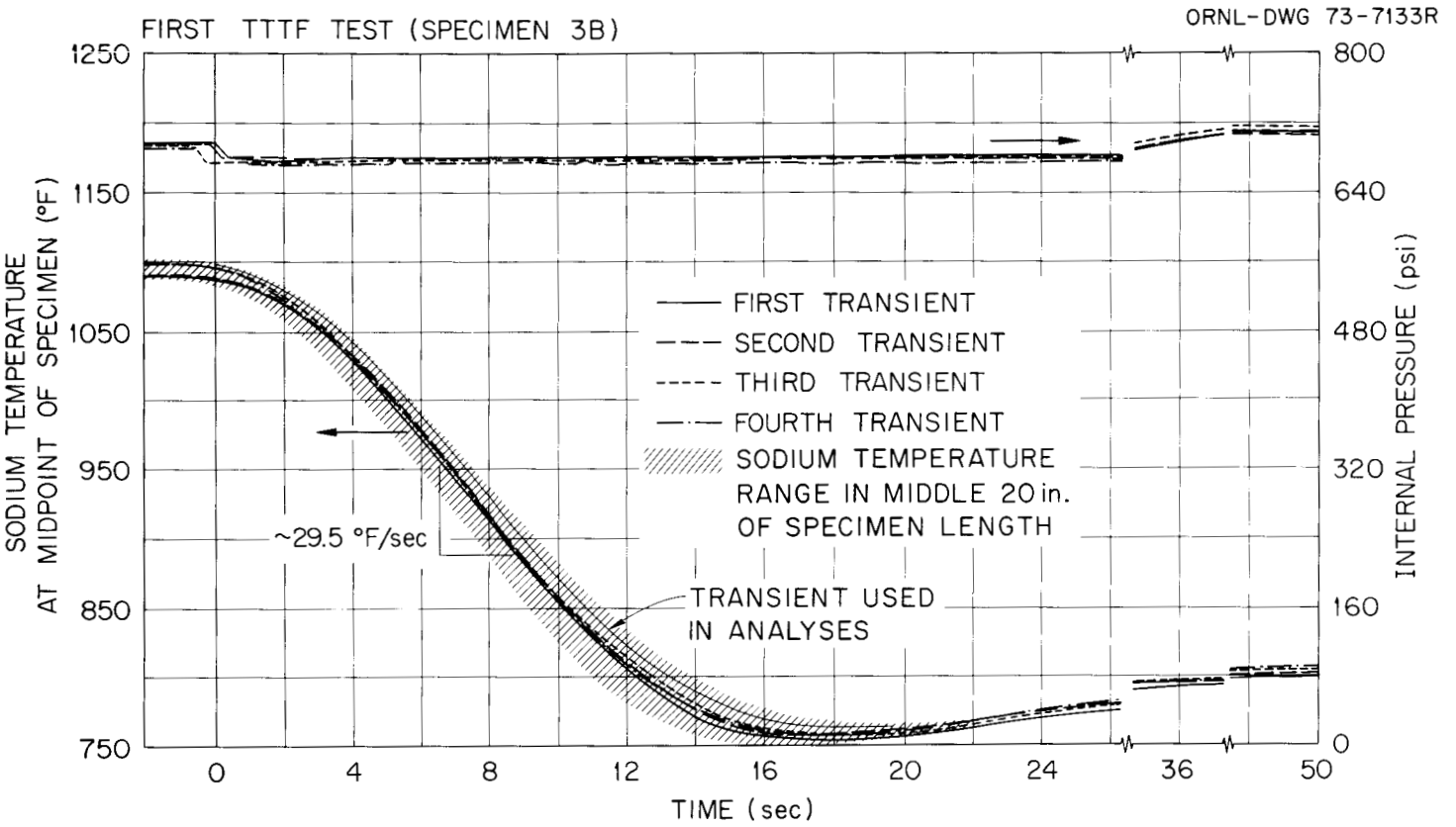

Fig. 5.37. Measured sodium temperature and pressure vs time from initiation of transient for first four transients. The temperature response curves shown were measured in the annulus at the midpoint of the test piece while the limits of the shaded band were determined by sodium thermocouples located in the annulus 10 in. upstream and downstream from the midpoint.

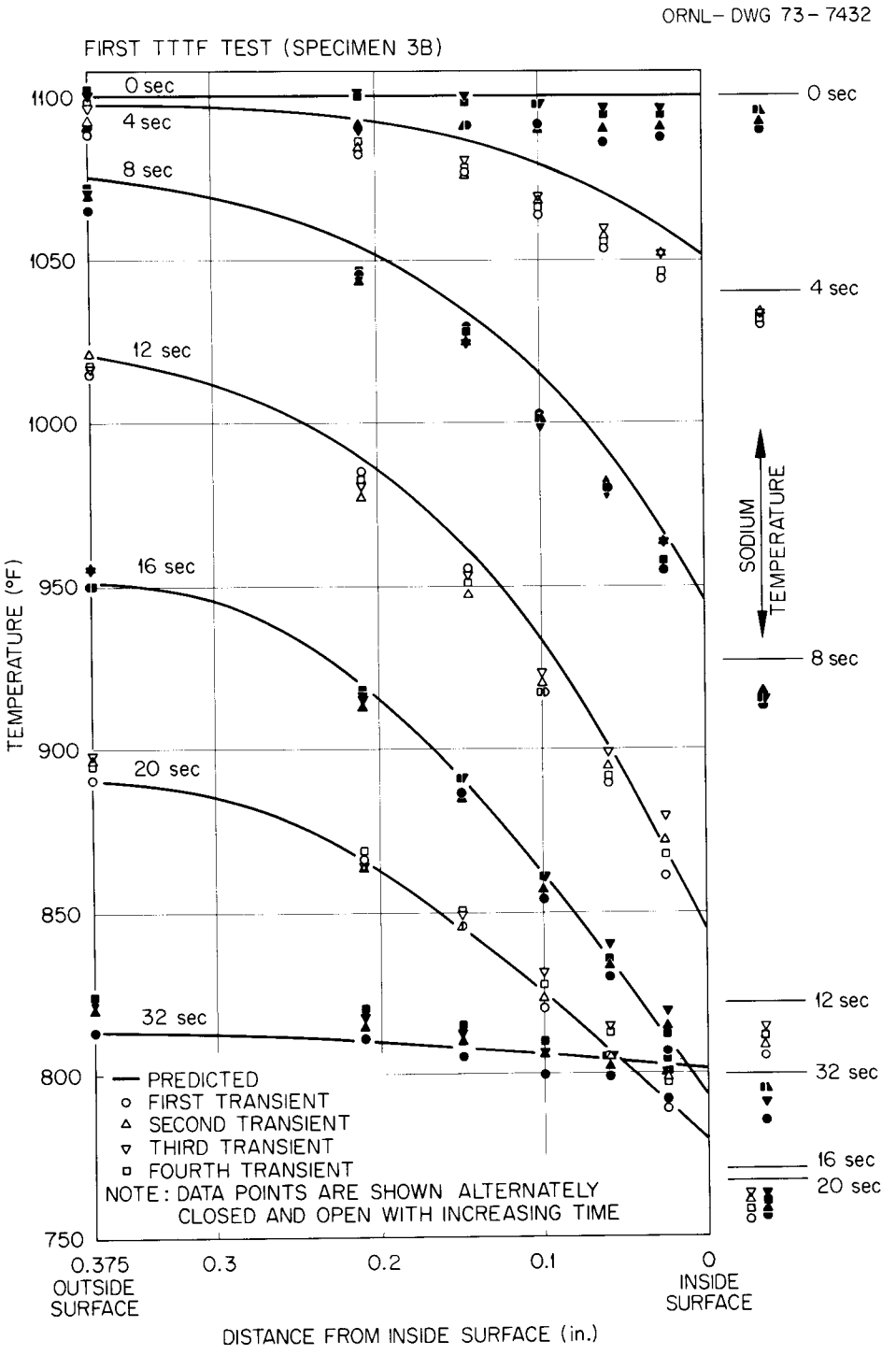

Fig. 5.38. Measured and predicted temperatures through the specimen wall at various times during the transient.

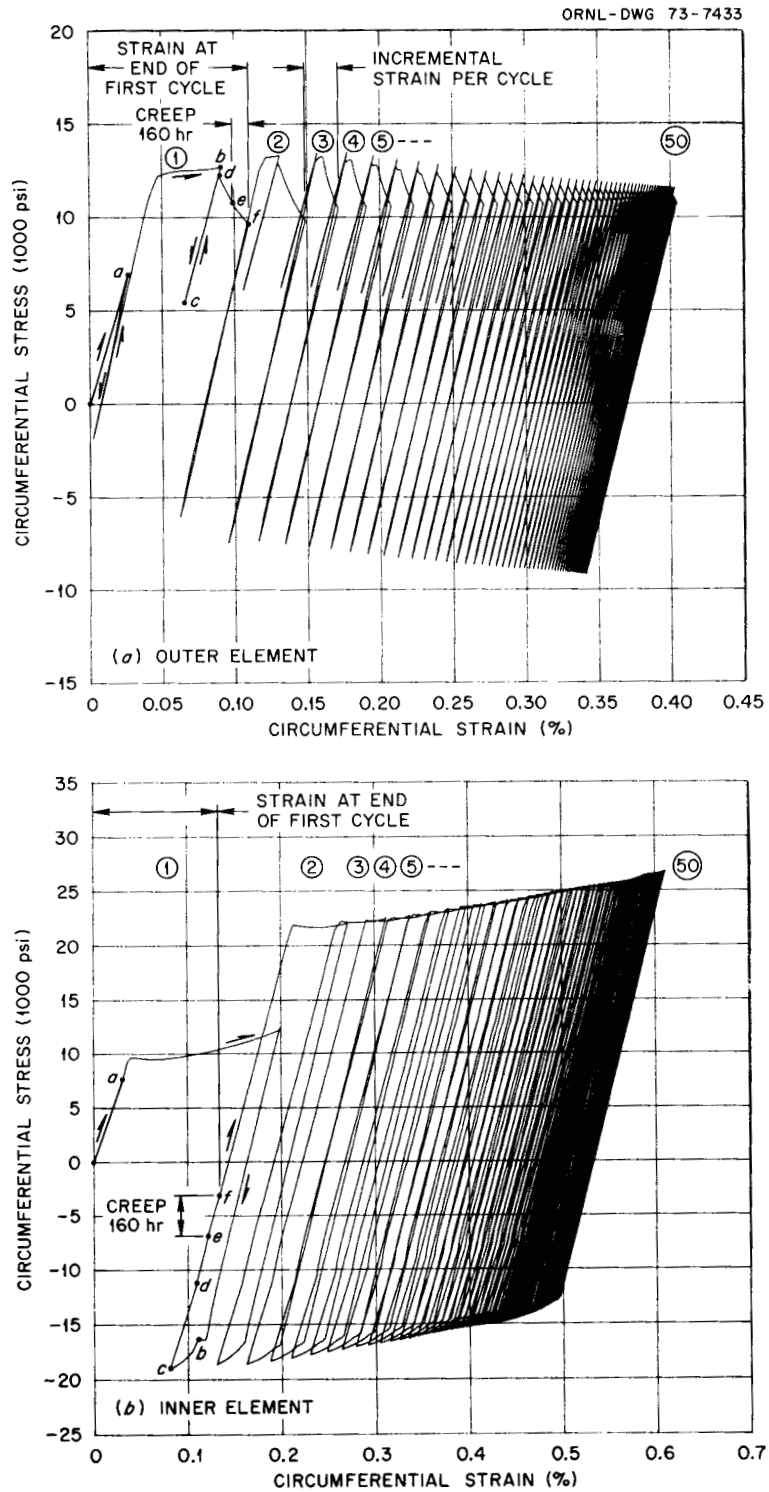

Fig. 5.39. Predicted circumferential stress-strain paths at the outside and inside surfaces for 50 cycles. The results shown are based on the reference analysis, and the lettered points correspond to the points labeled in the histograms of Fig. 5.29.

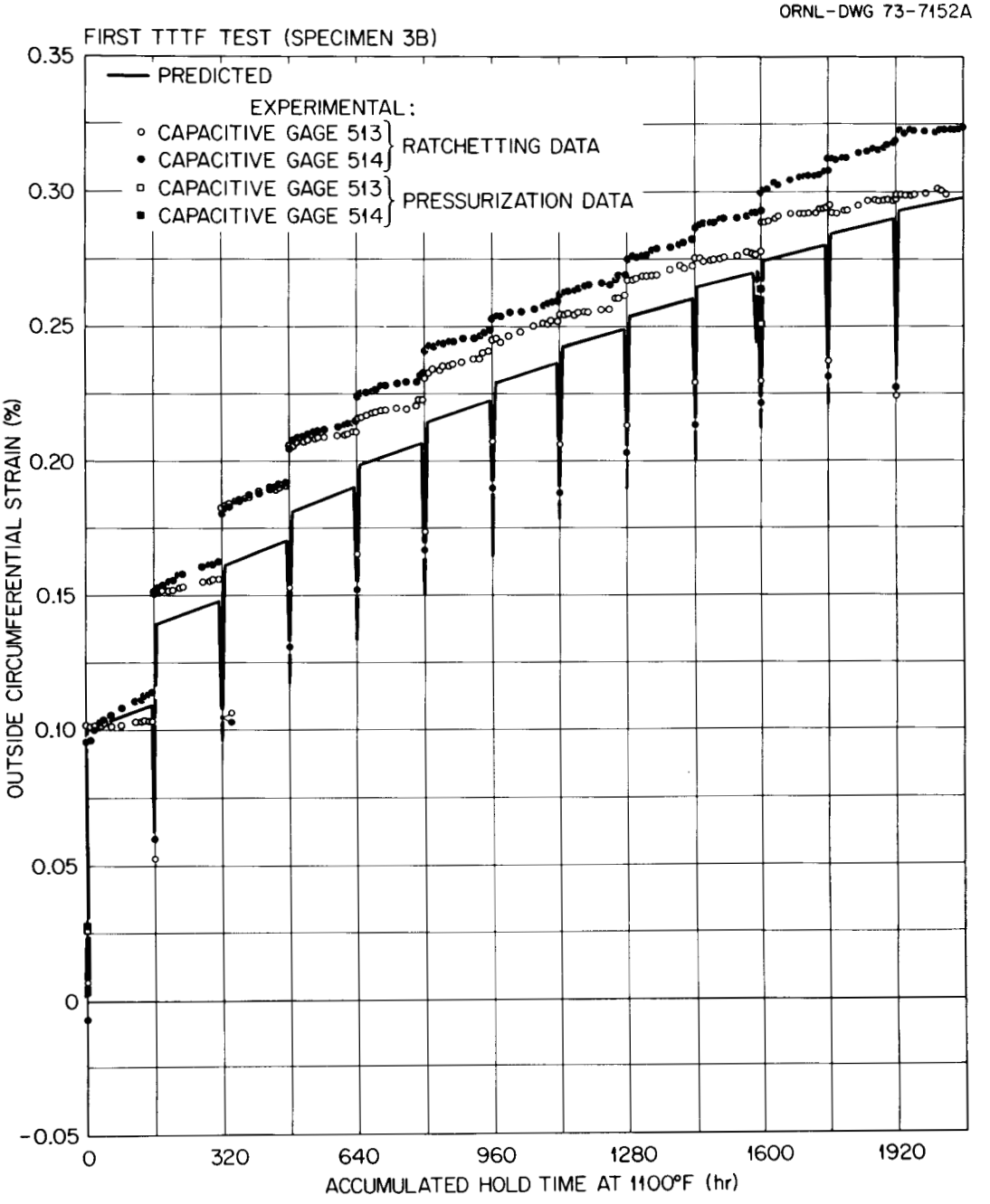

Fig. 5.40. Comparison of measured and predicted circumferential ratchetting strains for 13 test cycles. Predictions are from the reference analysis which was based on the creep law developed using all the data (see Fig. 5.36).

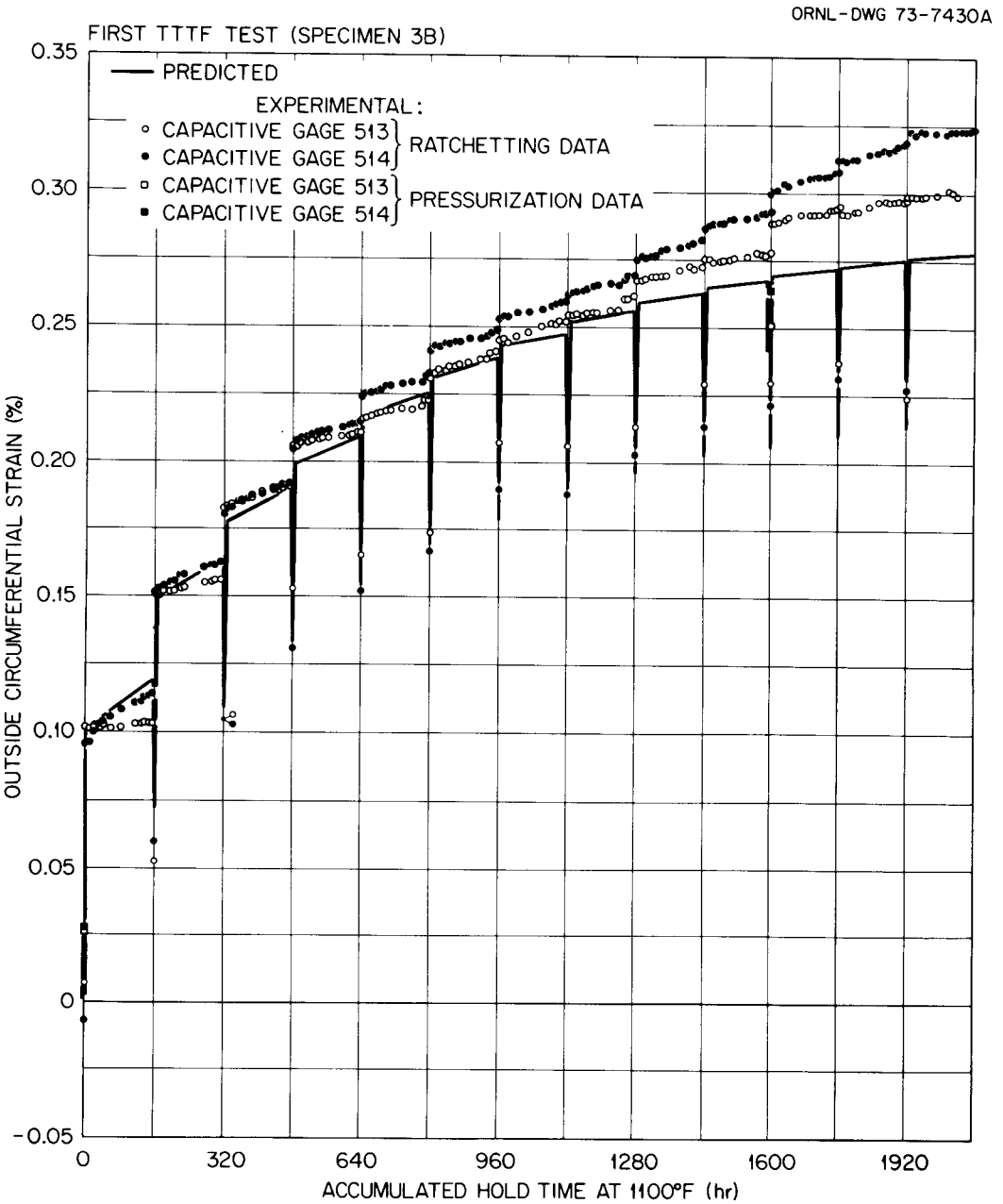

Fig. 5.41. Comparison of measured circumferential ratchetting strains with predictions based on the 1000 hr creep law (see Fig. 5.36).

for the initial pressurization and for a depressurization at the end of ten cycles.* Data corresponding to the minimum strain during each transient [see Fig. 5.39(a)] are also shown.

The net strains from the two capacitive gages agree reasonably well, although gage 513 seems to indicate more plastic (time-independent) strain and less creep (time-dependent) strain than gage 514. These differences are thought to be real. A possible explanation is the significant variation in properties that have been found around the circumference of the 8-in. pipe product form from which the ratchetting specimen was obtained.

The overall agreement between theory and experiment is good in both Figs. 5.40 and 5.41. As would be expected, the predictions shown in Fig. 5.40 underpredict the incremental deformations in the first few cycles while those shown in Fig. 5.41 agree well with the measured response for the first few cycles, but then begin to disagree for longer accumulated hold times. This behavior simply reflects the agreement between the creep laws and the actual uniaxial creep curves that were shown in Fig. 5.36, and it illustrates the significant role played by creep in the ratchetting process.

During the thermal downshocks the temperature differences between the specimen surface and the rods connecting the two ends of the capacitive gages increased very rapidly to about 150°F after approximately 20 sec. During these periods of rapidly changing temperatures, the distributions were not uniform along the gage rods, and consequently the thermal strain compensation to be applied to the gage readings could not be as precisely determined as during periods of near-isothermal conditions.

Despite this source of possible error, the detailed response measured during the transients is believed to be reasonably representative and is typified by the results shown in Fig. 5.42 for the first and fourth thermal transients. The measured and predicted (reference analysis) circumferential strains on the outer surface are shown in Fig. 5.42 as a function of time for the thermal downshock from 1100°F to 800°F, the depressurization at

---

*As explained previously, the test was interrupted for several days at the end of ten cycles by depressurizing the specimen and cooling it to room temperature. Testing was resumed by reheating to 1100°F, pressurizing, and proceeding with the next downshock.

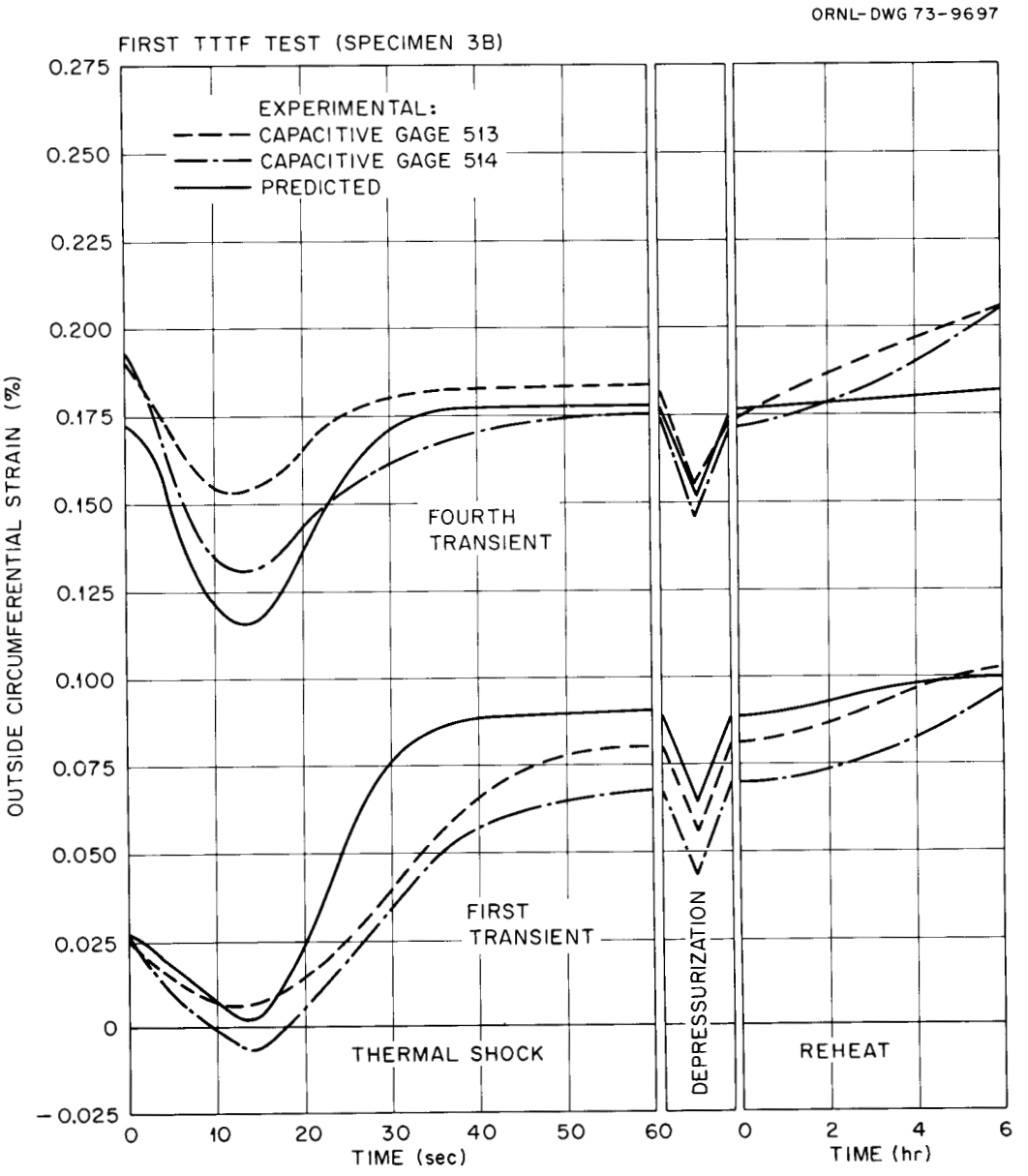

Fig. 5.42. Comparison of measured and predicted circumferential strains during the first and fourth thermal downshocks and the associated depressurizations and reheating periods. Predictions are based on the reference analysis.

800°F, and the subsequent reheating from 800°F to 1100°F. Qualitatively, the agreement between theory and experiment is reasonably good in Fig. 5.42. The analysis does appear to somewhat overestimate the increment of strain occurring during the downshock and underestimate the increment that occurs during the subsequent reheat.

The agreement between the measured ratchetting behavior and the inelastic analysis predictions is very encouraging. The results provide corroborative evidence in support of the interim constitutive equations recommended for use in design analyses of LMFBR components,[21] and they illustrate that detailed inelastic analyses based on current state-of-the-art procedures can give realistic predictions for use in design evaluations.

The final figure, Fig. 5.43, shows the predicted circumferential and axial strains accumulated on the outer surface of the pipe. Results from the reference analysis and from the other seven analyses described in the previous subsection are shown. In addition, cases 9 and 10 represent the predicted creep response over the same time period in the absence of thermal shocks based on the creep law that represented all the data and on the 1000 hr creep law, respectively. The band in Fig. 5.43 represents the measured response.

Two significant points can be made by comparing the predictions shown in Fig. 5.43. First, the pure creep cases (9 and 10) emphasize the significance of the progressive ratchetting caused by the thermal shocks. Second, the predictions are fairly sensitive to the various material behavior representations, or constitutive equation assumptions, used in the different analyses. The reference analysis gave the best overall results, although the nonlinear analyses with κ as a function of accumulated plastic strain also did well for relatively large cycle numbers.

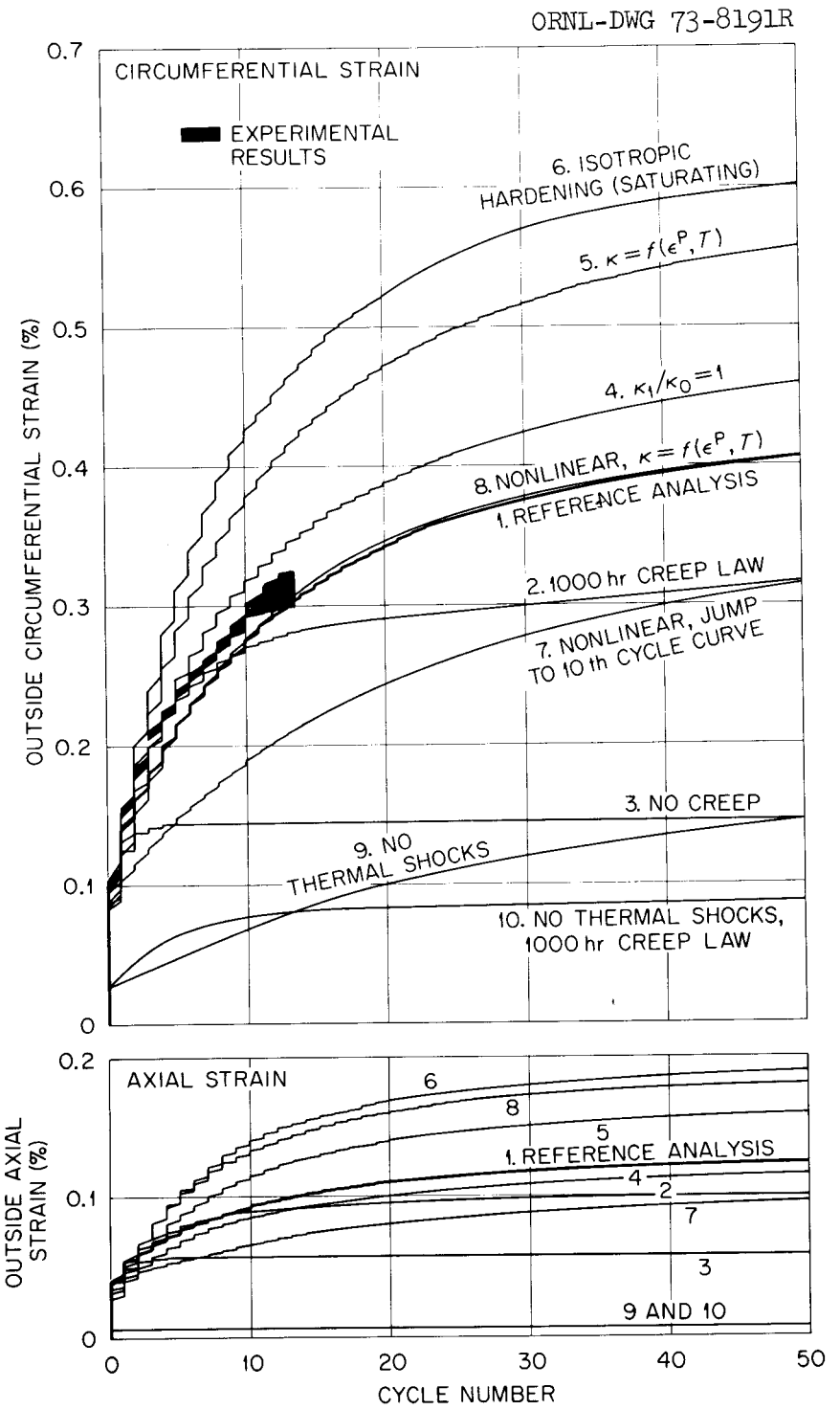

Fig. 5.43. Predicted outside circumferential and axial strains vs number of cycles for cases examined in analytical study.

6. DESIGN CRITERIA

G. T. Yahr

6.1. Studies of Shakedown and Ratchetting of Structures

G. T. Yahr W. K. Sartory
T. W. Pickel J. M. Corum

6.1.1. Comparison of Bree and O'Donnell methods for limiting ratchetting with cases run on PLACRE

Simplified ratchetting rules which are based on the Bree complete relaxation equations[31] were provided by ORNL for inclusion in a revision of RDT Standard F9-1T. Simplified ratchetting rules have been proposed for inclusion in the ASME Boiler and Pressure Vessel Code Case 1331 that are based on a method developed by O'Donnell and Porowski.[32]

Tables 6.1 and 6.2 list 51 cases that were analyzed earlier using the finite-element program PLACRE for thin-walled cylinders subjected to cyclic secondary stresses under elastic-plastic and creep conditions. The analyses[33] in Table 6.1 were originally conducted to determine whether Bree's complete relaxation equations could be used as an adequate criteria for limiting elastically calculated stresses so as to provide protection against ratchetting. The cases[34] in Table 6.2 are from a parameter study for the pipe thermal ratchetting tests[35] being conducted at ORNL. In general, only a few cycles were analyzed using PLACRE since the Bree complete relaxation method predicts the same amount of ratchet strain for each cycle. (The method based on the Bree equations becomes increasingly conservative as the number of cycles increases. In fact, this may be the principal weakness in this method since it may become extremely conservative when there are many cycles, as can be illustrated by case number 97B.) O'Donnell's method for limiting plastic and creep ratchetting have now been applied to these 51 cases. The average inelastic strains predicted by the three methods (PLACRE, ORNL-Bree, and O'Donnell) are compared in Tables 6.1 and 6.2.

Most of the cases in Table 6.1 were run with a sustained axial load and a cyclic angular edge rotation. In the method based on the Bree complete relaxation equation, the maximum equivalent linear secondary thermal stress

Table 6.1. Comparisons of O'Donnell's and Bree's ratchet strain estimates with results from ORNL PLACRE study

Case No.	P_L (ksi)	Q_R[a] (ksi)	S_t[b] (ksi)	Bree		O'Donnell		Maximum temperature (°F)	No. of cycles	Total creep time (hr)	Average inelastic strain			Comments
				$x'' = P_L/S_m$	$y'' = Q_R/S_m$	$\sigma'_p = P_L/S_y$	$\sigma'_t = S_t/S_y$				PLACRE[c] (%)	ORNL-Bree (%)	O'Donnell[d] (%)	
1	8.6	17.0	17.0	0.65	1.29	0.59	1.17	1100	5	0	0.016	0.090	0.05	Mechanical Q stress
4	8.6	17.0	17.0	0.65	1.29	0.59	1.17	1100	5	2,500	0.075	0.200	0.36	" " "
4A	8.6	17.0	17.0	0.65	1.29	0.59	1.17	1100	15	7,500	0.137	0.430	0.42	" " "
4B	8.6	17.0	17.0	0.65	1.29	0.59	1.17	1100	60	30,000	0.224	1.311	0.64	" " "
15	8.6	17.0	17.0	0.65	1.29	0.59	1.17	1100	5	5,000	0.101	0.230	0.41	" " "
16	8.6	17.0	17.0	0.65	1.29	0.59	1.17	1100	5	10,000	0.130	0.270	0.48	" " "
17	8.6	17.0	17.0	0.65	1.29	0.59	1.17	1100	5	100,000	0.277	0.390	1.08	" " "
11	11.5	5.1	5.1	0.87	0.39	0.79	0.35	1100	5	2,500	0.099	0.361	0.39	" " "
28	3.8	37.2	37.2	0.29	2.82	0.26	2.55	1100	5	2,500	0.045	0.181	0.21	" " "
29	3.8	50.0	50.0	0.29	3.79	0.26	3.42	1100	5	2,500	0.083	0.296	0.42	" " "
30	5.1	29.5	29.5	0.39	2.23	0.35	2.02	1100	5	2,500	0.054	0.172	0.25	" " "
31	5.1	50.0	50.0	0.39	3.79	0.35	3.42	1100	5	2,500	0.162	0.506		" " "
72	2.6	26.4	26.4	0.20	2.00	0.18	1.81	1100	5	2,500	0.010	0.074	0.02	" " "
73	2.6	26.4	26.4	0.20	2.00	0.18	1.81	1100	5	25,000	0.013	0.074	0.02	" " "
74	2.6	38.3	38.3	0.20	2.90	0.18	2.62	1100	5	2,500	0.020	0.127	0.07	" " "
75	2.6	38.3	38.3	0.20	2.90	0.18	2.62	1100	5	25,000	0.032	0.127	0.10	" " "
76	2.6	51.5	51.5	0.20	3.90	0.18	3.53	1100	5	2,500	0.035	0.186	0.18	" " "
77	2.6	51.5	51.5	0.20	3.90	0.18	3.53	1100	5	25,000	0.061	0.186	0.32	" " "
80	2.6	38.3	38.3	0.20	2.90	0.18	2.62	1100	5	2,500	0.032	0.127	0.07	" " "
81	2.6	38.3	38.3	0.20	2.90	0.18	2.62	1100	5	25,000	0.046	0.127	0.10	" " "
88	7.5	26.1	32.0	0.57	1.98	0.51	2.20	1100	5	2,500	0.240	0.293		Thermal Q stress
89	7.5	26.1	32.0	0.57	1.98	0.51	2.20	1100	5	5,000	0.240	0.333		" " "
90	7.5	21.1	26.9	0.57	1.60	0.51	1.85	1100	5	2,500	0.172	0.193	0.61	" " "
91	7.5	21.1	26.9	0.57	1.60	0.51	1.85	1100	5	5,000	0.170	0.238	0.70	Bree rules do not
92	7.5	15.1	18.9	0.57	1.15	0.51	1.30	1100	5	2,500	0.137	0.133	0.25	apply because
93	7.5	15.1	18.9	0.57	1.15	0.51	1.30	1100	5	5,000	0.139	0.183	0.30	creep occurs at
94	3.9	7.8	6.5	0.31	0.64	0.28	0.48	1250	5	120	0.019	0.010	0.00	both ends of cycle
97	2.6	38.3	38.3	0.20	2.90	0.18	2.62	1100	5	500	0.018	0.127	0.03	Mechanical Q stress
97A	2.6	38.3	38.3	0.20	2.90	0.18	2.62	1100	25	2,500	0.020	0.575	0.07	" " "
97B	2.6	38.3	38.3	0.20	2.90	0.18	2.62	1100	250	25,000	0.032	5.615	0.10	" " "

[a] Q_R is the maximum equivalent linear secondary thermal stress as defined in the Code.

[b] S_t is the maximum elastically calculated secondary stress. For mechanical Q, $S_t = Q_R$.

[c] The PLACRE strain values are the circumferential or axial inelastic strains on the inside surface and are slightly larger than the average.

[d] Where no value is given, the stress point is in region R_1 or R_2, and the O'Donnell method doesn't apply.

Table 6.2. Comparisons of O'Donnell's and Bree's ratchet strain estimates with results from ORNL PLACRE parameter study for pipe thermal ratchetting tests[a]

Case No.	P_L (ksi)	Q_R[b] (ksi)	S_t[c] (ksi)	Bree $x'' = P_L/S_m$	Bree $y'' = Q_R/S_m$	O'Donnell $\sigma'_p = P_L/S_y$	O'Donnell $\sigma'_t = S_t/S_y$	Maximum temperature (°F)	No. of cycles	Total creep time (hr)	Average inelastic strain: PLACRE[d] (%)	Average inelastic strain: ORNL-Bree (%)	Average inelastic strain: O'Donnell[e] (%)	Comments[f]
1	7.5	34.6	44.8	0.57	2.62	0.51	3.07	1100	10	5,000	0.324	0.966		Reference case, $\dot{T}$ = 30°F/sec
3	7.5	34.6	44.8	0.57	2.62	0.51	3.07	1100	10	5,000	0.375	0.966		κ_1/κ_0 = 1 in PLACRE
4	7.5	34.6	44.8	0.57	2.62	0.51	3.07	1100	10	5,000	0.398	0.966		No pressure removal at 800°F
5	7.5	34.6	44.8	0.57	2.62	0.51	3.07	1100	10	1,000	0.288	0.916		
6	7.5	34.6	44.8	0.57	2.62	0.51	3.07	1100	10	0	0.148	0.866		
7	7.5	29.0	36.5	0.57	2.19	0.51	2.51	1100	10	5,000	0.239	0.665		$\dot{T}$ = 20°F/sec
8	7.5	18.1	22.1	0.57	1.37	0.51	1.52	1100	8	4,000	0.122	0.220	0.39	$\dot{T}$ = 10°F/sec
9	7.5	18.1	22.1	0.57	1.37	0.51	1.52	1100	8	4,000	0.153	0.220	0.39	Same as 8 but with κ_1/κ_0 = 1
10	5.4	34.4	44.7	0.41	2.60	0.37	3.06	1100	10	5,000	0.163	0.462		
11	7.5	33.7	43.3	0.57	2.56	0.51	2.97	1100	5	2,500	0.271	0.500		$\dot{T}$ = 27.8°F/sec
12	7.5	32.5	51.5	0.57	2.46	0.51	2.85	1100	5	2,500	0.255	0.465		$\dot{T}$ = 25.4°F/sec
13	7.5	30.9	39.3	0.57	2.34	0.51	2.69	1100	5	2,500	0.233	0.424		$\dot{T}$ = 22.75°F/sec
14	7.5	28.7	36.1	0.57	2.17	0.51	2.48	1100	5	2,500	0.224	0.366		$\dot{T}$ = 19.6°F/sec
15	7.5	25.5	31.7	0.57	1.93	0.51	2.18	1100	5	2,500	0.179	0.287		$\dot{T}$ = 16.0°F/sec
16	7.5	19.8	24.3	0.57	1.50	0.51	1.67	1100	5	2,500	0.132	0.189	0.45	$\dot{T}$ = 11.25°F/sec
17	6.4	33.7	44.4	0.49	2.56	0.44	3.04	1100	5	2,500	0.197	0.360		$\dot{T}$ = 27.8°F/sec
18	5.4	32.5	43.6	0.41	2.46	0.37	2.99	1100	5	2,500	0.129	0.205		$\dot{T}$ = 25.4°F/sec
19	4.3	30.9	42.5	0.33	2.34	0.29	2.91	1100	5	2,500	0.082	0.155	0.45	$\dot{T}$ = 22.75°F/sec
20	3.2	28.7	40.4	0.24	2.17	0.22	2.77	1100	5	2,500	0.045	0.100	0.15	$\dot{T}$ = 19.6°F/sec
21	2.2	25.5	37.0	0.16	1.93	0.15	2.54	1100	5	2,500	0.025	0.055	0.03	$\dot{T}$ = 16.0°F/sec
22	1.1	19.8	30.7	0.08	1.50	0.07	2.11	1100	5	2,500	0.009	0.017	0.01	$\dot{T}$ = 11.25°F/sec

[a] In all cases, the normal temperature was 1100°F, and a ramp downshock to 800°F was applied at the beginning of each cycle. At 800°F in each cycle the pressure was removed, reapplied, and the pipe was heated to 1100°F at 50°F/hr. The 1100°F was then maintained until the beginning of the next cycle.

[b] Q_R is the maximum equivalent linear secondary thermal stress as defined in the Code.

[c] S_t is the maximum elastically calculated thermal stress.

[d] The PLACRE strain values are the circumferential or axial inelastic strain on the inside surface and are slightly larger than the average.

[e] Where no value is given, the stress point is in region R_1 or R_2, and the O'Donnell method doesn't apply.

[f] Each case is identical with Case 1 except as shown in tabulations or comments.

Q_R as defined in Section III of the ASME Boiler and Pressure Vessel Code is used. O'Donnell suggested that the maximum elastically calculated secondary stress S_t should be used. In most cases the maximum elastically calculated secondary stress is larger than Q_R. Again, most of the cases in Table 6.1 were run with a sustained axial load and a cyclic angular edge rotation and in these cases Q_R equals S_t.

The normalizing factor for the Bree and O'Donnell methods is different. The value of S_m given in Code Case 1331-7 is used as the normalizing factor in the Bree method. The minimum yield strength value, S_y, from the code case is used in the O'Donnell method. The S_m values are approximately 90% of the S_y values.

The most important conclusions made from an examination of Tables 6.1 and 6.2 are as follows:

1. Both the Bree and the O'Donnell methods are conservative relative to PLACRE in every case except for case No. 94 which falls outside the range of applicability of the rules because creep occurs throughout the cycle.

2. In some cases the Bree method is more conservative and in others the O'Donnell method is more conservative. The Bree method becomes especially conservative when there is a large number of cycles.

3. The Bree method provides for operation in the regions of mechanical ratchetting, R_1 and R_2. The O'Donnell method will not allow operation in those regions.

In conclusion it is noted that these cases were designed to test the Bree method rather than the O'Donnell method. Some attention should be given to designing cases that would most severely test the O'Donnell method.

6.1.2. Comparisons of simplified rules of ratchetting with experimental results from LMEC (Anderson) beams

A number of creep ratchetting tests[36] were conducted on 304 stainless steel beams at a constant temperature of 1200°F. The beams were subjected to a constant axial load and were repeatedly bent back and forth around cylinders of 80 in., 40 in., or 20 in. diameters. Although the conditions of these tests are outside the range of applicability of the simplified ratchetting rules based on Bree's complete relaxation equations, since creep

can occur throughout the cycle, comparisons were made because of the scarcity of ratchetting data to test the simplified rules.

Experimental data from the tests discussed in Ref. 36 are compared with predictions of simplified methods of analysis in Figs. 6.1 through 6.6. The experimental results are indicated by the test number. The predictions are based on the Bree complete relaxation equations[31] and on a method recently developed by O'Donnell and Porowski.[32] Two sets of predictions were made using the Bree complete relaxation equations; one was based on the measured properties for the material used in the tests[37] which are labeled "Bree," and the other was based on the material properties in Code Case 1331-8 in the manner prescribed in the simplified ratchetting rules recommended by ORNL which are labeled "ORNL." Only one set of predictions was made using O'Donnell's rules and they were based on the measured properties of the material. In every case except for test No. 21 the Bree method gave a conservative value of cumulative strain for the first seven cycles. The sixth cycle ratchet strain for test No. 21 was abnormally high. It was 1.69 times the second cycle ratchet strain, whereas in all other tests the sixth cycle ratchet strain was less than 0.6 times the second cycle ratchet strain. Therefore the experimental data for test No. 21 are questionable. Note that Bree was conservative at the end of five cycles for this specimen. Generally, Bree becomes more conservative as the number of cycles increases.

The O'Donnell predictions are too large to be plotted on the graphs for all the cases where there was some hold time. The first cycle predictions are shown by breaking the scale, but the predictions for subsequent cycles still fall off the graphs. For zero hold time cases the O'Donnell method predicts no ratchetting since the method is based on creep. This is of no practical consequence, since any real cycle takes some time to occur.

It is concluded from these figures that the Bree complete relaxation equations are conservative for these tests, even though the test conditions were outside the range of applicability of the equations.

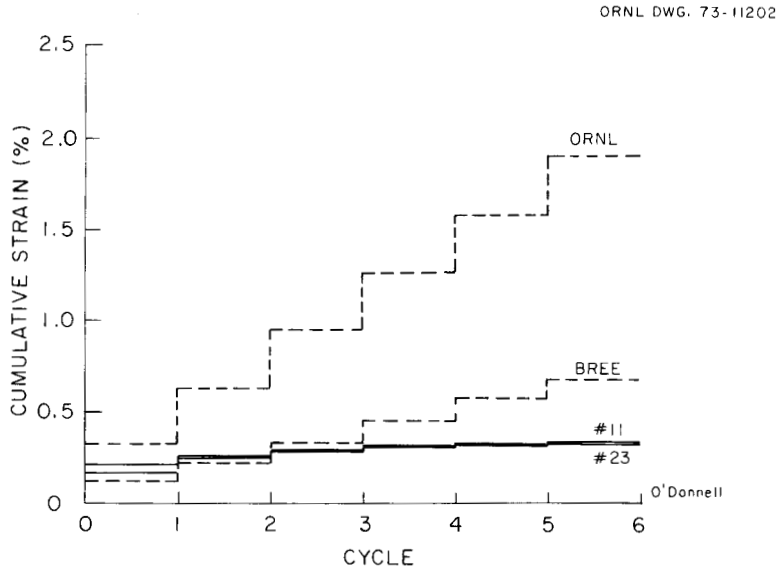

Fig. 6.1. Comparison of predictions with LMEC creep ratchetting test results. $\left(\frac{P_m}{\sigma_{y_{0.2}}} = 0.26;\ \frac{Q}{\sigma_{y_{0.2}}} = 3.82\ ;\ \text{no hold time}\right)$

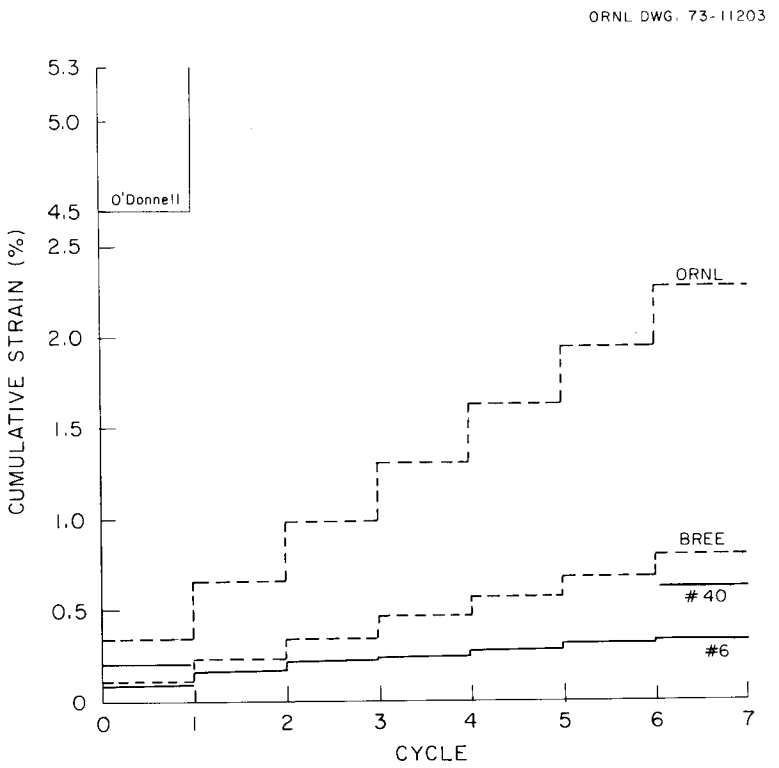

Fig. 6.2. Comparison of predictions with LMEC creep ratchetting test results. $\left(\frac{P_m}{\sigma_{y_{0.2}}} = 0.26;\ \frac{Q}{\sigma_{y_{0.2}}} = 3.82;\ 24 \text{ hr hold time}\right)$

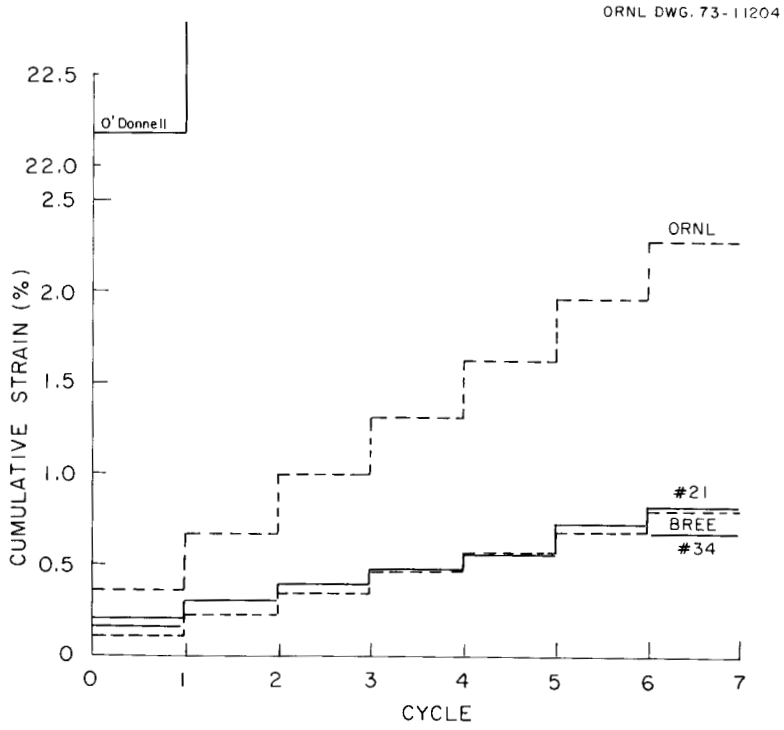

Fig. 6.3. Comparison of predictions with LMEC creep ratchetting test results. $\left(\frac{P_m}{\sigma_{y_{0.2}}} = 0.26;\ \frac{Q}{\sigma_{y_{0.2}}} = 3.82;\ 168\text{ hr hold time}\right)$

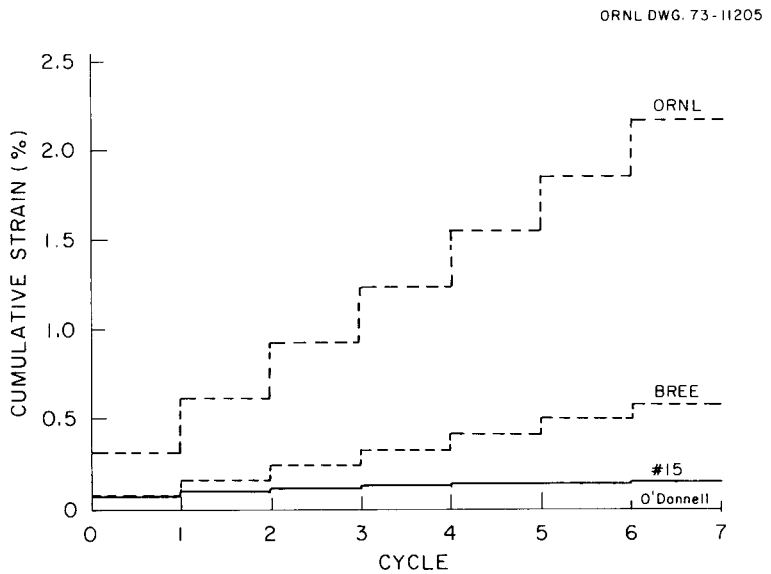

Fig. 6.4. Comparison of predictions with LMEC creep ratchetting test results. $\left(\frac{P_m}{\sigma_{y_{0.2}}} = 0.51;\ \frac{Q}{\sigma_{y_{0.2}}} = 1.92;\ \text{no hold time}\right)$

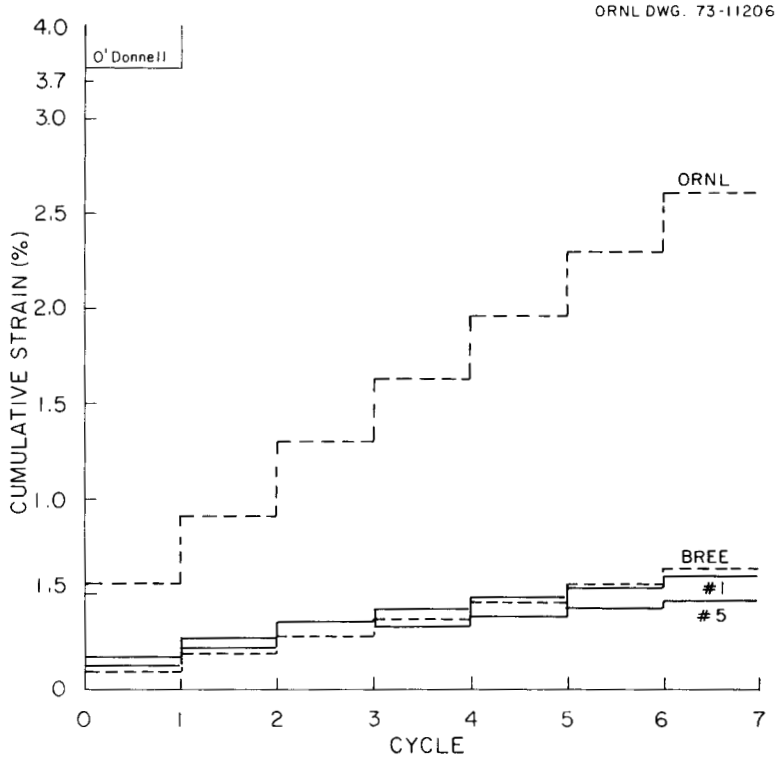

Fig. 6.5. Comparison of predictions with LMEC creep ratchetting test results. $\left(\frac{P_m}{\sigma_{y_{0.2}}} = 0.51;\ \frac{Q}{\sigma_{y_{0.2}}} = 1.92;\ \text{24 hr hold time}\right)$

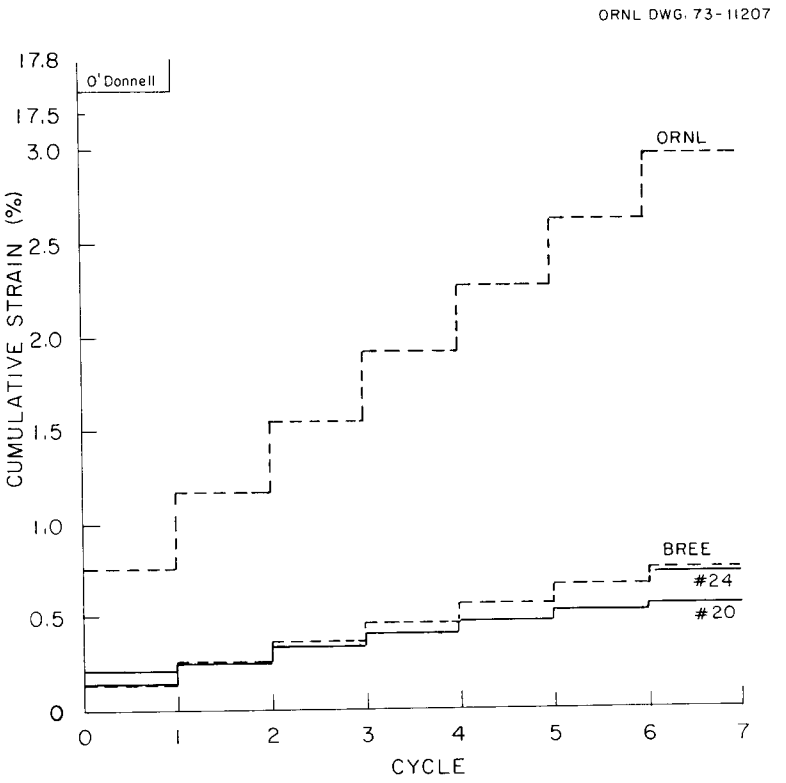

Fig. 6.6. Comparison of predictions with LMEC creep ratchetting test results. $\left(\frac{P_m}{\sigma_{y_{0.2}}} = 0.51;\ \frac{Q}{\sigma_{y_{0.2}}} = 1.92;\ 168 \text{ hr hold time}\right)$

6.2. Examination of K Factor Used in Code Case 1331 and Recommended Modifications

J. M. Corum

In ASME Boiler and Pressure Vessel Code Case 1331-8, a K factor* is used in the basic stress limits on primary membrane-plus-bending stress intensities and in the ratchetting rules. In the primary stress limits K is used to increase the allowable stress S_t in recognition of the fact that creep will reduce the actual maximum bending stress below the elastically calculated value. In the ratchetting rules, P_b from an elastic calculation is reduced by K to more realistically reflect the true maximum primary stress, which is a measure of the "driving force" for ratchetting.

To better understand the role of the K factor and the values which should be used, a number of elastic-creep and elastic-plastic-creep beam bending analyses were performed at Westinghouse-ARD by A. L. Snow and at ORNL, and the resulting inelastic stress distributions and maximum stresses were examined relative to the K factor. On the basis of these results it was concluded that the K factor currently used in the code case is a reasonable interim value for rectangular sections. However, the nomenclature in the code case should be changed to distinguish the factor used there from the more traditional K section factor as used in the 1972 Section III Winter Addenda. Also, the factor used in the code case should be dependent on the actual cross section being considered.

The results of the analyses performed at ORNL are represented in Figs. 6.7 through 6.12. Figures 6.7 and 6.8 show the steady-state creep stress distributions in a solid rectangular beam and in a tubular beam of circular cross section, respectively, for various values of n in the assumed steady-state creep law $\dot{\varepsilon}_c = A\sigma^n$. Although calculated for a specific bending moment and beam dimensions, these distributions are essentially independent of the

---

*The implied definition of K as used in the code case is the ratio of the elastically calculated maximum bending stress to the actual maximum bending stress. In the 1972 Section III Winter Addenda, K denotes the more traditional *shape factor* or *section factor* based on an elastic-ideally plastic material response.

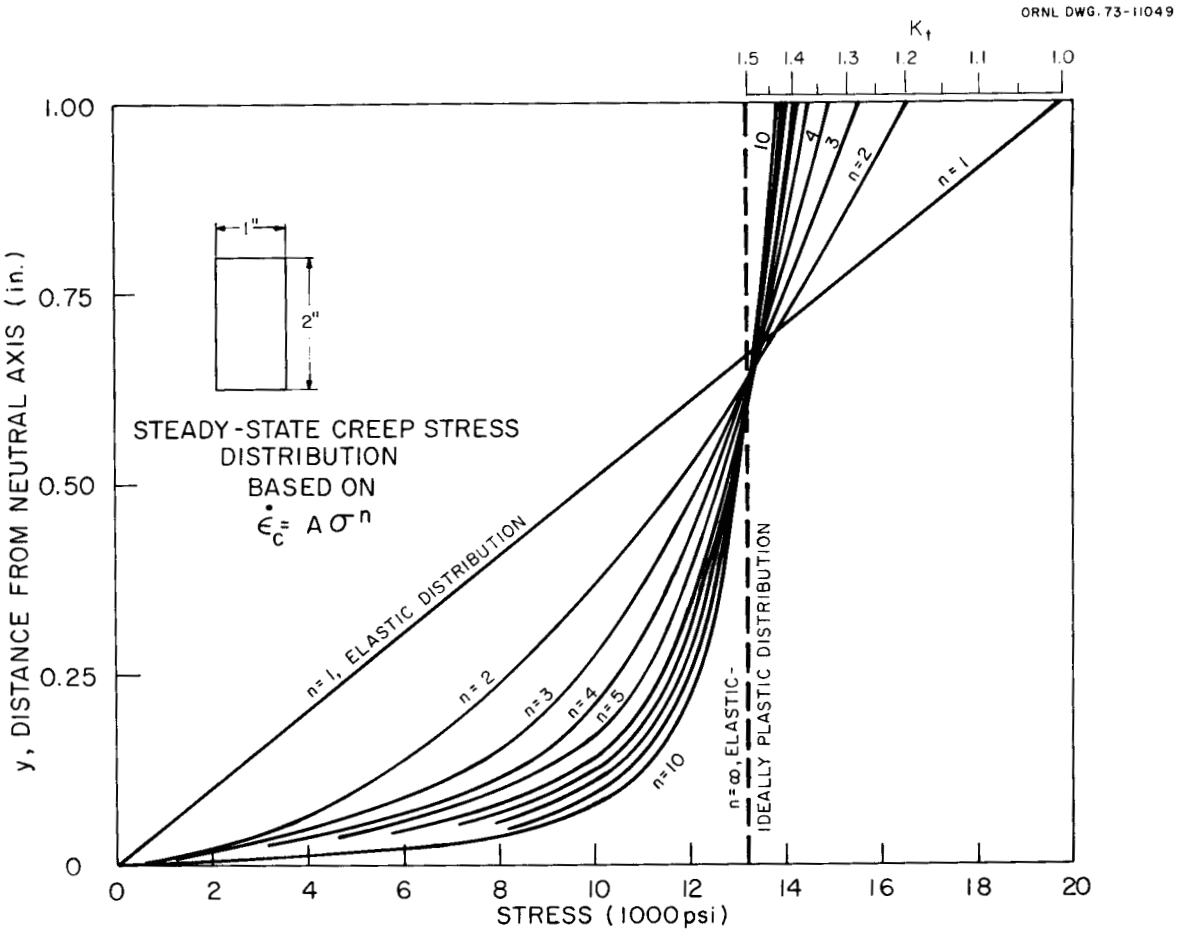

Fig. 6.7. Steady-state creep stress distributions across a rectangular beam in pure bending and having a steady-state creep law of the form $\dot{\varepsilon}_c = A\sigma^n$.

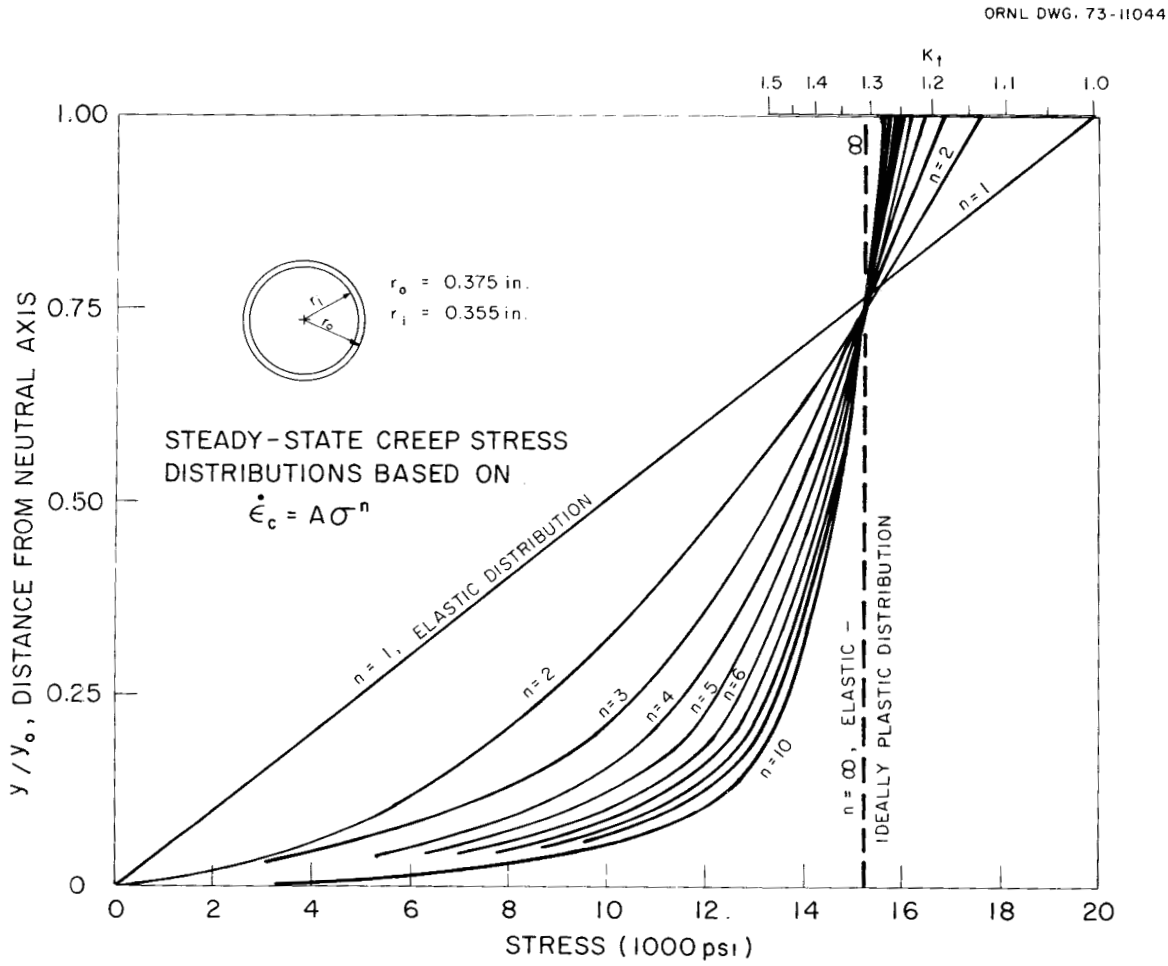

Fig. 6.8. Steady-state creep stress distributions across a thin circular tube in pure bending and having a steady-state creep law of the form $\dot{\varepsilon}_c = A\sigma^n$. Note that for the particular thickness used, the value of K_t for $n = \infty$ or for elastic-ideally plastic response is approximately 1.31. The limiting value as the thickness goes to zero is 1.27.

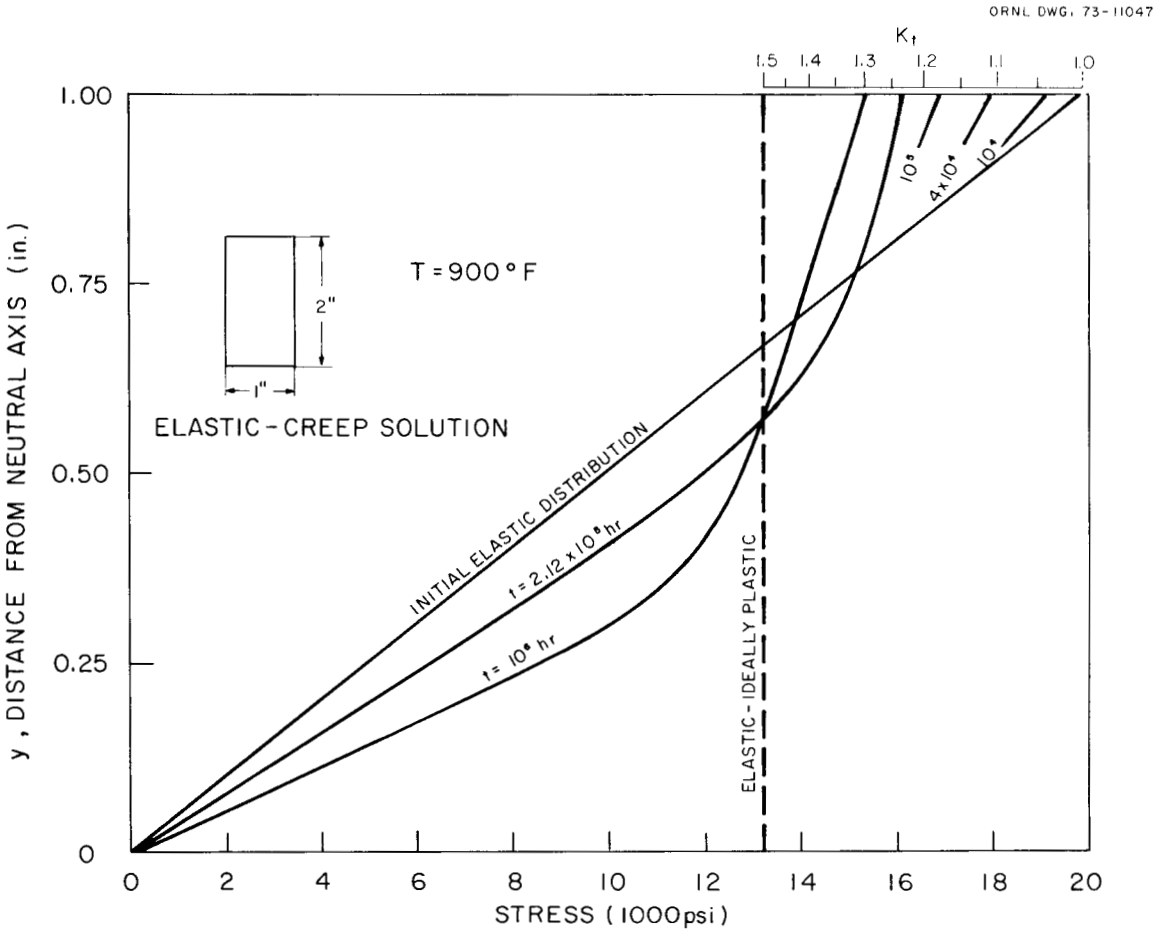

Fig. 6.9. Stress distributions for various times in a rectangular beam of type 304 stainless steel at 900°F. These calculations are based on the one-exponential creep law given in Ref. 32 and a maximum elastically calculated stress of $1.5S_{m_{1100°F}}$.

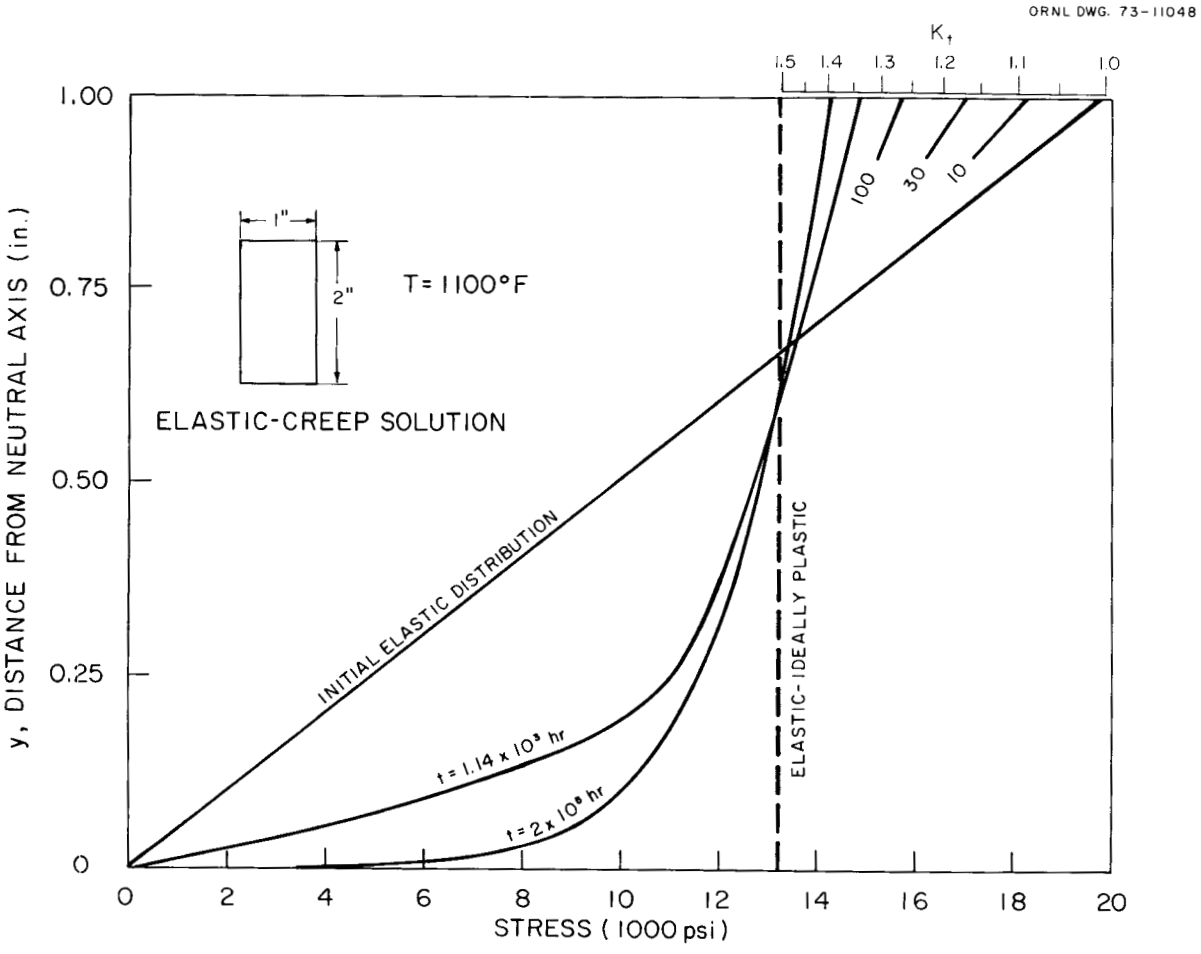

Fig. 6.10. Stress distributions for various times in a rectangular beam of type 304 stainless steel at 1100°F. These calculations are based on one-exponential creep law given in Ref. 32 and a maximum elastically calculated stress of $1.5S_{m_{1100°F}}$.

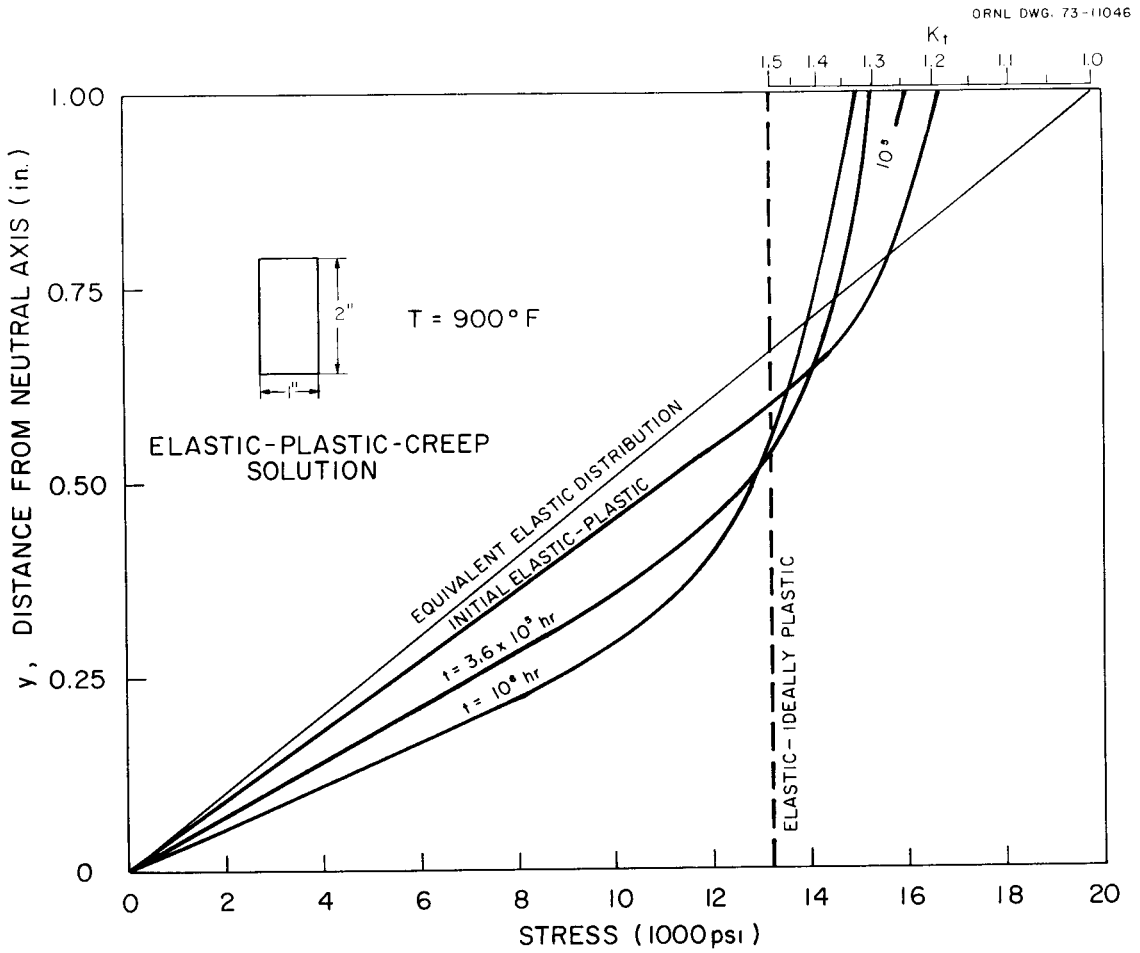

Fig. 6.11. Stress distributions for various times in a rectangular beam of type 304 stainless steel at 900°F. These calculations include initial elastic-plastic behavior based on the average stress-strain law given in Ref. 31. The maximum elastically calculated stress is $1.5S_{m_{1100°F}}$, and the creep behavior is based on the one-exponential creep law given in Ref. 32.

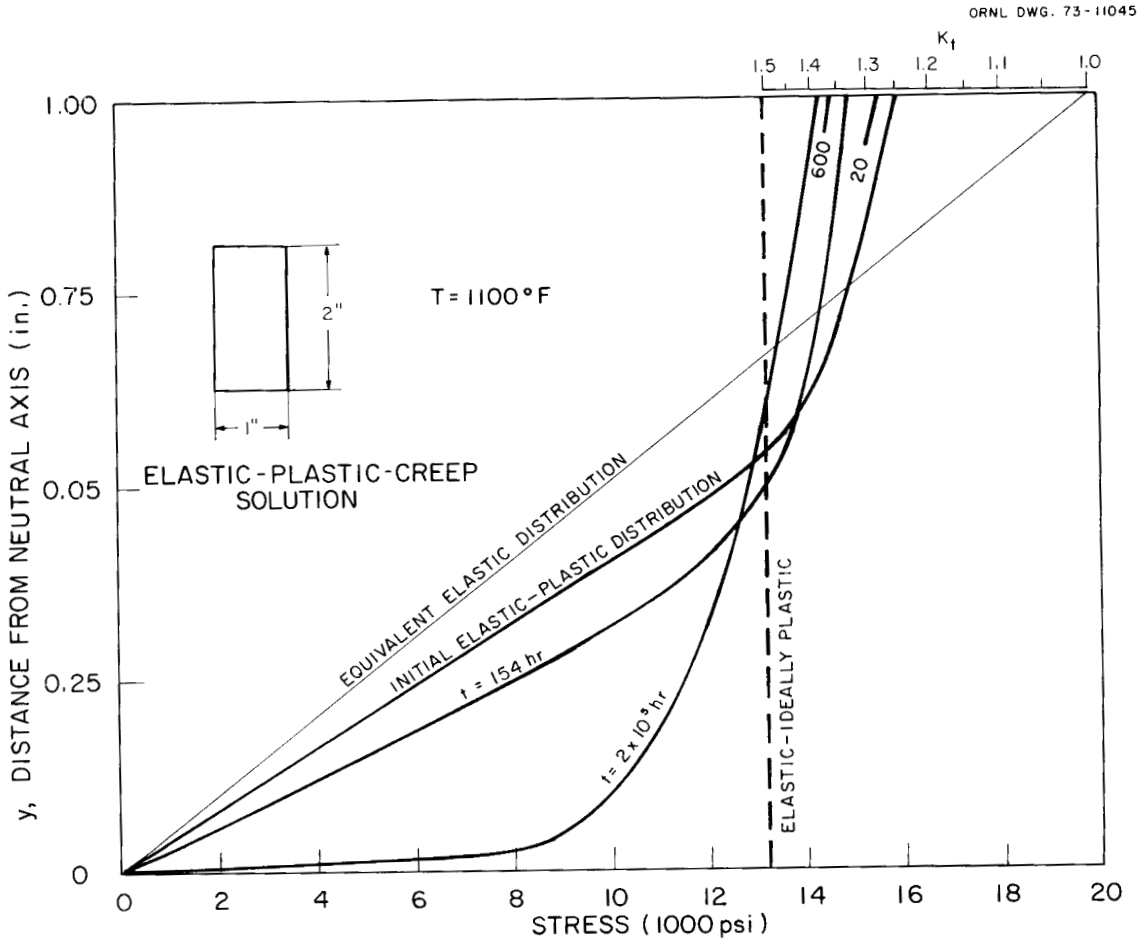

Fig. 6.12. Stress distributions for various times in a rectangular beam of type 304 stainless steel at 1100°F. These calculations include initial elastic-plastic behavior based on the average stress-strain law given in Ref. 31. The maximum elastically calculated stress is $1.5S_{m_{1100°F}}$, and the creep behavior is based on the one-exponential creep law given in Ref. 32.

stress levels and dimensions.* For the rectangular section, K varies from about 1.28 to 1.38 for n between 3 and 6, the usual range for the materials of interest at low stresses. Note that K = 1.5 for n = ∞ or for an elastic-ideally plastic response (this is the traditional section factor for a rectangular section).

Snow utilized the steady-state creep portion of the latest Blackburn creep equations (two-exponential) to examine types 304 and 316 stainless steel beams in the 900 to 1200°F temperature range. For elastically calculated stresses ranging from 5,000 to 15,000 psi he found that the ratios of the maximum steady-state stress to the elastic stress varied from 0.70 to 0.74, giving a K value ranging from 1.35 to 1.43.

These results show that the value of 1.25 used in the code case is reasonable and conservative for steady-state stress distributions in rectangular cross sections. On the same basis, however, Fig. 6.8 indicates that 1.25 is high for a thin circular tube. A comparable value to the 1.25 would be about 1.15 for the circular section.

In reality the creep response will consist of both primary and secondary creep. Also the "instantaneous" bending behavior can be elastic-plastic. Figures 6.9 and 6.10 show the stress distributions for a particular rectangular beam of type 304 stainless steel at 900 and 1100°F for various times. These calculations are based on Blackburn's one-exponential creep law and a bending moment producing a maximum elastic stress of $1.5S_m$ at 1100°F. These figures simply indicate that the appropriate K value is time and temperature dependent (as well as stress and material dependent). The code case value of 1.25 is still conservative for long times.

Figures 6.11 and 6.12 show results in which initial elastic-plastic response is included. These results, at 900 and 1100°F, are realistic for the conditions considered. The effect of the elastic-plastic behavior is to increase K and to move the 1.25 value toward conservatism.

---

*Actually the distributions for the tubular section are independent of dimensions only as the thickness approaches zero.

7. CORE STRUCTURES DESIGN CRITERIA AND DATA

W. J. McAfee
T. W. Pickel
W. K. Sartory

In connection with the compilation of design criteria for core structural components, the documentation of the general effects of irradiation on the high temperature mechanical properties of core structures materials is continuing. The representation of uniform and total elongation of type 304 stainless steel has been improved slightly by modification of the functional form and by obtaining fits on a logarithmic basis. That is

$$\mathrm{Ln(Elong.)} = \mathrm{Ln}\ (A_1 + A_2 e^{B\Phi^n}) \qquad (7.1)$$

where A_1, A_2, and B have been discussed previously[38] and n is a constant exponent of the fluence. By analyzing the function on a logarithmic basis, no weighting factor generally need be applied. Also, a more uniform interpretation of the limits on the fit can be obtained. One disadvantage of treating the data in this manner is that the result is somewhat more sensitive to round-off error both in the fit and in using the derived constants to independently calculate elongation values. The improved constants are listed in Table 7.1.

The reduction in area of irradiated and unirradiated type 304 stainless steel has also been fitted. The same approach was used as for the elongation data. However, since the available data do not indicate that a saturation value of RA has been reached with increasing fluence, no lower asymptote of the functional form was required. Thus, the function chosen was

$$RA = Ae^{B\Phi^n} \qquad (7.2)$$

where

$A = a_0 + a_1T + a_2T^2 + a_3T^3$

$B = b_0 + b_1T + b_2T^2$

T = Temperature (°F)/100

Φ = fluence/(10^{22}), ($E > 0.1$ MeV)

and n = constant

Table 7.1. Constants for equations fitted to elongation and reduction in area Data of types 304 and 316 stainless steel

Constant	Type 304 stainless			Type 316 stainless
	Uniform elongation (%)	Total elongation (%)	Reduction in area (%)	Uniform elongation (%)
A_1	0.50315	2.4647	0	1.5076
a_0	−30.256	−9.0829	−113.443	−265.66
a_1	21.854	18.93	59.041	92.076
a_2	−2.2187	−2.1777	−5.9812	−8.6473
a_3	.06315	.07554	0.18135	0.24766
b_0	−23.019	−30.718	0.20423	55.891
b_1	5.8113	8.2087	−.07879	−16.7309
b_2	−0.52067	0.75779	8.519×10^{-4}	1.5815
b_3	.0158	.02321	0	−.04839
n	0.71006	0.75234	0.65477	1.0
Std. dev. of fit	EXP (.3607)	EXP (.2736)	9.55	EXP (.4736)

A comparison of experimental data and fitted results is shown in Fig. 7.1. Experimental reduction in area data generally show more scatter than any other tensile property and this scatter is reflected in the degree to which the data have been fitted.

Data for type 316 stainless steel are also being considered. As with type 304 stainless steel, first consideration is being given to ductility (uniform and total elongation and reduction in area). Only uniform elongation data have been considered to date. The best fit of the available data has been obtained by using a similar function as was used for the analysis of the type 304 stainless steel elongation data, i.e.,

$$\mathrm{Ln}(\mathrm{Elong.}) = \mathrm{Ln}(A_1 + A_2 e^{B\Phi}) \ , \qquad (7.3)$$

where

A_1 = a constant

A_2, B = cubic polynomials in T

T = temperature (°F)/100

and Φ = fluence/(10^{22}), n/cm^2 (E > 0.1 MeV).

The use of a power on fluence, Φ, did not improve the fit for the type 316 data. The values of the derived constants are listed in Table 7.1. A comparison of experimental data and fitted values is shown in Fig. 7.2.

The above data correlations are being used in several ways in support of criteria compilation efforts. Generally, these correlations are used to extrapolate or interpolate to temperatures and/or fluences where data do not exist in sufficient quantity to allow statistical treatment. The elongation data are being studied in conjunction with creep-rupture data (both irradiation and unirraidated) as a basis for setting preliminary strain limits for core structures. These strain limits will apply to ductility limited strain, i.e., strain components that contribute to material failure. Presently, irradiation induced creep and volumetric swelling are not considered to be ductility limited. Reduction in area data are being used in studies of fatigue adjustment factors for irradiated material. This was discussed briefly in the last progress report[38] and is based on work by Brinkman et al.[39]

The compliation of recommended criteria is progressing, and the design rules are essentially complete. Included in the rules are preliminary guidelines to assess the potential for brittle fracture associated with embrittlement caused by irradiation. Presently, the main emphasis is on assessing

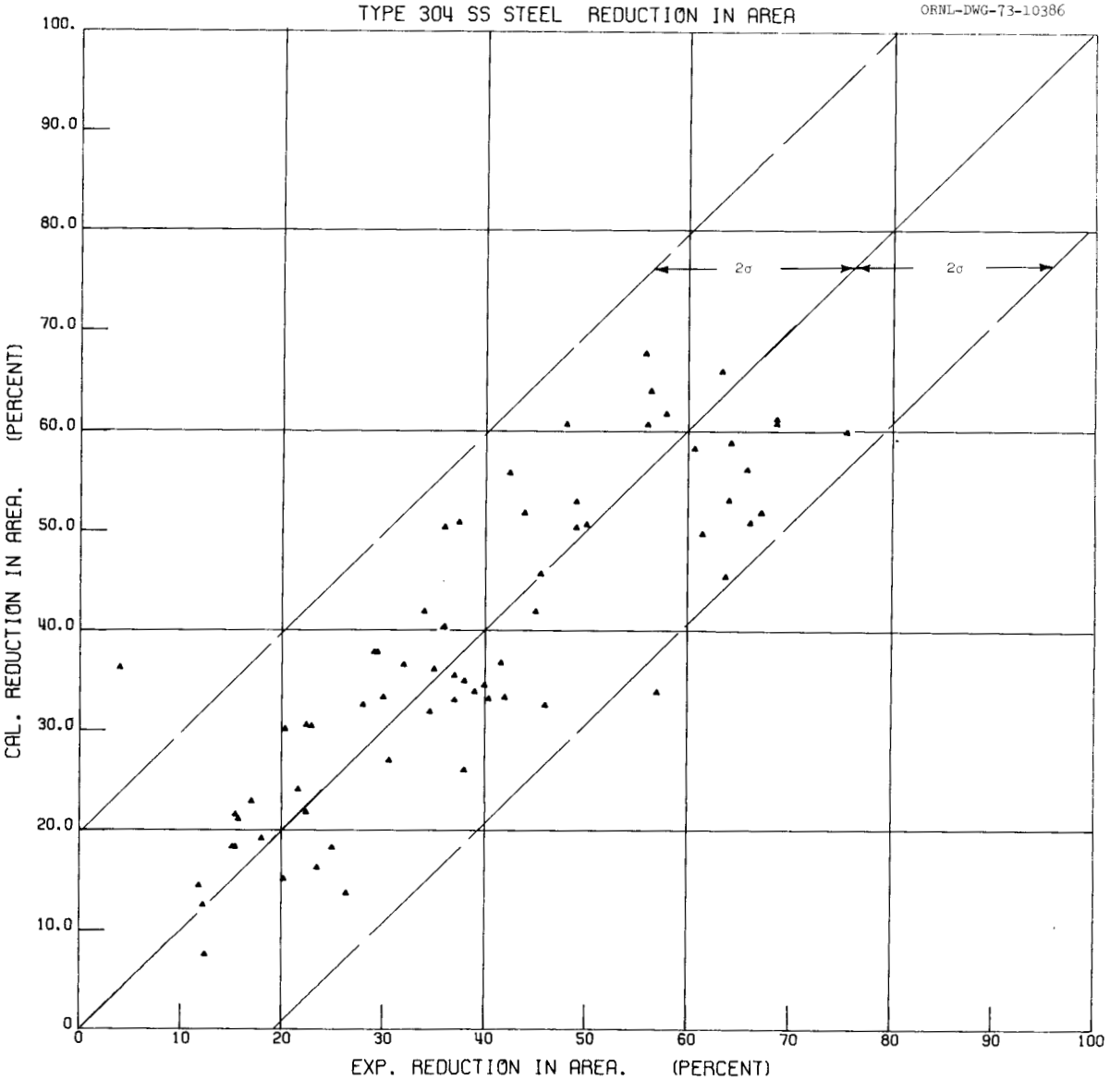

Fig. 7.1. Comparison of experimental and fitted values of reduction in area for annealed and irradiated type 304 stainless steel.

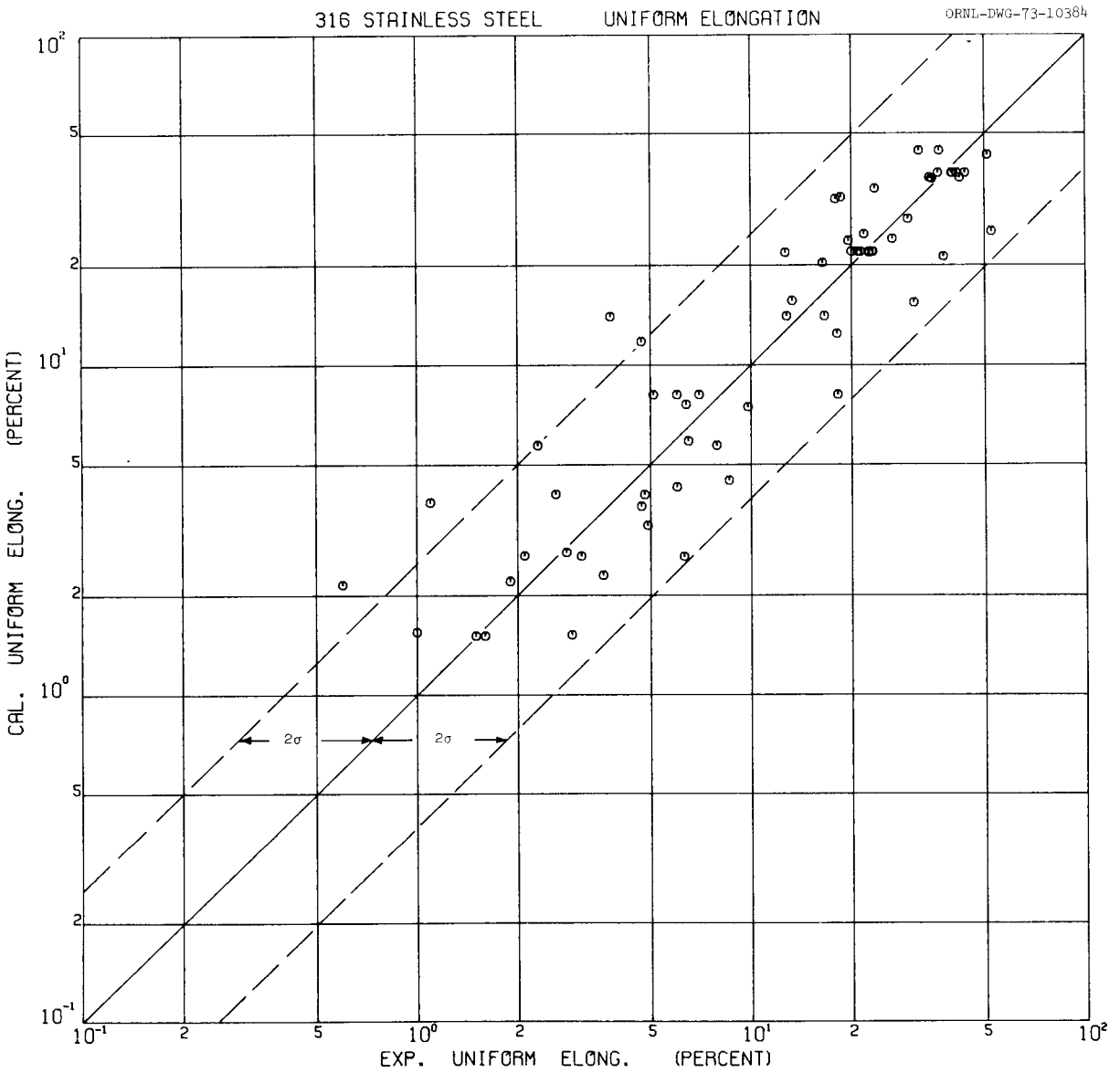

Fig. 7.2. Comparison of experimental and fitted values of uniform elongation for annealed and irradiated type 316 stainless steel.

proposed design limits and on developing new or additional limits where guidance is incomplete.

REFERENCES

1. W. J. McAfee, R. W. Swindeman, and R. D. Waddell, Jr., "Characterization of Structural Materials for Use in LMFBR Studies," pp. 133-47 in *High-Temperature Structural Design Methods for LMFBR Components Quart. Progr. Rep. Sept. 30, 1972,* USAEC Report ORNL-TM-4058, Oak Ridge National Laboratory, January 1973.

2. H. E. McCoy, "Characterization of Product Forms," pp. 196-201 in *High-Temperature Structural Design Methods for LMFBR Components Progr. Rep. October 1972 through March 1973*, USAEC Report ORNL-TM-4089, Oak Ridge National Laboratory, July 1973.

3. H. E. McCoy, "Mechanical Property Testing of Reference Heat of Type 304 Stainless Steel," pp. 89-102 in *Fuels and Materials Development Program Quarterly Progress Report for Period Ending Mar. 31, 1973*, USAEC Report ORNL-TM-4250, Oak Ridge National Laboratory, July 1973.

4. R. W. Swindeman, "Tensile Testing," pp. 206-07 in *High-Temperature Structural Design Methods for LMFBR Components Progr. Rep. October 1972 through March 1973*, USAEC Report ORNL-TM-4089, Oak Ridge National Laboratory, July 1973.

5. R. W. Swindeman and R. D. Waddell, Jr., "Mechanical Properties of Types 304 and 316 Stainless Steel," pp. 188-209 in *Fuels and Materials Development Program Quarterly Progress Report for Period Ending Dec. 31, 1971*, USAEC Report ORNL-TM-3703, Oak Ridge National Laboratory, March 1972.

6. R. W. Swindeman, "Variation of Short-Term Creep Properties with Annealing Conditions," pp. 202-05 in *High-Temperature Structural Design Methods for LMFBR Components Progr. Rep. October 1972 through March 1973*, USAEC Report ORNL-TM-4089, Oak Ridge National Laboratory, July 1973.

7. R. W. Swindeman, "Creep Testing," pp. 87-97 in *High-Temperature Structural Design Methods for LMFBR Components Quart. Progr. Rep. Mar. 31, 1972*, USAEC Report ORNL-TM-3845, Oak Ridge National Laboratory, June 1972.

8. K. C. Liu, "Elastic-Plastic Behavior Studies," pp. 2-11 in *High-Temperature Structural Design Methods for LMFBR Components Quart. Progr. Rep. June 30, 1972*, USAEC Report ORNL-TM-3917, Oak Ridge National Laboratory, September 1972.

9. K. C. Liu, "Elastic-Plastic Behavior Studies," pp. 2-22 in *High-Temperature Structural Design Methods for LMFBR Components Progr. Rep. October 1972 through March 1973*, USAEC Report ORNL-TM-4089, Oak Ridge National Laboratory, July 1973.

10. J. A. Clinard and J. M. Corum, "Verification and Qualification of CREEP-PLAST by Benchmark Problem Calculations," pp. 79-97 in *High-Temperature Structural Design Methods for LMFBR Components Progr. Rep. October 1972 through March 1973*, USAEC Report ORNL-TM-4089, Oak Ridge National Laboratory, July 1973.

11. E. T. Onat, *Representation of Creep of Metals*, USAEC Report ORNL-4783, Oak Ridge National Laboratory, August 1972.

12. W. N. Findley, "Multiaxial Creep Studies," pp. 10-21 in *"High-Temperature Structural Design Methods for LMFBR Components Quart. Progr. Rep. Sept. 30, 1972*, USAEC Report ORNL-TM-4058, Oak Ridge National Laboratory, January 1973.

13. J. M. Corum, "Two-Dimensional Elastic-Plastic-Creep Finite Element Computer Program CREEP-PLAST," pp. 77-97 in *High-Temperature Structural Design Methods for LMFBR Components Progr. Rep. October 1972 through March 1973*, USAEC Report ORNL-TM-4089, Oak Ridge National Laboratory, July 1973.

14. J. S. Crowell and S. K. Iskander, "General Three-Dimensional Thick Shell Elastic-Plastic-Creep Finite Element Computer Program EPACA," pp. 100-05 in *High-Temperature Structural Design Methods for LMFBR Components Progr. Rep. October 1972 through March 1973*, USAEC Report ORNL-TM-4089, Oak Ridge National Laboratory, July 1973.

15. W. Ramberg and W. R. Osgood, *Description of Stress-Strain Curves by Three Parameters*, Technical Note 902, National Advisory Commission for Aeronautics, July 1943.

16. Code Case 1331-7, *Interpretations of ASME Boiler and Pressure Vessel Code*, available from the American Society of Mechanical Engineers, 345 East 47th Street, New York, NY 10017.

17. *Steels for Elevated Temperature Service*, U.S. Steel Corporation, Pittsburgh, PA, third printing, 1952.

18. J. M. Corum and J. A. Clinard, "Inelastic Analyses of Beams B2, B3, and B4," pp. 51-65 in *High-Temperature Structural Design Methods for LMFBR Components Quart. Progr. Rep. Sept. 30, 1972*, USAEC Report ORNL-TM-4058, Oak Ridge National Laboratory, January 1973.

19. J. M. Corum and J. A. Clinard, "Elastic-Plastic-Creep Analysis of Circular Plate CP1," pp. 65-74 in *High-Temperature Structural Design Methods for LMFBR Components Quart. Progr. Rep. Sept. 30, 1972*, USAEC Report ORNL-TM-4058, Oak Ridge National Laboratory, January 1973.

20. J. M. Corum, M. Richardson, and J. A. Clinard, "Elastic-Plastic-Creep Tests and Analyses of Simply Supported Circular Plates," pp. 131-44 in *High-Temperature Structural Design Methods for LMFBR Components Progr. Rep. October 1972 through March 1973*, USAEC Report ORNL-TM-4089, Oak Ridge National Laboratory, July 1973.

21. RDT F9-1T, *Requirements for Nuclear Components at Elevated Temperatures* (supplement to ASME Elevated Temperature Code Case 1331), April 1973.

22. J. M. Corum, J. A. Clinard, and W. K. Sartory, "Cyclic Elastic-Plastic Analysis of Beam B6 and Comparisons with Test Results," pp. 115-31 in *High-Temperature Structural Design Methods for LMFBR Components Progr. Rep. October 1972 through March 1973*, USAEC Report ORNL-TM-4089, Oak Ridge National Laboratory, June 1973.

23. J. M. Corum and M. Richardson, "Elastic-Plastic-Creep Circular Plate Tests," pp. 89-93 in *High-Temperature Structural Design Methods for LMFBR Components Quart. Progr. Rep. Sept. 30, 1972*, USAEC Report ORNL-TM-4058, Oak Ridge National Laboratory, January 1973.

24. W. J. McAfee and M. Richardson, "Weldment Creep-Rupture Studies," pp. 145-7 in *High-Temperature Structural Design Methods for LMFBR Components Progr. Rep. October 1972 through March 1973*, USAEC Report ORNL-TM-4089, Oak Ridge National Laboratory, July 1973.

25. W. J. McAfee and M. Richardson, "Weldment Creep-Rupture Studies," p. 85 in *High-Temperature Structural Design Methods for LMFBR Components Quart. Progr. Rep. June 30, 1972*, USAEC Report ORNL-TM-3917, Oak Ridge National Laboratory, September 1972.

26. D. R. Harting, "Elevated-Temperature Test of Stiffened Shear-Lag Panel," pp. 153-70 in *High-Temperature Structural Design Methods for LMFBR Components Progr. Rep. October 1972 through March 1973*, USAEC Report ORNL-TM-4089, Oak Ridge National Laboratory, July 1973.

27. "Pipe Thermal Ratchetting Tests," pp. 168-95 in *High-Temperature Structural Design Methods for LMFBR Components Progr. Rep. October 1972 through March 1973*, USAEC Report ORNL-TM-4089, Oak Ridge National Laboratory, July 1973.

28. W. K. Sartory, "Inelastic Structural Analyses of TTTF Components," pp. 104-13 in *High-Temperature Structural Design Methods for LMFBR Components Quart. Progr. Rep. Sept. 30, 1972*, USAEC Report ORNL-TM-4058, Oak Ridge National Laboratory, January 1973.

29. W. K. Sartory, "Development of a Pipe-Wall Bending Element for Simple Ratchetting Analyses," pp. 48-51 in *High-Temperature Structural Design Methods for LMFBR Components Quart. Progr. Rep. Sept. 30, 1972*, USAEC Report ORNL-TM-4058, Oak Ridge National Laboratory, January 1973.

30. C. E. Pugh, "Creep Law Development for the ORNL Reference Heat of Type 304 Stainless Steel at 1100°F," pp. 31-43 in *High-Temperature Structural Design Methods for LMFBR Components Quart. Progr. Rep. Sept. 30, 1972*, USAEC Report ORNL-TM-4058, Oak Ridge National Laboratory, January 1973.

31. J. Bree, "Elastic-Plastic Behavior of Thin Tubes Subjected to Internal Pressure and Intermittent High-Heat Fluxes with Application to Fast-Nuclear-Reactor Fuel Elements," *J. Strain Analysis*, 2(3): (1967).

32. W. J. O'Donnell and J. Porowski, "Upper Bounds for Accumulated Strains Due to Creep Ratchetting," accepted for presentation at the Joint 1974 Pressure Vessels and Piping Division meeting of the ASME in Miami, and publication in the *ASME Transactions*.

33. T. W. Pickel *et al.*, "Study of Thermal Ratchetting Behavior and Elastic Design Requirements," pp. 190-213 in *High-Temperature Structural Design Methods for LMFBR Components Quart. Progr. Rep. Sept. 30, 1972*, USAEC Report ORNL-TM-4058, Oak Ridge National Laboratory, January 1973.

34. J. M. Corum and W. K. Sartory, "Predicted Ratchetting Behavior of Pipe Specimen," pp. 115-20 in *High-Temperature Structural Design Methods for LMFBR Components Quart. Progr. Rep. Sept. 30, 1972*, USAEC Report ORNL-TM-4058, Oak Ridge National Laboratory, January 1973.

35. J. M. Corum, "Pipe Thermal Ratchetting Tests," pp. 168-95 in *High-Temperature Structural Design Methods for LMFBR Components Progr. Rep. October 1972 through March 1973*, USAEC Report ORNL-TM-4089, Oak Ridge National Laboratory, July 1973.

36. W. F. Anderson, "Ratchetting Deformation as Affected by Relative Variations of the Loading Sequence," paper presented at ASME Pressure Vessel and Piping Meeting, New Orleans, September 1972.

37. W. K. Sartory, "Analysis of LMEC Ratchetting Tests," pp. 57-63 in *High-Temperature Structural Design Methods for LMFBR Components Quart. Progr. Rep. June 30, 1972*, USAEC Report ORNL-TM-3917, September 1972.

38. W. J. McAfee, T. W. Pickel, and W. K. Sartory, "Design Criteria for Core Structural Components," pp. 252-6 in *High-Temperature Structural Design Methods for LMFBR Components Progr. Rep. October 1972 through March 1973*, USAEC Report ORNL-TM-4089, Oak Ridge National Laboratory, July 1973.

39. C. R. Brinkman, J. M. Beeston, and G. E. Korth, *Fatigue and Creep-Fatigue Behavior of Irradiated Stainless Steels -- Available Data, Simple Correlations, and Recommendations for Additional Work in Support of LMFBR Design*, USAEC Report ANCR-1096, Aerojet Nuclear Company, February 1973.

INTERNAL DISTRIBUTION

Oak Ridge National Laboratory

1. S. E. Beall
2. E. E. Bloom
3. S. E. Bolt
4. C. R. Brinkman
5. J. W. Bryson
6. J. P. Callahan
7. D. D. Cannon
8. H. P. Carter
9. S. J. Chang
10. R. D. Cheverton
11. C. J. Claffey
12. J. A. Clinard
13. C. W. Collins
14-23. J. M. Corum
24. J. S. Crowell
25. F. L. Culler
26. W. G. Dodge
27. W. F. Ferguson
28. W. R. Gall
29-31. W. L. Greenstreet
32. A. G. Grindell
33. R. C. Gwaltney
34. W. O. Harms
35. S. K. Iskander
36. P. R. Kasten
37. R. T. King
38. K. C. Liu
39. T. S. Lundy
40. R. N. Lyon
41. R. E. MacPherson
42. W. R. Martin
43. W. J. McAfee
44. H. E. McCoy
45-47. H. C. McCurdy
48. J. G. Merkle
49. S. E. Moore
50. H. A. Nelms
51. P. Patriarca
52. T. W. Pickel
53-62. C. E. Pugh
63. M. Richardson
64. G. C. Robinson
65. W. K. Sartory
66-67. Myrtleen Sheldon
68. S. Siegel
69. G. M. Slaughter
70. J. E. Smith
71. R. W. Swindeman
72. D. B. Trauger
73. J. R. Weir
74. G. D. Whitman
75. L. V. Wilson
76. G. T. Yahr
77. H. C. Young
78. Patent Office
79-80. Central Research Library
81. Y-12 Document Reference Setion
82-91. Laboratory Records Department
92. Laboratory Records (RC)

Subcontractors and Consultants

93. Atomics International, P. O. Box 309, Canoga Park, CA 91304
    R. I. Jetter
94-96. Babcock & Wilcox Company, P. O. Box 835, Alliance, OH 44601
    W. E. Leyda
    C. C. Schultz
    D. B. Van Fossen
97-99. Battelle Memorial Institute, 505 King Ave., Columbus, OH 43201
    C. E. Jaske
    E. C. Rodabaugh
    G. H. Workman
100. Boeing Company, Aerospace Group, P. O. Box 3999, Seattle, WA 98124
    D. R. Harting
101-102. Brown University, Providence, RI 02912
    W. N. Findley
103. The Catholic University of America, Washington, DC 20017
    A. J. Durelli

104. Franklin Institute Research Laboratories, The Benjamin Franklin Parkway, Philadelphia, PA 19103
Zenons Zudans
105. General Electric Company, 175 Curtner Ave., San Jose, CA 95125
Y. R. Rashid
106. Pennsylvania State University, University Park, PA 16802
S. Y. Zamrik
107-109. Teledyne Materials Research Co., 303 Bear Hill Road, Waltham, MA 02154
T. Branca
W. E. Cooper
J. L. McLean
110. A. E. Carden, University of Alabama, University, AL 36586
111. E. P. Esztergar, 442 Westbourne St., La Jolla, CA 92037
112. R. H. Gallagher, Cornell University, Ithaca, NY 14850
113. R. D. Gilliland, University of Wisconsin, Milwaukee, WI 53201
114. W. J. O'Donnell, O'Donnell and Associates, Inc., 5100 Centre Avenue, Pittsburgh, PA 15232
115. E. T. Onat, Yale University, New Haven, CT 06520
116. G. H. Powell, Civil Engineering Dept., University of California, Berkeley, CA 94720

EXTERNAL DISTRIBUTION

117-118. Director, Division of Reactor Research and Development, U.S. Atomic Energy Commission, Washington, DC 20545
119. RRD Senior Site Representative, ORNL
120. Research and Technical Support Division, AEC-ORO, P. O. Box E, Oak Ridge, TN 37830
121-410. Given distribution as shown in TID-4500 under UC-79e, UC-79h, and UC-79k

☆U.S. GOVERNMENT PRINTING OFFICE: 1973-747-302/82